UNIVERSITÉ DU QUÉBEC À CHICOUTIMI

THÈSE PRÉSENTÉE À
L'UNIVERSITÉ DU QUÉBEC À CHICOUTIMI
COMME EXIGENCE PARTIELLE
DU DOCTORAT EN RESSOURCES MINÉRALES

PAR

HELIENE FERREIRA, M. Sc.

THE CORRELATION OF SEDIMENTATION PROCESSES AND LAND-USE THROUGH REMOTE SENSING: THE CASE STUDY OF THE JEQUIA LAGOON, ALAGOAS, BRAZIL

Décembre 2001

Bibliothèque
Paul-Émile-Boulet

UQAC
Université du Québec
à Chicoutimi

Mise en garde/Advice

Afin de rendre accessible au plus grand nombre le résultat des travaux de recherche menés par ses étudiants gradués et dans l'esprit des règles qui régissent le dépôt et la diffusion des mémoires et thèses produits dans cette Institution, **l'Université du Québec à Chicoutimi (UQAC)** est fière de rendre accessible une version complète et gratuite de cette œuvre.

Motivated by a desire to make the results of its graduate students' research accessible to all, and in accordance with the rules governing the acceptation and diffusion of dissertations and theses in this Institution, the **Université du Québec à Chicoutimi (UQAC)** is proud to make a complete version of this work available at no cost to the reader.

L'auteur conserve néanmoins la propriété du droit d'auteur qui protège ce mémoire ou cette thèse. Ni le mémoire ou la thèse ni des extraits substantiels de ceux-ci ne peuvent être imprimés ou autrement reproduits sans son autorisation.

The author retains ownership of the copyright of this dissertation or thesis. Neither the dissertation or thesis, nor substantial extracts from it, may be printed or otherwise reproduced without the author's permission.

DEDICATION

To the memory of my father "**Abelardo Ferreira da Silva**"

"Nothing can cure the soul but the senses, just as nothing
can cure the senses but the soul" (O. Wilde)

ABSTRACT

This study is focused on mapping the correlation between the land-cover change, sedimentation processes and the spectral radiance patterns along the Jequia estuary using field observations and reference information, laboratory spectral reflectance measurements and LANDSAT Thematic Mapper (TM) data. The Jequia estuary comprises the lagoon and its surrounding and a tidal channel to the Atlantic Ocean. It is inserted in Tertiary and Quaternary deposits covered mainly by sugar-cane crops and rare remains of the moist tropical forest. Bottom sediments along the lagoon were sampled and used to analyze their grain size distribution and mineral content by X-ray diffraction. Those samples were also used in an experiment where several sediment concentrations were simulated and their spectra's reflectance was determined. Silt is the predominating grain size within the lagoon. Quartz and kaolinite are the main minerals present within the silt and clay grain size fractions. Aerial photographs, satellite quick-look recorded in 1989 and a LANDSAT TM digital image recorded in 1990, were analyzed. The satellite data were analyzed through the photo-interpretation and quantitative approaches. Eight land-use units were mapped based on the aerial photographs and six land-use units were defined from the quick-look image. Despite the different scales within the data, we recognized that the most significant change in land-cover from 1968 to 1990 was the clearing of almost 100% of the moist tropical forest and its replacement by sugarcane crops. Overall, the digital results (0,48 to 0,82 μm) using standard classifiers indicate three water classes for the lagoon and ten land-use classes for the land surrounding the lagoon. The laboratory reflectance experimentation for suspended sediments demonstrates an overall increase of reflectance with increasing wavelength range for low and high concentrations. The reflectance for high sediment concentration shows a distinctive increase close to the TM4 range (0,82 μm). Although the correlation between the results was not precisely assessed, the results within this study demonstrate that any multidisciplinary approach is significantly facilitated using remote sensing techniques.

RÉSUMÉ

Cette recherche entreprise au Brésil concerne la lagune de Jequiá (située sur le littoral sud de l'État d'Alagoas dans le Nord-est brésilien), ses environs immédiats et le chenal (tidal) qui lui donne accès à l'Océan Atlantique. Son contexte géologique est constitué de dépôts tertiaires et quaternaires recouverts principalement par des cultures de canne à sucre et des vestiges de la forêt tropicale humide originelle. Cette étude a pour objectif de mettre en relief les corrélations existant entre les changements (les différentes variétés) de couvertures végétales, les processus de sédimentation et les modèles de radiances spectrales. Elle fut réalisée à partir des sources d'informations régionales disponibles, mais aussi au moyen d'observations sur le terrain, de mesures de réflectances spectrales réalisées en laboratoire et de données thématiques enregistrées par LANDSAT-Thematic Mapper (TM). Des échantillons de sédiments systématiquement recueillis dans le fond de la lagune et ses pourtours furent utilisés pour analyser, à partir de la diffraction par rayons X, la distribution des particules selon leurs dimensions et leurs contenus minéralogiques. Les échantillons servirent également à simuler diverses concentrations de sédiments et à mesurer corrélativement leurs réflectances spectrales en laboratoire. Les analyses effectuées montrèrent que les particules de la lagune avaient en majorité la dimension de la fraction du silt et que le quartz et le kaolin étaient les minéraux les plus nombreux dans les fractions du silt et de l'argile. Les données par télédétection furent analysées au moyen de la photo-interprétation et d'approches quantitatives fondées sur les photographies aériennes enregistrées en 1968 d'une part, le quick-look satellital de 1989 et l'image digitale enregistrée en 1990 par TM d'autre part. Huit unités d'utilisation du sol furent déterminées et cartographiées à partir de photographies aériennes. Six unités furent précisées à partir de l'interprétation d'images quick-look. En dépit des différentes échelles de données utilisées pendant la période considérée, la disparition quasi totale de la forêt tropicale humide originelle au profit de la culture de la canne à sucre s'est avérée le principal changement d'utilisation du sol. De plus, les classifications standard appliquées aux résultats digitaux dans le spectre de 0,48 à 0,82 µm permirent d'établir la présence de trois types d'eaux dans la lagune et de dix types d'unités de terrains dans la périphérie lagunaire. Les résultats en laboratoire relatifs aux sédiments en suspension montrent de plus, pour ce qui concerne les hautes et basses concentrations, un accroissement de la réflectance correspondant à une plus grande amplitude des longueurs d'ondes. Les échantillons de réflectance des concentrations élevées mettent en évidence un accroissement proche de 0,82 µm. Bien que toutes les corrélations existant entre les informations cartographiées n'aient pas toujours été définies de façon précise, il se révéla clairement que l'utilisation conjointe de la télédétection et des données obtenues sur le terrain permit de renforcer l'approche multi-disciplinaire et créa ainsi une synergie qui facilita grandement l'obtention de résultats significatifs.

ACKNOWLEDGEMENTS

This work was supported by the *Conselho Nacional de Pesquisa e Desenvolvimento* (CNPq) and the *Universidade Federal de Alagoas* (UFAL). I wish especially to thank the director of the thesis Prof. Gilles-H. Lemieux for all the scientific discussions and advices regarding the thesis and also for finding funds to acquire the LANDSAT full scene image. I wish to thank Prof. Denis W. Roy for answering all my doubts, Prof. Pierre Cousineau for his patience in clarifying the sedimentological infinite doubts. I wish to thank Prof. Jayanta Guha for all the encouragement during my four years of studying. My thanks are extended to the research team of the Remote Sensing Laboratory at the University of Quebec at Chicoutimi for the many hours they spent in assisting me in computer analysis. Thanks to Prof. Patrick Cliche from the CARTEL research team of Sherbrooke University for liberating the spectro-radiometer. Thanks to Prof. René Verreault for operating the spectro-radiometer that provided the data for chapter 5. I wish to thank the research staff of the *Núcleo de Pesquisas Tecnológicas* (NPT) at UFAL. Thanks to Prof. Nazare, Prof. Roberaldo and Prof José Leonaldo for their participation during field surveys. Thanks to Prof. Bento for the biological data. Thanks to Prof. Jader Onofre from the Federal University of *Ceara* and Prof. Rodrigo Ramalho from the Federal University of Alagoas for the letters of recommendation. Thanks to my students Jorima, Monica and Robson for their laboratory assistance. I wish to thank Richard from the petrochemical laboratory at UQAC, for his help on the sieve and LECO procedures. I wish also to thank the Department of Geology and Topography (GET) at UFAL for acquiring part of the satellite image. Thanks to Professor Milton for his kind help with the MacIntosh recording. Thanks to my daughters Thame and Thamires and to my sister Cristiene, and my family for their love and lots of patience for the long period I was not available to them. Thanks to the Guha clan for providing a family support that carried me through the numerous times I considered quitting my study. Thanks to my soul mates Angela, Marie, André, Myriam, Daniel and Malado who followed me through this road with their kind friendship.

I am very grateful to the members of the "extra muros" committee at UFAL who made possible all the arrangements for the thesis defense in Maceio, namely the Dean of Research Josealdo Tonholo as representant of the UQAC Dean, the president of the committee Roberaldo Carvalho de Souza and professor-witness José Leonaldo de Souza.

Finally, I wish to thank those I have omitted here and those who have chosen to help me in many different ways.

TABLE OF CONTENTS

CHAPTER 1

INTRODUCTION

1.1. Introduction

The analysis of remote sensing data has been proven to be very useful in mapping the water quality parameters for estuarine environments. It also enables the easy assess of temporal and spatial environmental changes on land-cover, mostly within regions lacking long-term data record.

Conventional method to estimate the water quality of lakes is assessed through qualitative and quantitative standard methods of analysis. The chemical and physical variations of the parameters controlling the water quality are characterized by those methods. Since the early eighties, the analyses of the water quality of lakes have been done through the characterization of the water optical properties (organic, inorganic content and suspended sediments) recorded on remote sensing products. Over the last two decades, the suspended sediment existing on heterogeneous and homogeneous lakes has been considered as a major optically active parameter controlling the quality of water bodies.

The *Jequia* study area, comprising the *Jequia* lagoon and the tidal channel is the focus of this study (Figure 1.1). Remote sensing techniques were selected in this work to analyze the spatial and temporal variability of water quality parameters. These techniques were selected due to lack of previously water quality data within the study area coupled with the high cost and time consuming of conventional methods. It has been widely reported that remote sensing methods are particularly appropriate for regions presenting few ground truth data.

1.1.1 *Statement of the problem*

Large and extensive industrial mono-cultivation such as sugar-cane production (industrial plumes), wastes rejected by growing and crawling urban settlements along rivers and lakes and all their subsequent impacts (mangroves clearing, slope erosion,

silting, inorganic plumes) on the ecosystems, have led to mislead the study of the natural and anthropogenic processes to an extent where it becomes a difficult task to characterize them.

The *Jequia* lagoon (Figure 1.2) was chosen as a representative depositional environment presenting several impacts such as the clearing of mangroves areas, dumping of urban wastes along the tidal channel, silting near *Jequia da Praia* town, sediment plumes, blooms of algae and an oil-like plume on its western arm.

This brings us to the following questions:

a) Can sedimentation processes and land-use changes be mapped through remote sensing techniques ?

b) Can correlations between sedimentation processes and land-use be detected ?

c) Can sediment and pollutant plumes be mapped through remote sensing technique ?

d) Can sediment and pollutants be distinguished using digital laboratory reflectance ?

The major part of this study relies on the analysis of the patterns of spectral and digital water quality signatures. The signatures were recorded in the visible, near infrared and medium infrared wavelength ranges by the LANDSAT Thematic Mapper (TM) and a spectro-radiometer. The spatial and spectral resolution of the thematic mapper available image offered, at that time, the best available opportunity of mapping water quality parameters of the *Jequia* lagoon and assessing the changes on land-cover surrounding it. The feasibility and the spectral resolution of the spectro-radiometer provide the optical data to the characterization of several concentrations of clastic sediment sampled along the lagoon in 1990. Sediment plumes and an oil-like substance and phytoplankton plumes are the controlled water quality factors mapped during three field surveys in November 1989,

March 1990 and July 1992, along the lagoon (Figure 1.1). The changes on land-cover patterns were also assessed along the study area.

The bottom sediments (Figure 1.2) along the lagoon were sampled during the 1990 survey. The analyses of the bottom sediments are used to characterize the depositional environment and the related transport processes prevailing along the lagoon during the survey sampling. Samples of water were taken to a laboratory to determine their conductivity was determined. The bathymetry of the *Jequia* lagoon was estimated using data (Table 1.1), from the same sites where sediments were sampled. These data were also used to group the sediment samples in the zones described in the third chapter, and to elaborate an original bathymetric map for the *Jequia* lagoon (Figures 1.3 and 1.4).

The major aims of this thesis are: the characterization of the optical spectral reflectance for several concentrations of suspended sediments, the correlation of reflectance to mineral type and size (their distribution patterns) and the detection of major land-cover changes along the study area.

This thesis is presented in four interrelated parts (Chapters 2, 3, 4 and 5). The first chapter concerns the outline of the problem defined along the *Jequia* lagoon. The second chapter describes the regional environmental aspects of the study area.

The third part of this study attempts to characterize the deposition and transport mechanisms related to the grain size distribution of the bed clastic sediments. A textural parametric analysis based on grain size data treated by sieve, hydrometer and moment methods, coupled with field observation and existing data was performed.

The fourth part of this thesis deals with the analysis of the digital irradiance data detected along the visible, red and near infrared wavelength ranges by the TM in 1990. These data are the basis for the characterization of the water quality parameters of the *Jequia* lagoon. The general environmental changes on land-cover along the *Jequia* estuary

are also described. The data comes from a LANDSAT TM quick-look image recorded in November 1989, and some reference data and aerial photographs recorded in 1968.

The fifth chapter of this work attempts to characterize the optical properties of the sampled sediments under two states within the 485-820 nm range; suspended load (several concentrations) and dry samples. That characterization is based on the spectra-reflectance patterns detected through a laboratory simulation performed in March 1996.

1.2 Regional environmental setting

1.2.1 Localization

The *Jequia* study area presents an approximated area of 60 km^2. It is located on the south-eastern coast of the *Alagoas* state in the northeastern part of Brazil. The study area comprises two major ecosystems; the *Jequia* lagoon and the *Jequia* tidal channel (Figure 1.1). The study area is considered within this study as an estuarine-lagunar system, therefore the expressions *Jequia* estuary or *Jequia* estuarine-lagunar system are used throughout this work in an interchangeable way.

The *Jequia* lagoon receives a maximum discharge of 1,45 m^3/sec and a minimum discharge of 1,33 m^3/sec (Cavalcante *et al.* 1993) from the *Jequia* River, its major tributaries. These results were empirically derived from the mean discharge of the *Coruripe* River located in the *Coruripe* watershed in the southern part of the *Jequia* estuary.

The *Jequia* lagoon has a water surface area of about 16 km^2, a width varying from 200 m to 1000 m and a depth varying from 1 to 11 m. The *Jequia* tidal channel has a length of 7,5 km connecting the *Jequia* lagoon to the Atlantic Ocean and a width varying from 50 to 200 m.

1.2.2.Historical data

The fishing community states the historical clear state (pure water) and fish diversity an the recreational potential value of the *Jequia* lagoon. The tidal channel was used also as a transportation route for sugar-cane products.

The oil-pollutant plume in the western branch of the *Jequia* lagoon, urban waste plumes along the sides of the tidal channel and punctual silting near the *Jequia* town was recognized during two surveys in 1989. Clearing of mangroves along the tidal channel was assessed during the 1990 surveys. Periodic floods are reported from the fishing community. The oil-plume, the suspended sediments and the urban wastes are the most important factors that might control the water quality of the study area.

The types of pollution recognized within the plumes along the study area are likely to come from the industrial effluents from the Sinimbu and Porto Rico sugar-cane and alcohol plants and distilleries. These plants are located respectively at 7 and 17 km from the main input of water into the lagoon. Rossetto (1985) established that *vinhaça* presents the major potential to pollute the rivers along the Brazilian coast. The *vinhaça* is constituted mostly of organic matter by solids (2 to 6%) and minor amounts of calcium, potassium and magnesium. He also points that the Biochemical Oxygen Demand (BOD) pH, temperature and suspended solids are the main polluted indicators or tracers. The *vinhaça* usually presents BOD of 20 000 to 35 000 mg/L and temperature ranging from 85° to 90°C. The *Jequia* pollution also comes from the human activities (urban wastes) of *Jequia* town that has about 1 000 inhabitants and lacks sanitary infrastructure.

The low values (Figure 1.5) of dissolved oxygen in the water are explained by Barros *et al.* (1992) as the result of a large quantity of pollutants in that lagoon. They suggest that the water quality of the lagoon has been significantly damaged.

The *Cansançao do Sinimbu* plant and distilleries have dumped from 1985 to 1988 (Barbosa, 1990), during the harvest period, about 239 tons of Biochemical Oxygen Demand BOD wastes (mainly *vinhaça*) into the *Jequia* river. The dumped organic load equals to a waste disposal for a population of about 4 438 000 inhabitants (Barbosa, 1990). The *Industrial Porto Rico* plant and distillery had dumped 295 tons of *vinhaça* in the tributaries of the *Jequia* river during the same period. This corresponds to an organic load equivalent to waste disposal for a population of about 5 460 000 inhabitants. The *vinhaça* is also used along the *Jequia* estuary as a soil fertilizer compound. This residual compound, having a particularly high oxygen demand, is a potential polluting chemical compound for lakes and soils (Gloria and Orlando, 1983; Vasconcelos and Oliveira, 1985). In addition, sugar-cane waste waters coming from the washing of barometric columns (equipment) are also industrial effluents dumped into the *Jequia* ecosystem (Barbosa 1990).

Moreover, all the urban wastes from the *Jequia da Praia* town located in the right part of the lagoon outlet have also been dumped into the tidal channel.

In the early phases of this study, the two main punctual sources of pollution were assessed in qualitative terms during two field surveys in November 1989 and March 1990. A pollutant plume containing an oil like substance floating on the water surface in the western portion of that lagoon and sediment plumes were recognized all over this latter. Pollutant plumes were observed along both margins of the tidal channel and are believed to come mainly from urban sewage dumped by the *Jequia da Praia* and *França* towns.

Field works were conducted in order to identify the regional impacts on land-use occurring within the natural environment of the *Jequia* estuary. The information was gathered from qualitative field descriptions and from a survey realized with the fishing association of the *Jequia da Praia* town. Plankton, nekthos and benthos species and some physical and chemical water parameters such as Secchi depth, surface water temperature, water turbidity and the gradient of salinity were determined by Barros *et al.,* (1992). Low

and high tide physical parameters were also measured (Figure 1.5). The results presented by Barros *et al.* (1992) indicate that the water column of the *Jequia* lagoon presents a homogeneous distribution of the parameters measured, as well as the water column of the tidal channel.

FIGURES AND TABLES FOR CHAPTER 1

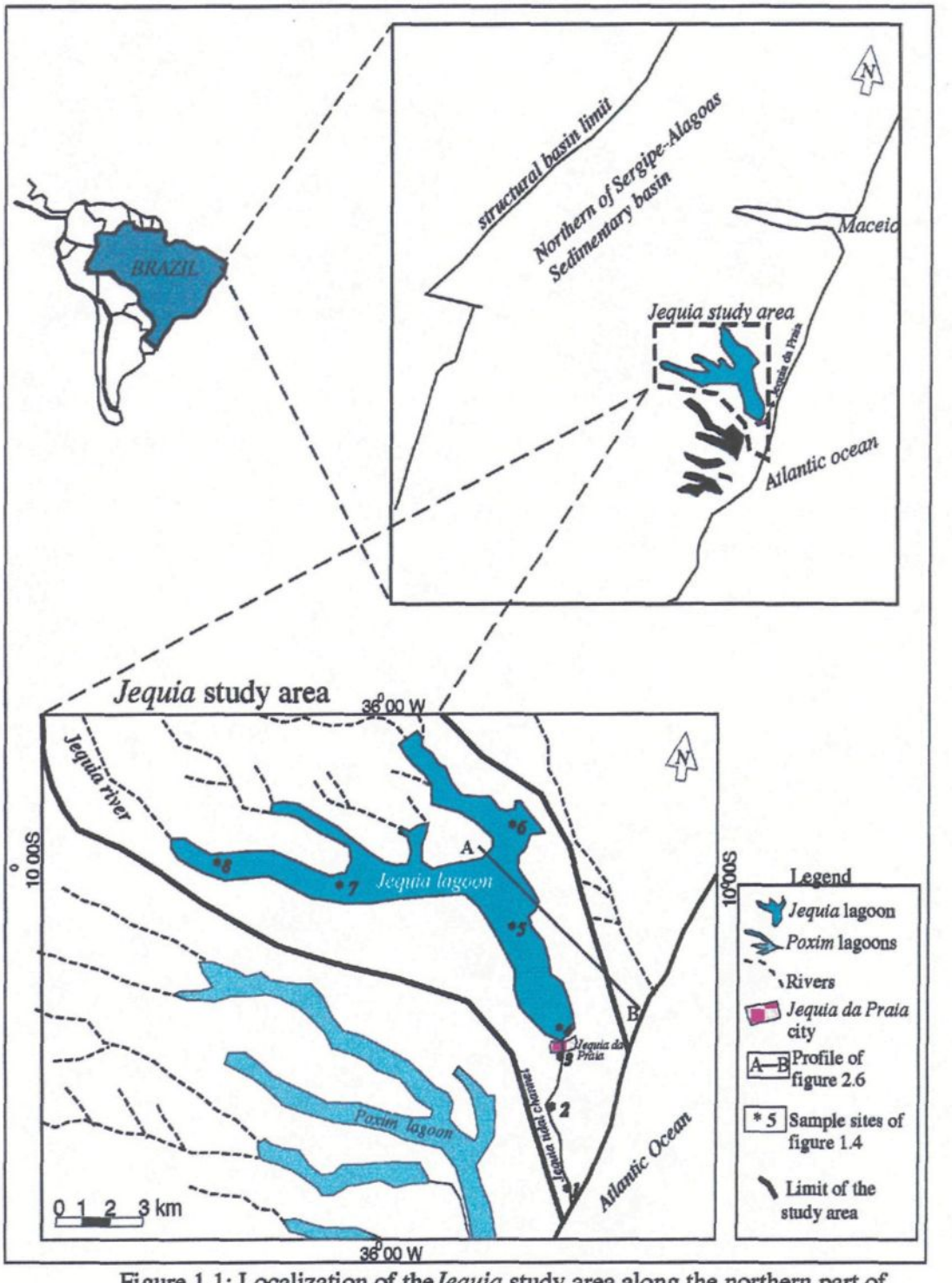

Figure 1.1: Localization of the*Jequia* study area along the northern part of *Sergipe-Alagoas* sedimentary basin in the northeast of Brazil

(a)

(b)

Figure 1.2 : Land use patterns along the Jequia estuarine-lagoon systems. Oblique serial view from mid (a) and outlet portion (b) of the Jequia lagoon recorded on November 1990.

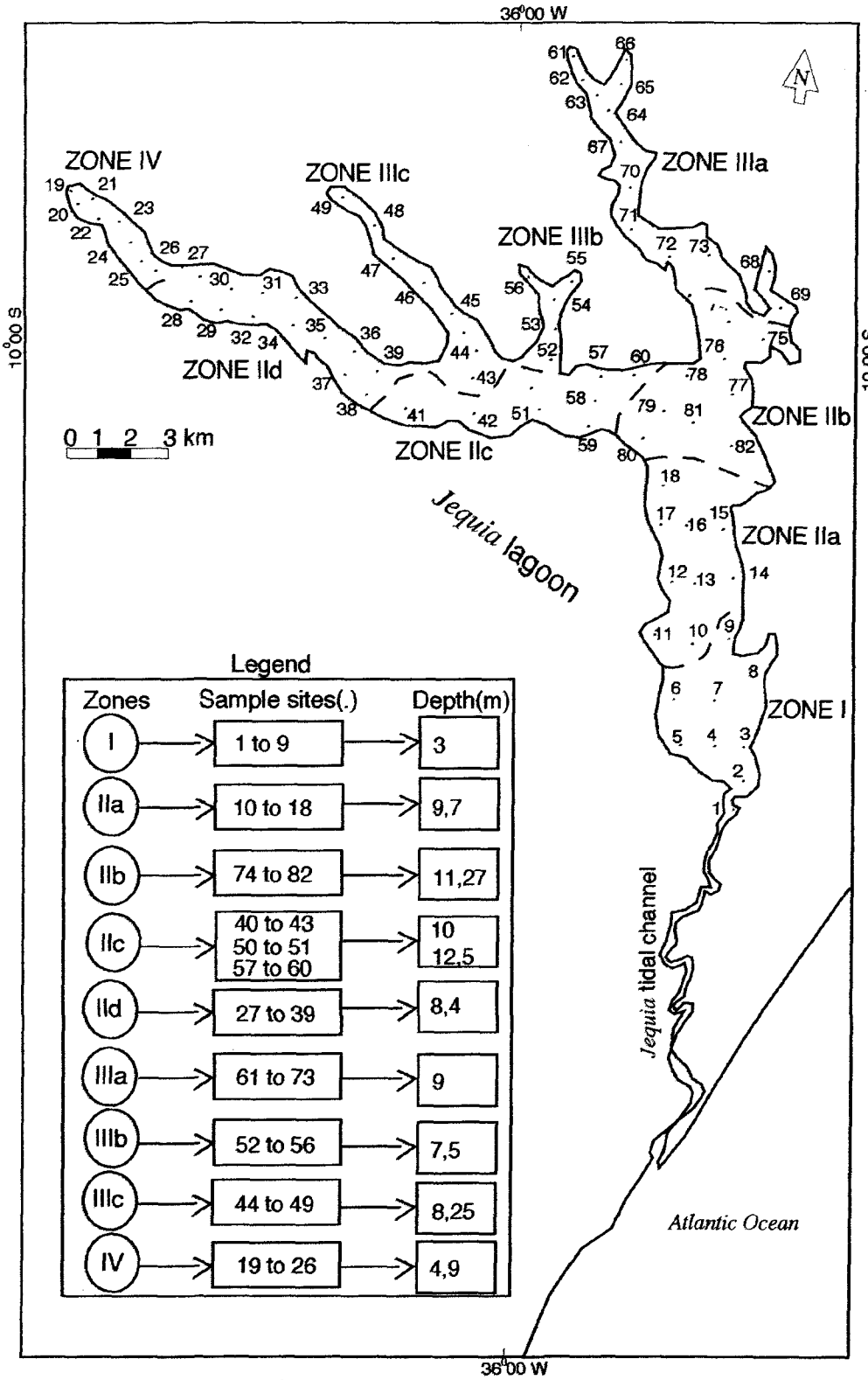

Figure 1.3 . Map of the sample sites of the bottom sediments of *Jequia* lagoon, *Alagoas*, Brazil. Sites within each zone were grouped based on the bathymetric data.

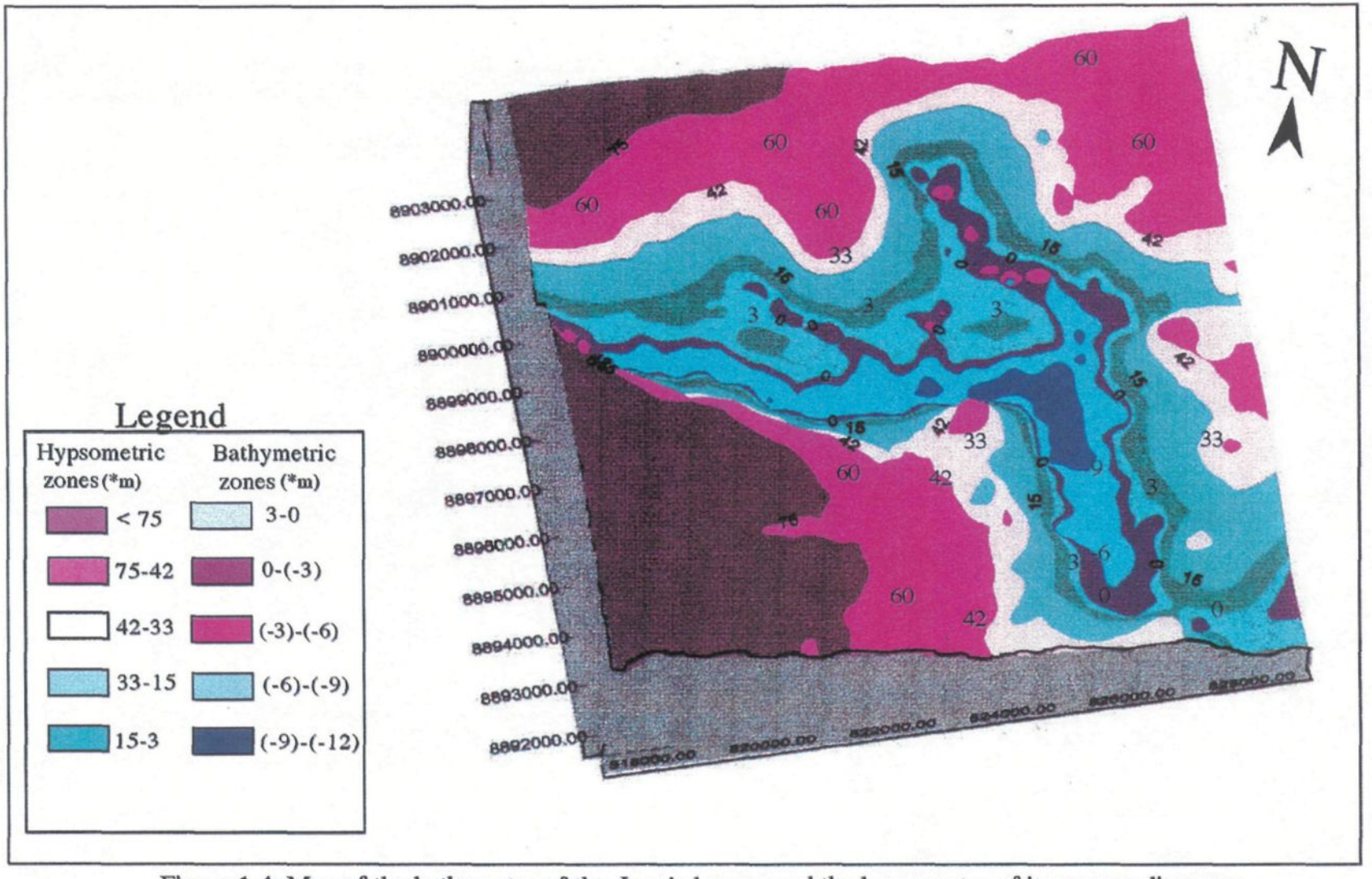

Figure 1.4: Map of the bathymetry of the *Jequia* lagoon and the hypsometry of its surrounding area.

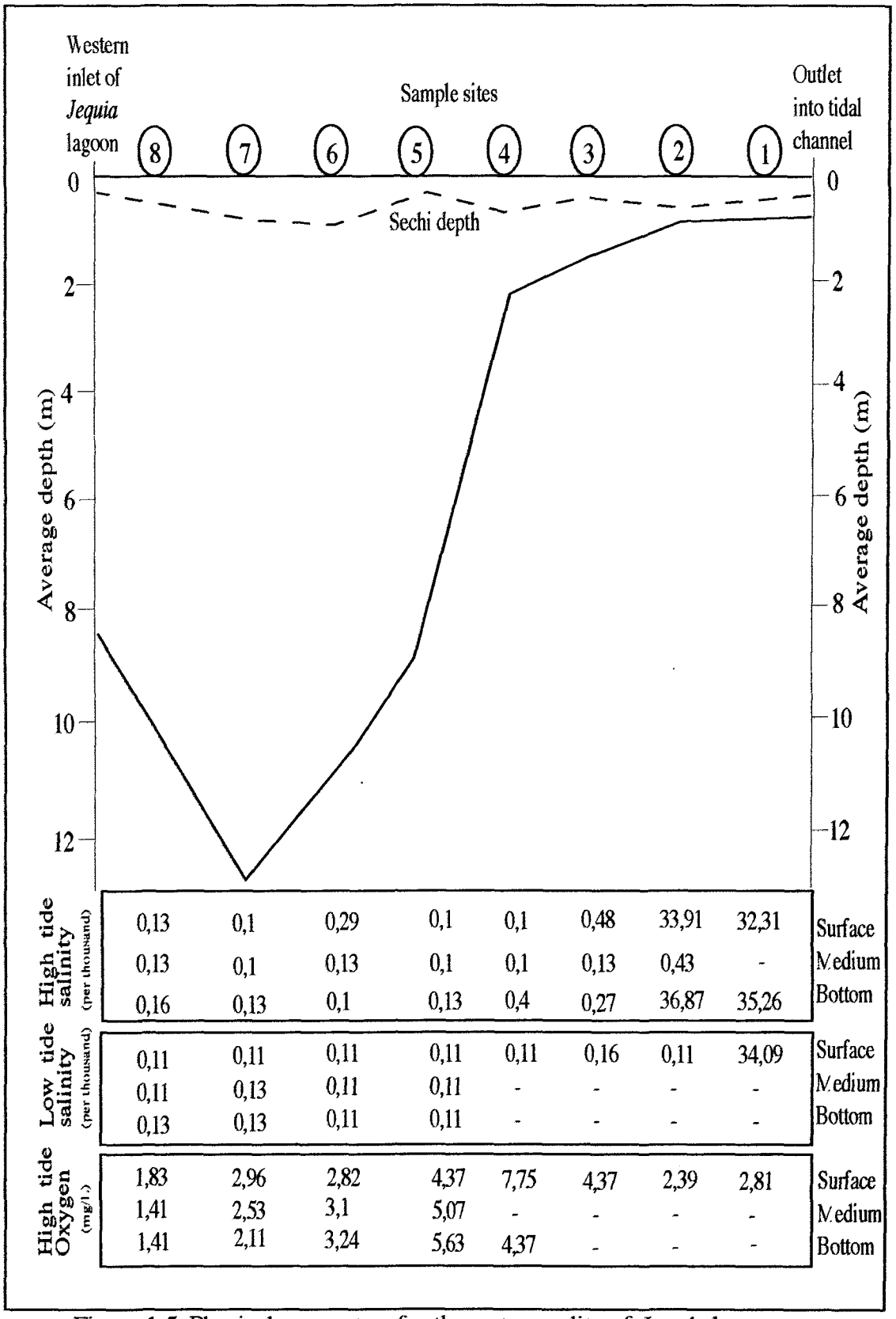

Figure 1.5. Physical parameters for the water quality of *Jequia* lagoon. Modified from Barros *et al.*, 1990. Sample sites are shown on figure 1.2

Sites of zone I	Conductivity(mohs/cm)	Depth (m)
1	0.2145	0.8
2	0.1943	1.2
3	.	2
4	.	3
5	.	2.5
6	.	0.8
7	.	6.5
8	.	4.5
9	.	3.5
10	.	10
11	.	9
12	.	4
13	.	12
14	.	10
15	.	11
16	.	13
17	.	9
18	.	10

Sites of zone IIIb	Conductivity(mohs/cm)	Depth (m)
40	.	6.5
41	.	10
42	.	12
43	.	12
50	0.1846	13
51	.	12
52	0.3054	12
53	.	6
54	.	7
55	.	5.5
56	0.2086	7

Sites of zone IIb	Conductivity(mohs/cm)	Depth (m)
74	0.2106	12
75	.	10.5
76	.	9
77	.	12
78	.	10
79	.	13
80	.	12
81	.	12
82	.	11

Sites of zone IIIc	Conductivity(mohs/cm)	Depth (m)
28	0.1482	9
29	.	9
30	0.1488	8.5
31	.	9
32	.	9
33	0.1735	8
34	.	8.5
35	0.1768	8
36	.	8
37	.	9
38	0.2034	12
39	.	6
44	.	8.5
45	.	8
46	.	8
47	.	8
48	.	8
49	.	9

Sites of zone IIIa	Conductivity(mohs/cm)	Depth (m)
61	.	8
62	.	8
63	.	8
64	.	8
65	.	8
66	.	5.5
67	.	10
68	.	5
69	.	10.5
70	0.1924	5.5
71	0.1982	5
72	.	10
73	0.2106	9

Sites of zone IV	Conductivity(mohs/cm)	Depth (m)
19	.	4
20	0.2081	4.5
21	.	4
22	0.1852	5
23	.	6
24	0.1755	6
25	.	4.5
26	0.1748	6
27	.	8

Table 1.1: Bathymetric raw data and conductivity data determined in situ along the zones of the *Jequia* lagoon, *Alagoas* , Brazil

CHAPTER 2

DESCRIPTION OF THE REGIONAL PHYSICAL ASPECTS

2.1 General geography

The *Jequia* estuarine-lagunar system pertaining to the watershed of *Jequia* is located on the eastern part of the homogeneous micro-region of the *Sao Miguel dos Campos* Mesa along the *Alagoas* coast (Figure 1.1). It is limited by the geographical coordinates of 9° 30' 00" S to 10° 05' 00" S and 36° 00' 00" W to 36° 30' 00" W. The *Jequia* lagoon and tidal channel are the major notable environments of the study area. The *Jequia* lagoon with a surface area of about 16 km^2 and a branched out form suggesting flooding events, is the third in length and the deepest (16 m) lagoon along the coast *alagoana*. It corresponds to the old mouth of the *Jequia* River closed by Quaternary terraces that resulted from the last glacial period. The *Barra D'agua, Manibu, Sapucais, Barra Seca* and *Taquara* being its tributaries. The lagoon is connected to the Atlantic Ocean via a tidal channel that has a length of about 8 km and a width ranging from 50 to 200 m.

Drainage of the *Jequia* River begins in *Tanque D'arca Serra* in the southern *Borborema* Planalt escarpment. It runs to the eastern portion crossing the Tertiary *Barreiras* Group or Formation and Quaternary deposits.

Controlled by the climatic oscillations operating during the Tertiary and Quaternary period, the phytogeographic aspects along the *Jequia* watershed have already been subjected to severe environmental changes. These changes were marked by replacement of the original tropical moist forest by adapted secondary phenotypes. The original tropical forest that dominates along the *Barreiras* Formation is classified as the *ombrophilous* forest. Before the sixties this forest has presented growth leading to heights of 30 to 40 m and stems with diameter larger than 1 m. The environmental changes produced by a severe clearing, an intense forest fire (Assis, 2000) and by climatic oscillations have reduced the ombrophylous forest density, the width of the leaves and the trees to a height less than 15 m. Their stem diameter was reduced to a few centimeters (Assis, 1999).

The Quaternary paleoclimate variations lead to the replacement of the original *ombrophylous* forest ecotypes (phanerophytes) to new species presenting no protection of their foliate gems. The new or secondary phenotypes are seasonably dependent and are classified in phytoecological regions (Assis, 1999) as semi-deciduous and deciduous forests. They are dependent on the periods of dry season: a first period of 90 to 120 days of biological dryness and a second one corresponding to 120 to 150 days. The semi-deciduous forests during the dry period lose 20 to 50% of their leaves and the deciduous forests might lose up to 50% of their leaves (Assis, 2000). Assis (1998) has estimated that for an approximate area of 14 695 km^2 of forests (ombrophylous and *estacional*), 13 901 km^2 corresponds to the clearing processes. The remaining forest corresponds approximately to 794 km^2, that is, less than 3% along the *alagoas* coast. We have estimated, using a planimeter, that within the *Jequia* study area (60 km^2), the remains of tropical forest are less than 2% (less than 5 km^2). Within this study the ombrophylous forests were not differentiated from *estacional* forests.

Ab'Saber (1992) emphasizes the intense clearing of dense forest along the sandy resting areas during the fifties and its replacement by homogeneous forest of coconuts (*Cocus Nucifera*). Along the *Jequia* study area the coconut crops predominate near the tidal channel margins.

These land-cover changes are expressive and noticeable along the flood plains, the dissected valley slopes, the mesa's plateau, and the marine and fluvial terraces of the *Jequia* study area.

Red-yellow podzolic soils with clayey fragipan associated with red-yellow latosol podzolic soils predominate along the *Jequia* estuary (Wake *et al.*, 1983). Mangrove soil types and hydromorphic soils predominate along the *Jequia* channel. Dystrophic gley humic soils predominate along the western portion of the *Jequia* lagoon. Koffler *et al* (1985) have described that 55% of crops are cultivated on red-yellow podzolic soils, 35% on red-yellow latosol soils and 10% on alluvial and hydromorphic soils.

A map of the soil and vegetation types based on previous regional mapping realized in 1984 (Projeto RADAMBRASIL) for the *Jequia* watershed is summarized in figure 2.1.

2.2. Geomorphological aspects

The geomorphological evolution of the *Jequia* estuary is closely related to fluctuations of sea levels during the Pleistocene (Figure 2.2). Sea level fluctuations have controlled the evolution of the Quaternary plains along Brazilian east coast (Dominguez *et al.,* 1981; Bittencourt *et al* .,1982 1983; Barbosa, 1986; Vilas Boas *et al.,* 1985).

Around 17 000 years B.P. the sea level was 110 m below the present level, therefore, close to the continental shelf limit. Within the last Holocene transgression, the sea level had risen progressively until 5 000 – 5 200 years BP when it has reached 5 m above the present sea level (Dominguez *et al.,* 1981; Martin *et al.*, 1980 a).

Two distinctive geomorphological units (Dantas *et al.,* 1986) were mapped along the *Jequia* estuary, the plains and the coast mesas denominated as *tabuleiros* (Figure 2.3).

2.2.1. Plains

The Quaternary deposits attain thickness of 3 to 4 m. They consist of well-sorted sands along the littoral (5,5 km), coarse and poorly sorted sands along the fluvial region and mud along the mangrove areas. This region was subjected to transgressions that left two levels of terraces along the coast. A first level of 8 to 10 m dates back to 120,000 BP, and a second of 3 to 5 m, dates back to 5 100 BP (Barbosa, 1986).

Barbosa (1986) refers to a hooked spit (30 m high) of sandy bar (sandstones, unconsolidated sands, and coarse sands rich in shells) tending southwestward and displacing the mouth of the *Jequia* River to the South. These sediments occur as stratified

layers with cross, tabular and channeled bedding (Barbosa, 1986). The tributaries of the *Jequia* River are inserted into a wider fluvial plain.

2.2.2. Mesas

Mesas are composed of colored clays, coarse sandstones and conglomerate with varying thickness and occur along an NE-SW zone of the coast. Cliffs, ravines and *boçorocas* (gullies) are frequent along this compartment.

Interfluvial plains were cut by natural abrupt channels margin within the sediments of the *Barreiras* Formation, while the geomorphic pattern of dissection was developed through other sediments and basement rocks. The wider mesas developed declivity of 0% to 3% and wide and flat valleys with steep banks. They occur along the left bank of the middle and downstream of the *Jequia* River.

This geomorphological unit is also occupied by homogeneous dissected subunits that present two classes of declivity and a deepening of their drainage. One of the subunit occurs along the left side of the *Jequia* lagoon and presents a deepening of 21 to 42 m with an average slope dip of 8%, and another subunit shows deepening of 45 to 65 m and an average slope dip of 18%.

2.3. Geological context

The *Jequia* estuary belongs to the northern part of the *Sergipe-Alagoas* Sedimentary Basin that is located (Figure 1.1) on the northeastern Brazilian Atlantic Margin. The entire *Sergipe-Alagoas* basin is approximately 330 km long and 80 km wide, occupying an area of 26,000 km^2 onshore, and offshore out to a water depth of 1 000 m (Guimaraes, 1988).

The sedimentary filling of this basin reaches a thickness of up to 10 000 m and is associated with the extensive rifting process that controlled the evolution of the Atlantic Divergent Margins during Early Cretaceous (Castro, 1989). Syn and post-rift sedimentation represent the dominant deposits (Figure 2.4).

The stratigraphy of the *Sergipe-Alagoas* sedimentary basin comprises one of the most complex sedimentation processes, mapped along the Brazilian eastern-coast (Castro 1989). Historically, it has been studied for petroleum exploration (Lana, 1990). A scheme modified from the general stratigraphy proposed by Castro 1989 for the *Sergipe-Alagoas* sedimentary basin (Figure 2.4) summarizes the geological units mapped along *Jequia* estuary.

The main lithological units (Figure 2.5) occurring within the study area and its surrounding are the *Coruripe* Subgroup comprising Mesozoic sedimentation, the *Barreiras* Formation representing the clastic Cenozoic sedimentation and the Quaternary deposits (Gomes, 1980).

The *Coruripe* Subgroup (Schaller, 1969) represents the rift valley stage of the *Sergipe-Alagoas* Basin and occurs along the *Jequia* valley. The *Coruripe* Subgroup is in conformable to unconformable contact with the pre-rift rocks (Castro 1989).

Stratigraphically, the *Coruripe* Subgroup comprises, from top to bottom the *Coqueiro Seco, Penedo,* and *Barra de Itiuba* Formations. Those Formations contain clastic sediments with local thickness of more than 5 000 m.

The *Coqueiro Seco* Formation comprises immature and heterogeneous sandstones, horizons of foliated conglomerates and silt, and rare carbonate rocks. The *Penedo* Formation (800 m thick) consists of gray, yellow and poorly sorted classified sandstones with intercalations of shale and micaceous silts. It also comprises rare sequences of clay and impure calcareous rocks showing cross and convoluted structures. The *Barra de*

Itiuba Formation, with a thickness of 200 m, consists of calcareous shales intercalated by fine and poorly sorted sandstones, microcrystalline calcareous and ostracoid conquines, and remains of fishes.

The *Barreiras* Formation represents the lithological unit that covers most of the area (95%) of the *Jequia* watershed (Figure 2.4). The Barreiras term has been used indistinctly with reference to the unconsolidated or weakly consolidated continental sediments. It comprises layers and lens of clastic sediments ranging from gravel, arkosic sands to claystones that occur as a narrow and long band along the Atlantic coast. The presence of erosional unconformities and great lithological variations within the Barreiras unit causes some difficulties to its stratigraphic designation. It is not a simple sedimentary unit, but contains more than one formation. Therefore a classification of the *Barreiras* Formation based only on the lithostratigraphy, has been proposed. Correlation between erosional and aggradation surfaces have been used within this classification (Bigarella, 1975). The *Barreiras* sedimentation is the result of a high energy transport process carrying significant flow of sand and mud, filling deep fault basins (grabens) along the continental margin during the Tertiary. Pre-Cambrian crystalline basement rocks occur along the upper stream of the *Jequia* watershed.

The *Barreiras* Formation is composed of poorly consolidated conglomerate sandstones and occurs as extensive tabular beds along the entire Brazilian coast with average thickness varying from 60 to 300 m. The tabular nature of the *Barreiras* deposits creates a smooth topographic relief that drops off sharply at the coast line and forms a series of spectacular cliffs extending for tens and sometimes hundreds of kilometers. The *Barreiras* sediments were deposited unconformably above all the older strata in the *Sergipe-Alagoas* basin, and covers about 95% of the basin onshore, therefore limiting severely geological field work (Castro, 1989). The origin of the *Barreiras* sedimentation is related to the formation of lateritic soils during climatic changes. Periods of tectonic

stability alternated by periods of instability where erosion was followed by formation of lateritic soils (Dantas *et al.*, 1986).

The Quaternary sedimentation (Figure 2.6) occurs along the river valleys and mainly along the littoral. It includes sediments from fluvial, eolian, fluvial-marine and fluvial-lacustrine origin. They are sandy-clay, shells, organic matter, wood, and marine deposits. The sedimentation includes the coarse and well-sorted sands with remains of carapaces and concentration of heavy mineral, calcareous ropes, sandy and clay-silty rocks containing organic matter (mangrove areas) with algae shells.

The Pleistocene marine terraces comprise well-sorted sandy distributed along the fossil cliffs of the *Barreiras* Formation. They stand at altitudes of 8 to 10 m above the present sea level.

The narrow strips of Holocene marine terraces contain sandy sediments and stand at altitudes around 4 m above the present sea level.

2.4. Climatological context

The climatic characteristics of the region were established from 1927 to 1942 by the climatological norms from the *Coruripe* station located 30 km from the *Jequia da Praia* district (*Superitendencia do Desenvolvimento do Nordeste-SUDENE,* 1965).

The climatic condition estimated for *Jequia* watershed was based on a monthly normal hydric balance transposed from data recorded at the *Coruripe* meteorological Station. The hydric balance (Souza, 1994) was normalized using the Thornthwaite-Mather model (Thornthwaite *et al.*, 1955b). It was considered within the model that the soil of the study area has an average storage potential of 100 mm. The results are illustrated on figure 2.7.

The hydric balance comprises the pluvial precipitation (P), potential evapotranspiration (ETP), water availability (P-ETP), storage (AR), variation of storage (VAR), hydric excess (EXC), superficial runoff (ESC) and real availability of water (RDA/ETP).

The RDA/ETP rate indicates the degree of monthly humidity in this region. Values below 2 and above 1, corresponding to March, April and August were classified as semi-humid period.

The months with values of RDA/ETP higher than 2, were classified as completely humid, and correspond to May, June and July. February, October and November were classified as semi-arid (RDA/ETP of 0,5 to 1) and November, December and January as completely arid (RDA/ETP of 0,5).

The hydric deficiency of the *Jequia* watershed occurs from September to February. It varies from semi-arid to completely arid, with annual values of 240 mm distributed over 181 days. The hydric excess was observed from May to August, with a total annual value of 444 mm distributed over 123 days. Water availability (P-ETP) occurs from March to August. It is considered a humid period with an amount of 540 mm distributed over 182 days.

2.5. Socio-economic considerations

The *Jequia* estuarine-lagunar system marks the boundary between the municipalities of *Sao Miguel dos Campos* and *Coruripe*. The southwestern bank belongs to *Sao Miguel dos Campos* and the northeastern bank belongs to *Coruripe*. The geopolitical limits of the *Jequia* estuary might add some economic and political constraints to decision-making concerning its regional environmental planning. The municipality of *França* is located on the southern portion of that lake.

The *Porto Rico* and *Cansançao do Sininbu plants*, and the *Jequia da Praia* (1 000 inhabitants) district, which extend to both banks are located respectively along the upper *Jequia* estuary and the outlet (Zone I). The land-use development activities along the *Jequia* estuary system are summarized in table 2.1.

The mixed farming (polyculture) of coconut, coffee, rice, corn, manioc, beans, potatoes, and bananas has been mostly replaced by sugar-cane culture. Coconut has been cultivated along the resting areas, near the tidal channel. Fishing is the primary economic activity of the inhabitants of these small towns.

Clay, kaolin, sand and brittle-rock materials are the mineral resources that have been exploited in this region. During the sixties, petroleum was the main mineral exploration. The available water supply system depends on the *Manibu* River and on water well. There is no data available on the treatment of these water resources. There is no public sewage.

Marinho, 1994 reports the environmental legislation that regulates the land-use along the study area. It includes the regulation of preservation and conservation of the mangrove areas, the restriction to implementation of any tourist business and the dumping of effluents from the distilleries and sugar-cane plants into rivers.

Even though, a state governmental administrative bureau regulates the environmental legislation, there is no sustainable monitoring program towards the maintenance of that legislation.

FIGURES AND TABLES FOR CHAPTER 2

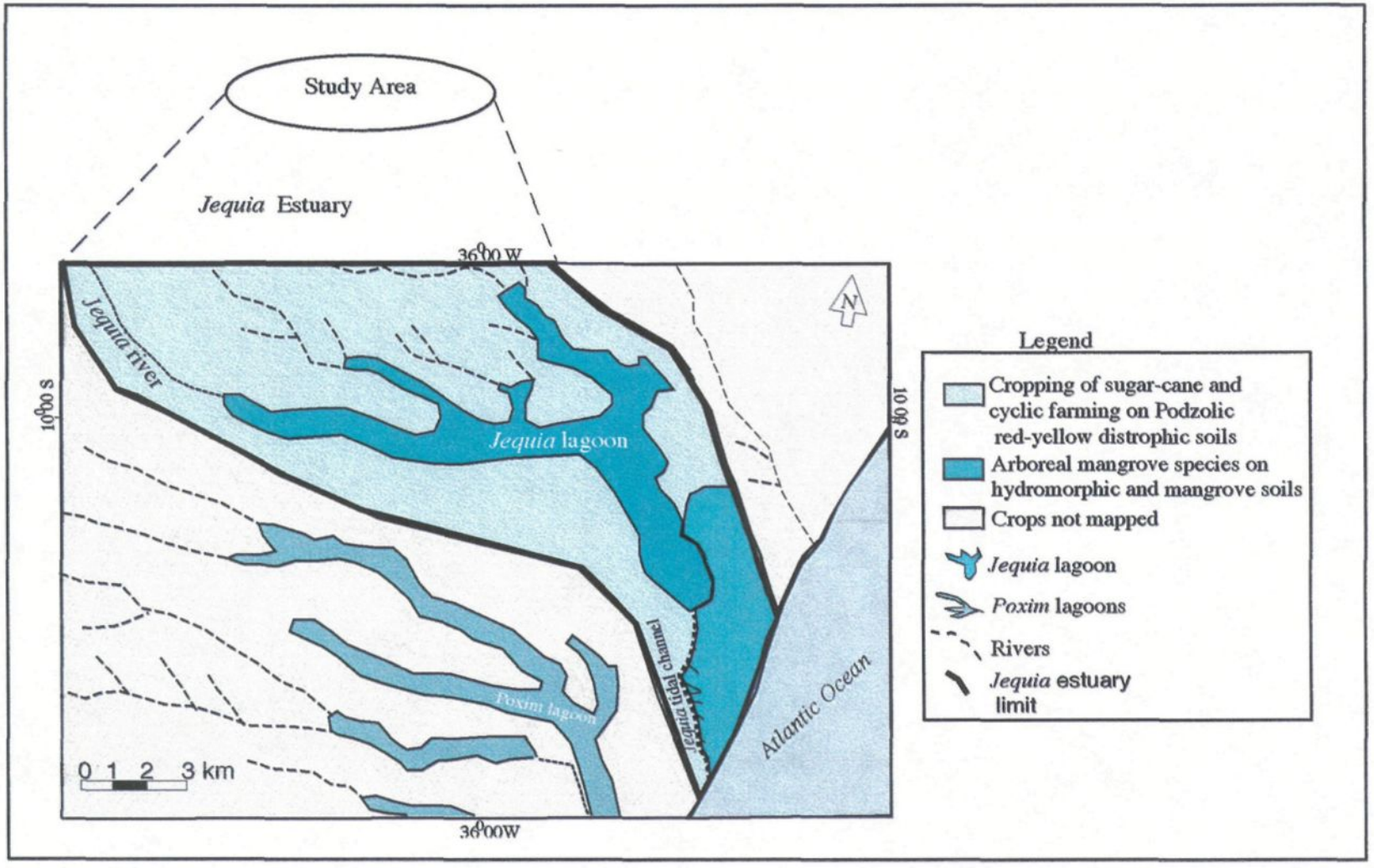

Figure 2.1. Regional vegetation and soil map for *Jequia* estuary. Modified from Dantas *et al.*, 1984.

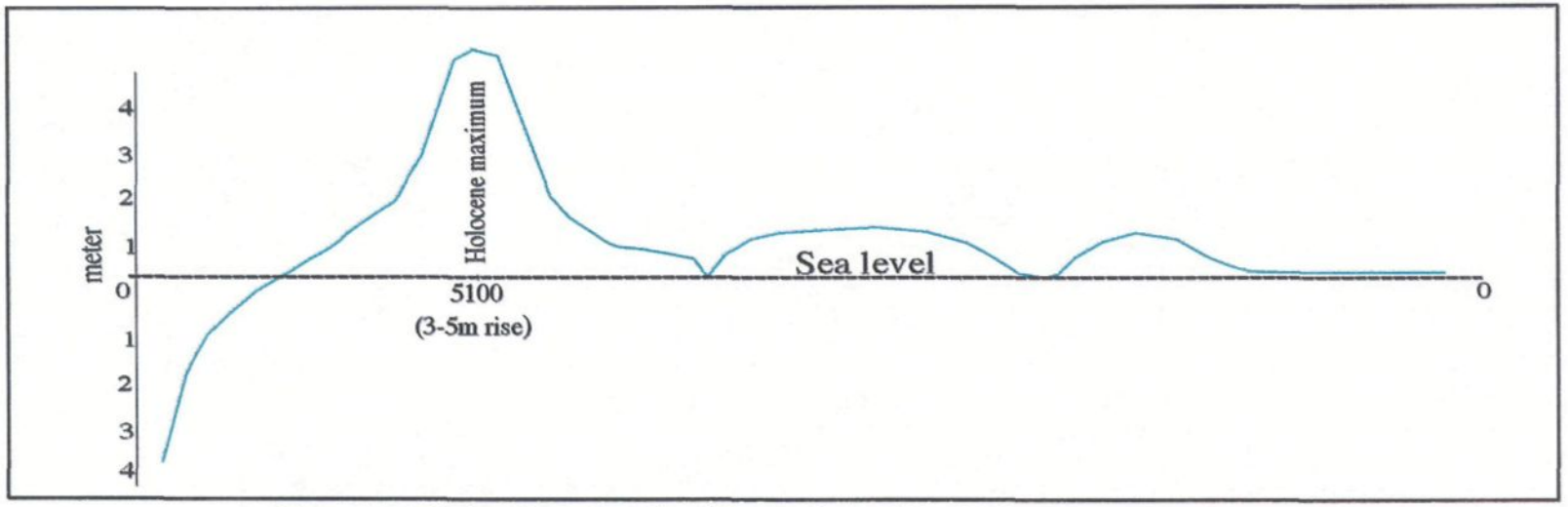

Figure 2.2. Estimation of sea level fluctuations (BP x 7000 y) along the Alagoana coast. Modified from Dominguez *et al.*, 1981.

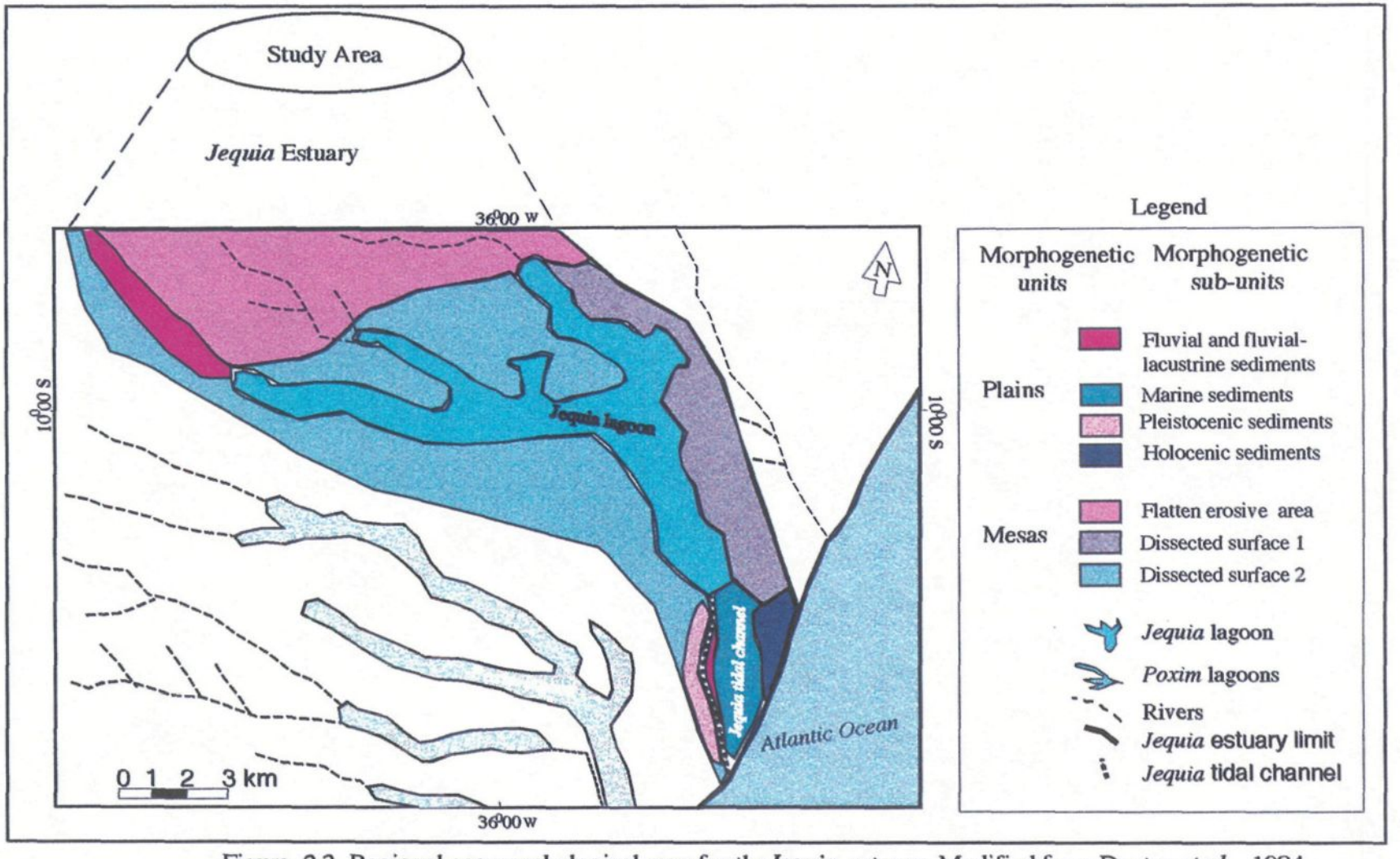

Figure 2.3. Regional geomorphological map for the*Jequia* estuary. Modified from Dantas *et al.*, 1984.

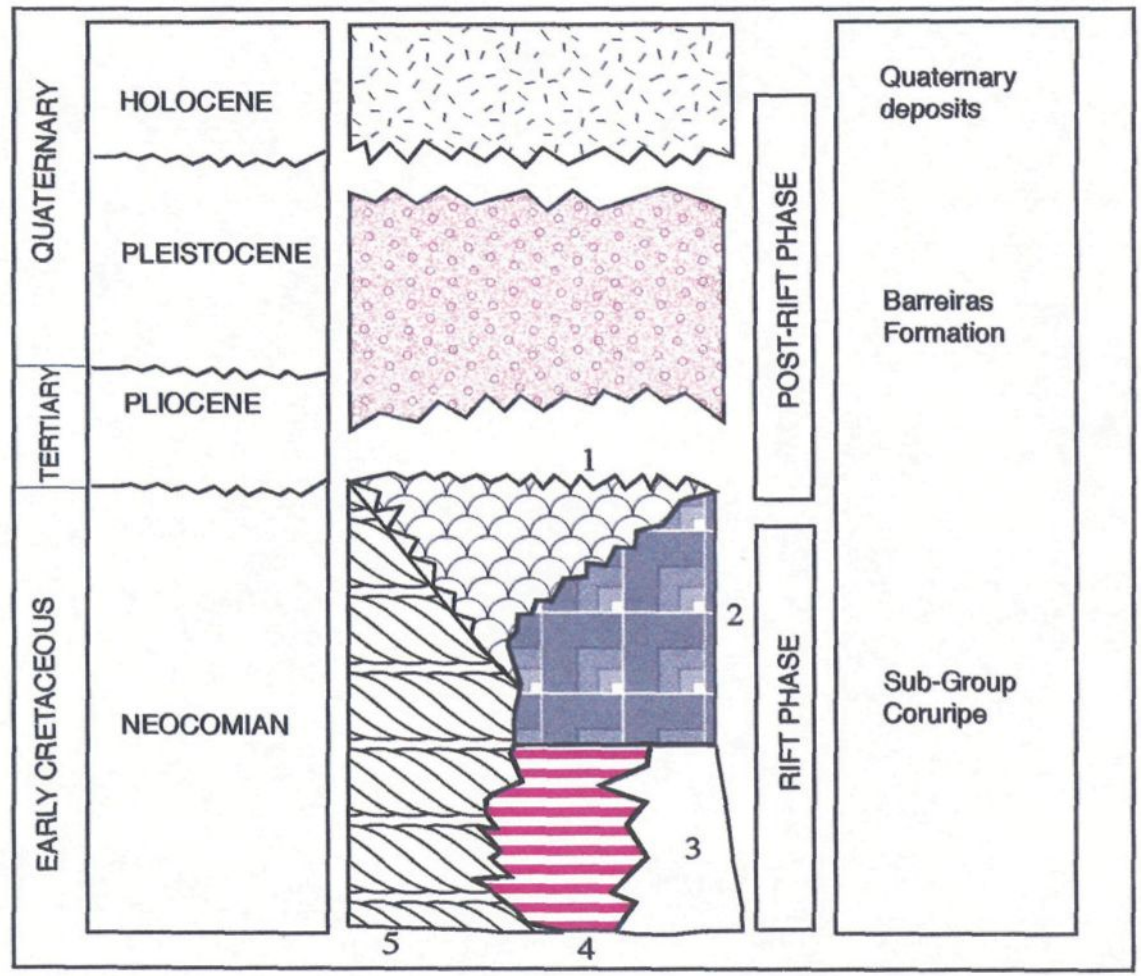

Figure 2.4. Stratigraphic scheme of the *Jequia* estuary. Modified from Castro 1989. Stratigraphic units 1-*Coqueiro Seco* Formation, 2-*Morro do Chaves* Formation, 3-*Barra de Itiuba* Formation, 4-*Penedo* Formation and 5- Muribeca Formation

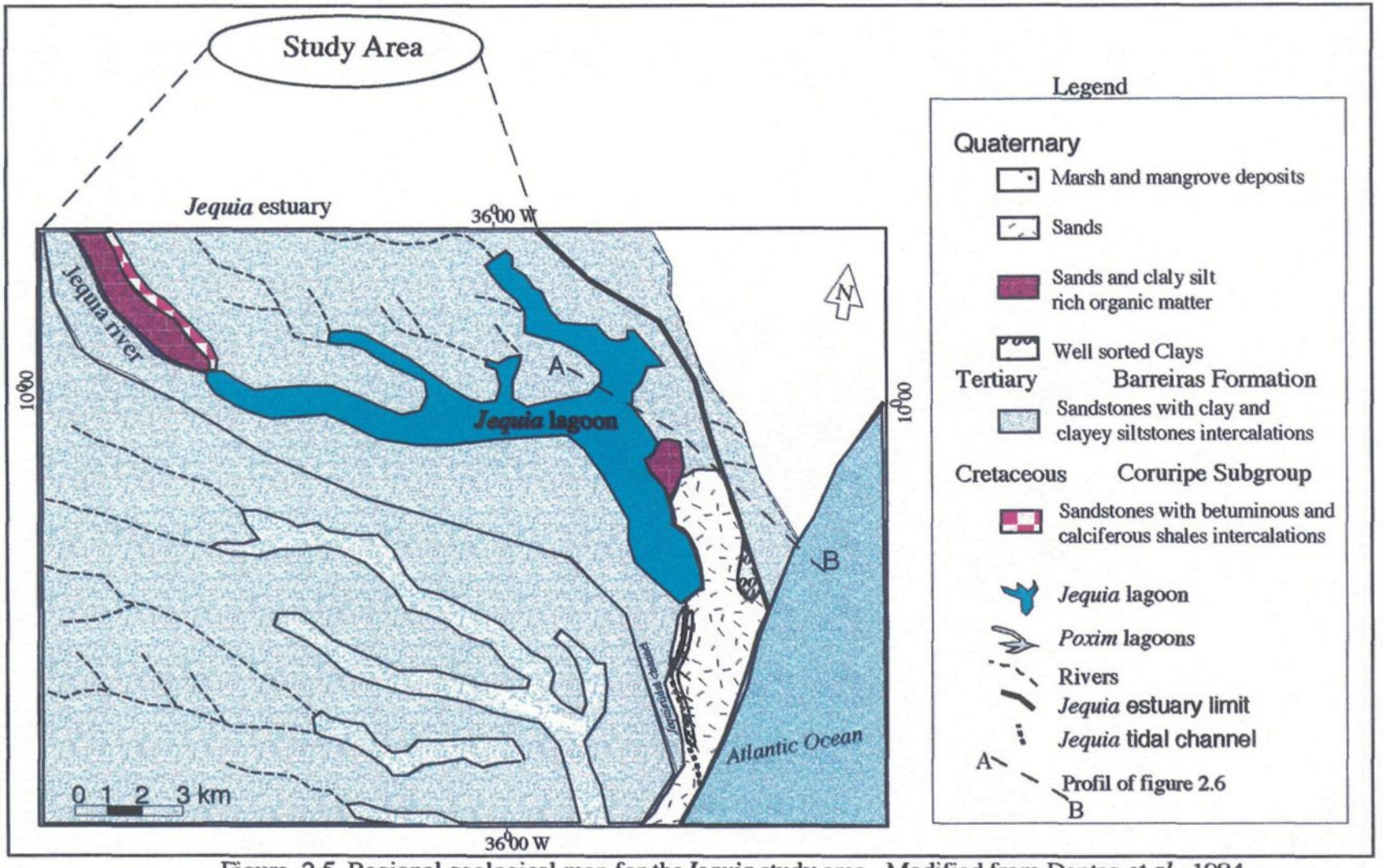

Figure 2.5. Regional geological map for the *Jequia* study area. Modified from Dantas *et al.*, 1984.

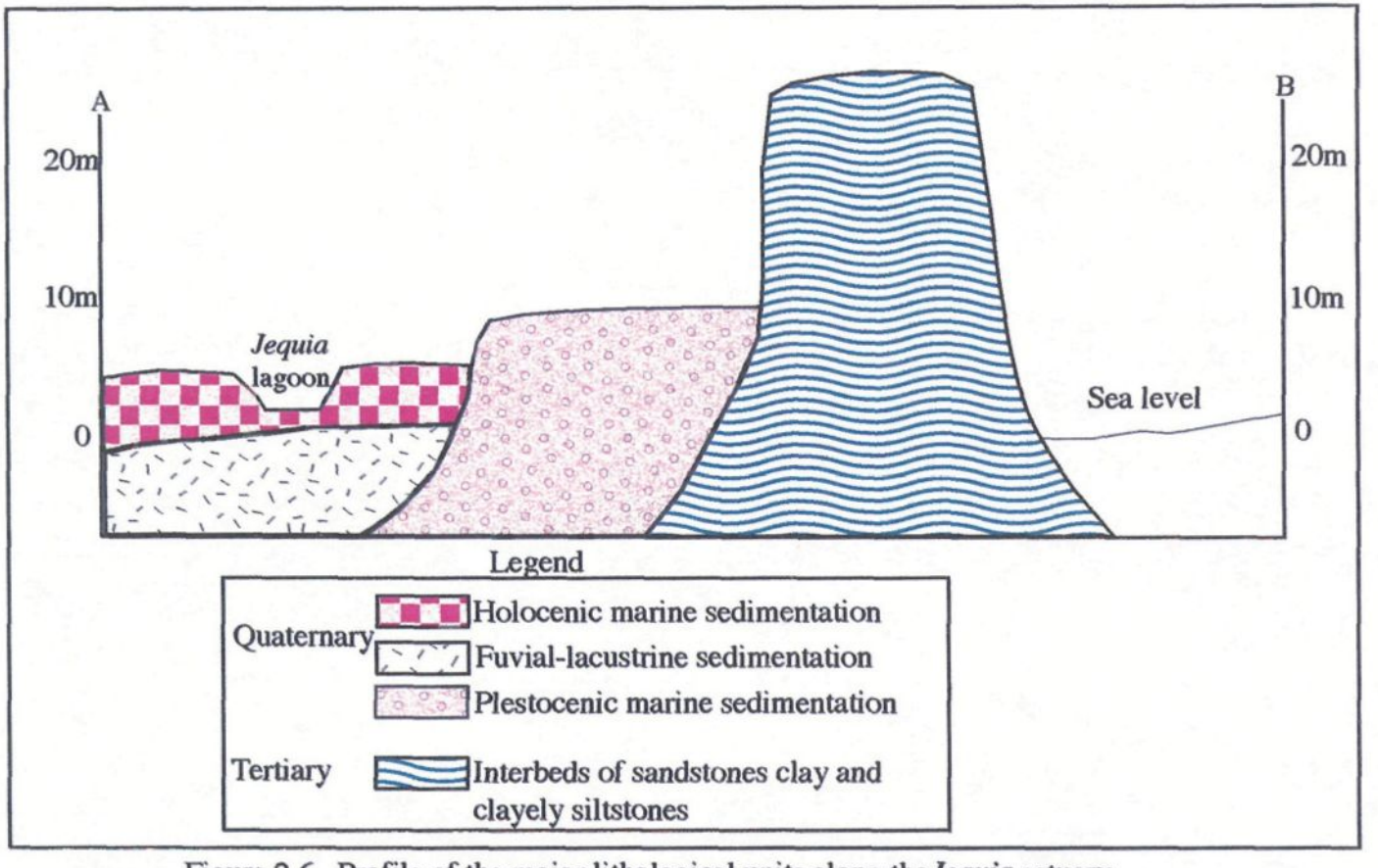

Figure 2.6. Profile of the major lithological units along the*Jequia* estuary. Modified from Barbosa 1986. Section A-B is shown in figure 1.1.

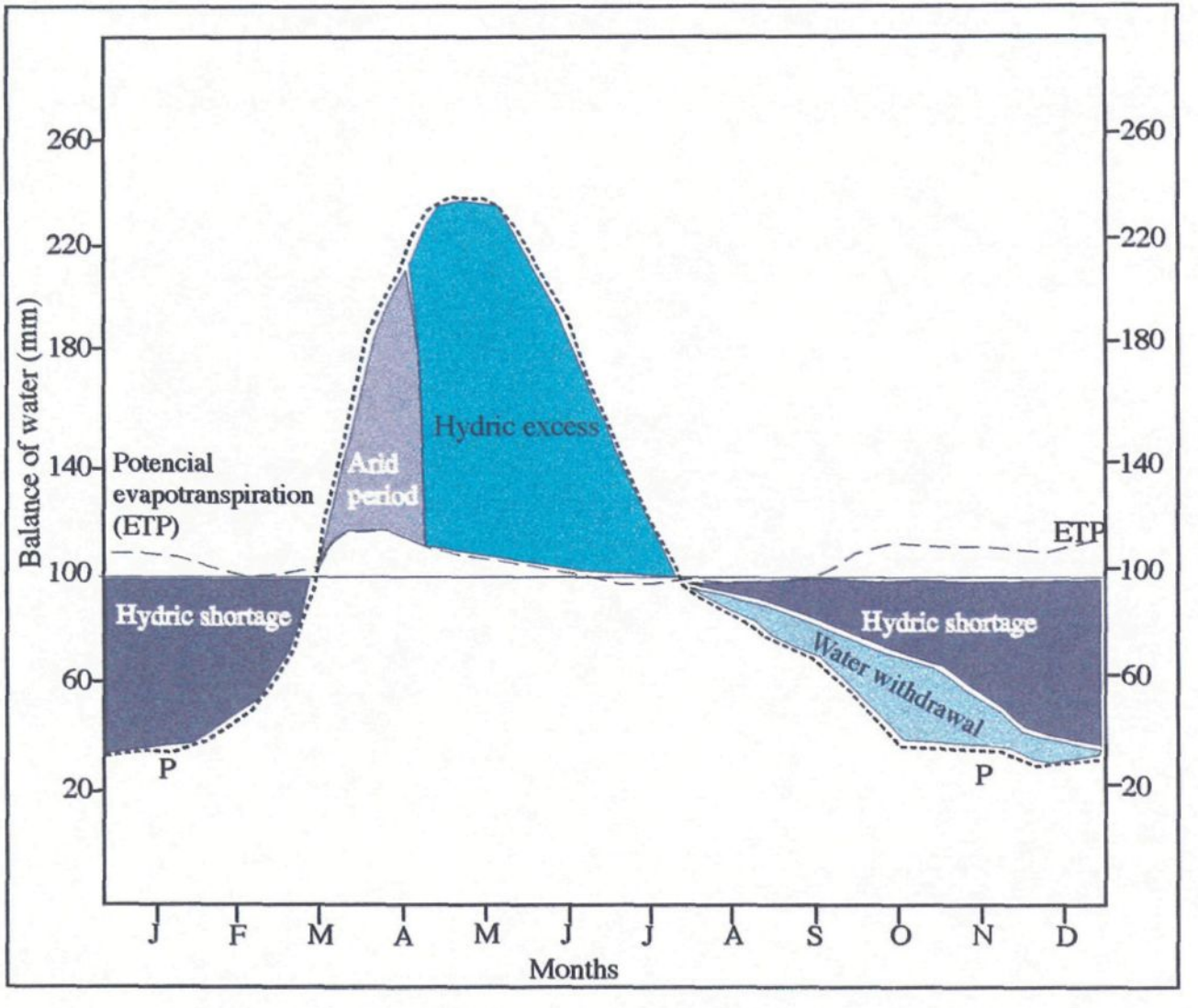

Figure 2.7. Normalized hydric budget for the *Jequia* watershed (Souza, 1993)

LAND-USE PATTERNS RELATED ACTIVITIES	ESTIMATED AREA(%)	ANTHROPOGENIC DESCRIPTION	GEOLOGICAL-GEOMORPHOLOGICAL UNITS
INDUSTRIAL CROPPING	87	SUGAR-CANE PRODUCTS	TERTIARY MESAS
FARMING	2	COFFEE, MANIOC COCONUT	QUATERNARY FLOOD PLAINS MESAS SLOPE
MINERAL EXTRACTION	1.5	KAOLIN, SAND, BRITTLE ROCKS	TERTIARY DISSECTED MESAS
URBAN SITES	5	*JEQUIA DA PRAIA, FRANCA, PORTO RICO CANSANCAO DO SINIMBU*	HOLOCENIC AND PLEISTOCENIC TERRACES
PRESERVED ENVIROMENTAL ZONES	1	MANGROVES FOREST	HOLOCENIC TERRACE
NATURAL ENVIRONMENTS	3.5	DENSE FOREST, MANGROVES	QUATERNARY FLUVIAL PLAINS

Table 2.1. Scheme of the land-use patterns related to the major activities developed along *Jequia* estuary. A total area of 80 km was used to derive the proportion of area for each activities.

CHAPTER 3

CHARACTERIZATION OF THE CLASTIC SEDIMENTS

3.1. Introduction

This chapter attempts to describe the mechanism of transport and deposition along the *Jequia* lagoon environment (Figure 1.1), based on textural parametric analysis using the bottom sediment's sample along that lagoon. Results from sieve, hydrometer and moment analyses are compared and discussed. Therefore the characterization of the mechanisms of transport and deposition of bottom sediments in the *Jequia* lagoon environment is the main goal of this chapter.

The water of the *Jequia* lagoon contains; floating oil-like substance, suspended inorganic matter (sediments), floating organic matter, industrial waste, anthropogenic urban discharges and vinasse an acid chemical compound.

The bottom sediment samples of the *Jequia* lagoon were grouped within nine zones. Each zone was selected and analyzed according to their grain size distribution using the data treated through the sieve, the hydrometer and moment method. Some samples from figure 1.2 were discharged or neglected after a preliminary analysis, since they present incomplete results and a bias distribution between the combined results from the sieve and hydrometer method. Sieve and hydrometer data should be complementary in those samples. Therefore, only few samples from Zones I, II, III and IV are considered in this chapter.

The mineralogy of the sediments was done through X-Ray diffractometric (X-RD) methods. X-ray, as any other wavelength radiation, pertains to the electromagnetic spectra therefore following the same law as any other radiation. The X-ray beam is parallel and strictly monochromatic with wavelength (Reynolds, 1989). The specific optical characteristic of X-ray is that it diffracts or reflects the radiation only at very few angles and it is measured them from the diffracted planes. On the contrary, the visible energy reflects radiation at all angles and it is measured from the normal. Bragg's law states the principles that define the diffraction of X-rays. Moreover, the diffraction is the result of

the relationship between the radiation (l), the incident angle (q) and the space between the atom's planes (Moore *et al.*, 1989) of a given mineral.

The sediment samples (2 g) with size less than 2 mm (passed through the 200 mesh) used in the diffraction analysis were previously centrifuged (1 750 rpm) to enable the separation of clay from silt. Several samples selected from Zones I, IIb, IIIa and IV were centrifuged during 10 minutes to separate the clay minerals from the silt. The separation was possible only for few samples. These samples were used to identify the minerals by X-ray diffraction. The difficulty after centrifugation was due to the interlayering of clay and silt recognized within the samples.

A general petrography of the minerals was realized through a binocular optical device (*loupe*). The recognized minerals and their estimation are grouped on table 3.1a.

The most significant petrography characteristic we have recognized within the minerals was the form and size of the quartz grains. The grains of quartz within Zones I and IV show smaller size and roundness compared to the others. The grains of quartz within the others' zones are much larger and present angular form.

The concentration of total organic carbon was done through the oxidative combustion (LECO) method and by applying cold hydrogen peroxide (H_2O_2) with concentration of 30% to the selected sediment samples (2 g). The H_2O_2 removes the inorganic carbon content from the sediment samples. The remaining carbon was deduced as of organic origin. The 2 g sample of sediment was heated during 1 hour in a high temperature furnace (550°C) before applying the hydrogen peroxide. The carbon lost within the samples after heating is assumed to be of organic origin. Therefore the total carbon inorganic and organic was estimated from the weight loss on heating (Table 3.1b). The carbon estimation was developed in the Petrochemical Laboratory of the Department of Applied Sciences at the University of Quebec in Chicoutimi on June of 1996.

3.2. Previous sedimentological work along the *Jequia* estuary

The *Jequia* estuary has been the site of hydrocarbon exploration studies since late 1950s. The discovery of commercial oil and gas accumulation (1957) in the southern portion of this lagoon led to an increased number of studies along the *Sergipe-Alagoas* basin, where the *Jequia* estuary is located. These studies are concerned mainly with the stratigraphy and the sedimentation related to oil exploration along the *Jequia* estuary. Some general structural aspects have been also discussed. They rely on the analysis and interpretation of seismic and well data, on gravimetric data and on regional mapping.

Saldanha *et al.* (1975) have described the Serra dos Martins unit within the Barreiras Formation. It occurs along the northeast part of *Jequia* city and comprises fine and conglomerate sands. The sands show a wide range of colors and along the lower mesas the sands are intercalated with silt and clay. They also defined the transport of the sediments of Serra dos Martins as typically of graded suspension, rolling and bottom suspension.

Lira *et al.* (1992) present the only available data (Figure 1.4) along the *Jequia* lagoon. They have estimated some chemical parameters (salinity and oxygen) and recognized the biological species within the lagoon.

This study relies on grain size and X-ray analyses and attempts to characterize the deposition and transport mechanism prevailing within the environment of the bottom clastic deposits of the *Jequia* lagoon. It also aims to support regional mapping and municipal planning along the *Jequia* study area.

Despite the inaccurate character of grain size analysis, one might achieve useful information related to the mechanism of transport and deposition of sediments and their grain size distribution in a given environment. Another goal of this study is to present correlation between grain size and reflectance data, more precisely the particle size of the sediments and their spectral patterns.

The sediments filling *Jequia* lagoon are mostly derived from the erosion of Tertiary continental conglomerate sandstone sequences (*Barreiras* Group), erosion of Cretaceous syn rift clastic sediments, Quaternary fluvial-delta sediments and marine deposits (Figure 2.6).

3.3. Description of the textural parametric methods

3.3.1. Introduction

A sedimentologic mapping of the bottom sediments of *Jequia* lagoon was carried out in March 1990. Eighty-two samples were collected during this survey.

The sediment samples were grouped in five zones (I, IIa, IIb, IIc, IId, III, and IV) to enable a better discrimination of their plots in cumulative frequency curves (Figure 3.1 to Figure 3.30). The graphic estimation of grain fractions for Zones I to IV are summarized on table 3.3. The cumulative frequency curves were performed using selected raw data grouped on tables 3.4, to 3.11. Within the sampled sediments, only few cumulative curves were possible to be derived from the samples of Zones I (sites 3, 4, 6 and 7) and IV (sites 19, 20, 22 and 23). Within Zone IIIa, only samples sites 62 and 65 have performed cumulative curves. Along Zone IIb that corresponds to the deepest part of the lagoon four cumulative curves were derived. The rest of the cumulative curves were derived from Zones IIa, IIc, IId, III and IIIc.

The bathymetric data (Table 1.1) were used to group and differentiate the zones. Only the data within discernible zones (I, IIb, IIIb and IV) were treated and analyzed in this chapter. Water conductivity (Table 1.1) and bathymetric data of the *Jequia* lagoon were measured in the same sediment sites sampled.

Field notes concerning the environmental impact of land-use along the *Jequia* estuary were taken. Some general information was also acquired from a survey done by the Fishing Association of the *Jequia da Praia* district.

The bottom sediments of the lagoon are the major available source of data used in this study. These sediments were analyzed using sieve and hydrometer data. The grain size data were also treated by the moment method after the studies of Friedman (1962), Kaddah (1974) and Moussa (1977). The main advantage of the moment method is that it enables the construction of frequency distributions and derived textural parameters for clastic sediment, with less extensive samples and very low cost. Advanced methods are usually prohibitive and not as practicable as the moment method.

In this study, a wide revision of the several contributions to textural parametric analysis on clastic sediments was done. The analyses of textural parametric data have been exhaustively reported during the beginning of the twentieth century. In the fifties, sixties and seventies a great contribution to grain size studies came from the works of Griffiths (1953), Folk (1957), Sternberg (1961) Spencer (1963), Passega (1964) Sahu (1964), Weiser *et al.* (1968), Folk (1966), Passega (1969), Lynts (1966), Visher (1969), Solohub *et al.* (1970), Swift *et al.* (1972), Kaddah (1974), Moussa (1977), Sengupta (1979) and McLaren (1979). We have noticed that during the last two decades the researches approaching grain size have been reduced. Several contributions come from the works of Bagnold *et al.* (1980), Kennedy (1984), Sengupta (1984), Sengupta *et al.* (1991) and Mazunder (1994).

Few recent studies present advances and refinements in understanding the sediment properties (their grain size distribution and mineral type) and related spectra's reflectance. We refer to the works of Zbinden (1981), Illenberger (1992), Gibbs and Chakrapani (1994), Oldfield and Yu (1994), Sutherland and Lee (1994), Kothyari (1995), Mazumder (1994) and Kranck *et al.* (1996). We point out the special contribution from Zbinden (1981) along the Normand Breton gulf. She presents a multidisciplinary approach relating

the micro granulometric aspects of some clastic sediments based on the moment method and the spectral properties of coastal water using LANDSAT- MSS data.

The statistical parameters used within this study include the average grain size, the uniformity or sorting measure and the asymmetry or peakness measures. The average grain size measures comprise the computed graphic mean-Md_f (McCammon, 1962a) and the median-Mz_f; the measure of sorting corresponds to the quartile deviation-Qd_f, computed graphic standard deviation-Gs_f and inclusive graphic standard deviation-IGs_g; and the measures of asymmetry comprise the Phi quartile skewness-Qsk_f, the graphic skewness-Gs_f, the inclusive graphic skewness-IGs_f and the computed skewness-Cs_f. The peakness measures include the computed kurtosis-Cku_f and the graphic kurtosis-Gku_f. The Md_f, Cs_f. Cku_f and the Mz_f (50%) were also computed using the results processed by the Statview software. The statistical measures were empirically and manually (calculator) computed based on the concepts of Folk (1957 and 1966) as follows:

$$Md_f = (10\%+25\%+50\%+75\%+90\%)/5 \qquad \text{equation 3.1}$$

$$Mz_f = (f16+ f50+ f84)/3 \qquad \text{equation 3.2}$$

$$Qd_f = (f75+ f25)/2 \qquad \text{equation 3.3}$$

$$Gs_f = (f84- f16)/2 \qquad \text{equation 3.4}$$

$$IGs_f = [(f84- f16)/4] + [(f95- f5)/6.6] \qquad \text{equation 3.5}$$

$$Qsk_f = (f25+ f75-(2\ Md_f/2)) \qquad \text{equation 3.6}$$

$$Gsk_f = (f16+ f84- 2(f50))/(f84- f16) \qquad \text{equation 3.7}$$

$$IGsk_f = [(f16+ f84- 2(f50))]/[2(f84- f16)]+ \\ +[(5+f95- 2(f50))]/[2(f95- f5)] \qquad \text{equation 3.8}$$

$$Gku_f = (f95- f5)/2.44(f75-.f25) \qquad \text{equation 3.9}$$

The results computed with the above textural parameters are grouped in tables 3.11a, b, c and d respectively for Zones I, IIb, IIIa and IV.

The sieve percentiles were computed through graphic determination using simple intercepts from cumulative curves. This procedure is less time-consuming. The hydrometer percentiles of less than 10%, 25%, 50%, 75%, 90% and above 90% were computed using the results processed by the Statview software. These percentiles were used in the empirical computation of the sieve and moment textural or statistical parameters. Since the sediments present a general homogeneous distribution within the cumulative curves, we considered for this study, that the percentiles of 84%=(75%+90%)/2, 16% =(10%+25%)/2, 5% =10% and 95%= 90%. These parameters (f) were computed from selected samples within Zone I (sites 3, 4, 6, 7), Zone IIb (sites 76, 80, 81), Zone IIIa (sites 56, 62, 65) and Zone IV (sites 19, 20, 22, 23, 24).

The above textural parameters have been considered as environmentally sensitive. They might also trace the prevailing mechanisms of transport and deposition of the sediments in a given environment (Folk *et al.*, 1957, Passega, 1964, Visher, 1969, Solohub, 1970, Allen, 1971 and McLaren, 1979).

3.3.2. Description of the sieve method

The granulometric distribution of the bottom sediments presented in this chapter, are defined through the following methods. Part of the data subjected to sieve and hydrometer techniques were not combined and also were developed in different laboratory conditions and at different periods. The samples that showed bias trend derived probably from sieve operational errors, were neglected. Only the composite combined sieve and hydrometer data were considered within this study. Those methods fit the overall objective of this study, that is, to present the correlations between the sedimentation processes (grain size distribution), land-use changes and the spectral reflectance for the study area targets. It was also dependant of the laboratory facilities and the inaccessibility of other techniques.

Sieving has been widely used to characterize and distinguish clastic sediments from different and similar environments. In the case of this study, we attempted to characterize a unique environment through data treated by sieving and sedimentation settling rate (hydrometer) methods.

Conceptually, grain size data have the unit phi (f) expressed as the logarithm in the base two of the particle size (Fritz *et al.*,1988). This mathematical base used in textural analysis can be written as:

$f = -\log 2\ d/d_0$ equation 3.10

in which;

$d_0 = 1mm$,

f: dimensionless

The sieve method can be adjusted for coarse or fine sediments. In this study, it was set for sediments classified according to the *Associação Brasileira de Normas Tecnicas* (ABNT) scale. A comparison between the ABNT grade grain scale and the Udden-Wentworth one is illustrated in table 3.2a.

The procedures used to treat the sieve and hydrometer data were based on the norms of the ABNT that presents similarity to the U. S Bureau of Standards norms.

The sample zones were selected to construct cumulative frequency curves for the sieve and hydrometer data. The data treated through the method of moment correspond to few samples within Zones I, IIb, IIIa and IV.

The plot of cumulative frequency curves shown was selected from the best shaped-fit curves from all cumulative frequency curves performed for the 80 sample sites. Due to errors during the laboratory procedure in several samples, only few cumulative curves

were constructed. The constructed curves are from sites 3, 4, 6 and 7 of Zone I, sites 76, 80, 81 and 82 of Zone IIb, sites 62 and 65 of Zone IIIa, and sites 19, 20, 22, 23 of Zone IV are analyzed within this study. The graphic estimation (%) of the grain fraction is presented in table 3.30 a, b, c and d respectively for Zones I, IIb, IIIa and IV.

3.3.3. Description of the hydrometer method

The hydrometer gravitational sedimentation method has been widely applied to the determination of the content of silt and clay within a given sediment population. The goal of this study is the comparative analysis of the distribution of grain size data using the hydrometer method and sieve method.

The theoretical principle of this method is the settling rate of a particle defined by the Stokes' law. This law stipulates that the rate of deposition of a particle is related to its diameter. This law is written as:

$Sdr = Di \div TxV$ in which (equation 3.11)

Sdr: Sedimentation rate

Di:Diameter of grain (mm)

T:Time-average (from the start of the experiment to the beginning of hydrometer reading)

V:Velocity of deposition (cm/s)

The procedure used in the hydrometer method is described in appendix II. The hydrometer data were computed manually following the concept of Lambe, 1967. It was also used in the Casagrande nomographic method. The Casagrande's method (Lambe, 1967) accepted by the American Society of Testing Materials (ASTM) in 1958 is also

based on Stoke's law as described above. It is an integrate graphic procedure which involves data computation based on the following expressions:

$V = Zr / t$ in which, (equation 3.12)

V: Velocity of deposition (cm/seg),

Z: Hydrometer height (cm)

r: Hydrometer reading (dimensionless)

t: time (seconds)

$T: 1800m / ds - dl$ in which, (equation 3.13)

T: Time-average

m: Liquid viscosity ($gsec/cm^2$)

ds: Particles density (g/cm^3)

dl: Liquid density (g/cm^3)

The percentage of fine particle for each range of grain size was determined using the equation (Lambe, 1967) written as follow:

$N = (G/G-1)\ (V/P)\ (g_{H2O})\ (R_1-R_2) \times 100\%$ (equation 3.14)

in which,

N: Percentage of fine,

G: Specific gravity of solids,

V: Volume of suspension,

P: Weight of dry soil,

g_{H2O}: The unit weight of water calibrated

R_1: Hydrometer reading in suspension

R_2 : Hydrometer reading in distilled water

The terms Z and r of the equation 3.12, corresponding to the hydrometer height and reading, are interdependent variables. The height from which the particles were settling was calibrated graphically for each hydrometer reading. The average time was determined from the beginning of the experiment to the moment of the first hydrometer reading. The hydrometer grain size diameters for the 80 samples were manually computed using equation 3.14. Several samples were discarded since they presented laboratory errors during hydrometer reading.

The hydrometer data were computed through Statview software. Some grain size measures and the percentiles were done graphically. The computed hydrometer percentiles were the 10%, the 25%, the 50%, the 75% and 90%. The hydrometer grain size diameters for the 80 samples were empirically computed using equation 3.14 (Lambe, 1967).

The sieve hydrometer (combined) raw data, comprising the grain size (mm), the raw weight, the cumulative weight percent and the cumulative percentage determined using standard methods mentioned above, are grouped in tables 3.3 to 3.10.

3.3.4. Description of the method of moment

The method consists of a series of computation procedures of selected standard statistical or textural parameters whereby the entire frequency distribution enters into the determination. Other methods use a few selected percentiles. Moussa (1977) proposes a procedure that computes the statistical measures through the moment method. This

concept uses the sieve screen opening and weight frequency for computing the phi mean and phi standard deviation. The procedure comprises adding or subtracting a constant to a sediment group of data. The results change the mean but do not change the standard deviation.

The textural parameters computed from the moment method were calculated for 4 selected sieve samples within Zones I, IIb, IIIa and IV. The results are grouped respectively in table 3.12 for Zones I and IIb and in table 3.13 for Zones IIIa and IV.

There are two overall advantages of using the method of moment to determine textural parameters, relatively to conventional methods. One refers to the data analysis that includes the entire frequency distributions of a given sediment population and the second refers to the simplification of computation procedures, especially when it is carried out manually. Within this study, all the moment data were computed manually using a pocket calculator. Sieve and hydrometer methods included only the percentile-intercept methods and were in part computed manually and through graphic method (Statview percentiles).

According to Moussa's concept, the larger phi values of a size grade are identical to the mesh size of the respective sieve expressed in phi value. This concept enables using the screen opening (mesh size) of the sieves directly in the computation procedure of statistical measures through the moment method. Therefore, we used the weight percentage frequency of raw sieve data. The Moussa's values of screen opening, corresponding to the sieve number used in this study (16 to 200), were used in the computation of the moment textural parameters. The constant added to the data is one-half class interval (1/2if = 0,25)

The textural parameters empirically computed through the method of moment (Moussa, 1977) are: the moments designated mean-MXd, the sample moment phi mean-MXf, the phi moment standard deviation-Msf, the moment skewness-Msk and the moment

kurtosis-Mku. The moment measures were manually computed using respectively the equations 3.15 to 3.23.

$MXd_f = \sum M1 / \sum Wf$ where (equation 3.15)

in which;

MXd_f : Moment designate mean

M1: First class interval

Wf: Weight frequency (%)

Mf: MXd-1/2i f where (equation 3.16)

MXd: Moment designate mean

i_f : Classs interval=0.25

$Ms_f = (Md2)^{1/2}$ (equation 3.17)

in which;

Ms_f : Moment standard deviation

Md2: Second moment variance

$Msk = (Md3)^2/(Md2)^3$ (equation 3.18)

in which;

Msk: Moment skewness

Md2= Second moment variance

Md3 = Third moment variance

$Mku = (Md4)/(Md2)^2$ (equation 3.19)

in which;

Mku: The moment kurtosis

Md4 = Fourth moment variance

Md2= Second moment variance

$Md1 = Md1 - MXd$ (equation 3.20)

in which;

Md1: First moment variance

Mxd: Moment designated mean

$Md2 = M2-(M1)^2$ (equation 3.21)

$Md3 = M3-3(M1M2) + 2(M1)^3$ (equation 3.22)

$Md4 = M4-4(M1M3) + 6((M1)^2(M2))-3(M1)^4$ (equation 3.23)

The empirical textural measures determined through the moment method are grouped in tables 3.13 and 3.14. Within these tables, the first column corresponds to the used sieve number designation. The second column represents the corresponding sieve opening values (sop) suggested by Moussa, 1977. The third column is grouping the sieve data in weight frequency (Wf). The fourth, fifth, sixth and seventh columns correspond to the computation of the class intervals (M1, M2, M3, M4) by multiplying the weight frequency per the sieve opening. The first moment class interval corresponds to the moment designated mean. The data grouped within the tenth row are the moment variances (D1, D2, D3, D4) computed by dividing the total class intervals by the total weight frequency. Also grouped along that row are the moment designated mean (MXd) and the moment sample mean (Mf). The last row includes the deviation (Md1, Md2, Md3, Md4) measures

computed by using equations 3.20, 3.21, 3.22 and 3.23. The moment standard deviation, the moment skewness (Msk) and the moment kurtosis (Mku) are also grouped along the same row.

The similar values within the measures of dispersion (mean and standard deviation) indicate a unimodal pattern for the lagoon sediments. The sieve mean and standard deviation also indicates a unimodal character for these sediments. The computed measures of asymmetry or peakness (skewness and kurtosis) are not significant due to the wide range of values determined. The sieve and hydrometer skewness and kurtosis show similar behavior, that is, no significance.

The textural parameters or grain size measures such as sorting, symmetry and dispersion, derived from data treated through several methods, present an expressing quantitative significance. They might reflect the energy gradients responsible for their transport and deposition, and enable the reconstruction of a given sedimentologic environment.

3.4. Analysis and interpretation of the textural parametric empirical data

3.4.1. Introduction

The grain size data analyzed through sieve and hydrometer methods and through the method of moment are the basic statistical data that support the following assumptions and considerations. First, we analyze the range of grain size distributed along the lagoon and, second, we discuss the transport and deposition mechanism that can be characteristically based on the statistical parameters.

Since the main goal of this study is the characterization of a single environment, (*Jequia* lagoon) receiving eroded materials mostly from a relatively uniform geological unit (the Group *Barreiras*), only the combination of a few computed (Statview curves)

percentiles were considered to be representative of the textural parameters. Moreover, the widespread homogeneity of sediments along that lake enables the treatment of the available data using simpler methods, such as the moment method.

3.4.2. Discussion of the textural parameters

The computed Mdf and graphic percentile results from Zone I (site 4), Iib (site 81), IIIa (site 65) and Zone IV (site 22) were converted to C (mm) and M (mm) parameters. Since Passega's diagram requires at least 30 samples from a single sediment population, the C and M of these study results representing few samples were not projected into his diagram. Therefore the characterization of the mechanism of transport and deposition of the lagoon is deduced from a simple analysis of the absolute computed C and M values (Table 3.2b), because of tractive current deposits following the concept of Passega (1957).

The statistically derived data of the clastic sediments of *Jequia* lagoon were computed using sets of random combinations of four selected groups along the lagoon. This set suffices to provide an assessment of the patterns of transport and deposition mechanisms of the sediments prevailing into that environment at the survey period.

The interpretation of textural parametric data is done through the analysis of absolute statistical values, and is based on the plot of bivariate and simple diagrams.

The overall patterns of percentage cumulative curves shown in figures 3.1 to 3.30, suggests a very homogeneous distribution of clastic sediments along *Jequia* lagoon. The graphic estimation (percentage) grouped in table 3.3 indicates mean values for the clay, silt and sand fractions respectively of 10, 48,3 and 15 within Zone I (sites 3, 4, 6 and 7). Within Zone IIb the mean values for the clay, silt and sand fractions are respectively 5,6, 56 and 2,6. The mean values within Zone IIIa, for the clay, silt and sand fractions are respectively of 5, 62,5 and 0,5 and within Zone IV the mean value for the clay, silt and sand fractions are respectively of 10,5, 64 and 7. These fractions demonstrate the

homogeneous and unimodal distribution of clay, silt and sand at the bottom of the lagoon. Silt is the fraction that predominates most within all zones. Exception is remarked for the site 6 of Zone I. During the sampling survey, a very intense slope erosion was recognized near that site. This event might justify the dominance of sand fractions within site 6. The clay fraction predominates within Zone IV and IIIa, which represent the main entry of sediments into the lagoon.

The non-steeper nature of cumulative curves suggests a very poor sorting process for these lake sediments. The absolute values of raw weight and weight percentage indicate a dominance of grain size in the range of 2 to 9 phi, matching the range size for silt and clay sediments.

The estimation of the variation on grain size fractions during sieving indicates that 70% of these sediments fall within a range size among 2 to 7 phi (fine sand-silt), the remaining 30% left falling in the grain range below 7 phi (silt-clay). We estimate that the fractions with diameters larger than 8 phi do not exceed 10%.

A precise computation of the proportion of the sediment size above 8 phi was not performed. We point out the frequent interlayering of silt and clay preventing a precise separation of clay from the silt fraction in almost all samples. Therefore, clay minerals were mixed with silt particles within the range of grain size lower than 7 phi.

The sieve sample mean (Mdf) from Inman (1952) and the sieve mean (Mzf) from Folk (1957) reflect the overall average size of a given sediment population. They are sensitive measures for showing the prevailing sediment patterns of deposition and transport of the source supplying these sediments into the lagoon.

In the study-case of *Jequia* lagoon bottom clastic sediments, the mean is not a sensitive measure for the population of clastic sediments, since it does not enable an overall analysis for samples within each zone.

Most samples within each zone pertain to a specific mean value. Therefore each sample was analyzed as pertaining to a unique related pattern of deposition and provenance.

Trask (1930) defines the median as the measure of the sediment population which has half of the raw weight grain as finer, and half as coarser; and the 50% value computed in the interception of the cumulative curves. The median within this study is not an environmentally sensitive parameter for the clastic sediments of *Jequia* lagoon. No significant information was gathered from the median statistical measure.

The sorting measure (the standard deviation and moment standard deviation) of the bed clastic sediment population (s and Ms) suggests an environment dominated by transport under low energy. Therefore, the absolute values of standard deviation and mean of Zone I show greater sorting processes compared to Zones III and IVwhich show a poor sorted character for these sediments.

Several absolute values of textural statistical parameters suggest a platykurtic character and a very poor sorting pattern for the clastic sediments of *Jequia* lagoon, within the four selected sediment zones.

The sediment population represented in Zones I, III and IV supports a poor sorted character for these clastic deposits. For Zone II the constant mean values, even though varying from sample site to sample site, suggest a bimodal character for the sediments along these sites.

The analysis of the skewness and kurtosis suggests a fine-skewed character with values concentrated in the range of 1,5 to 0,5. It also shows a strong platykurtic pattern with absolute values around 0 for Zones I, II and III and ranging from 0 to -1 for Zone IV.

Considering that strong platykurtic curves suggest a bimodal character, the values found for the population of sediments grouped in Zone IV indicate a bimodal distribution for these deposits. The bivariate plots of skewness versus kurtosis (Figures 3.31 to 3.35) indicate a poor sorted and platykurtic character for Zones I, II and IV. These textural parameters show poor correlation for sediments wihtin Zone III.

The computed hydrometer absolute values for the mean (6,2 to 6,6) suggest a symmetric and unimodal pattern for the *Jequia* sediments. The measures of uniformity and the standard deviation ranging from 1,6 to 1,7 indicate a poorly sorted character for the sediment population grouped in all zones.

The analysis of the above diagrams suggests a strong to fine-skewed character for the sediments with values concentrated in the range of 0,2 to 0,4. They also present a strong platykurtic pattern with absolute values ranging from -1,1 to -1 for Zones I, II and III and ranging from -0,6 to -1,1 for Zone IV. These results show a good agreement with the sieve data for the bimodal tendency of distribution for these deposits.

The designated mean and the measure of asymmetry, which are the equivalent measures to the sorting statistical measure determined through the moment method, are not sensitive to deposition related patterns. The absolute values (Tables 3.12, 3.13 and 3.14) for the moment and sieve textural parameters show slight variations from zone to zone.

Absolute values of standard deviation indicate an overall pattern of moderately well sorted sediments within Zones I, IIb and IV. The values range from 0,4 to 0,8 for Zone I, 0,6 to 1 for Zone II, 0,5 to 0,8 for Zone III and 0,7 to 0,9 for Zone IV. A tendency towards moderately to poorly sorted for Zone II sediment deposits is noticeable.

The standard deviation values grouped respectively for Zones I and IV suggest a moderately sorted pattern for these sediments even though some values are around zero.

Absolute standard deviation values for Zones II and III suggest a poorly sorted character for these deposits, even though some values are around zero.

The analysis of the bivariate diagram of skewness and kurtosis for all zones suggests a strong platykurtic character for the sediment population in all zones. The absolute values of skewness and kurtosis are around zero, indicating a near symmetrical pattern for these clastic deposits.

The absolute values of C and M within table 3.2b indicate that the sediment population of the lagoon might be controlled mainly by traction and near bottom suspension. The major mineralogical phases identified occur very often within tropical basins. The finer quartz grains might remain in suspension near the bottom of the lagoon. The clay particles (kaolinite) predominate in simple single suspension along the water column. Assuming that there is a seasonally regular distribution pattern of these minerals along the lagoon, we might establish correlation between that distribution and the spectral reflectance response from these sediments.

Considering the major results of the textural parameters, we assume the existence of an overall dominant unimodal distribution for the sediments mapped along the bottom of the *Jequia* lagoon. This pattern might also indicate a unique source of supply feeding that environment. This assumption finds an easily supported argument since the *Jequia* study area is fed by a specific geological unit (*Barreiras* Group) which covers more than 95% of the study area.

The correlations between the sediment properties (grain size, mineral type) characterized in this last chapter and their specific reflectance patterns are discussed in the subsequent chapters 4 and 5.

3.5. Characterization of the minerals using X-ray diffraction patterns and thin section descriptions within the bottom sediments of the *Jequia* lagoon

3.5.1. Introduction

The particles occurring along the water column of the *Jequia* lagoon are natural organic (phytoplankton species), natural inorganic matters (sediments) and anthrophogenic (oil-like substance) matter. The inorganic particles are considered mainly derived from the erosion of the Tertiary clastic sediments and from fluvial and braided stream origin.

The grain size distribution using data treated by the hydrometer and sieve method enables the assumption that the bottom sediments present a very similar unimodal pattern for all the zones sampled. It is assumed that the suspended inorganic loads are derived mainly from the re-suspension of the bed load material especially along the shallow zones (I and IV).

The mineralogy of the bottom sediments of the *Jequia* lagoon was determined by X-ray powder diffraction methods. The same sample sites and zones used on the simulation of different concentrations of suspended sediments were analyzed by X-ray diffraction. Due to the small sample size and the goals of this mineralogical identification, no pretreatment was performed.

Two groups of samples were separated after sieving. The first group of sediments presented fractions among 63 and 2 microns and a second group with fractions lower than 2 microns. The former fractions quantitatively dominated (75%) in all samples while the latter fractions represented less than 20% of the sediments on the bottom of the lagoon for all sediment samples.

The two microns fractions were repeatedly subjected to centrifugation during 10 minutes to separate silt from clay minerals. The silt and clay fractions in all samples were

highly intercalated and not enough samples were available to repeat the centrifugation. Therefore the fractions with size less than 2 microns might have detected a significant percentage of silty mineral by X-ray.

3.5.2. Analysis of the mineral within the bottom sediments using X-ray diffraction patterns

The mineralogical homogeneity of these sediments is expressed by the single assembling of quartz and kaolinite. Therefore, we assume that within the suspended sediments the major inorganic material identified using X-ray diffraction (XRD) and petrographic identifications were quartz and kaolinite. These results show good agreement with the mineralogy expected for those tropical environments.

Two groups of fractions were selected from Zones I, IIb, IIIa and IV to determine the mineralogy by X-ray diffraction. The sediment fractions smaller than 63 microns shown in figures 3.36 to 3.37 and sediment fractions smaller than 2 microns in figures 3.38 and 3.39 were subjected to XRD for the four zones selected.

The peak positions were obtained by scanning at 0,01°2q intervals using CuKa radiation. X-ray patterns were recorded up to 50° (2d). The qualitative analyses of X-ray results indicate sharp reflections at about 7,2Å and 3,35Å for the sediments of Zones I and II and at about 7,2Å and 3,34Å for sediments from Zones III and IV. Those peaks correspond respectively to the presence of kaolinite and quartz within the zones. Therefore, we deduce that quartz is the phase that predominates in the fractions larger than 63 microns, and kaolinite is the one in the fractions smaller than 2 microns. Kaolinite is the major clay mineral present in the selected samples, followed by illite identified with reflections at about 5,1Å and 5,2Å in all zones except Zone IV.

X-ray results indicate qualitatively that for fractions smaller than 63 microns there is a slight dominance of quartz compared to clay minerals. The description of thin sections for those fractions also indicates the dominance of coarse quartz compared to clay minerals.

For fractions smaller than 2 microns, kaolinite is the slightly dominating mineral. Therefore we assume that within the bottom sediments of the *Jequia* lagoon, kaolinite is the dominant clay mineral.

Assuming that the suspended inorganic loads of the water column of the *Jequia* lagoon represent part of the bed load material, it is deduced hereafter that the assemblage of kaolinite+quartz is the suspended inorganic matter recorded by the satellite LANDSAT TM sensor. Therefore the major water quality parameter controlling the overall reflectance pattern along the lagoon is the sediments.

Quartz representing the heaviest phase in that assemblage tends to settle in the bottom of that lake or to concentrate in the deepest water layers, according to Stooke's law. Therefore, we assume that the suspended inorganic matter is mostly composed of kaolinite+illite. It is believed that quartz in the water column plays a significant role in the residual reflectance detected by satellite sensors, due to intense backscatter effects of the water columns. These effects are very strong along shallow lakes, which is the case of some zones of the *Jequia* lagoon.

Exception can be stated for the sediment sites within Zone IIb, which present an average depth of 11 m (table 1.1), and are referred as the clear water sites of the lagoon.

The XRD patterns recording the peak of illite for Zones I, II and III support a diagenetic continental origin for the sediments of the lagoon. The clay minerals detected by the XRD are typically of highly weathered tropical environments with advanced leaching process.

3.5.3. Estimation of the total organic and inorganic carbon by LECO and peroxide methods.

The main biogenetic solid components mapped along the *Jequia* lagoon by Lira *et al.*, 1991, comprise primarily the resident phytoplankton (56%) and nekton (19%). Results of some organic samples are shown in table 3.1a.

The LECO (Laboratory Equipment Corporation) and peroxide analysis were used to estimate the relative amount of total organic and inorganic carbon dissolved within the suspended matter along the *Jequia* lagoon (Tables 3.1a and 3.1b).

The four zones and corresponding sample sites, through X-ray analysis, were selected to estimate the amount of organic carbon by LECO and by applying peroxide. The peroxide analysis showed an explosive character for all samples.

The LECO results for the four zones selected show variations in the percentage of organic carbon from 2,5 to 5,3% for Zones IIb and IIIa respectively, and for 6,9 to 8,9% for Zones I and IV respectively. The population of sediments mapped along Zone I was identified as the major organic trap in the *Jequia* lagoon.

The results indicate that the sediments of the *Jequia* lagoon showing a high proportion of organic matter come from Zones I and IV. The spectral reflectance data show a very good agreement with the sedimentologic results. The higher spectral radiance recorded by the LANDSAT TM sensors in June 1990 is mainly due to the sediments in the blue (TM1) range and to the great influence of the organic matter within the green (TM2) for these zones. The spectral signature of solid (phytoplankton) or dissolved organic matter recorded for these zones is overlapped by the suspended sediment reflectance.

Homogeneous and mixed target, present in the *Jequia* lagoon, is difficult to be distinguished. Therefore, we believe that a residual reflectance for these water quality

parameters mapped through digital methods represent a mixed plume composed of a mineral assemblage determined by quartz+kaolinite and organic matter fixed to it.

The above considerations enable the assumption that several mixed homogeneous water targets are hardly distinguished using standard classifiers and fairly set of field data. It is believed that non-parametric classifiers enable a more performed and accurate classification of homogeneous targets.

The vinasse presenting a very high rate of daily sodium dumped into the *Jequia* River is mixed with the sediment and phytoplankton plumes. Although vinasse is an adequate compound to fertilize the soil, into water bodies it becomes a very acid chemical compound leading to lower levels of oxygen and pH (Rossetto, 1980).

The concentration of total organic carbon was performed by the oxidative combustion (LECO) method. It was also estimated by applying hydrogen peroxide to the dry sediment samples. In the latter method, the organic carbons were removed from the sediment samples by means of a cold concentration of 30% of hydrogen peroxide (H_2O_2). The digestion of the organic matter by the hydrogen peroxide in all samples was followed by a growing reaction in the following order: Zone IIIa > Zone IIb> Zone I> Zone IV. The total organic matter digested by the peroxide in the four zones is shown in table 3.1b. The results from the combustion (LECO) method for the same four zones of samples grouped are also in table 3.1b.

FIGURES AND TABLES FOR CHAPTER 3

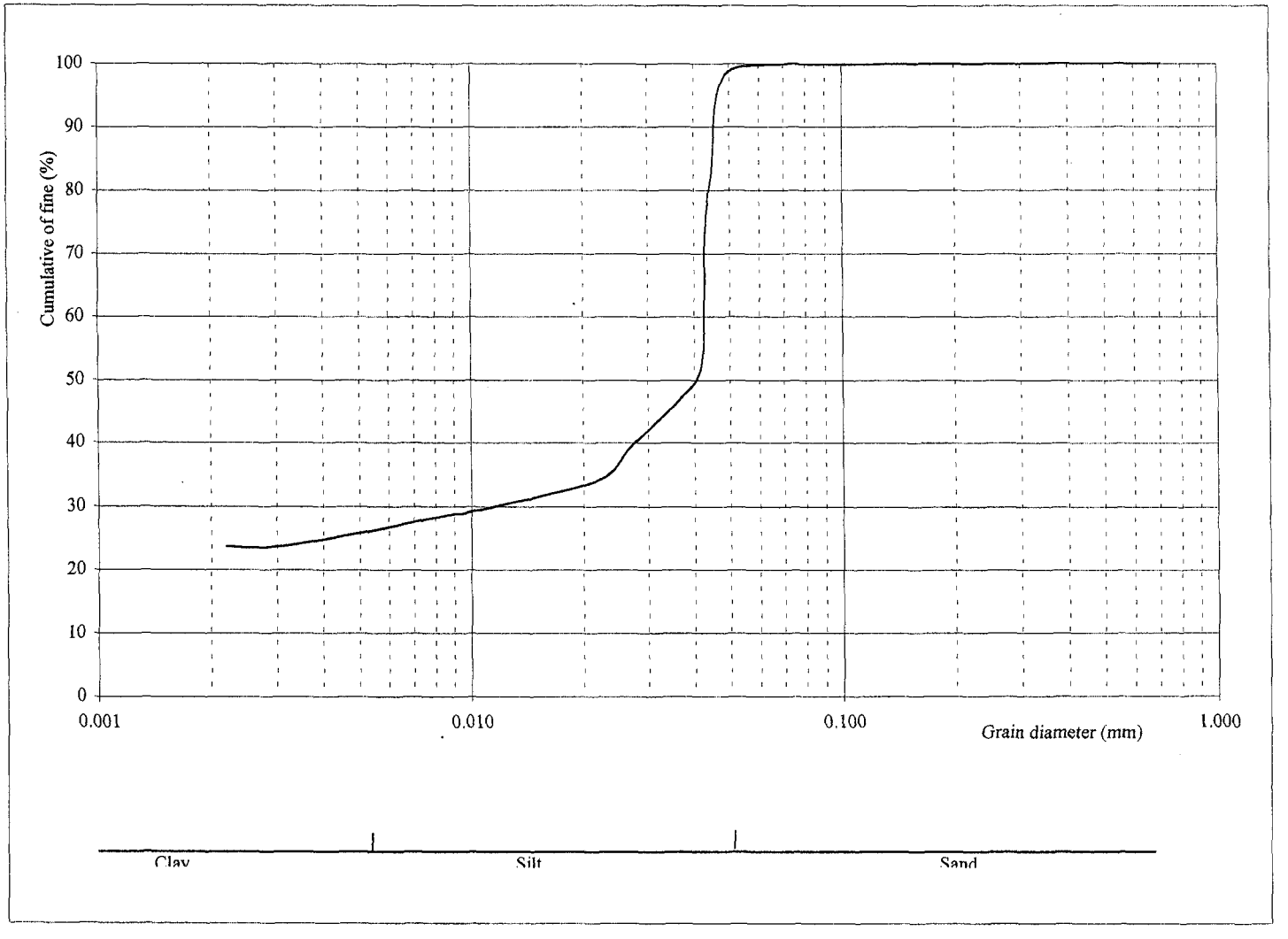

Figure 3.1. Combined Sieve and Hydrometer raw data Zone I(3) from the bottom sediments of the Jequia lagoon.Alagoas.Brazil

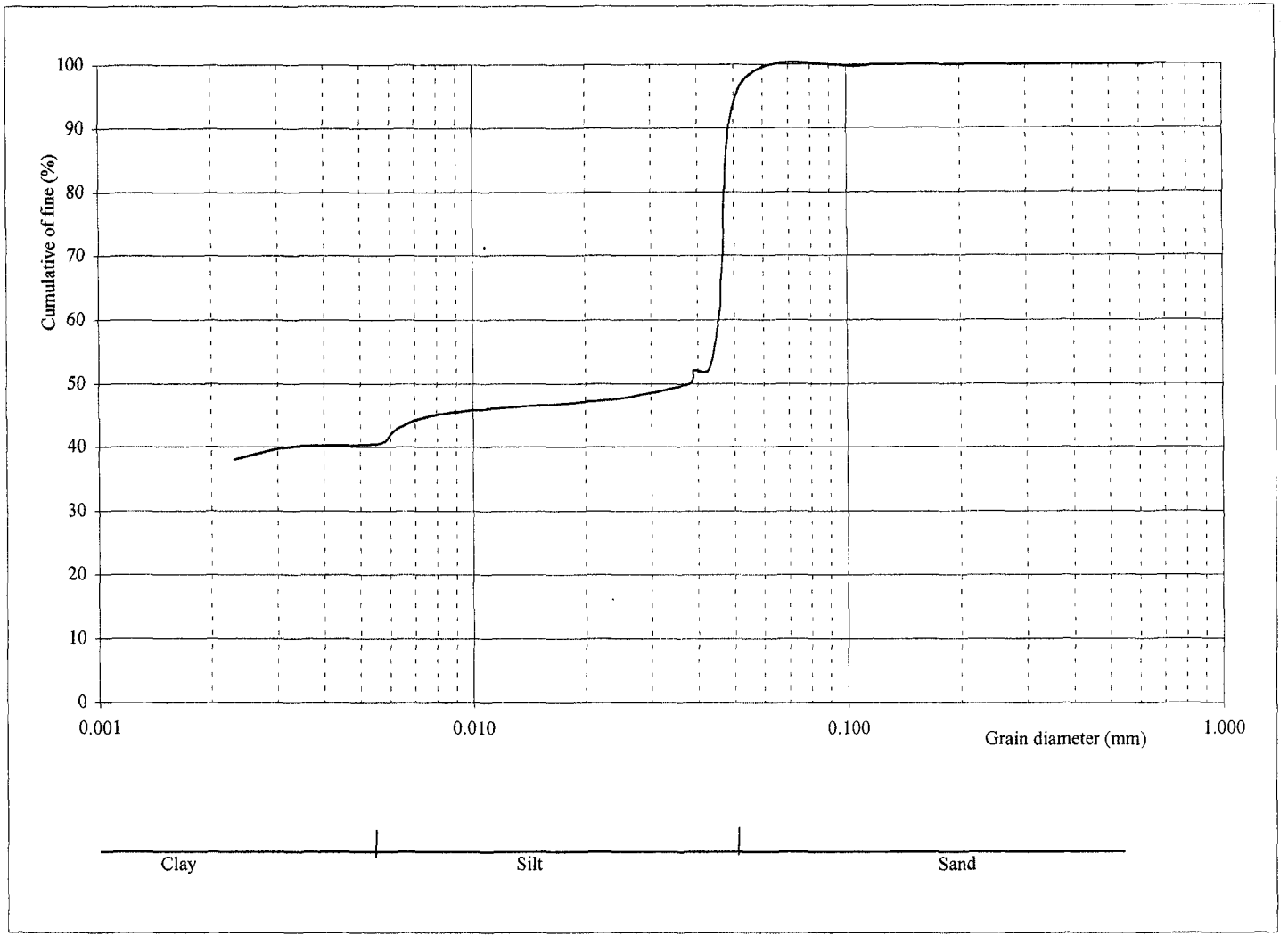

Figure 3.2.Combined sieve and hydrometer raw data Zone I(4) from the bottom sediments of the *Jequia* lagoon.Alagoas.Brazil

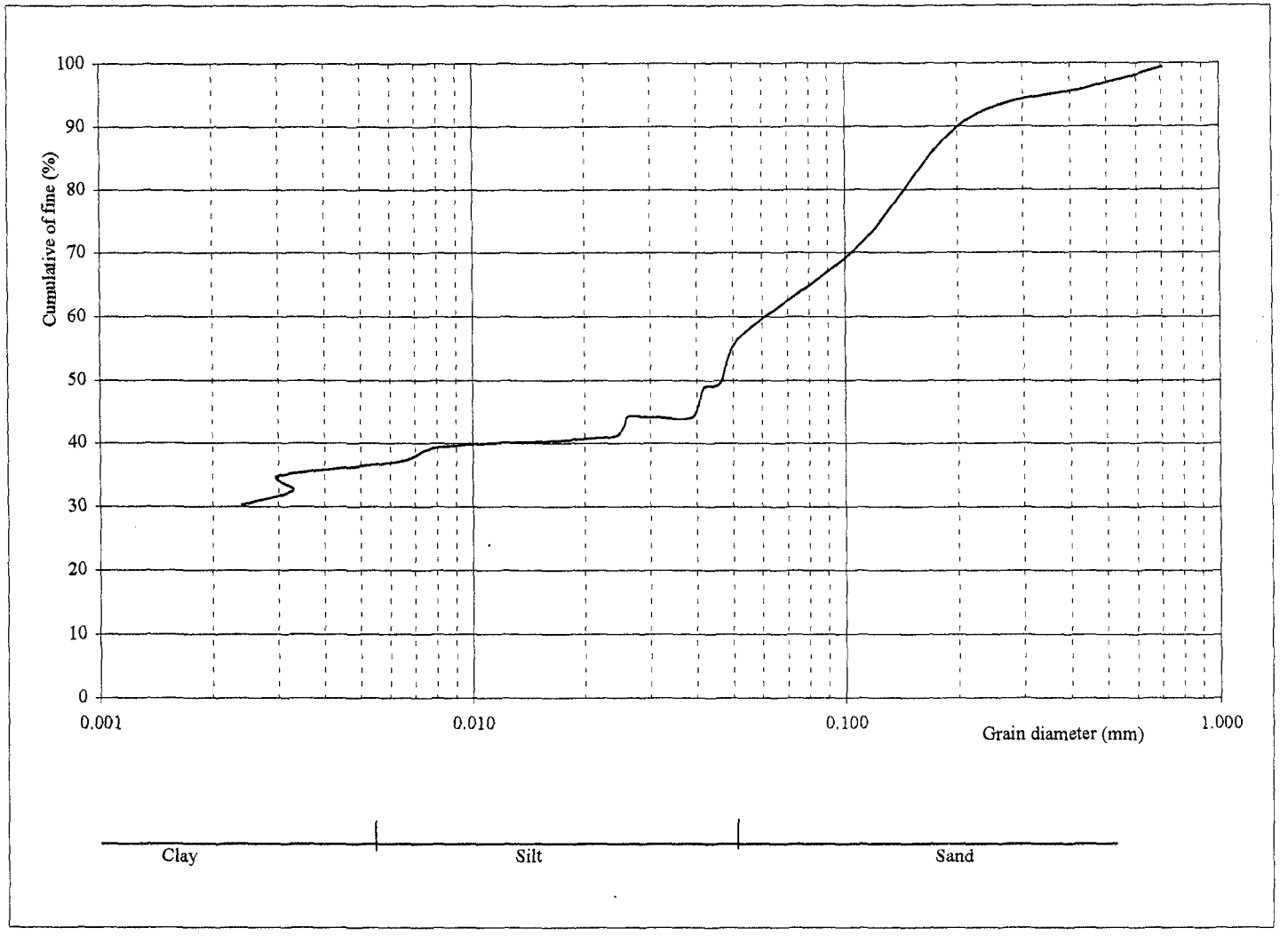

Figure 3.3. Combined sieve and hydrometer raw data Zonel(6) from the bottom sediments of the *Jequia* lagoon.Alagoas.Brazil

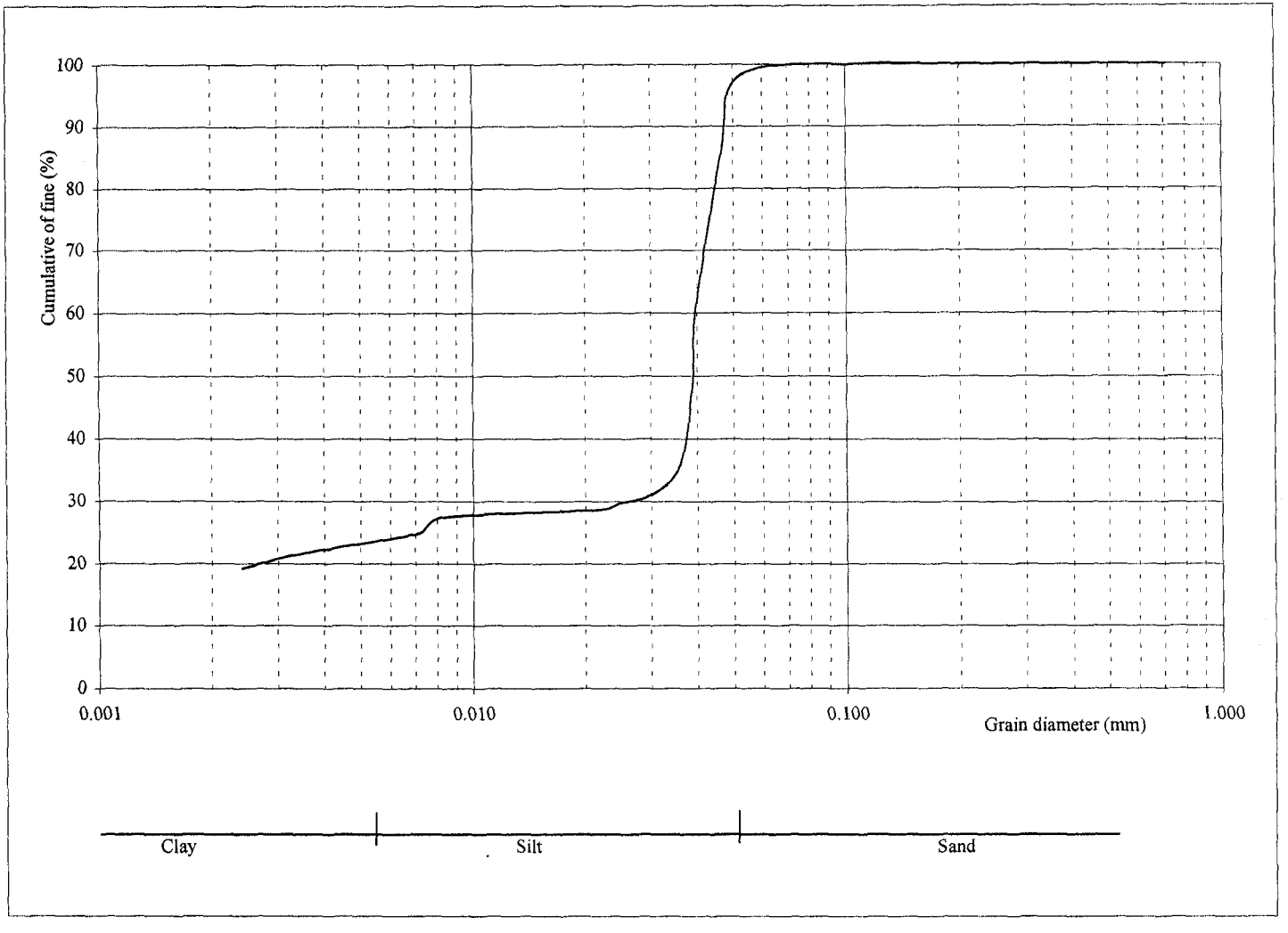

Figure 3.4.Combined sieve and hydrometer rwa data Zone I(7) from the bottom sediments of the *Jequia* lagoon. Alagoas.Brazil

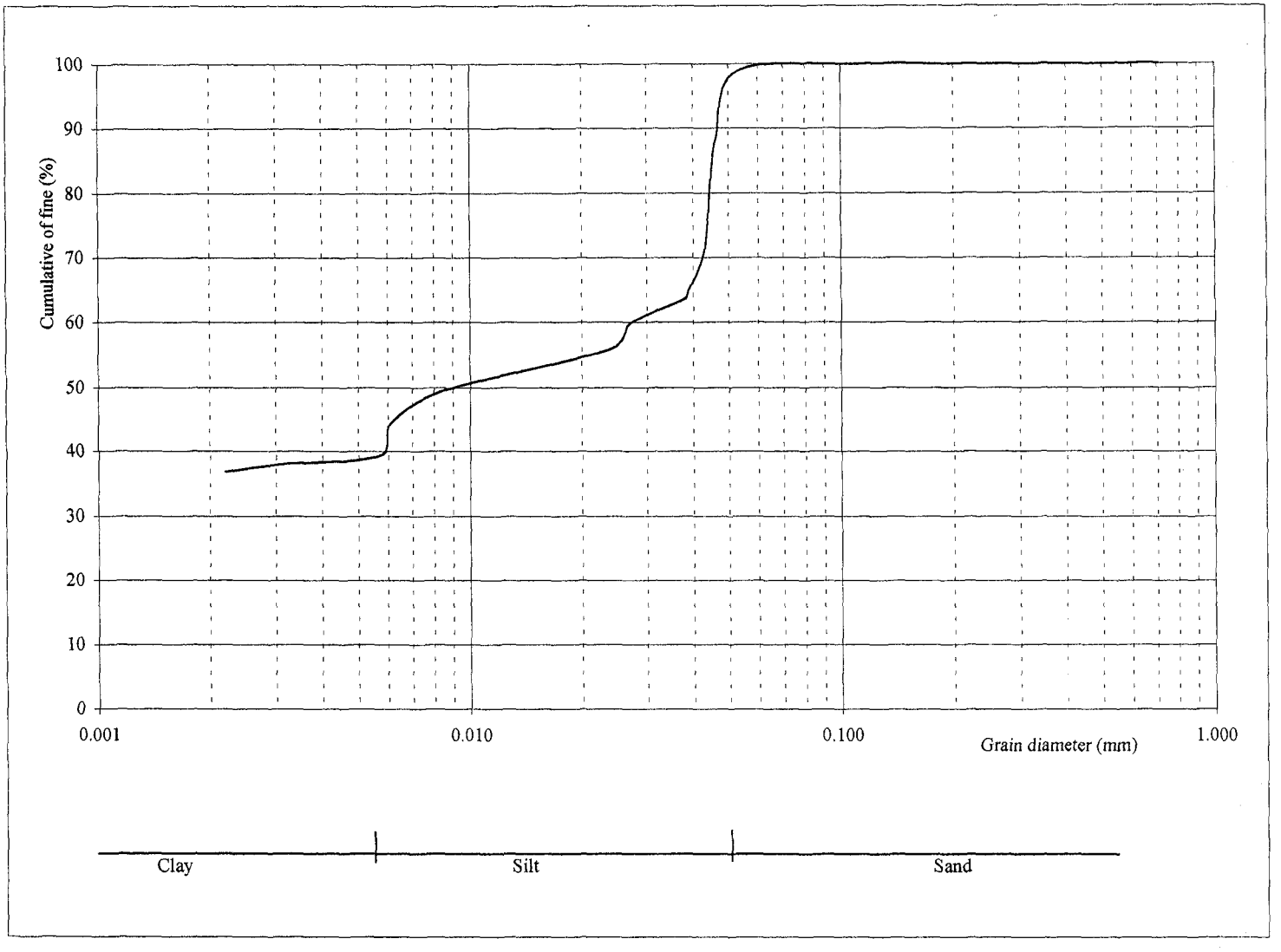

Figure 3.5. Combined sieve and hydrometer raw data Zone IIa(10) from the bottom sediments of the *Jequia* lagoon.Alagoas Brasil.

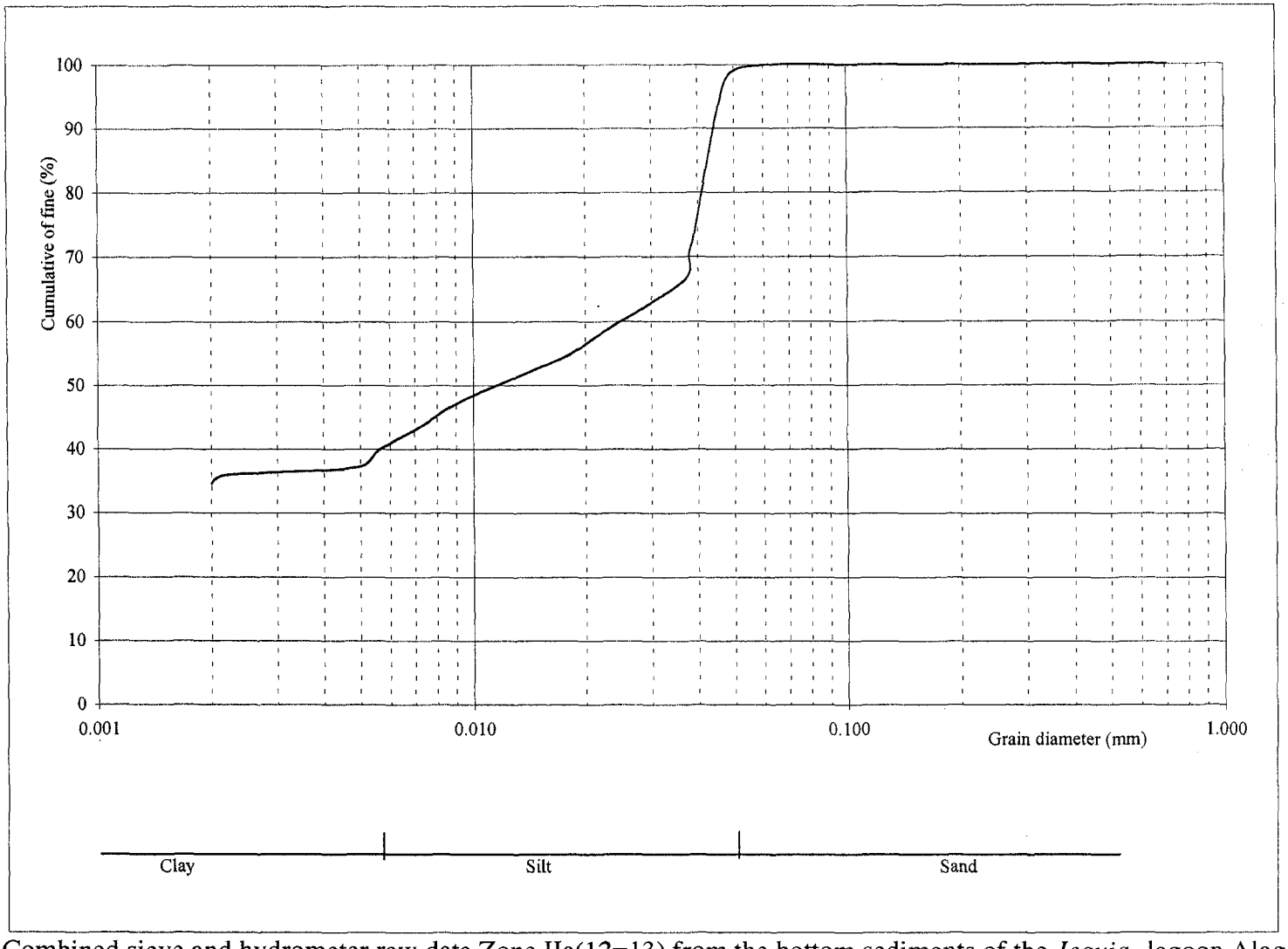

Figure 3.6.Combined sieve and hydrometer raw data Zone IIa(12=13) from the bottom sediments of the *Jequia* lagoon.Alagoas.Brazil

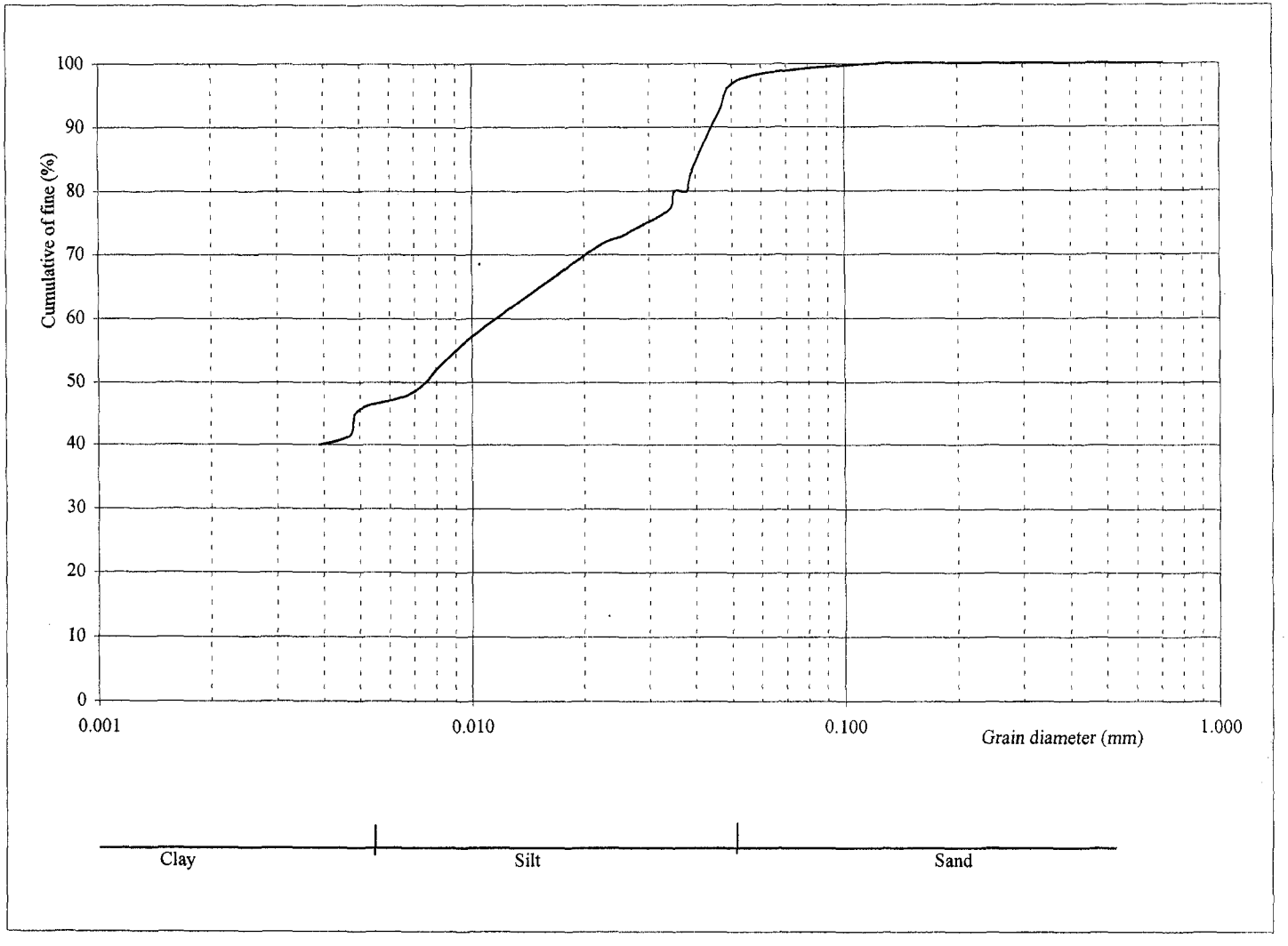

Figure 3.7.Combined sieve and hydrometer raw data Zone IIa(15) from the bottom sediments of the *Jequia* lagoon.Alagoas. Brazil

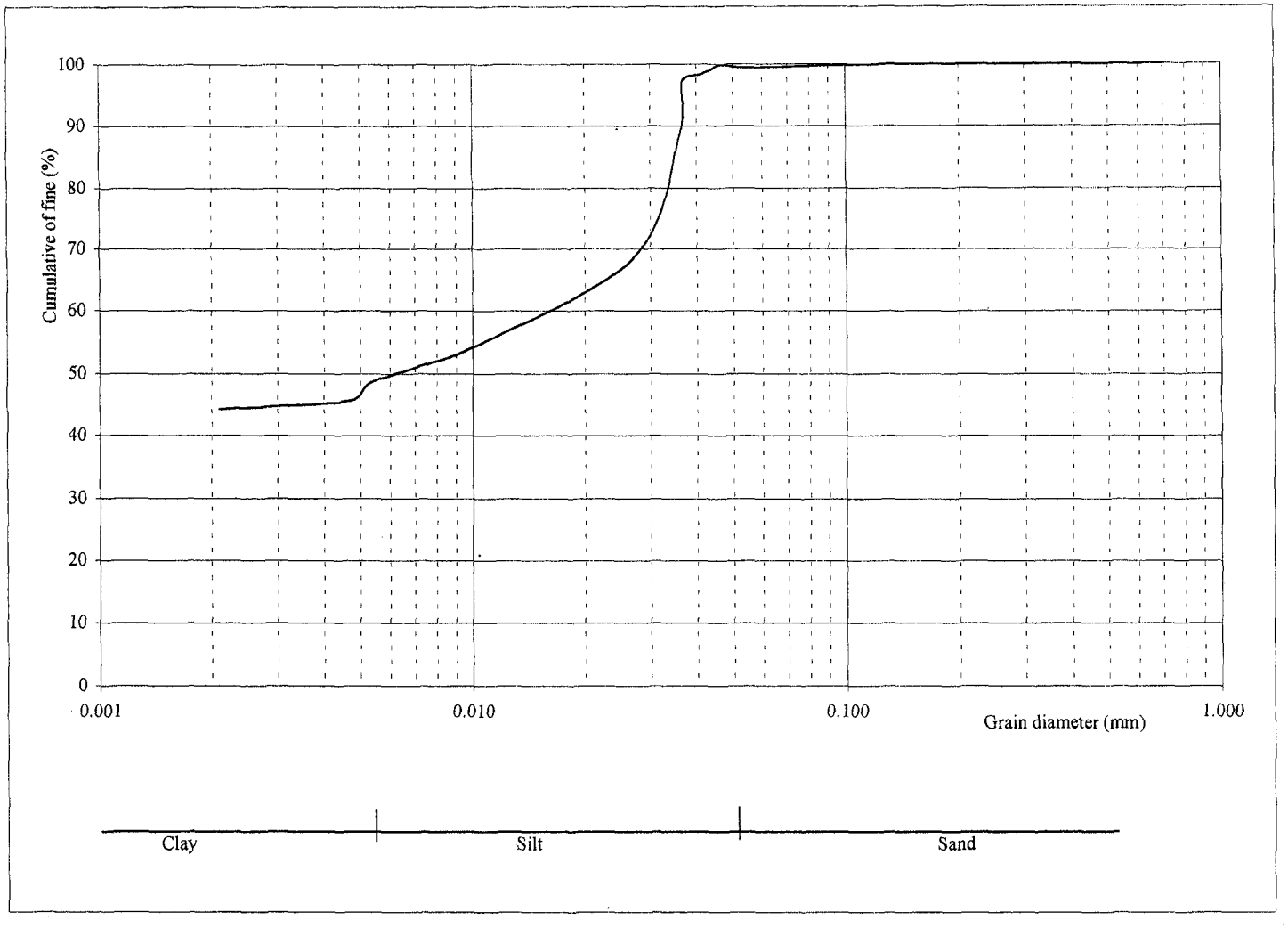

Figure 3.8.Combined sieve and hydrometer raw data Zone IIa(16) from the bottom sediments of the *Jequia* lagoon.Alagoas.Brazil.

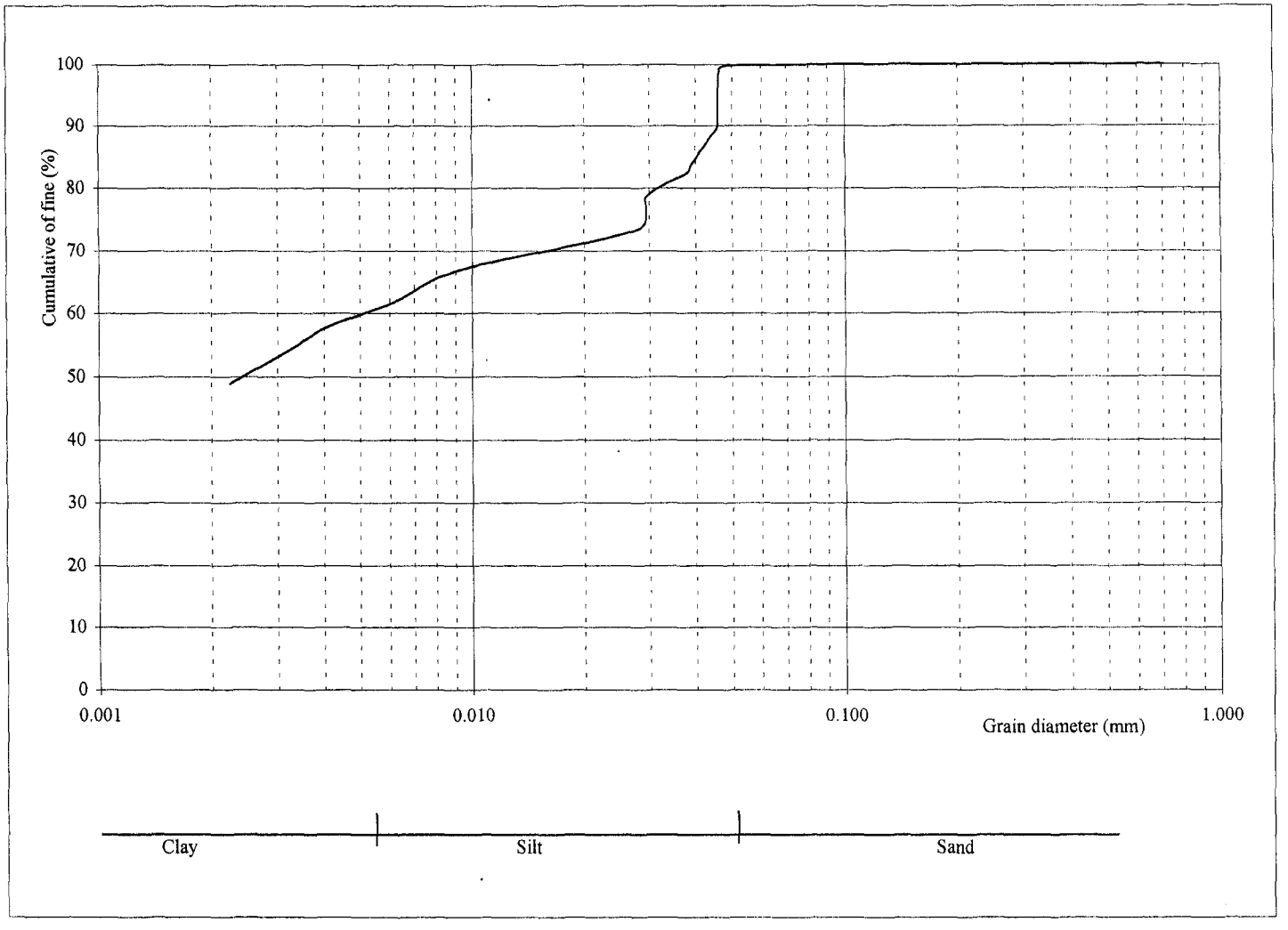

Figure 3.9.Combined sieve and hydrometer raw data ZoneIIa(17) from the bottom sediments of the *Jequia* lagoon.Alagoas.Brazil.

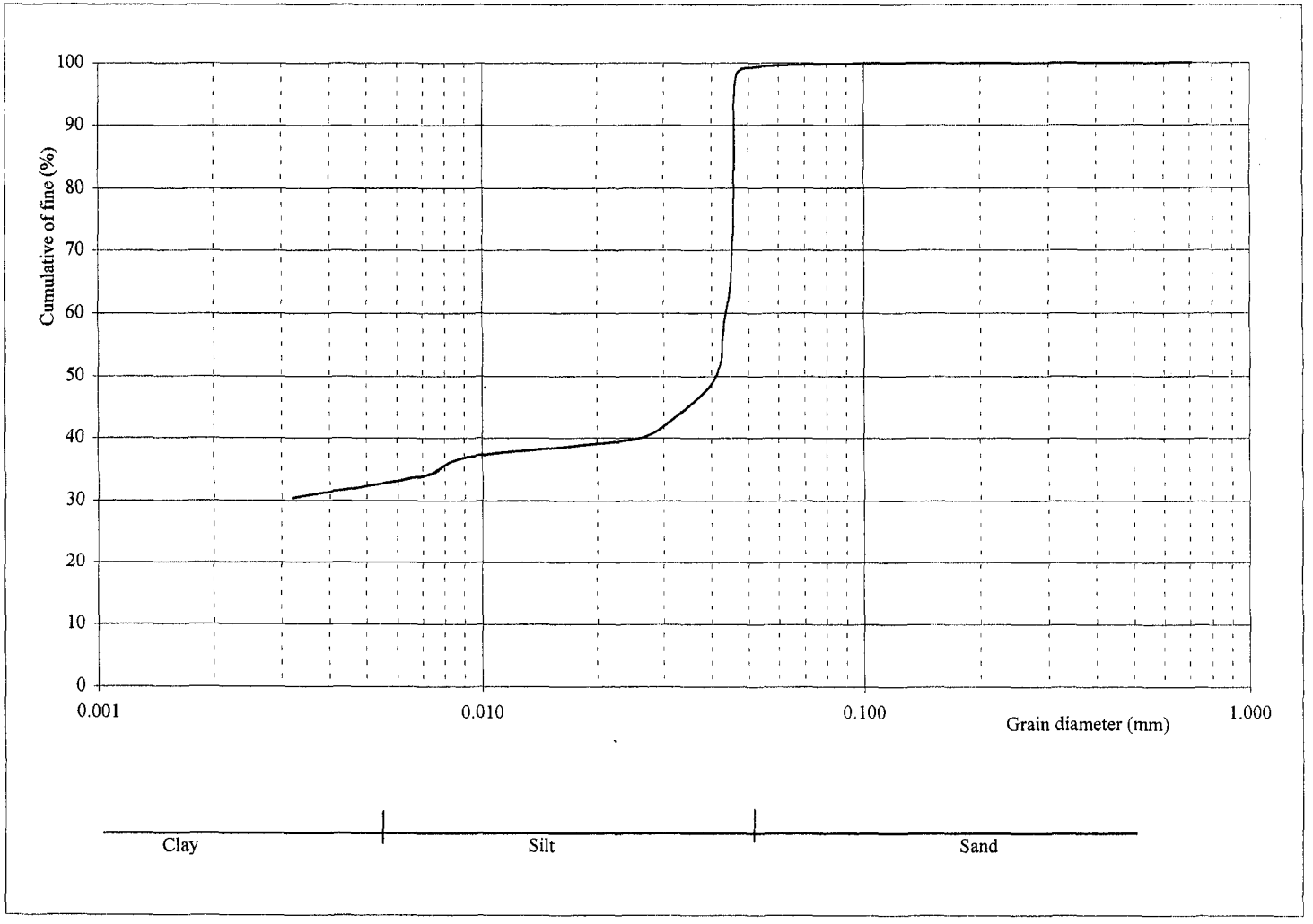

Figure 3.10.Combined sieve and hydrometer raw data Zone IIb(76) from the bottom sediments of the *Jequia* lagoon.Alagoas.Brazil

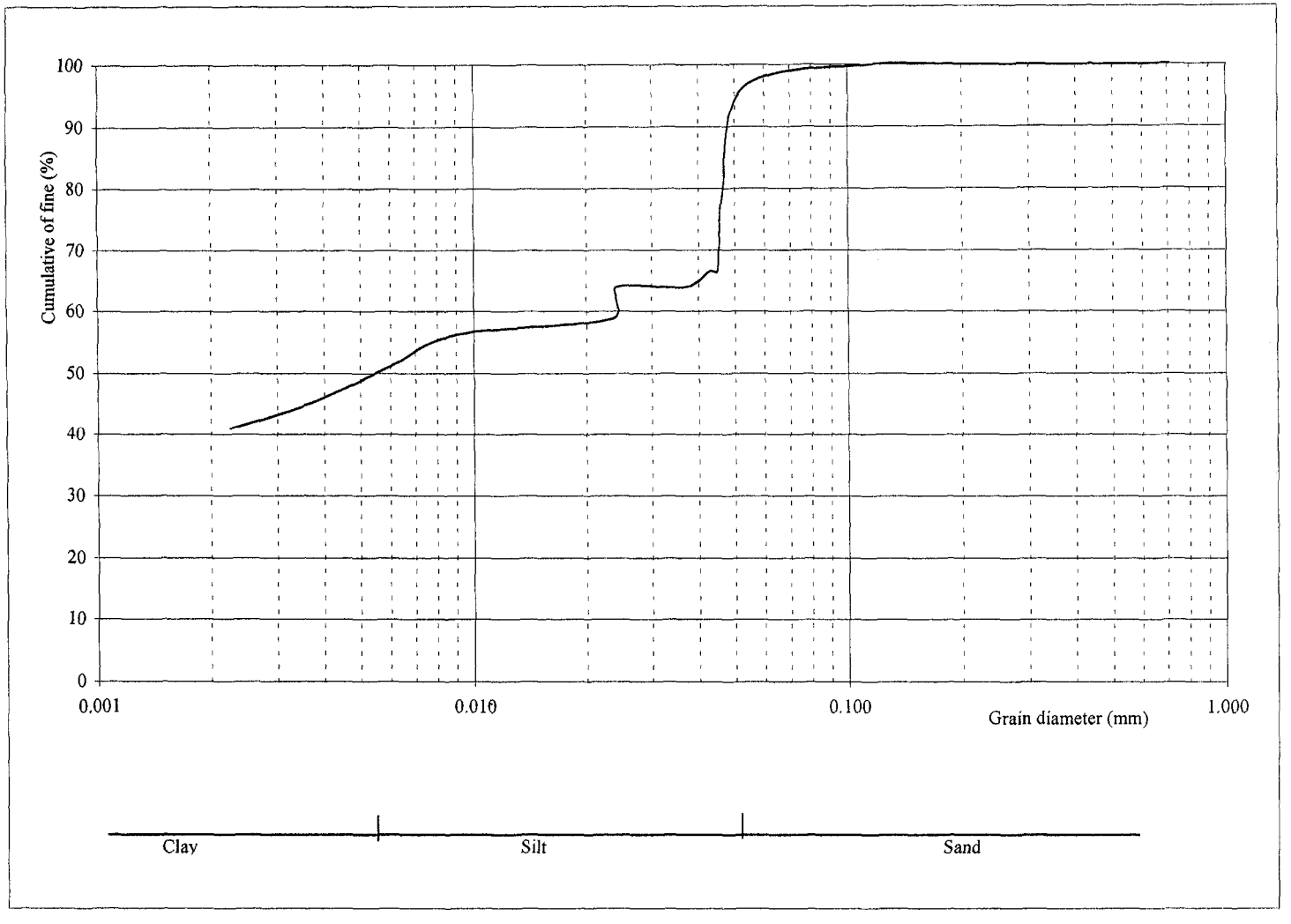

Figure 3.11.Combined sieve and hydrometer raw data Zone IIb(80) from the bottom sediments of the *Jequia* lagoon.Alagoas.Brazil

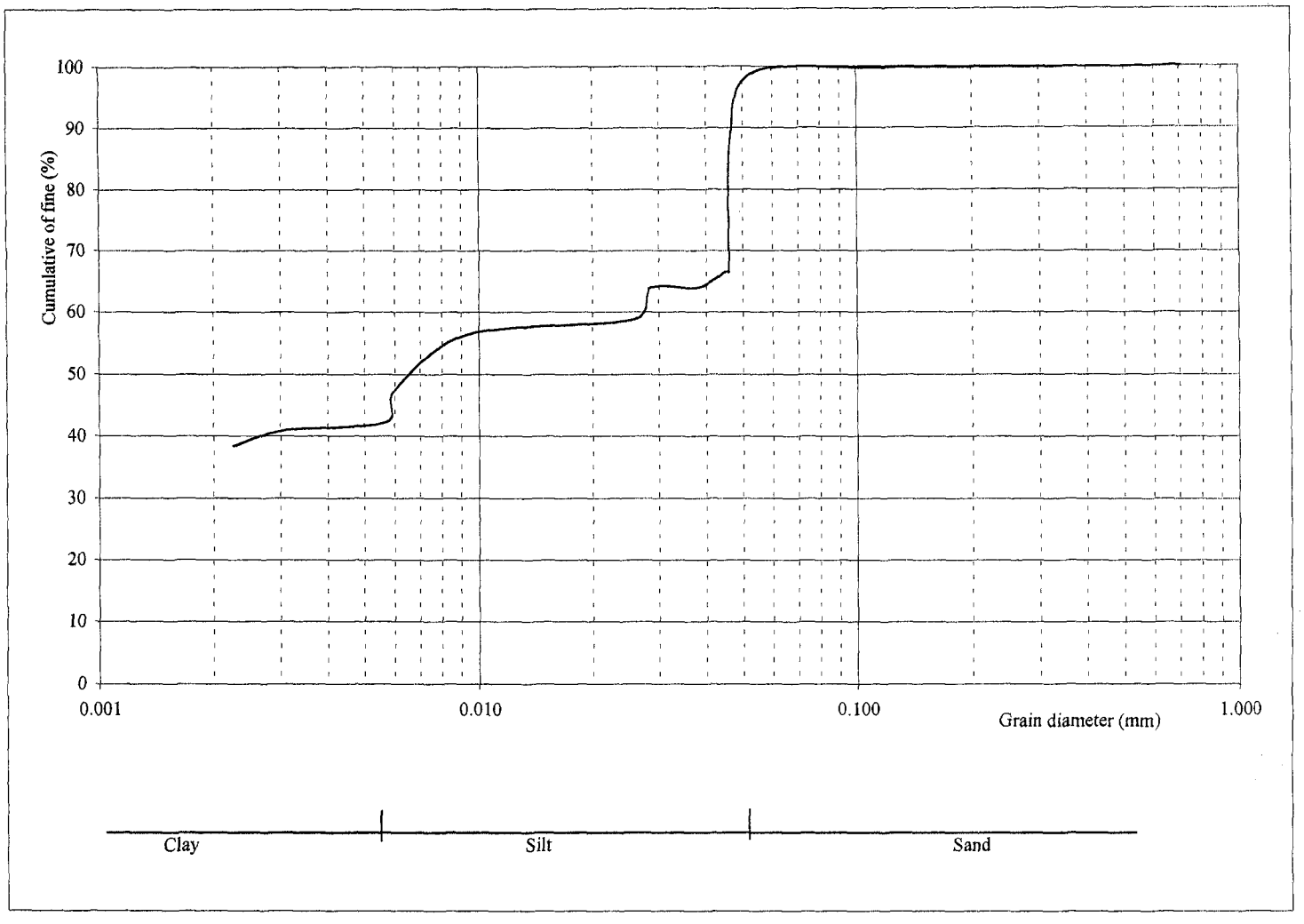

Figure 3.12.Combined sieve and hydrometer raw data Zone IIb (81) from the bottom sediments of the *Jequia* lagoon.Alagoas.Brazil.

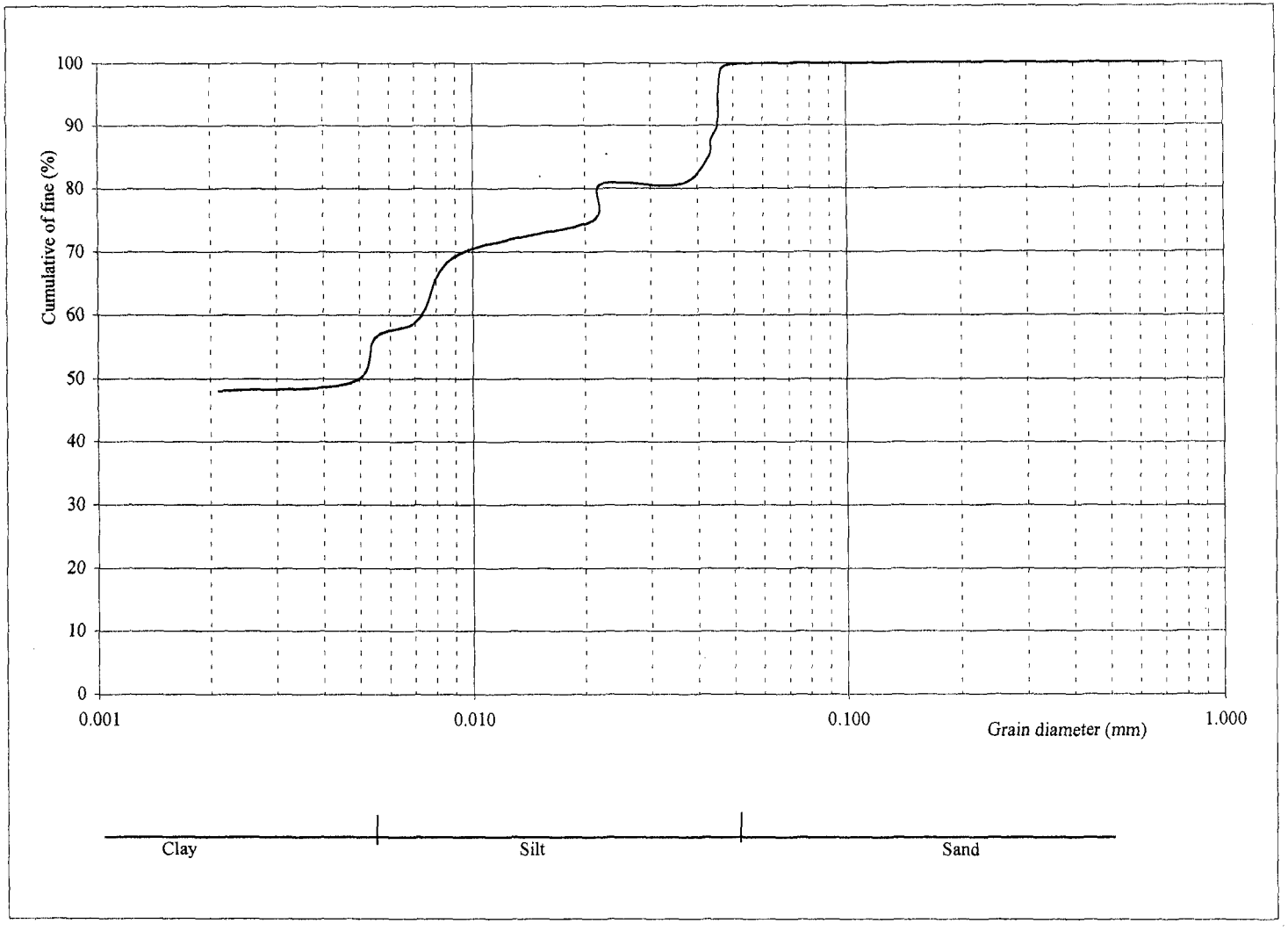

Figure 3.13.Combined sieve and hydrometer raw data Zone IIb(82) from the bottom sediments of the *Jequia* lagoon.Alagoas.Brazil.

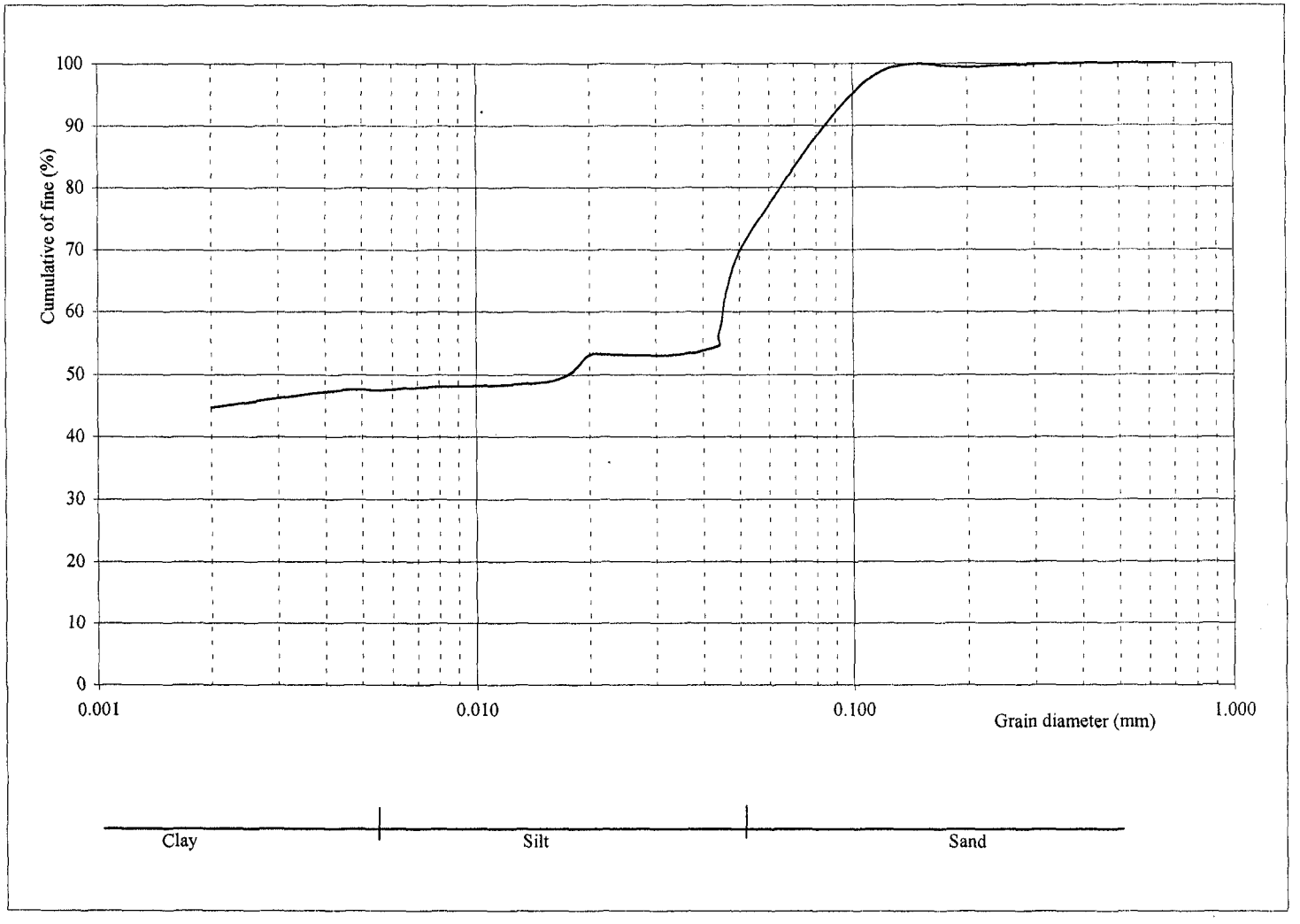

Figure 3.14.Combined sieve and hydrometer raw data Zone IIc(50) from the bottom sediments of the *Jequia* lagoon.Alagoas.Brazil.

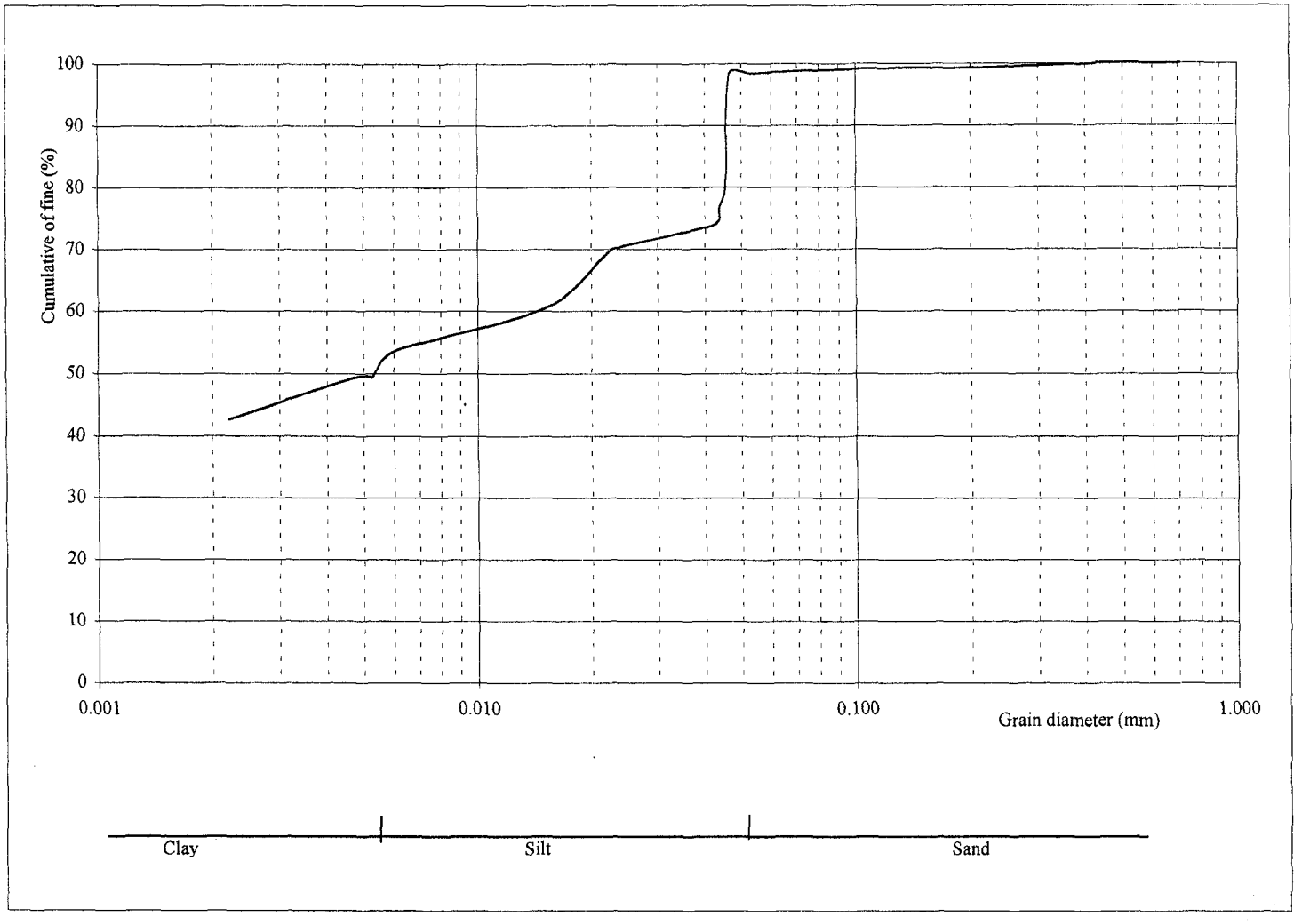

Figure 3.15.Combined sieve and hydrometer raw data Zone IId(27) from the bottom sediments of the *Jequia* lagoon.Alagoas.Brazil

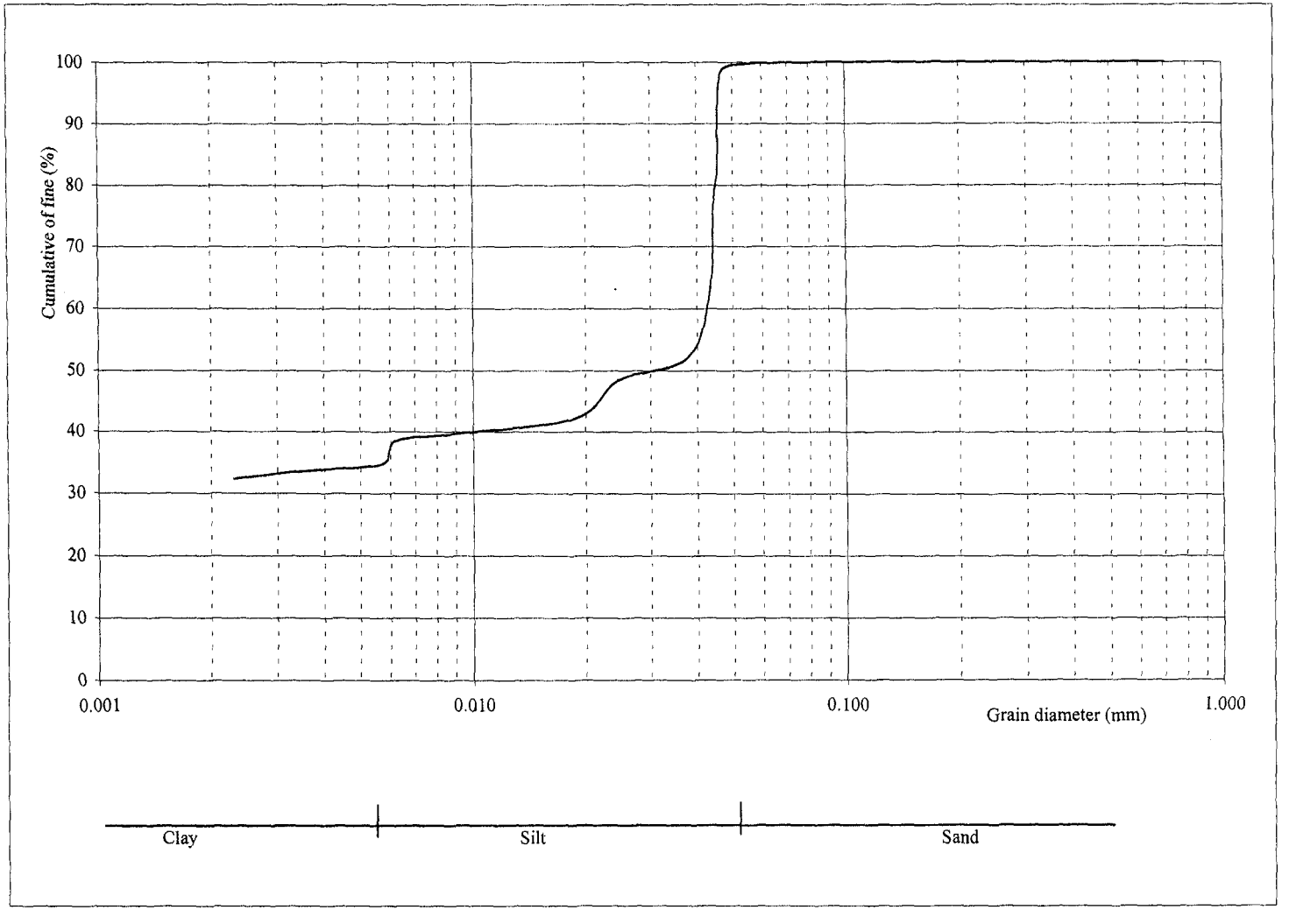

Figure 3.16.Combined sieve and hydrometer raw data Zone IId(29) from the bottom sediments of the *Jequia* lagoon.Alagoas.Brazil

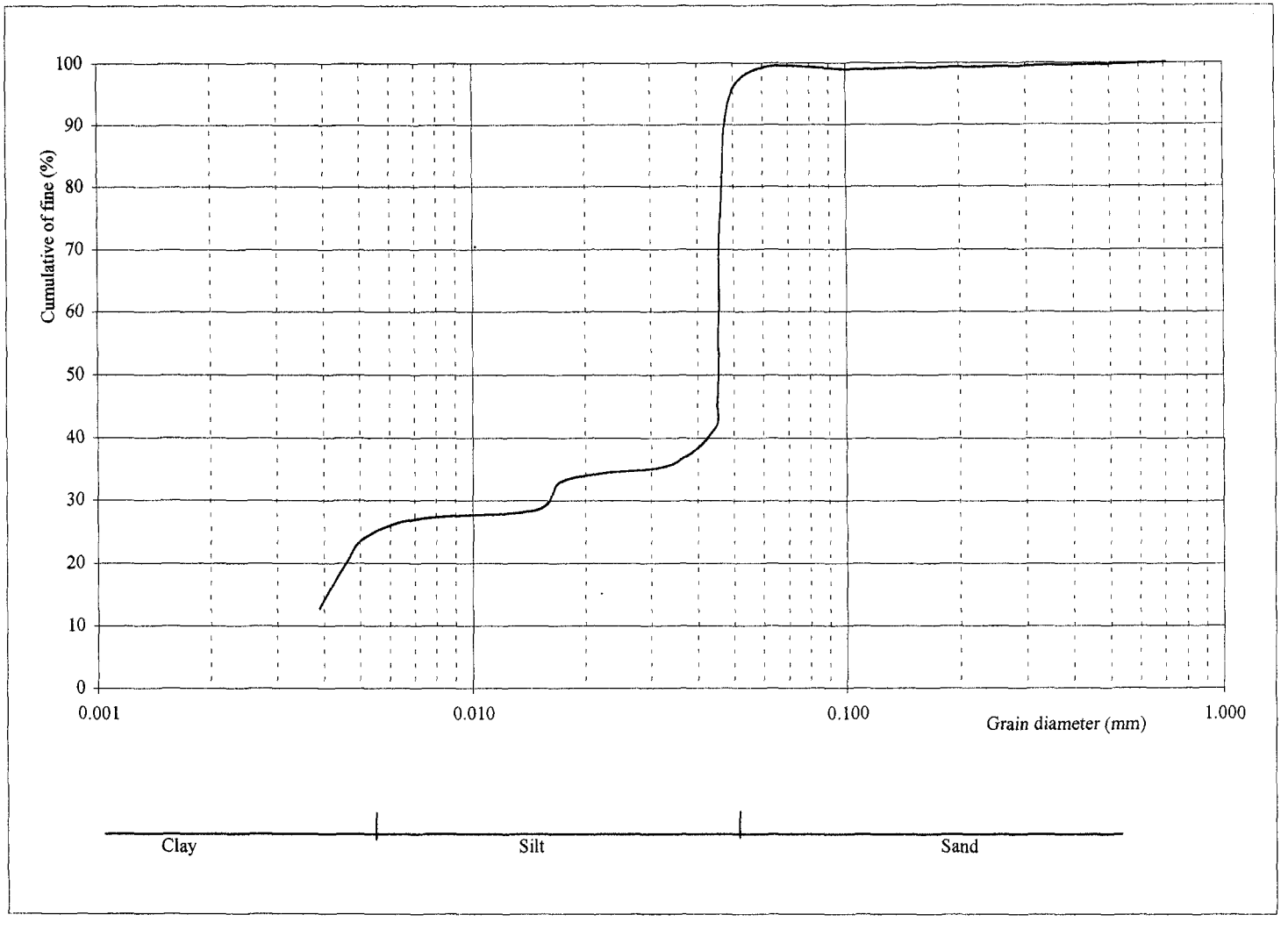

Figure 3.17.Combined sieve and hydrometer raw data Zone IId(37) from the bottom sediments of the *Jequia* lagoon.Alagoas.Brazil.

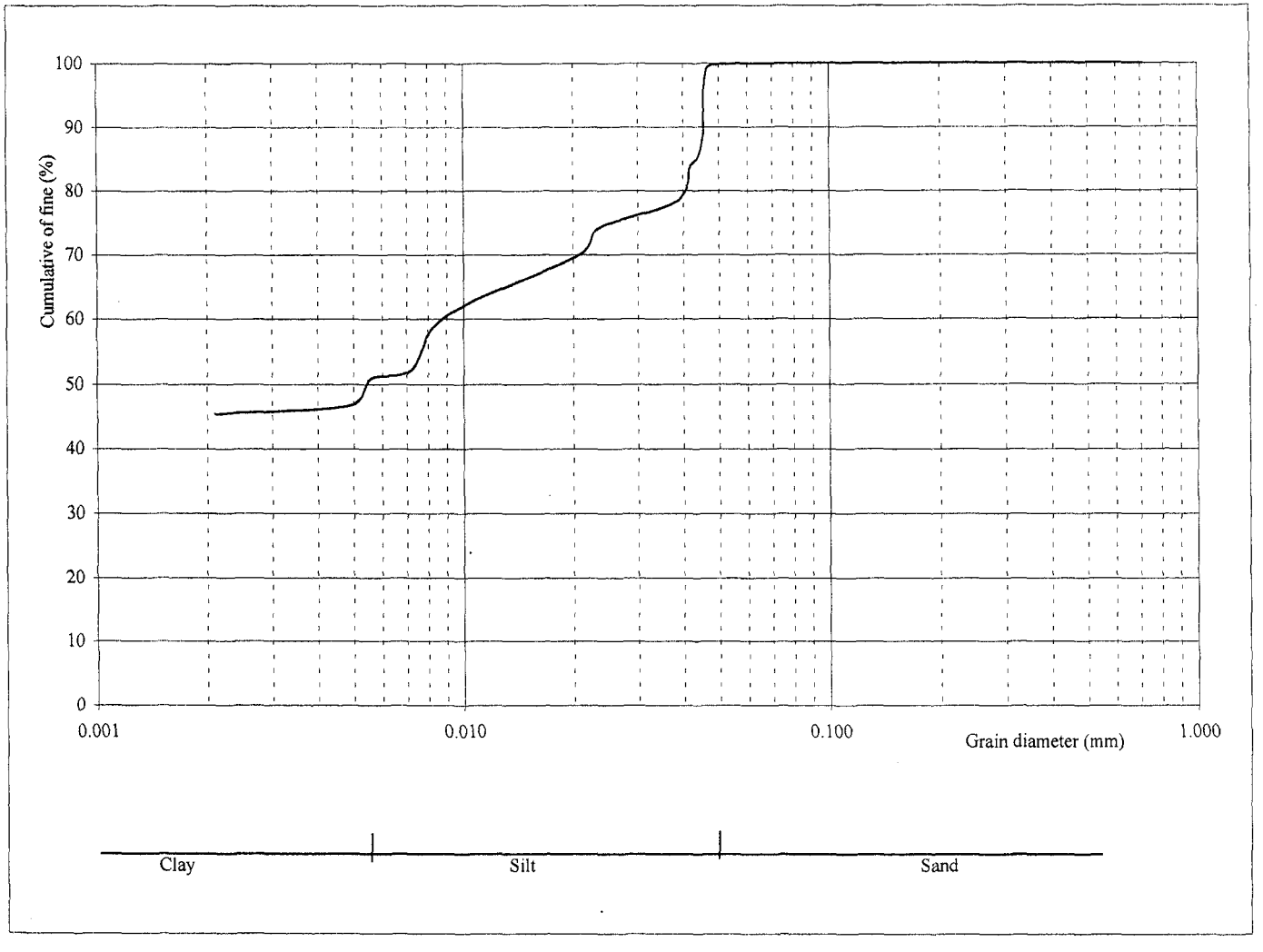

Figure 3.18.Combined sieve and hydrometer raw data Zone IIIa(62) from the bottom sediments of the *Jequia* lagoon.Alagoas.Brazil

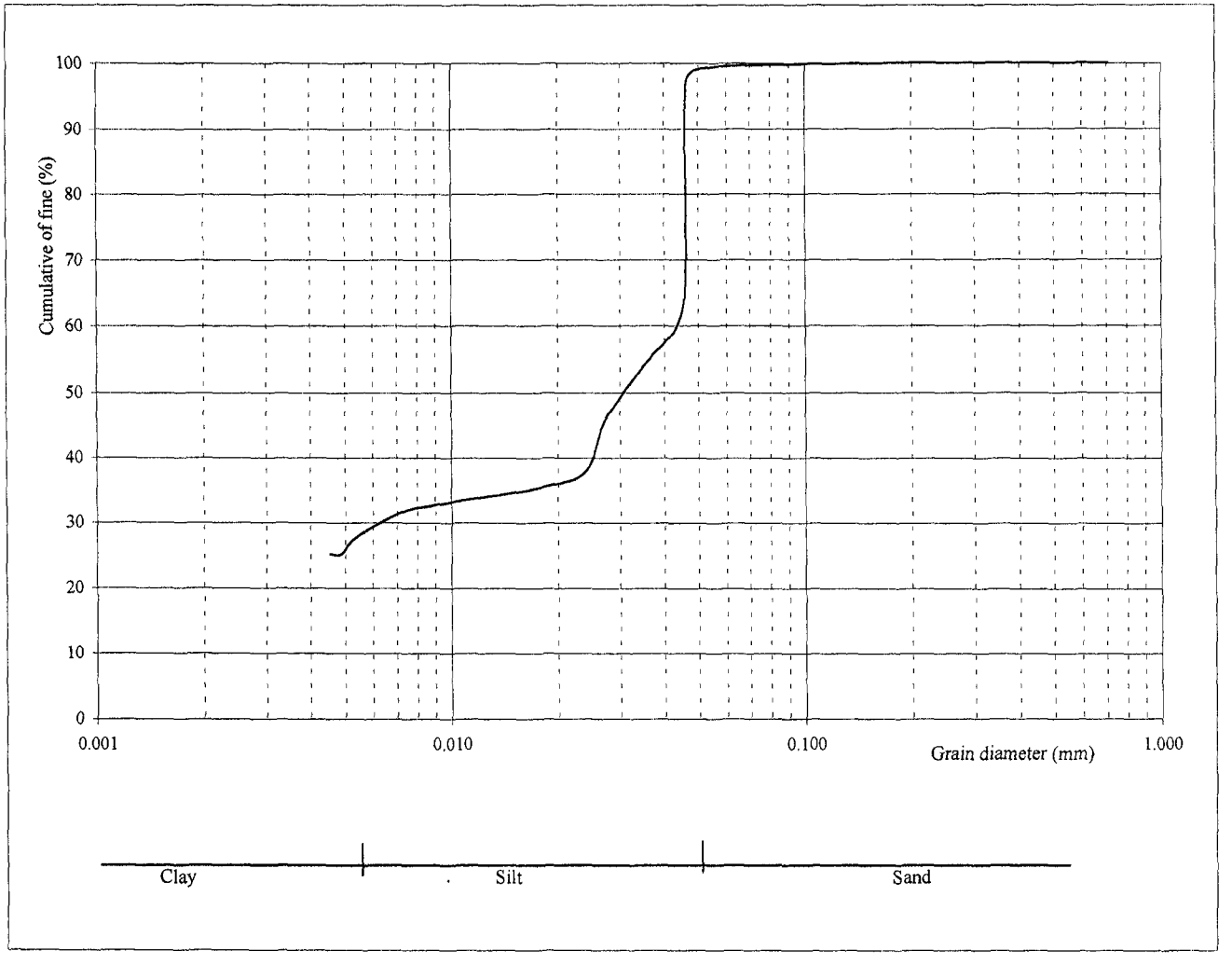

Figure 3.19.Combined sieve and hydrometer raw data Zone IIIa(65) from the bottom sediments of the *Jequia* lagoon.Alagoas.Brazil

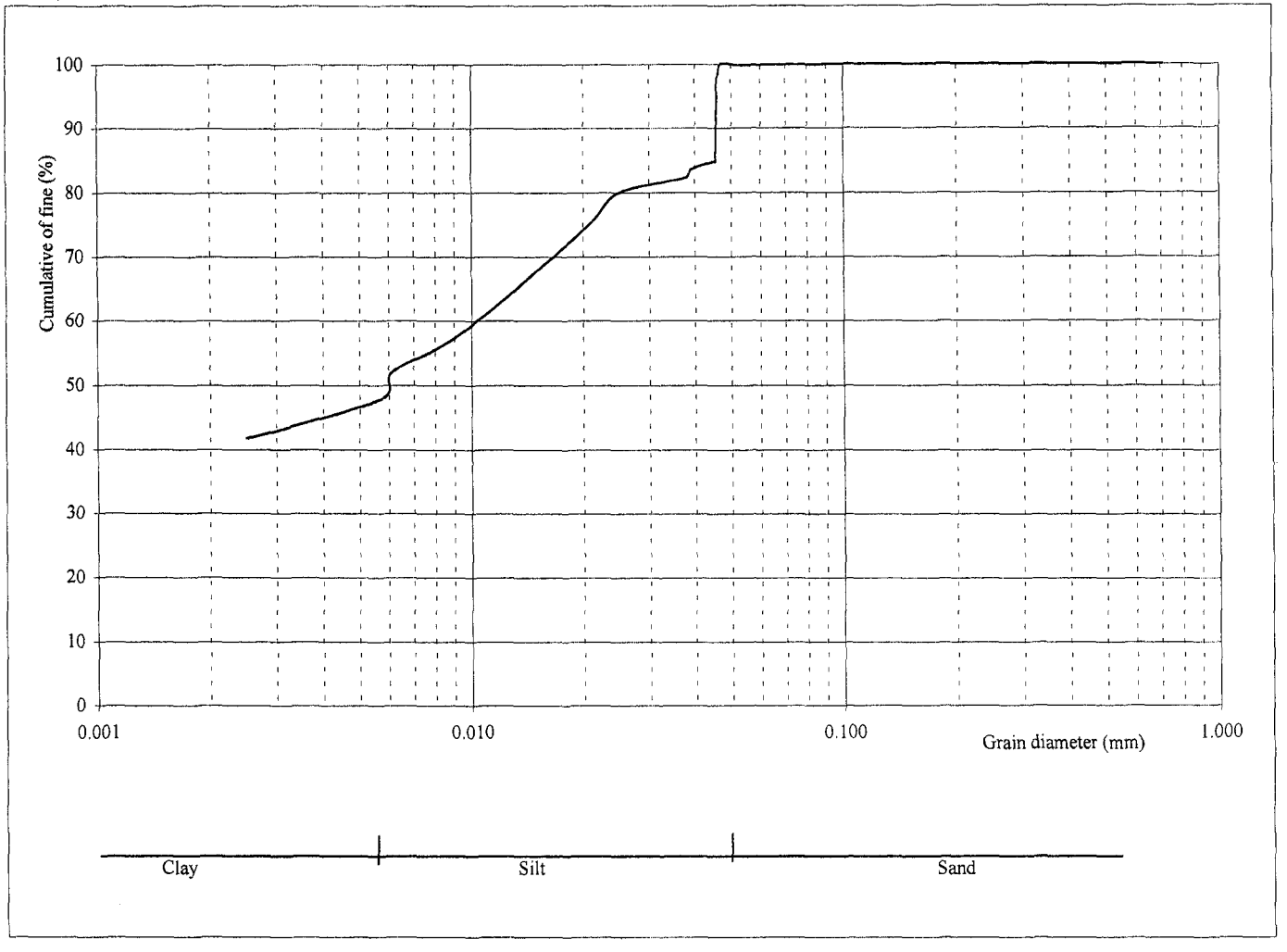

Figure 3.20.Combined sieve and hydrometer raw data Zone IIIb(52) from the bottom sediments of the *Jequia* lagoon.Alagoas.Brazil.

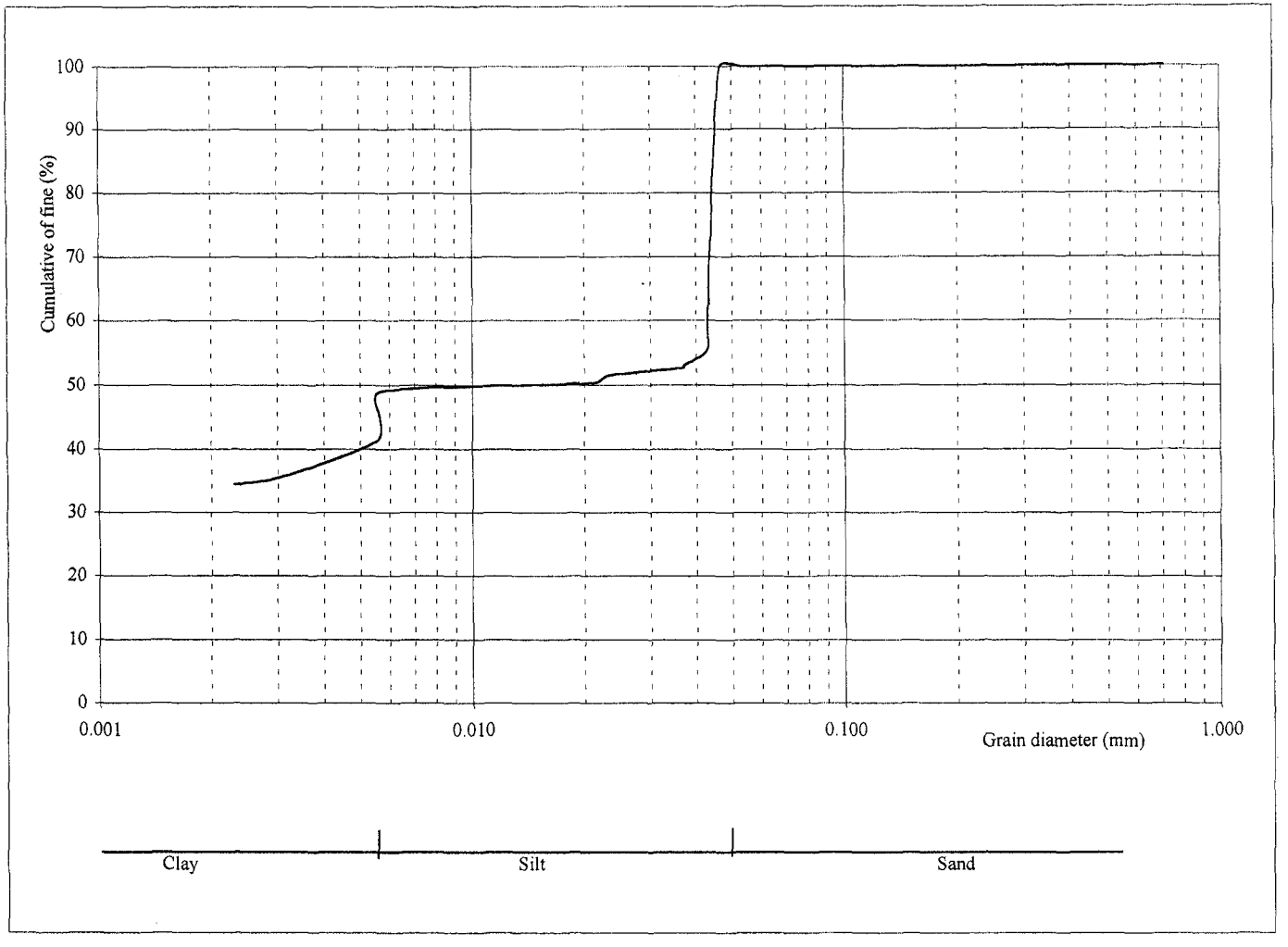

Figure 3.21.Combined sieve and hydrometer raw data Zone IIIb(53) from the bottom sediments of the *Jequia* lagoon.Alagoas.Brazil

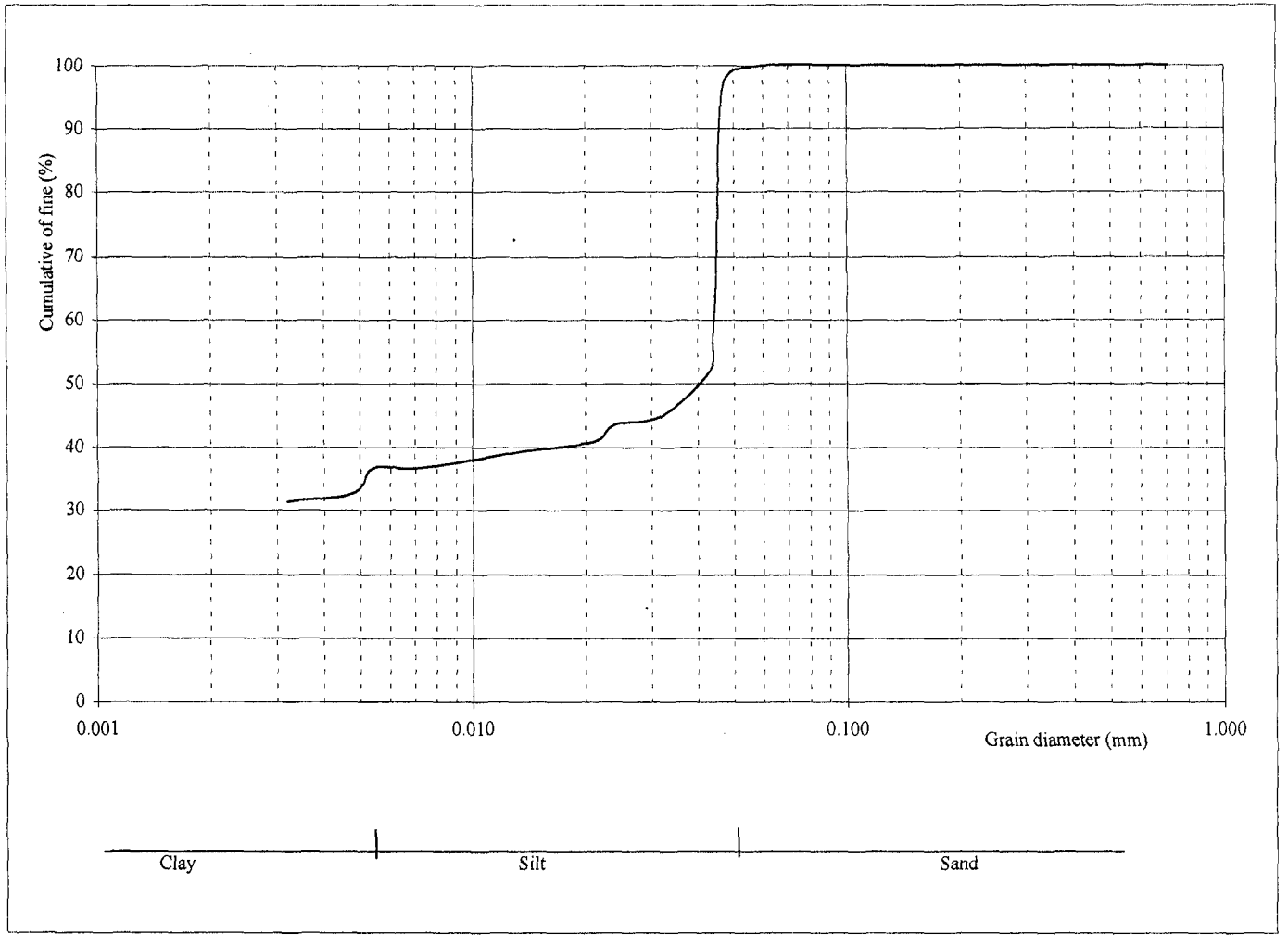

Figure 3.22.Combined sieve and hydrometer raw data Zone IIIb(54) from the bottom sediments of the *Jequia* lagoon.Alagoas.Brazil

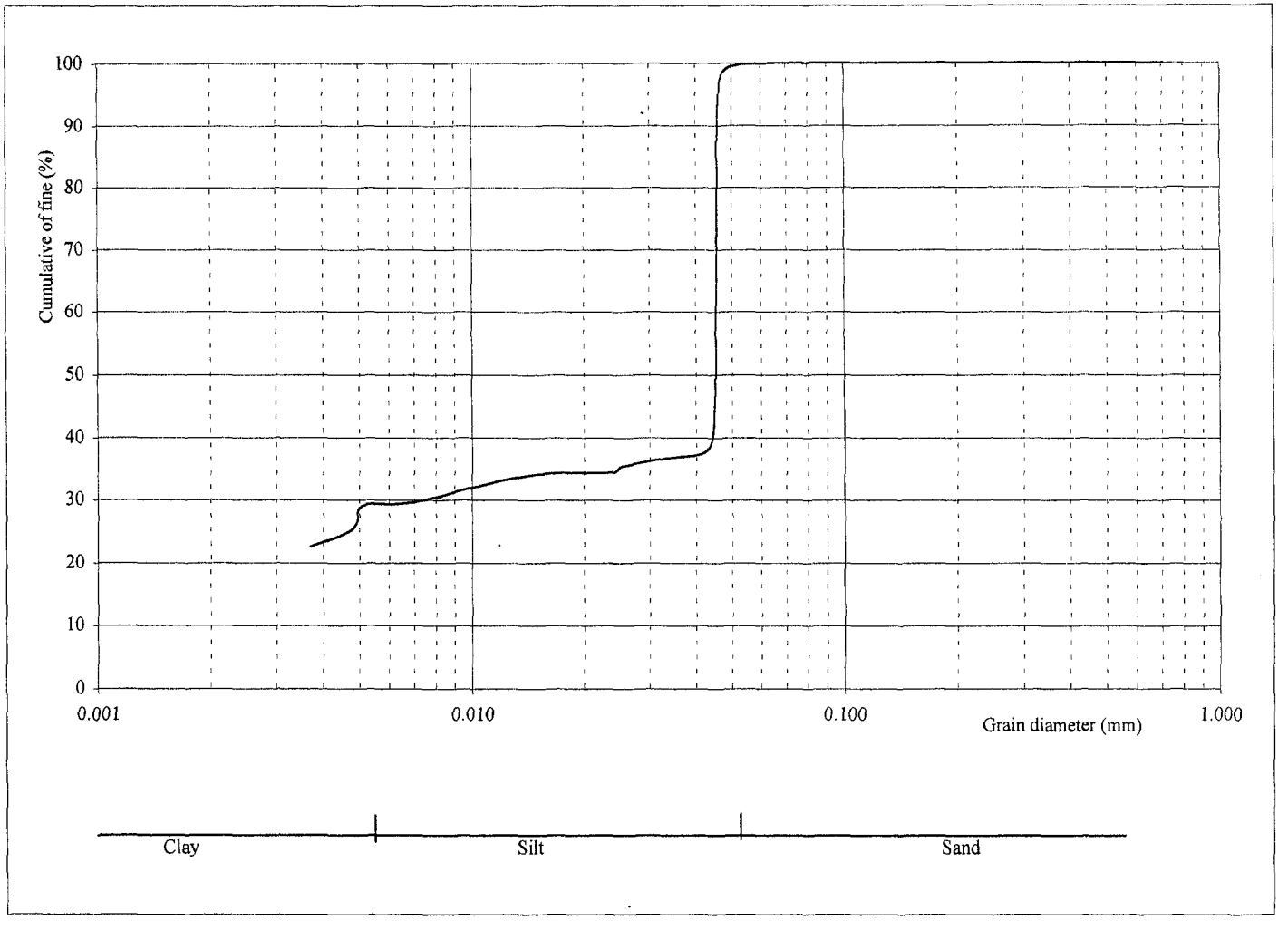

Figure 3.23.Combined sieve and hydrometer raw data Zone IIIb(56) from the bottom sediments of the*Jequia* lagoon.Alagoas.Brazil.

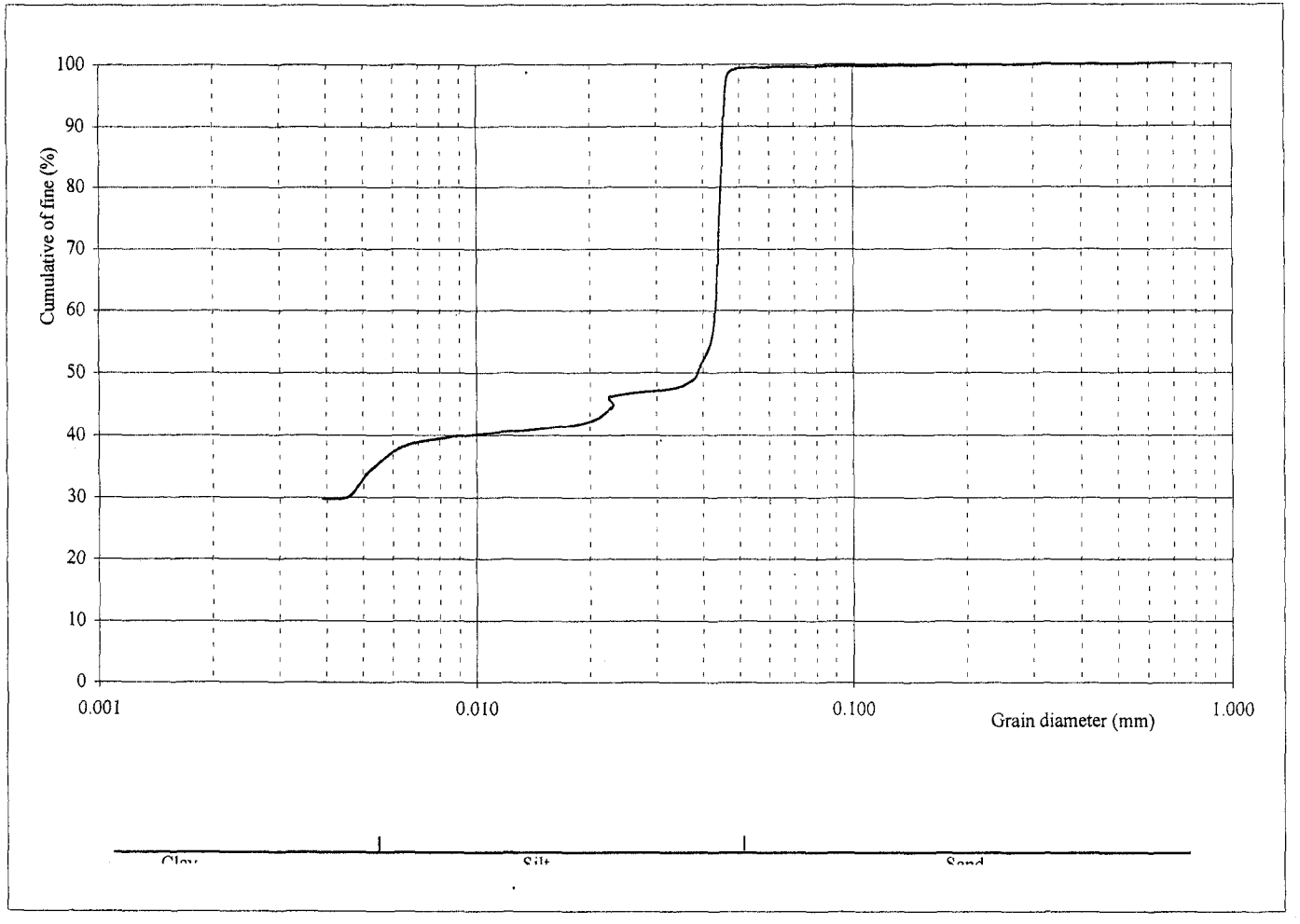

Figure 3.24.Combined sieve and hydrometer raw data Zone IIIc(50) from the bottom sediments of the*Jequia* lagoon.*Alagoas* .Brazil

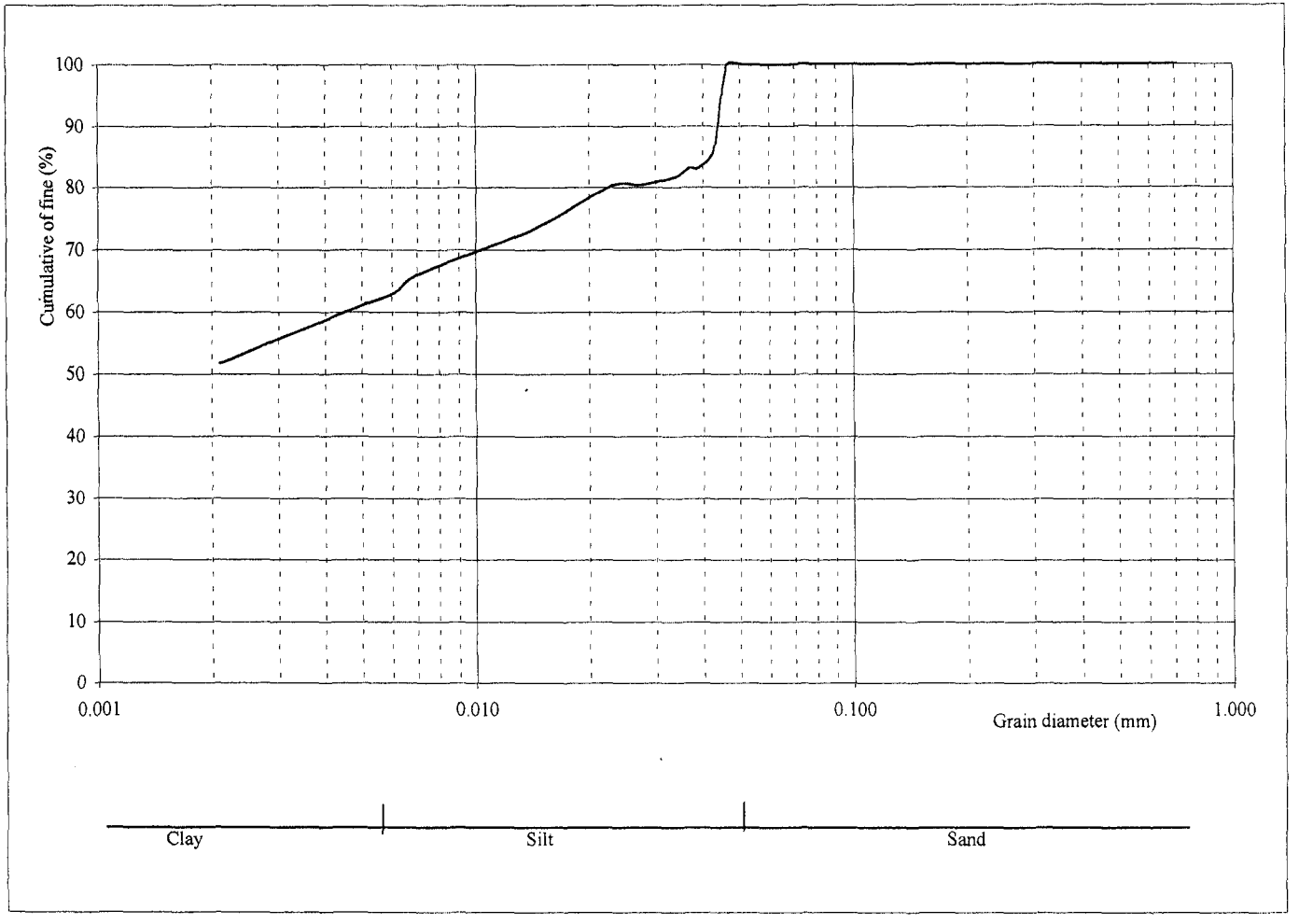

Figure 3.25.Combined sieve and hydrometer raw data Zone IIIc(46) from the bottom sediments of the *Jequia* lagoon.Alagoas.Brazil

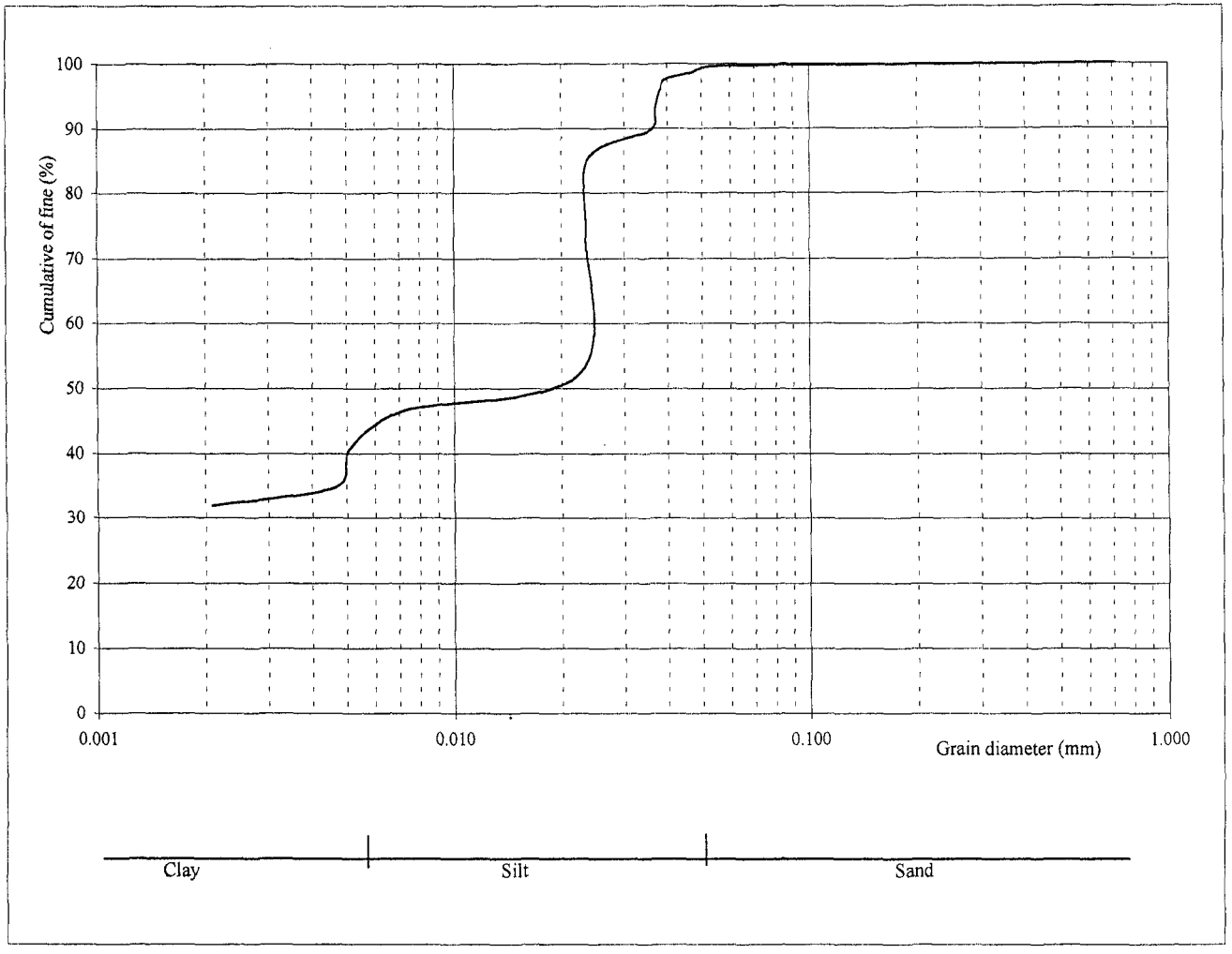

Figure 3.26.Combined sieve and hydrometer raw data Zone IV(19) from the bottom sediments of the *Jequia* lagoon.Alagoas.Brazil

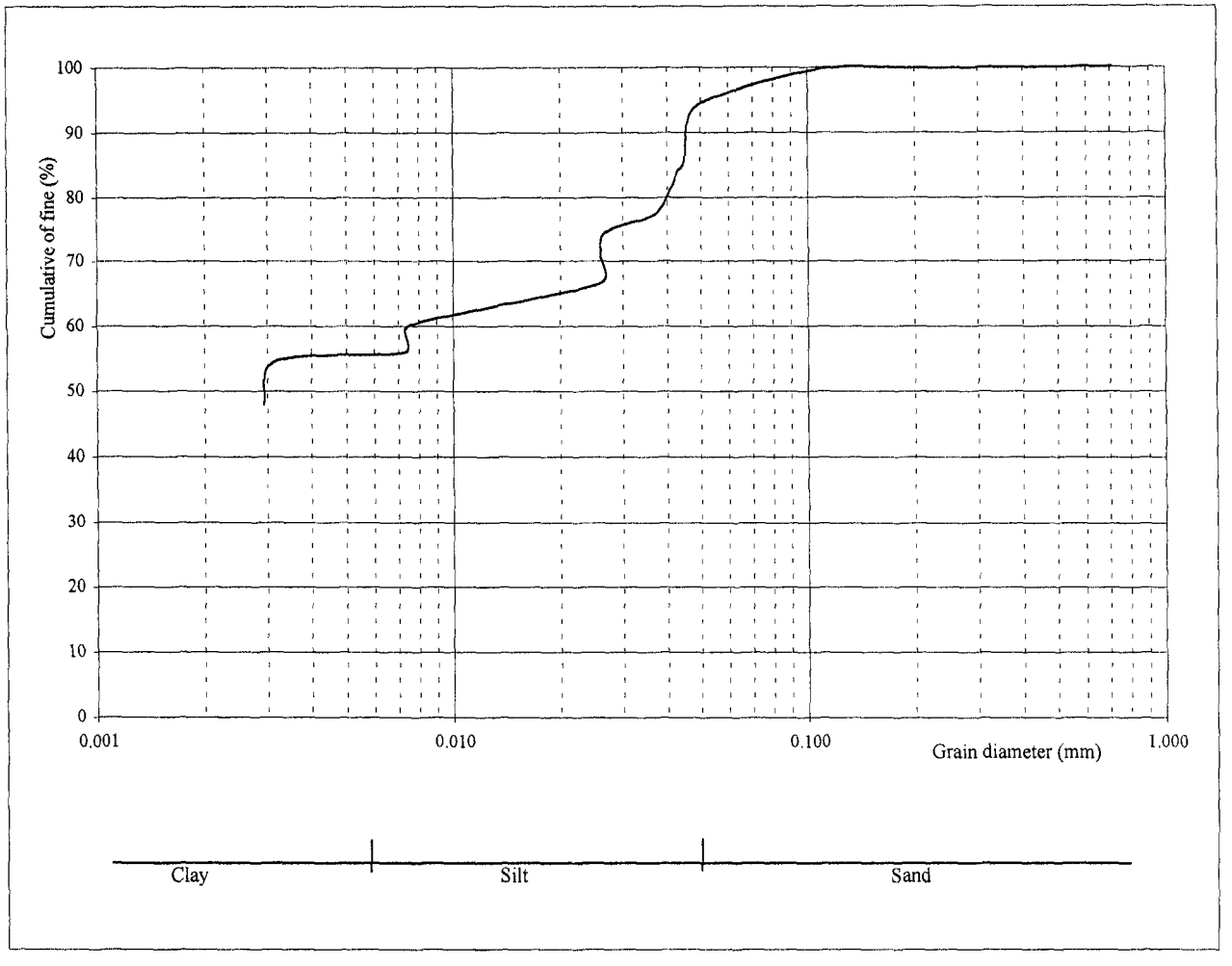

Figure 3.27.Combined sieve and hydrometer raw data Zone IV(20) from the bottom sediments of the *Jequia* lagoon.Alagoas.Brazil

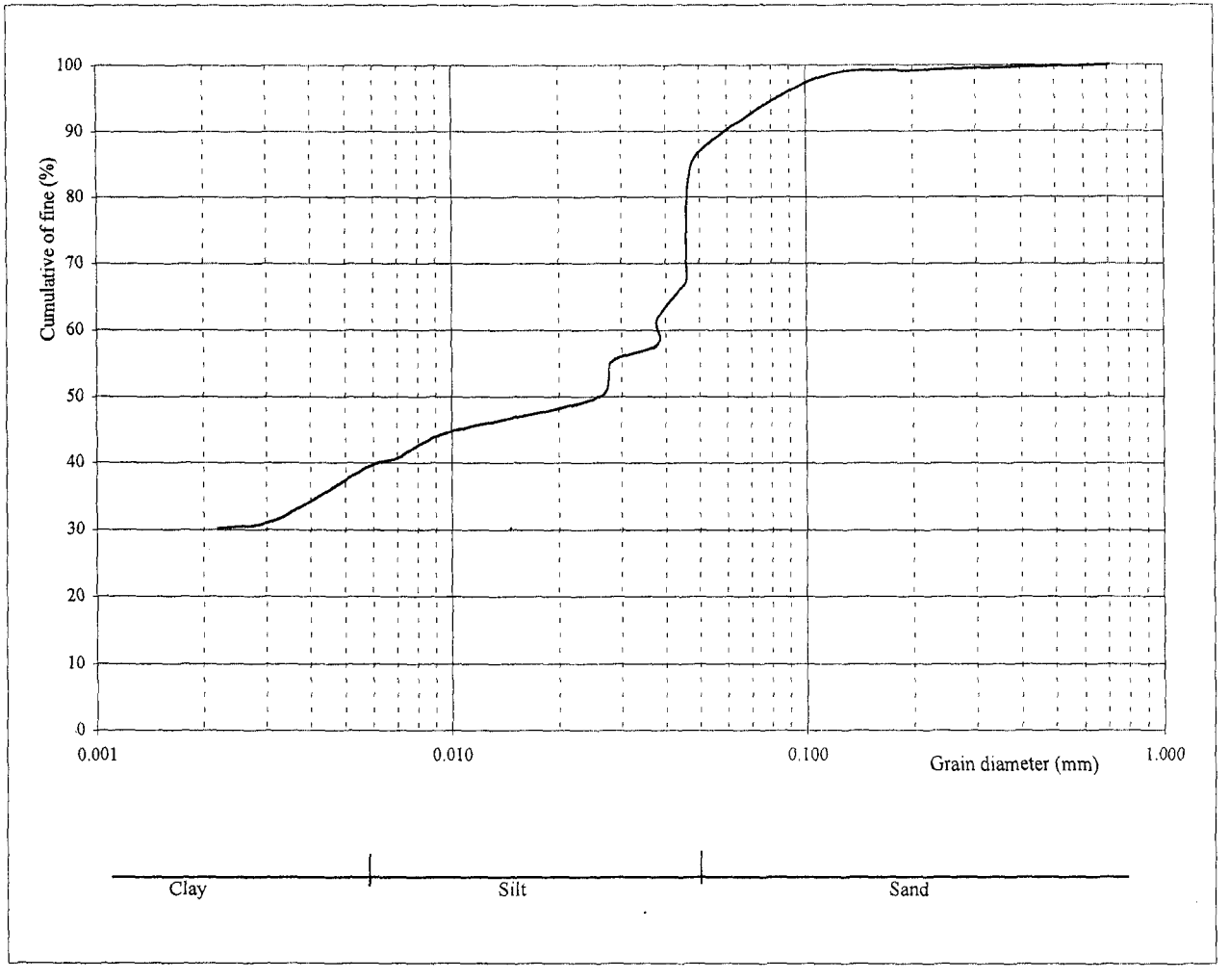

Figure 3.28.Combined sieve and hydrometer raw dataZone IV(22) from the bottom sediments of the *Jequia* lagoon.Alagoas.Brazil

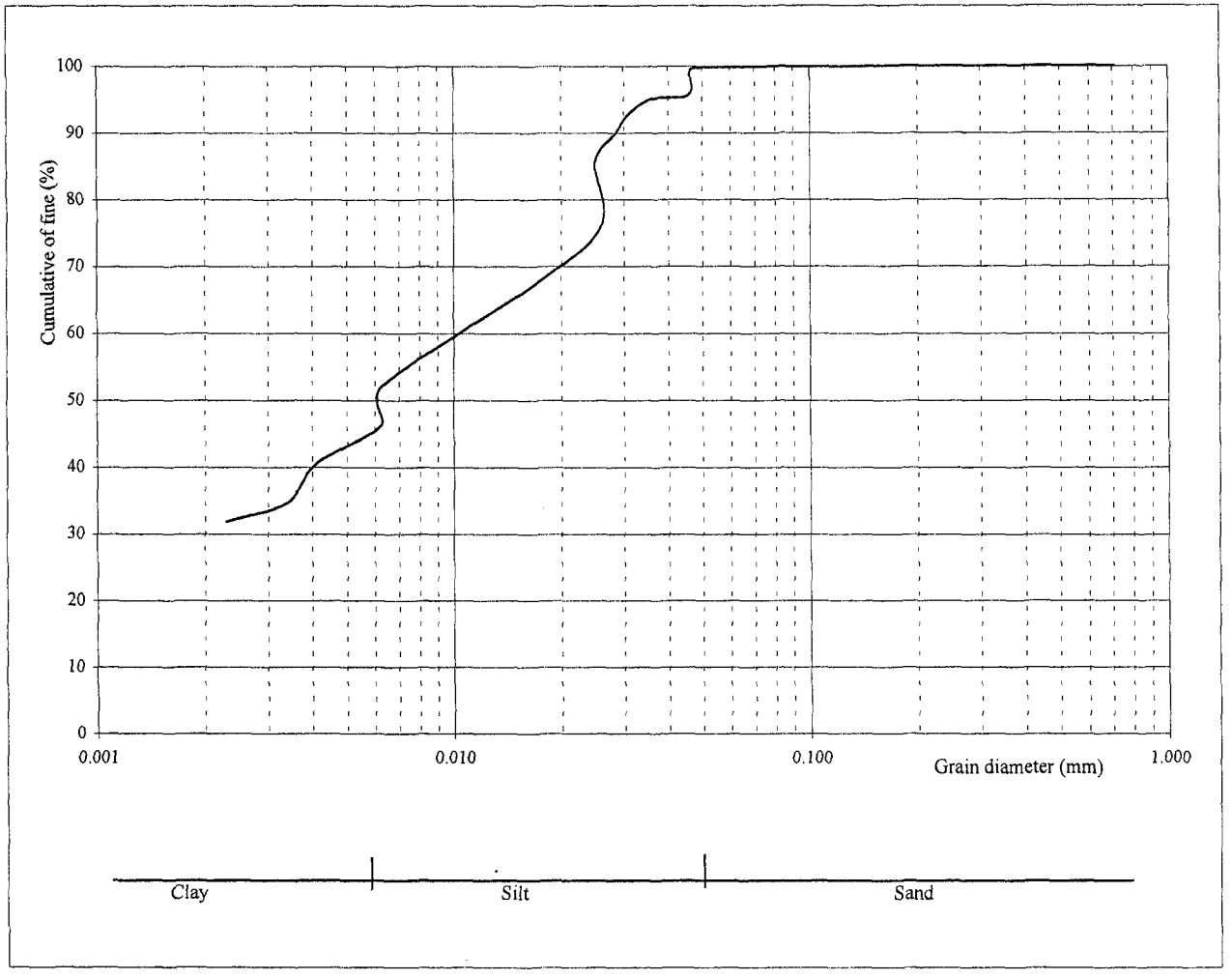

Figure 3.29.Combined sieve and hydrometer raw data Zone IV(23) from the bottom sediments of the *Jequia* lagoon.Alagoas.Brazil

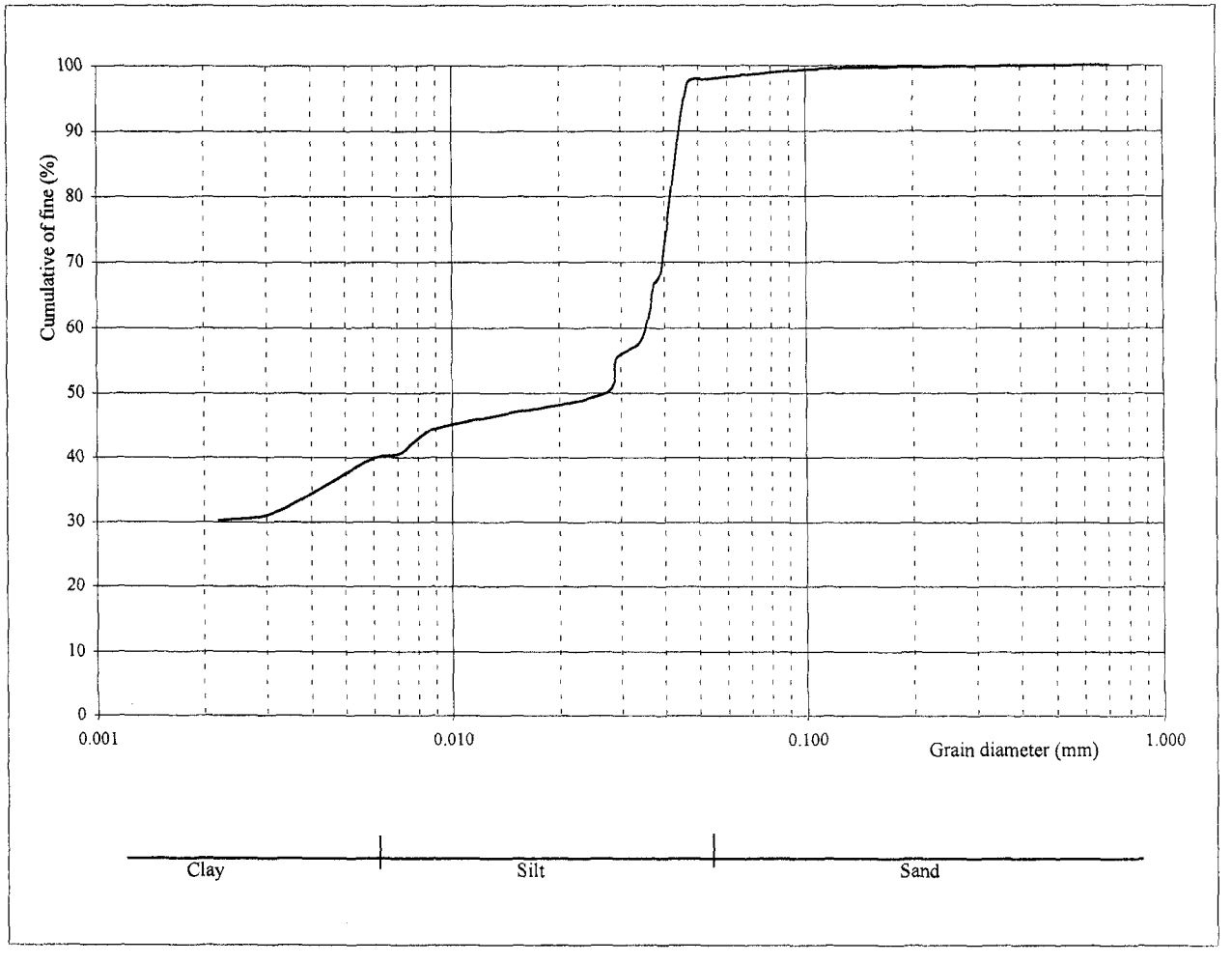

Figure 3.30.Combined sieve and hydrometer raw data Zone IV(24) from the bottom sediments of the *Jequia* lagoon.Alagoas.Brazil.

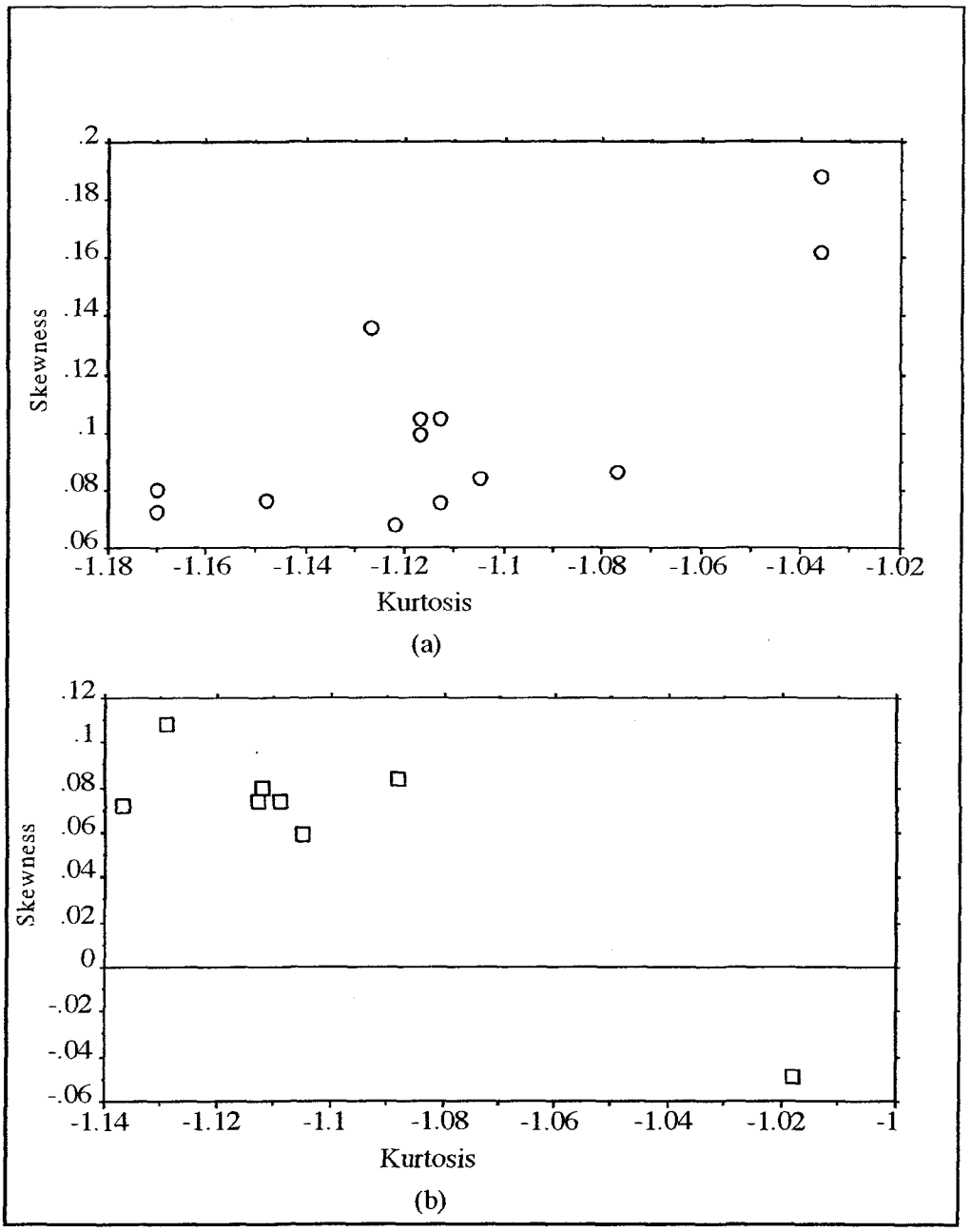

Figure 3.31: Bivariate plot of graphic textural parameters (skewness xkurtosis) of the clastic sediments of the *Jequia* lagoon, *Alagoas*, Brazil. Data from zone I (a) and zone II (b)

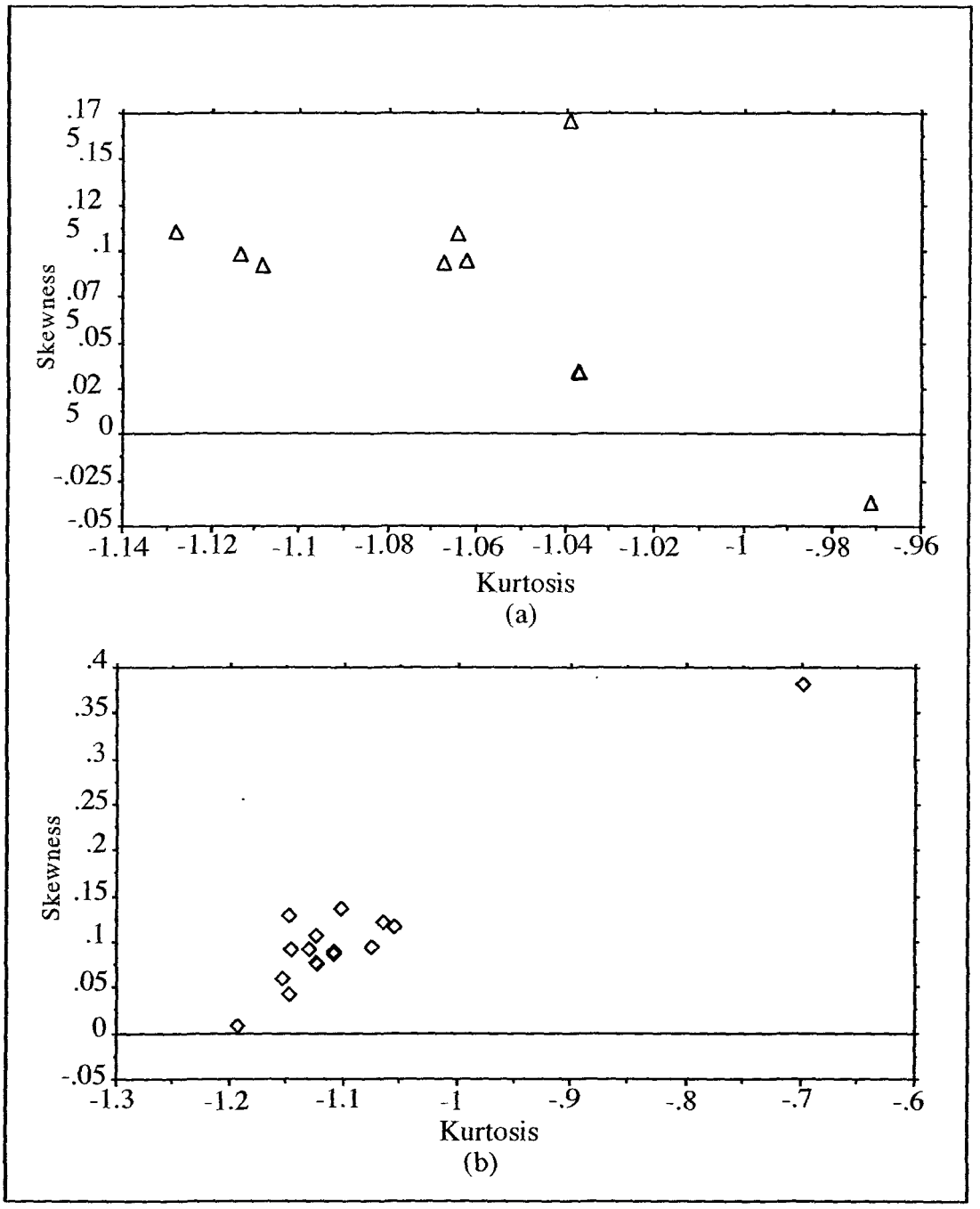

Figure 3.32: Bivariate plot of graphic textural parameters (skewness x kurtosis) of the clastic sediments of the *Jequia* lagoon, *Alagoas*, Brazil. Data from zone III (a) and zone IV(b)

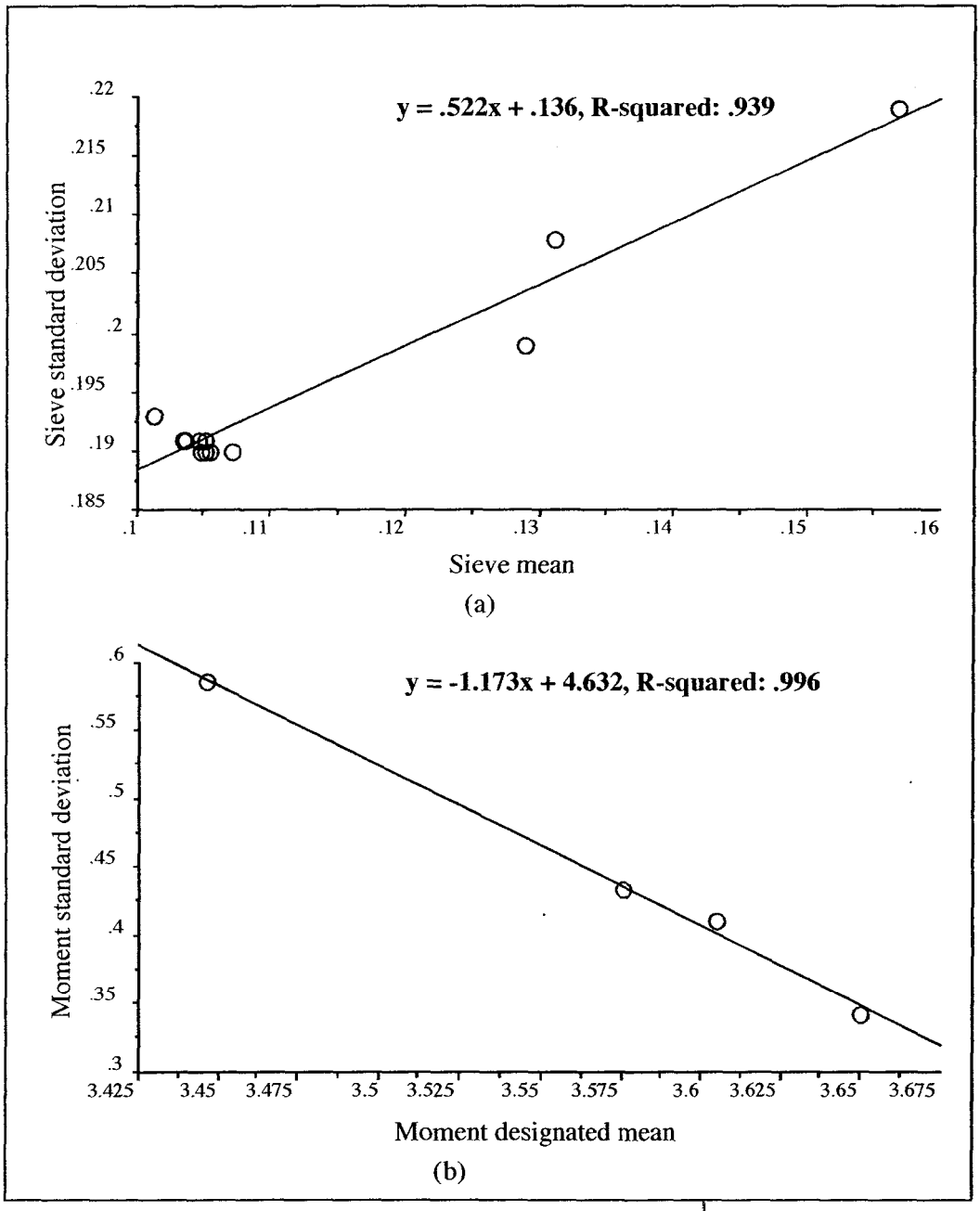

Figure 3.33: Simple regression between the sieve mean and standard deviation (a) and the moment sorting and mean grain size(b)

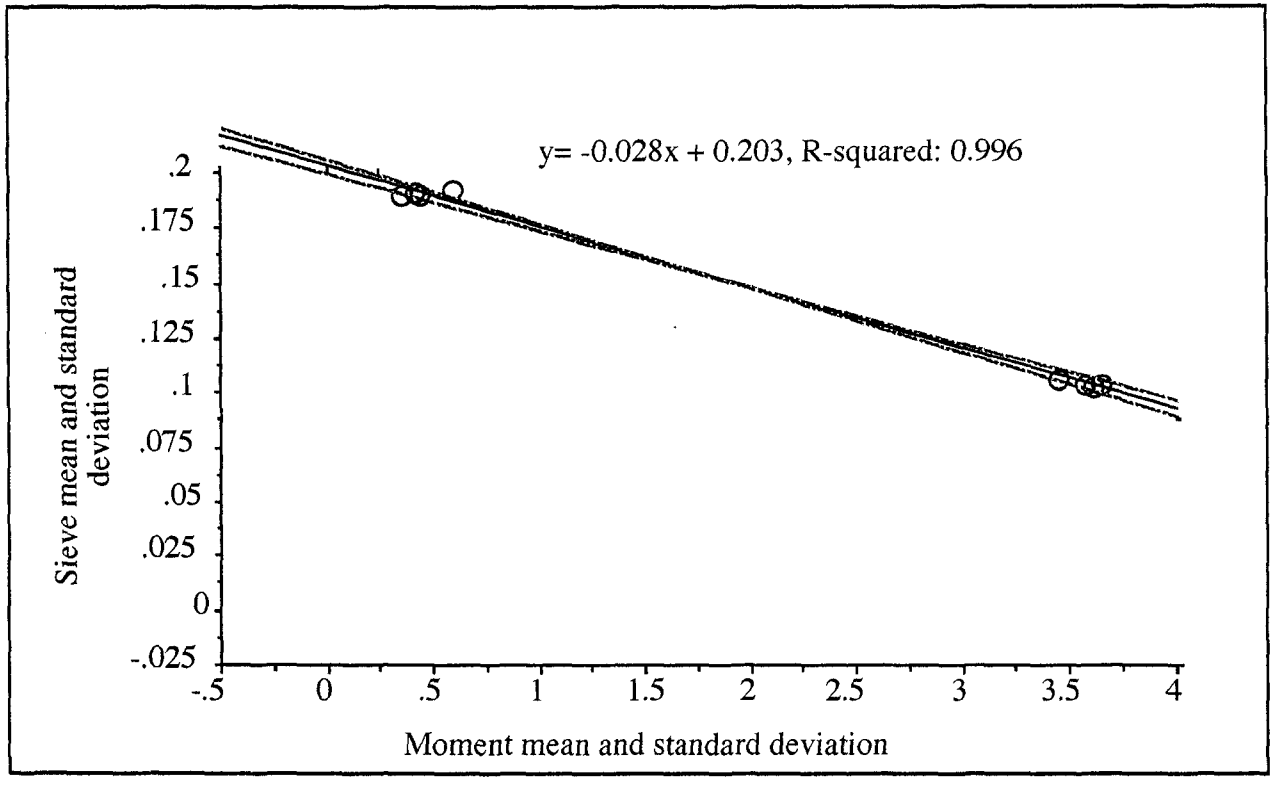

Figure 3.34: Correlation between the sieve and moment statistic measures for the Jequia sediments

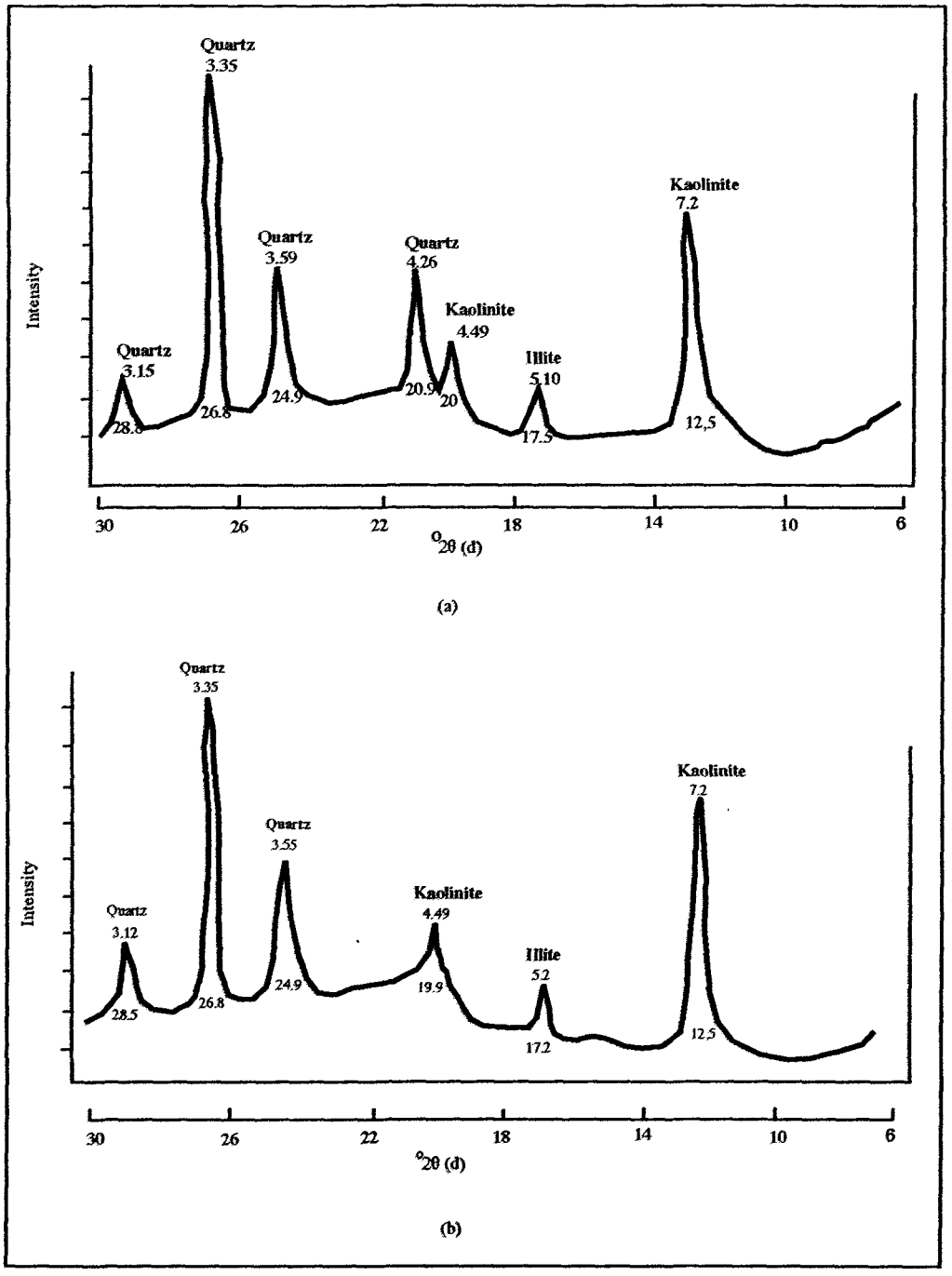

Figure 3.35: Diffraction peaks of the mixture of bottom clay minerals of *Jequia* lagoon, Alagoas, Brazil. Sieve sample < 63 micro from zone I-1 (a) and zone II-80(b).

Kaolinite (trimorphous with Dickite, Nacrite)-$Al_2Si_2O_5(OH)_4$

Illite(Hydromuscovite)-$KAl_2(OH)_2[AlSi_3(O,OH)_{10}]$

Quartz-SiO_2

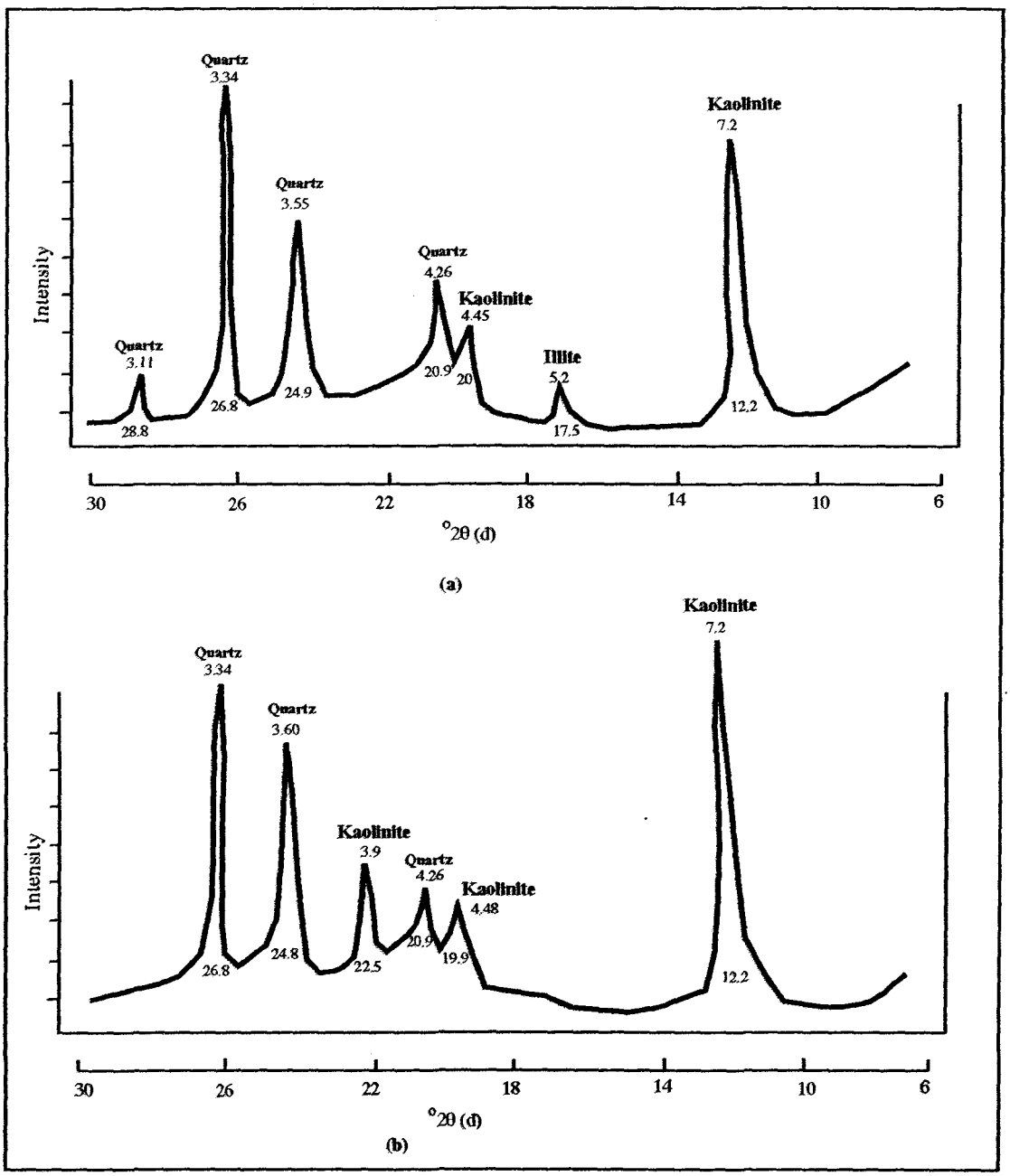

Figure 3.36: Difraction peaks of the mixture of the bottom clay minerals of the*Jequia* lagoon, *Alagoas*, Brazil. Sieve sample < 63 micro from zone III-6 (a) and zone IV-19(b).

Kaolinite (trimorphous with Dickite, Nacrite)-$Al_2 Si_2 O_5 (OH)_4$

Illite(Hydromuscovite)-$KAl_2(OH)_2 [AlSi_3 (O,OH)_{10}]$

Quartz-SiO_2

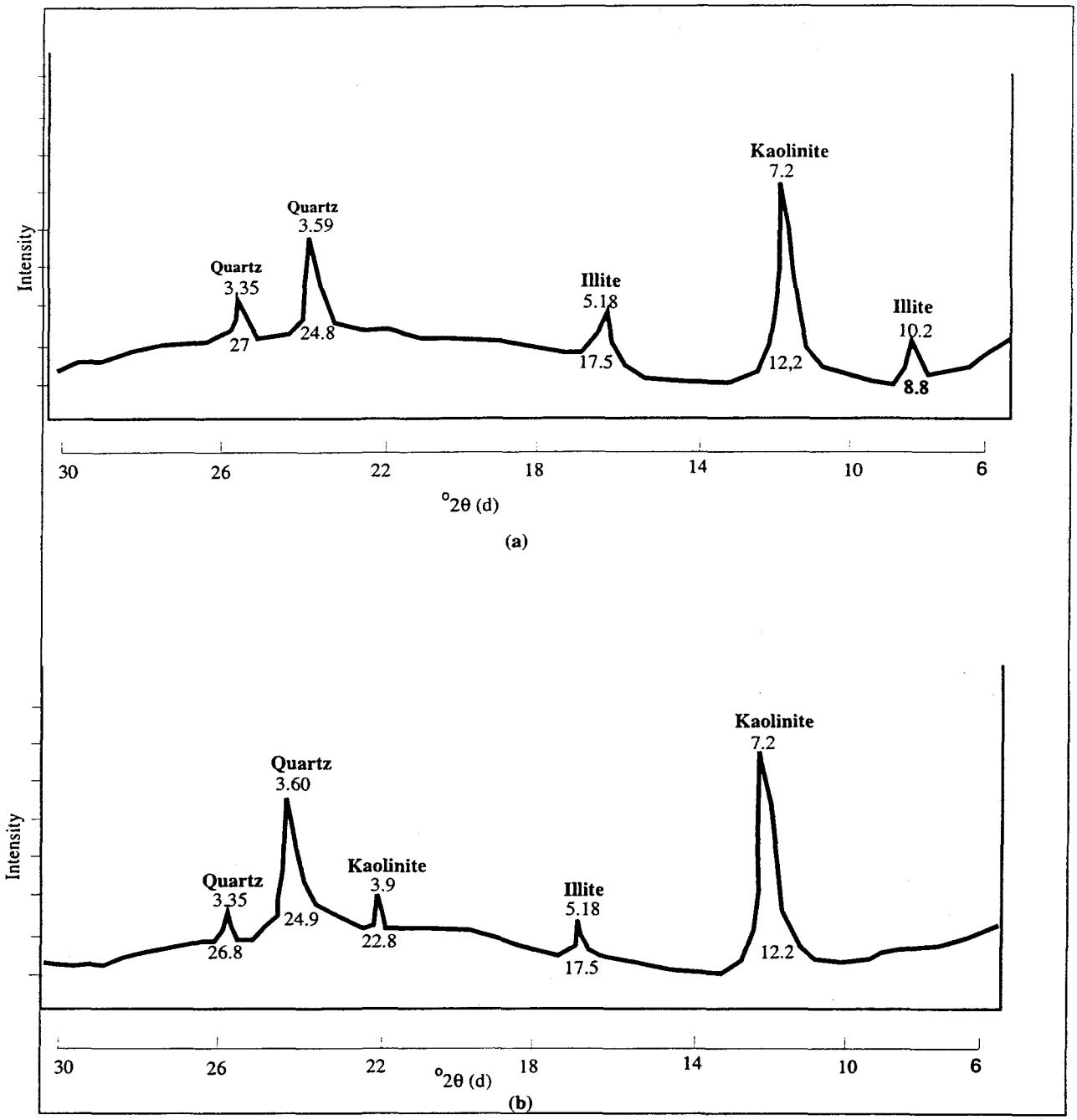

Figure 3.37: Difraction peaks of the mixture of bottom clay minerals of *Jequia* lagoon, *Alagoas*, Brazil. From Sieve samples with size <2 micro from Zone I-site1(a) and Zone II-site80(b)

Kaolinite (trimorphous with Dickite,Nacrite)-$Al_2Si_2O_5(OH)_4$

Illite(Hydromuscovite)-$KAl_2(OH)_2[AlSi_3(O,OH)_{10}]$

Quartz-SiO_2

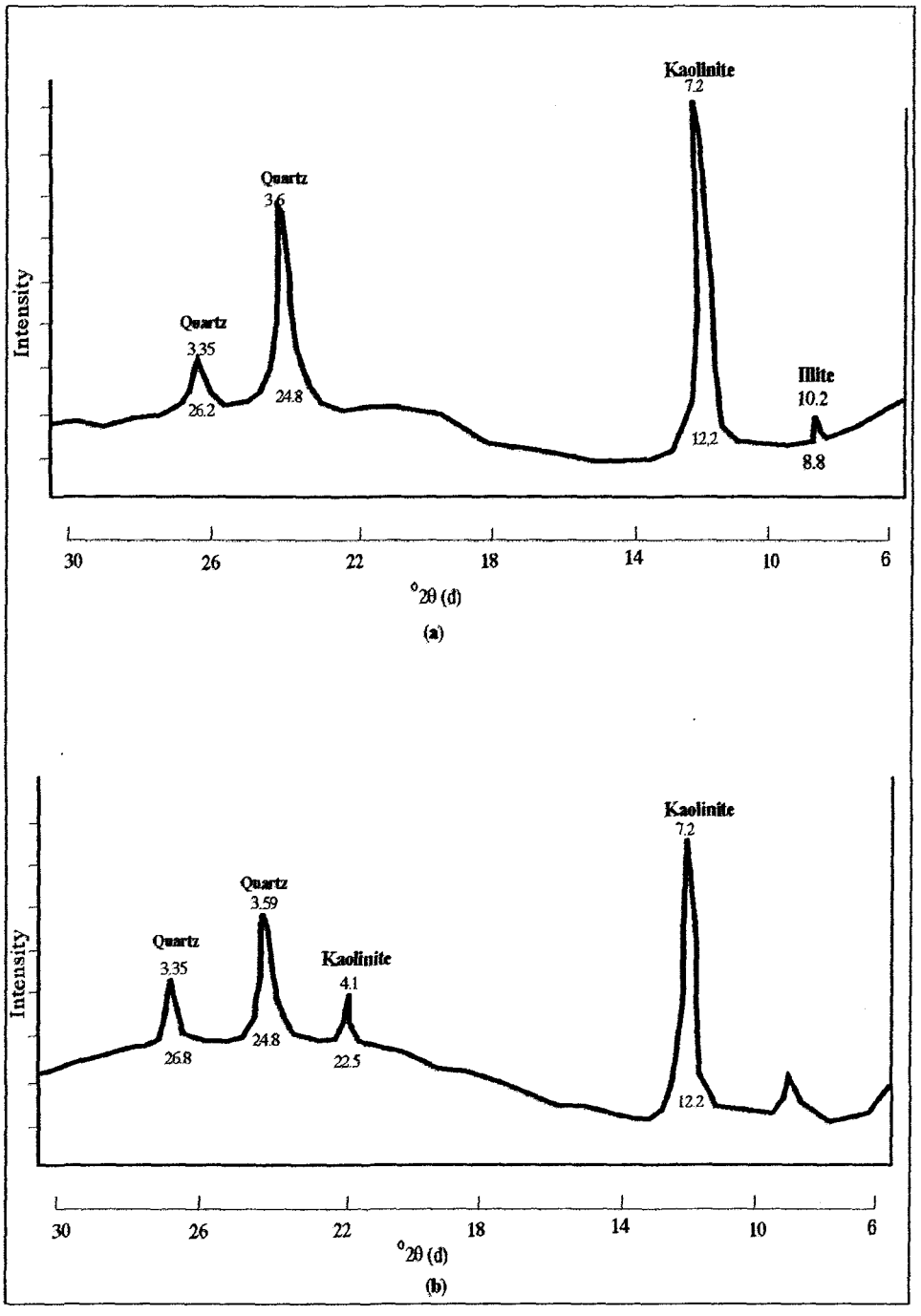

Figure 3.38: Difraction peaks of the mixture of the bottom clay minerals of the*Jequia* lagoon. *Alagoas.* Brazil. From Sieve samples with size < 2 micro from Zone III-site6 (a) and Zone IV-site19(b).

Kaolinite (trimorphous with Dickite, Nacrite)-$Al_2 Si_2 O_5(OH)_4$
Illite(Hydromuscovite)-$KAl_2(OH)_2[AlSi_3(O,OH)_{10}]$
Quartz-SiO_2

	Zone I	Zone IIb	Zone IIIa	Zone IV
Minerals and organic matter	Quartz (99,5%)	Quartz (99,9%)	Quartz (99,7%)	Quartz (99%)
	Mica (0,3%)	Opaque (0,05%)	Opaque (0,1%)	Mica (0,02%)
	Opaque (0,05%)	Wood (0,05%)	Quartz (0,1%)	Rest shell (0,5%)
	Rest shell (0,1%)	-	Leaves (0,1%)	Leaves (0,2%)

(a)

	Zone I	Zone IIb	Zone IIIa	Zone IV
LECO (%)	6,9	2,5	5,3	8,9
Peroxide (%)	7,7	3,65	3,2	8,65

(b)

Table 3.1 Petrographic characteristics (a) and carbon estimates (b) of the bottom sediments of the *Jequia* lagoon. LECO method and peroxide method.

Grade grain size scales (mm)	Sand	Silt	Clay
ABNT	4,8-0,05	0,05-0,005	<0,005
Udden Wentworth	2-0,0765	0,0765-0,0041	<0,0041
	Mud		

(a)

Passega Parameters	Zone I	Zone IIb	Zone IIIa	ZoneIV
C	1 800	1 600	1 590	1 620
M	3 800	3 600	2590	3 620

(b)

Table 3.2. Comparison between two standard grain size grade scales (a). Computation of the C and M Passegas's parameters (b) for the bottom sediments of the *Jequia* lagoon..

Grain Fractions(%)	Zone I(3)	Zone I(4)	Zone I(6)	Zone I(7)	Mean(ZoneI)
Clay	8	2	10	5	10
Silt	70	55	20	70	48.3
Sand	2	3	45	5	15

(a)

Grain Fractions(%)	Zone IIb (76)	Zone IIb(80)	Zone IIb(81)	Mean(ZoneIIb)
Clay	4	10	3	5.6
Silt	75	46	48	56
Sand	1	5	2	2.6

(b)

Grain Fractions(%)	Zone IV(19)	Zone IV(20)	Zone IV(22)	Zone IV(24)	Mean(ZoneIV)
Clay	12	10	10	10	10.5
Silt	70	60	60	67	64
Sand	5	10	10	3	7

(d)

Grain Fractions(%)	Zone IIIa(62)	Zone IIIa(65)	Mean (ZoneIIIa)
Clay	5	5	5
Silt	55	70	62.5
Sand	0	1	0.5

(c)

Table 3.3. Graphic estimation of grain fractions for Zones I(a), IIb(b), IIIa(c) and IV(d) from cumulative curves.

zoneI(3)	zoneI(3)	zone I (3)	zoneI(3)	zoneI(4)	zoneI(4)	zone I(4)	zoneI(4)
Raw weight	Cumulative weight %	Combined sieve-hydromter grain diameter(mm)	Cumulative % finer	Raw weight	Cumulative weight %	Combined sieve-hydromter grain diameter(mm)	Cumulative % finer
0	0	0.71	100	0	0	0.71	100
0	0	0.45	100	0.02	0.042	0.45	99.95
0.03	0.059	0.21	99.94	0	0.042	0.21	99.95
0.04	0.138	0.11	99.86	0.09	0.235	0.11	99.76
0.26	0.653	0.053	99.34	1.22	2.851	0.053	97.14
2.28	5.177	0.0465	94.82	13.9	32.65	0.0465	67.35
		0.045	83.9			0.46	61.79
		0.043	73.48			0.043	52.28
		0.042	52.48			0.039	52
		0.037	47.23			0.038	49.91
		0.027	39.36			0.024	47.53
		0.022	34.12			0.019	47
		0.0095	28.86			0.0081	45.15
		0.009	28.8			0.0062	42.78
		0.0055	26.24			0.0059	40.45
		0.003	23.61			0.0033	40
		0.0022	23.61			0.0023	38.02

zoneI(6)	zoneI(6)	zone I(6)	zoneI(6)	zoneI(7)	zoneI(7)	zone I(7)	zoneI(7)
Raw weight	Cumulative weight %	Combined sieve-hydromter grain diameter(mm)	Cumulative % finer	Raw weight	Cumulative weight %	Combined sieve-hydromter grain diameter(mm)	Cumulative % finer
0.35	0.728	0.71	99.27	0	0	0.71	100
1.57	3.994	0.45	96	0	0	0.45	100
2.56	9.319	0.21	90.68	0	0	0.21	100
9.38	28.82	0.11	71.18	0	0	0.11	100
6.87	43.11	0.053	56.89	1.05	1.722	0.053	98.28
27.33	99.96	0.0465	49.5	8.03	14.89	0.0465	85.1
		0.042	48.77			0.0395	59.74
		0.039	44.13			0.039	48.99
		0.031	44.13			0.036	35.84
		0.029	44.13			0.03	31.06
		0.026	44.13			0.025	29.87
		0.024	41			0.022	28.67
		0.0082	39.4			0.0082	27.48
		0.0064	37.16			0.0073	25.09
		0.003	34.84			0.0058	23.89
		0.0034	32.51			0.0034	21.5
		0.0024	30.19			0.0024	19.12

Table 3.4.Combined sieve and hydrometer rawdata for Zone-I (sample sites) from the bottom sediments of the*Jequia* lagoon.*Alagoas* .Brazil

ZoneIIa(10)	ZoneIIa(10)	ZoneIIa(10)	ZoneIIa(10)Cum%
Raw weight	Cumulative weight %	Combined sieve-hydromter grain diameter(mm)	Cumulative % finer
0	0	0.71	100
0.02	0.049	0.45	99.95
0	0.049	0.21	99.95
0	0.049	0.11	99.95
0.42	1.092	0.053	98.9
7.37	19.4	0.0465	88.6
		0.045	83.82
		0.043	71.12
		0.039	64.77
		0.038	63.5
		0.024	59.69
		0.027	55.88
		0.0085	49.53
		0.00615	44.52
		0.0057	39.37
		0.0032	38.1
		0.00222	36.83

ZoneIIa(13=12)	ZoneIIa(13=12)	ZoneIIa(13=12)	ZoneIIa(13=12)
Raw weight	Cumulative weight %	Combined sieve-hydromter grain diameter(mm)	Cumulative % finer
0	0	0.71	100
0	0	0.45	100
0.03	0.071	0.21	99.93
0.02	0.118	0.11	99.88
0.15	0.474	0.053	99.52
1.6	4.27	0.0465	95.73
		0.36	73.02
		0.038	70.37
		0.037	66.38
		0.0225	58.42
		0.0275	54.43
		0.0095	47.8
		0.0074	43.81
		0.0056	39.83
		0.0049	37.17
		0.00215	35.85
		0.00205	34.52

ZoneIIa(15)	ZoneIIa(15)	ZoneIIa(15)	ZoneIIa(15)
Raw weight	Cumulative weight %	Combined sieve-hydromter grain diameter(mm)	Cumulative % finer
0	0	0.71	100
0	0	0.45	100
0.01	0.03	0.21	99.97
0.05	0.181	0.11	99.82
0.71	2.331	0.053	97.67
1.73	7.57	0.0465	92.43
		0.039	82.71
		0.038	79.86
		0.035	79.86
		0.034	77
		0.022	72.73
		0.025	71.3
		0.01	57.04
		0.007	48.48
		0.005	45.63
		0.0047	41.35
		0.0039	39.93

ZoneIIa(16)	ZoneIIa(16)	ZoneIIa(16)	ZoneIIa(16)
Raw weight	Cumulative weight %	Combined sieve-hydromter grain diameter(mm)	Cumulative % finer
0	0	0.71	100
0.02	0.052	0.45	99.95
0.02	0.104	0.21	99.89
0.04	0.209	0.11	99.79
0.18	0.684	0.053	99.32
0.59	2.24	0.0465	99.81
		0.043	98.8
		0.041	98.2
		0.0375	97.76
		0.0365	96.87
		0.036	88.41
		0.027	68.45
		0.01	54.19
		0.0073	51.34
		0.0053	48.48
		0.0047	45.63
		0.0021	44.21

zoneIal(17)	zoneIIa(17)	zoneIIa(17)	zoneIIa(17)
raw weight	Cumulative weight %	Combined sieve-hydrometer grain diameter(mm)	Cumulative % finer
0	0	0.71	100
0	0	0.45	99
0	0	0.21	99.35
0.01	0.021	0.11	99.98
0.11	0.258	0.053	99.74
0.3	0.904	0.0465	99.09
		0.046	90.16
		0.045	88.87
		0.039	83.72
		0.038	82.43
		0.0295	78.57
		0.028	73.42
		0.0093	66.98
		0.0062	61.82
		0.0041	57.96
		0.0032	54.09
		0.00225	48.94

Table 3.5. Combined sieve and hydrometer rawdata for Zone-IIa(sample sites) from the bottom sediments of the*Jequia* lagoon.Alagoas.Brazil

Zone IIb(76)	Zonellb(76)	Zonellb(76) Combined hydrometer	Zonellb(76) sieve-grain	Zonellb(76)
Raw weight	Cumulative weight %	diameter(mm)		Cumulative % finer
0	0		0.71	100
0	0		0.45	99.92
0.04	0.08		0.21	99.9
0.02	0.12		0.11	99.88
0.26	0.643		0.053	99.36
0.71	2.072		0.0465	97.9
			0.046	83.1
			0.045	65.95
			0.043	56.72
			0.042	51.44
			0.385	47.48
			0.0245	40.89
			0.0285	39.57
			0.0091	36.93
			0.0074	34.35
			0.00585	32.98
			0.0032	30.34

Zone IIb(80)	Zonellb(80)	Zonellb(80) Combined hydrometer	Zonellb(80) sieve-grain	Zonellb(80)
Raw weight	Cumulative weight %	diameter(mm)		Cumulative % finer
0	0		0.71	100
0.02	0.055		0.45	99.95
0.01	0.082		0.21	99.92
0.02	0.137		0.11	99.86
1.27	3.687		0.053	96.31
6.17	20.92		0.0465	79.08
			0.0455	71.61
			0.045	66.5
			0.043	66.5
			0.037	63.94
			0.024	63.94
			0.0235	58.82
			0.009	56.27
			0.006	51.15
			0.004	46.04
			0.0031	43.48
			0.00225	40.92

Zonellb(81)	zonellb(81)	zonellb(81) Combined hydrometer	zonellb(81) sieve-grain	zonellb(81)
Raw weight	Cumulative weight %	diameter(mm)		Cumulative % finer
0	0		0.71	100
0.04	0.17		0.45	99.83
0.03	0.297		0.21	99.7
0.02	0.382		0.11	99.62
0.2	1.234		0.053	98.76
2.65	12.52		0.0465	87.48
			0.046	71.62
			0.046	66.5
			0.045	66.5
			0.038	63.94
			0.0285	63.94
			0.026	58.82
			0.00935	56.27
			0.006	47.32
			0.0057	42.2
			0.0031	40.92
			0.00225	38.37

Zonellb(82)	Zonellb(82)	Zonellb(82) Combined hydrometer	Zonellb(82) sieve-grain	Zonellb(82)
Raw weight	Cumulative weight %	diameter(mm)		Cumulative % finer
0	0		0.71	100
0	0		0.45	100
0	0		0.21	100
0	0		0.11	99.9
0.08	0.166		0.053	99.83
0.42	1.042		0.0465	98.96
			0.0455	90.37
			0.0435	87.55
			0.043	84.72
			0.036	80.49
			0.022	80.49
			0.021	74.84
			0.0091	69.47
			0.0072	59.31
			0.0055	56.48
			0.0048	49.42
			0.0021	48.01

Table 3.6. Combined sieve and hydrometer rawdata for Zone-IIb(sample sites) from the bottom sediments of Jequia lagoon.Alagoas.Brazil.

ZoneIId(27)	ZoneIId(27)	ZoneIId(27) Combined sieve-hydrometer grain	ZoneIId(27)
Raw weight	Cumulative weight %	diameter(mm)	Cumulative % finer
		0.71	100
		0.45	100
		0.21	99.3
0	0	0.11	99.19
0	0	0.053	98.39
0.02	0.7	0.0465	98.25
0.03	0.805	0.0455	79.64
0.13	1.26	0.044	76.9
0.14	1.75	0.043	74.15
		0.036	72.78
		0.023	70.03
		0.0215	68.66
		0.015	60.42
		0.006	53.55
		0.0053	49.43
		0.0048	49.43
		0.0022	42.57

Zone IId(29)	Zone IId(29)	Zone IId(29) Combined sieve-hydrometer grain	Zone IId(29)
Cumulative weight %	Raw weight	diameter(mm)	Cumulative % finer
0		0.71	100
0		0.45	100
0	0	0.21	100
0.021	0	0.11	99.98
0.358	0	0.053	99.64
1.982	0.01	0.0465	98.01
	0.16	0.0456	81.91
	0.77	0.0445	76.95
		0.0435	63.3
		0.038	52.13
		0.0245	48.41
		0.0189	42.2
		0.0093	39.72
		0.0062	38.48
		0.0057	34.75
		0.0035	33.51
		0.0023	32.27

ZoneIId(37)	ZoneIId(37)	ZoneIId(37) Combined sieve-hydrometer grain	ZoneIId(37)
raw weight	Cumulative weight %	diameter(mm)	Cumulative % finer
0	0	0.71	100
0.1	0.35	0.45	99.65
0.1	0.7	0.21	99.3
0.1	1.05	0.11	98.95
0.36	2.31	0.053	97.69
5.39	21.26	0.0465	78.74
		0.0455	51.34
		0.0452	45.63
		0.0445	41.35
		0.034	35.65
		0.022	34.22
		0.017	32.79
		0.015	28.52
		0.0071	27.09
		0.0052	24.24
		0.0046	19.96
		0.00395	12.63

Table 3.7.Combined sieve and hydrometer rawdata for Zone-IId(sample sites)of the bottom sediments of *Jequia* lagoon.*Alagoas* .Brazil.

ZoneIIc(45)	zoneIIc(45)	zoneIIc(45)	zoneIIc(45)	ZoneIIc(46)	ZoneIIc(46)	ZoneIIc(46)	ZoneIIc(46)
Raw weight	Cumulative weight %	Combined sieve-hydrometer grain diameter(mm)	Cumulative % finer	Raw weight retained	Cumulative weight %	Combined sieve-hydrometer grain diameter(mm)	Cumulative % finer
0	0	0.71	100	0	0	0.71	100
0.02	0.081	0.45	99.92	0	0	0.45	100
0.04	0.243	0.21	99.76	0	0	0.21	100
0.03	0.365	0.11	99.63	0	0	0.11	100
0.08	0.69	0.053	99.31	0.03	0.075	0.053	99.92
0.38	2.237	0.0465	97.76	0.04	0.176	0.0465	99.82
		0.043	57.62			0.043	85.99
		0.039	50.42			0.039	83.13
		0.038	48.98			0.037	83.13
		0.034	47.54			0.034	81.7
		0.0225	46.09			0.027	80.26
		0.023	44.66			0.023	80.26
		0.019	41.78			0.014	73.09
		0.007	38.9			0.007	65.93
		0.0053	34.57			0.0061	63.06
		0.0046	30.25			0.0046	60.19
		0.0039	29.68			0.0021	51.6

ZoneIIc(50)	ZoneIIc(50)	ZoneIIc(50)	ZoneIIc(50)
Raw weight	Cumulative weight %	Combined sieve-hydrometer grain diameter(mm)	Cumulative % finer
0	0	0.71	100
0	0	0.45	100
0.3	0.69	0.21	99.31
0.87	2.699	0.11	97.3
10.82	27.68	0.053	72.32
12.36	56.23	0.0465	63.77
		0.045	58.74
		0.044	55.94
		0.044	54.54
		0.034	53.14
		0.022	53.14
		0.16	53.14
		0.02	48.95
		0.00715	48
		0.0056	47.55
		0.0044	47.55
		0.002	44.75

Table 3.8.Combined sieve and hydrometer rawdata for Zone-IIc (sample sites) from the bottom sediments of Jequia lagoon.Alagoas.Brazil

Zoneiiib(52)	Zoneiiib(52)	Zoneiiib(52) Combined sieve-hydrometer grain	Zoneiiib(52)
Raw weight	Cumulative weight %	diameter(mm)	cumulative % finer
0	0	0.71	100
0	0	0.45	100
0	0	0.21	100
0	0	0.11	100
0.04	0.14	0.053	99.86
0.1	0.49	0.0465	99.51
		0.455	84.8
		0.045	84.8
		0,038	83.54
		0.039	82.27
		0.0245	79.74
		0.0205	74.68
		0.0095	58.22
		0 .0081	51.89
		0.00585	48.1
		0.0031	43.03
		0.0025	41.77

Zoneiiib(53)	Zoneiiib(53)	Zoneiiib(53) Combined sieve-hydrometer grain	Zoneiiib(53)
raw weight retained	Cumulative weight %	diameter(mm)	cumulative % finer
0	0	0.71	100
0	0	0.45	100
0.04	0.101	0.21	99.9
0	0.101	0.11	99.9
0	0.101	0.053	99.9
0.1	0.355	0.0465	99.64
		0.043	60.83
		0.043	55.54
		0.037	52.9
		0.037	52.57
		0.023	51.37
		0.021	50.25
		0.0057	48.93
		0.00585	44.98
		0.0055	40.99
		0.0031	35.7
		0.0023	34.38

Zoneiiib(54)	Zoneiiib(54)	Zoneiiib(54) Combined sieve-hydrometer grain	Zoneiiib(54)
Raw weight	Cumulative weight %	diameter(mm)	Cumulative % finer
0	0	0.71	100
0	0	0.45	100
0	0	0.21	100
0	0	0.11	100
0.11	0.361	0.053	99.64
1.24	4.43	0.0465	95.57
		0.45	66.06
		0.44	57.17
		0.043	51.73
		0.032	44.92
		0.024	43.56
		0.021	40.83
		0.014	39.47
		0.0072	36.75
		0.0054	36.75
		0.0048	32.67
		0.0032	31.31

Zoneiiib(56)	Zoneiiib(56)	Zoneiiib(56) Combined sieve-hydrometer grain	Zoneiiib(56)
Raw weight retained	Cumulative weight %	diameter(mm)	cumulative % finer
0	0	0.71	100
0	0	0.45	100
0	0	0.21	100
0	0	0.11	100
0.11	0.286	0.053	99.71
0.94	2.733	0.0465	97.27
		0.455	64.95
		0.45	45.18
		0.043	38.12
		0.033	38.71
		0.025	35.3
		0.024	34.45
		0.014	33.88
		0.007	29.65
		0.0051	29.08
		0.0048	25.41
		0.0037	22.59

Zoneiiia(62)	Zoneiiia(62)	Zoneiiia(62) Combined sieve-hydrometer grain	Zoneiiia(62)
raw weight retained	Cumulative weight%	diameter(mm)	Cumulative % finer
0	0	0.71	100
0	0	0.45	100
0	0	0.21	100
0.02	0.029	0.11	99.97
0.09	0.163	0.053	99.84
0.5	0.909	0.0465	99.09
67g		0.0454	87.88
		0.044	85.14
		0.042	83.76
		0.0385	78.27
		0.0235	74.15
		0.021	70.03
		0.009	60.42
		0.0072	52.18
		0.0058	50.8
		0.0049	48.88
		0.0021	45.31

Zoneiiia(65)	Zoneiiia(65)	Zoneiiia(65) Combined sieve-hydrometer grain	Zoneiiia(65)
Raw weight	Cumulative weight%	diameter(mm)	Cumulative %
0	0	0.71	100
0	0	0.45	100
0.01	0.043	0.21	99.96
0.03	0.174	0.11	99.83
0.12	0.699	0.053	99.3
0.5	2.88	0.0465	97.12
		0.0455	63.07
		0.037	55.5
		0.034	52.98
		0.027	45.41
		0.024	37.84
		0.0175	35.32
		0.0093	32.8
		0.0072	31.54
		0.0054	27.75
		0.0049	25.23
		0.00455	25.23

Table 3.9.Combined sieve and hydrometer rawdata for Zone-IIIb(sample sites) from the bottom sediments of Jequia lagoon.Alagoas.Brazil

zoneIIIc(45) raw weight retained	zoneIIIc(45) Cumulative weight %	zoneIIIc(45) cumulative % finer	zoneIIIc(45) Combined sieve-hydrometer grain diameter(mm)	zoneIIIc(46) raw weight retained	zoneIIIc(46) Cumulative weight %	zoneIIIc(46) cumulative % finer	zoneIIIc(46) Combined sieve-hydrometer grain diameter(mm)
0	0	100	0.71	0	0	100	0.71
0.02	0.081	99.92	0.45	0	0	100	0.45
0.04	0.243	99.76	0.21	0	0	100	0.21
0.03	0.365	99.63	0.11	0	0	100	0.11
0.08	0.69	99.31	0.053	0.03	0.075	99.92	0.053
0.38	2.237	97.76	0.0465	0.04	0.176	99.82	0.0465
		57.62	0.043			85.99	0.043
		50.42	0.039			83.13	0.039
		48.98	0.038			83.13	0.037
		47.54	0.034			81.7	0.034
		46.09	0.0225			80.26	0.027
		44.66	0.023			80.26	0.023
		41.78	0.029			73.09	0.014
		38.9	0.007			65.93	0.007
		34.57	0.0053			63.06	0.0061
		30.25	0.0046			60.19	0.0046
		29.68	0.0039			51.6	0.0021

Table 3.10. Combined sieve (a) and hydrometer data (b) for zone IIIc(sample sites) of the bottom sediments of the Jequia lagoon, Alagoas, Brazil

ZoneIV(19)	ZoneIV(19)	ZoneIV(19)	ZoneIV(19)	ZoneIV(20)	ZoneIV(20)	ZoneIV(20)	ZoneIV(20)
Raw weight(g)	Cumulative weight %	Combined sieve-hydrometer grain diameter(mm)	Cumulative % finer	Raw weight(g)	Cumulative weight %	Combined sieve-hydrometer grain diameter(mm)	Cumulative % finer
0	0	0.71	100	0	0	0.71	100
0.05	0.119	0.45	99.88	0.06	0.103	0.45	99.9
0.04	0.214	0.21	99.79	0.03	0.154	0.21	99.85
0.02	0.261	0.11	99.74	0.09	0.309	0.11	99.7
0.1	0.5	0.053	99.5	2.64	4.869	0.053	95.13
0.43	1.53	0.0465	98.47	18.82	37.4	0.0465	62.6
		0.0395	97.5			0.045	85.32
		0.038	95.57			0.043	83.98
		0.037	92.67			0.041	81.32
		0.036	89.78			0.037	77.32
		0.024	85.43			0.027	74.65
		0.0235	73.85			0.026	70.65
		0.0225	52.13			0.026	66.65
		0.0071	46.33			0.0075	59.99
		0.0051	40.54			0.0074	55.99
		0.00465	34.75			0.0032	54.65
		0.0021	31.85			0.00295	47.99
Zone IV(22)	ZoneIV(22)	ZoneIV(22)	ZoneIv(22)	ZoneIV(23)	ZoneIv(23)	ZoneIv(23)	ZoneIv(23)
Raw weight(g)	Cumulative weight %	Combined sieve-hydrometer grain diameter(mm)	Cumulative % finer	Raw weight(g)	Cumulative weight %	Combined sieve-hydrometer grain diameter(mm)	Cumulative % finer
0.02	0.052	0.71	99.95	0	0	0.71	100
0.08	0.262	0.45	99.74	0	0	0.45	100
0.21	0.813	0.21	99.18	0.01	0.0272	0.21	99.97
0.42	1.916	0.11	98.08	0.02	0.081	0.11	99.91
3.82	11.94	0.053	88.06	0.04	0.19	0.053	99.81
2.26	17.87	0.0465	82.13	0.12	0.517	0.0465	99.48
		0.046	68.23			0.046	95.57
		0.0452	66.7			0.036	95
		0.038	61.67			0.031	92.67
		0.038	57.74			0.0265	89.78
		0.028	55.11			0.0025	85.43
		0.026	49.86			0.00245	73.85
		0.0098	44.61			0.0063	52.13
		0.007	40.68			0.0063	46.33
		0.0058	39.36			0.0041	40.54
		0.0032	31.5			0.0034	34.75
		0.00225	30.18			0.0023	31.85
ZoneIV(24)	ZoneIV(24)	ZoneIV(24)	ZoneIV(24)				
Raw weight(g)	Cumulative weight %	Combined sieve-hydrometer grain diameter(mm)	Cumulative % finer				
0	0	0.71	100				
0.02	0.055	0.45	99.95				
0.07	0.249	0.21	99.75				
0.13	0.61	0.11	99.39				
0.55	2.138	0.053	97.89				
0.35	1.11	0.0465	96.89				
		0.039	68.23				
		0.0375	66.7				
		0.036	61.67				
		0.034	57.73				
		0.029	55.11				
		0.027	49.86				
		0.0091	44.61				
		0.0072	40.68				
		0.0058	39.36				
		0.0032	31.5				
		0.0022	30.18				

Table 3.11.Combined sieve and hydrometer rawdata for Zone-IV(sample sites) of the bottom sediments of Jequia lagoon,Alagoas,Brazil

Textural Parameters	Zone I(3,4)	Zone I(5)	ZoneI(6)	ZoneI(7)
Mdϕ	0.1048	0.1310	0.1034	0.1034
Mzϕ	0.0943	0.1138	0.0921	0.0921
σ	0.1900	0.2080	0.1910	0.1910
Qdϕ	0.0290	0.0635	0.0375	0.0375
Gσϕ	0.1140	0.1452	0.1112	0.1112
IGσϕ	0.1170	0.1059	0.1159	0.1159
Cskϕ	2.3530	1.7610	2.3520	2.3520
Qskϕ	-0.031	-0.037	-0.031	-0.031
Gskϕ	0.6880	0.2305	0.7840	0.7840
Iskϕ	0.3440	0.8279	1.8830	1.8830
Ckuϕ	4.3970	1.8210	4.3830	4.3830
Gkuϕ	3.4300	1.4690	2.7650	2.7650
Mode	.	0.0440	.	.

(a)

Textural Parameters	Zone IIb(76)	Zone IIb(80)	Zone IIb(81)
Mdϕ	0.1288	0.1046	0.1054
Mzϕ	0.2056	0.0943	0.3265
σ	0.1990	0.1910	0.1900
Qdϕ	0.0780	0.0295	0.0290
Gσϕ	0.1363	0.2290	0.1875
IGσϕ	0.1334	0.1241	0.1541
Cskϕ	1.8760	2.3500	2.3520
Qskϕ	-0.1916	-0.0296	-0.0294
Gskϕ	1.1530	1.0292	1.2613
Iskϕ	0.7920	1.0988	1.0876
Ckuϕ	2.4230	4.3870	4.3990
Gkuϕ	1.5494	3.3380	2.8120
Mode	0.0440	.	0.0460

(c)

Textural Parameters	Zone IV(19)	Zone IV(20)	Zone IV(23)	Zone IV(24)
Mdϕ	0.1050	0.1070	0.1012	0.1036
Mzϕ	0.1020	0.1510	0.0890	0.0923
σ	0.1900	0.1900	0.1930	0.1910
Qdϕ	0.0240	0.0230	0.0315	0.0290
Gσϕ	0.2000	0.2040	0.2045	0.2280
IGσϕ	0.1533	0.1720	0.1628	0.1743
Cskϕ	2.3800	2.3610	2.3330	2.3540
Qskϕ	-0.0190	-0.0190	-0.0300	-0.0276
Gskϕ	1.1600	0.9550	1.0090	0.8990
Iskϕ	1.1170	0.9250	0.9324	0.8680
Ckuϕ	4.4020	4.4280	4.3090	4.3930
Gkuϕ	3.0050	3.2250	3.1740	2.8120
Mode	.	0.0260	0.0060	.

(b)

Textural Parameters	Zone IIIa(56)	Zone IIIa(62)	Zone IIIa(65)
Mdϕ	0.1568	0.1050	0.1034
Mzϕ	0.1378	0.0945	0.0202
σ	0.2190	0.1910	0.1910
Qdϕ	0.1290	0.0290	0.0290
Gσϕ	0.3535	0.2275	0.1205
IGσϕ	0.2448	0.1739	0.0716
Cskϕ	1.3530	2.3520	2.3510
Qskϕ	-0.1252	-0.0290	-0.1034
Gskϕ	0.9264	0.8769	0.1340
Iskϕ	0.8786	0.7934	0.4939
Ckuϕ	0.4730	4.3920	4.3800
Gkuϕ	0.7132	3.2150	2.8052
Mode	0.4500	.	.

(d)

Table 3.12. Computed textural parameters for zones I(a), IV(b), IIb (c) and III(d) of the bottom sediments of the *Jequia* lagoon, Alagoas, Brazil

Sieve designation-standard and alternate*	Sieve opening-Moussa's values	Zone I(4) Weight frequency-Wf	Zone I(4) M1	Zone I(4) M2	Zone I(4) M3	Zone I(4) M4
1.19mm-16*	-0.25	0	0	0	0	0
595μm-30*	0.75	0.042	0.0315	0.0236	0.0177	0.0132
420μm-40*	1.25	0.042	0.0525	0.0656	0.082	0.10253
297μm-50*	1.75	0.235	0.4112	0.7196	1.259	2.203
149μm-100*	2.75	2.851	7.84	21.56	59.29	163.04
74μm-200*	3.75	32.65	122.437	459.14	1721.77	6456.638
TOTAL	-	35.82	130.772	481.5	1782.24	6621.996

D1	D2	D3	D4	Moment designated Mean(Xd)	Moment sample Mean(Mϕ)	-
3.65	13.44	49.76	184.86	3.65	3.4	
Moment	Moment	Moment	Moment	Moment standard	Moment	Moment
Deviation-Md1	Deviation-Md2	Deviation-Md3	Deviation-Md4	Deviation(σ)	Skewness-Msk	Kurtosis-Msk
0	0.1175	3.846	0.014	0.343	9119.4	1.0145

(a)

Sieve designation-standard and alternate*	Sieve opening-Moussa's values	Zone IIb(80) Weight frequency-Wf	Zone IIb(80) M1	Zone IIb(80) M2	Zone IIb(80) M3	Zone IIb(80) M4
1.19mm-16*	-0.25	0	0	0	0	0
595μm-30*	0.75	0.055	0.0412	0.0309	0.023	0.0174
420μm-40*	1.25	0.082	0.1025	0.1281	0.16	0.2001
297μm-50*	1.75	0.137	0.2397	0.4196	0.7342	1.285
149μm-100*	2.75	3.687	10.139	27.882	76.678	210.865
74μm-200*	3.75	20.92	78.45	294.18	1103.2	4137.01
TOTAL	-	24.881	88.972	322.64	1180.8	4349.4

D1	D2	D3	D4	Moment designated Mean-Xd	Moment sample Mean(Mϕ)	-
3.575	12.967	47.46	174.815	3.575	3.325	
Moment	Moment	Moment	Moment	Moment standard	Moment	Moment
Deviation-Md1	Deviation-Md2	Deviation-Md3	Deviation-Md4	Deviation(σ)	Skewness (Msk)	Kurtosis-Msk
0	0.1894	-0.231	0.458	0.4352	7.845	12.77

(b)

Table3.13.Computed moment textural parameters using selected sieve data from ZoneI-site 4(a) and Zone IIb-site80(b).

Sieve designation-standard and alternate	Sieve opening-Moussa's values	ZoneIIIa(65) Weight frequency-Wf	ZoneIIIa(65) M1	ZoneIIIa(65) M2	ZoneIIIa(65) M3	ZoneIIIa(65) M4
1.19mm-16	-0.25	0	0	0	0	0
595μm-30	0.75	0	0	0	0	0
420μm-40	1.25	0.043	0.05375	0.0671	0.0839	0.10498
297μm-50	1.75	0.174	0.3045	0.5328	0.933	1.632
149μm-100	2.75	0.699	1.9222	5.286	14.54	39.98
74μm-200	3.75	2.88	10.8	40.50	151.87	569.53
TOTAL	-	3.796	13.08	46.385	167.43	611.25

D1	D2	D3	D4	Moment designated Mean(Xd)	Moment sample Mean(Mϕ)	-
3.446	12.22	44.106	161.02	3.446	3.196	

Moment Deviation-Md1	Moment Deviation-Md2	Moment Deviation-Md3	Moment Deviation-Md4	Moment standard Deviation(σ)	Moment Skewness-Msk	Moment Kurtosis Msk
0	0.345	-0.382	0.693	0.587	3.554	5.8223

(a)

Sieve designation-standard and alternate	Sieve opening-Moussa's values	Zone IV(20) Weight frequency-Wf	Zone IV(20) M1	Zone IV(20) M2	Zone IV(20) M3	Zone IV(20) M4
1.19mm-16	-0.25	0	0	0	0	0
595mm-30	0.75	0.103	0.0773	0.0579	0.0434	0.0325
420mm-40	1.25	0.154	0.1925	0.240	0.300	0.376
297mm-50	1.75	0.309	0.541	0.9463	1.656	2.898
149mm-100	2.75	4.87	13.39	36.83	101.28	278.52
74mm-200	3.75	37.4	140.25	525.93	1972.3	7395.99
TOTAL	-	42.84	154.45	564.004	2075.57	7677.81

D1	D2	D3	D4	Moment designated Mean-Xd	Moment sample Mean(Mϕ)	-
3.605	13.165	48.45	179.22	3.605	3.355	

Moment Deviation-Md1	Moment Deviation-Md2	Moment Deviation-Md3	Moment Deviation-Md4	Moment standard Deviation(σ)	Moment Skewness (Msk)	Moment Kurtosis Msk
0	0.169	-0.2286	0.43	0.411	10.83	15.056

(b)

Table 3.14. Computed moment textural parameters using selected sieve data from Zones IIIa(a) and IV(b)

CHAPTER 4

CHARACTERIZATION OF SPECTRAL SIGNATURES FROM THE SUSPENDED MATTER AND LAND-USE TYPES OF THE STUDY AREA

4.1. Introduction

The *Jequia* lagoon, presenting mostly clastic sediments as the major water quality parameter described in chapter three, is the main focus of this chapter.

In this study, pollutant plumes were recognized on the western portion (Zone IV) of the *Jequia* lagoon. The mixed pollutant plumes comprise a suspended sediment plume, a phytoplankton (algae) plume and an oil-like substance plume. We assume that the oil-like substance plume is related to the vinasse that degrades the water quality by lowering the pH and the dissolved oxygen. Two plumes of sediment in Zone I and III of the *Jequia* lagoon were also recognized. These plumes are considered to be the major parameters or variables controlling the water quality of that lake.

This chapter is devoted to the study of the spectral reflective signatures of the water quality parameters of the *Jequia* lagoon and the overall variability in land-use change of the region surrounding that lagoon. This chapter is divided in two parts. Part I is concerned with the overall changes in the patterns of land-use between two sets of data recorded by different sensors in 1968 and in 1989 respectively. This part is also concerned with the detection of changes in land-use surrounding the lagoon and with the characterization of spectral signatures or albedo patterns of water quality parameters along that lake. Albedo is hereafter considered as the fraction of reflected radiation coming only from the sun, following the concept of Iqbal (1983). There is a distinction from the albedo patterns to the reflectance patterns simulated in laboratory within this study. Therefore, spectral reflectance signatures or patterns and irradiation produced by the sun and the water quality targets are used in an interchangeable way, throughout this chapter.

Sugar-cane fields, farming crops, roads, urban sites and bare soil are the land-use targets studied along the *Jequia* estuary. Photo interpretation of a LANDSAT quick-look image recorded in 1989 and aerial photographs recorded in 1968 are used to map the land-use changes along the *Jequia* study area. A maximum likelihood classification on a

LANDSAT-TM computerized image recorded in 1990 is also used to address those changes. Part II aims to characterize the spectral signatures of suspended matter along the water column of the *Jequia* lagoon. It also attempts by different techniques and methodologies to discriminate or distinguish the plumes qualitatively recognized in the water surface of that lagoon during field surveys. It also aims to map the horizontal distribution of the sediment plumes of the lagoon, using the digital TM data in the visible and near-infra-red wavelength ranges recorded in June 1990, and taking into account a few chemical and physical reference data sets. The irradiation signatures are expressed as a proportion of radiant energy arriving at the surface of the study area during June 11, around 9:45 a.m. in 1990. The energy was detected by the sensor Thematic Mapper (TM) of the LANDSAT 5 satellite.

The suspended matter recognized in the *Jequia* lagoon, consists of a mixed plume containing suspended sediments, algae (phytoplankton) and an oil-like substance (Zone IV) whose spectral pattern might show subtle differences from each other. The other plumes along the lagoon comprise only suspended sediment and water. Therefore, the specific goals of part II are: to distinguish the pollutant plume from the sediment and organic (phytoplankton) plume in Zone IV and to differentiate the mixed plume from the other plumes in Zones I, IIb and IIIa (Figure 1.2) using their reflectance patterns.

The major discharge into the *Jequia* lagoon comes dominantly from the *Jequia* River entering the *Jequia* lagoon in Zone IV (Figure 2.1). Small rivers feed the *Jequia* lagoon within Zones III.

The water of the *Jequia* River has been classified as type 2 (Marinho 1994). Type 2 waters imply that the water is not adequate for human consumption, nor for farming or recreation activities. Therefore the water classified as type 2 requires previous treatment against contamination before any use. There is no historical data on water quality parameters within the *Jequia* watershed.

Thereby, the field observations done in November 1989 and March 1990 enabled the assessment of the quality of the *Jequia* water. The water of the *Jequia* lagoon presents a general homogeneous character. Exception is recognized for the mixed plumes of Zone IV. The Zones II and III exhibit plume containing dominant sediment matter. Within the outlet of the lagoon (Zone I), part of the plume consists of sediments and mangrove.

4.2. Description of the LANDSAT thematic mapper (TM) image used in this study

The original Earth Resources Technology Satellite (ERTS) launched during the seventies is the current LANDSAT series. The LANDSAT 5, launched in March 1984, carried two earth-observing sensors: the flight Thematic Mapper (TM) and the Multispectral Scanner (MSS). The former sensor enables the detection of more information, due to its performing spatial and spectral resolution. The thematic mapper sensor operates in seven spectral bands TM1, TM2, TM3, TM4, TM5, TM6, TM7 and presents a spatial resolution of 30 m for six bands and 120 m for band TM6 (for thermography).

The targets of interest in this study present specific spectral signatures or albedo for the TM bands of the visible wavelength ranges of TM1 (blue), TM2 (green) and TM3 (red), the near infra-red TM4 band and the middle infra-red TM5 band. For this study, these last five thematic mapper bands were chosen for a scene of 6 120 pixels per line and 3 088 lines per band. The sensor had a field of view of 15,39 degrees and a scan rate of 13,99 lines/sec. Each reflective band was sensed by an array of 16 detectors. The overall imagery size was 6 120 pixels per 3 088 lines centered at -9,6563 degrees of latitude and -36,2322 degrees of longitude.

The *Jequia* multispectral image was recorded on a computer compatible tape (CCT) from the Thematic mapper sensor captured from LANDSAT 5 and managed by the Brazilian National Institute of Spatial Research (INPE) in partnership with NASA. The

TM bands were recorded during the peak of water excess around 9:45 a.m., on June 11, 1990 and were acquired with geometric and radiometric corrections.

The Thematic mapper tapes were processed in sections of 1024 x 1024 pixels, by the PCI Image Analysis System Software on a Sun UNIX based computer station at the Remote Sensing Laboratory of the Department of Human Sciences of the University of Quebec at Chicoutimi.

PART I

4.3. Prediction of land-use changes within the *Jequia* area during the last three decades

4.3.1. Introduction

Part I of this chapter has two major objectives. The first goal is to identify the overall variability in land-use types between two sets of data recorded on two separate datés. These products are aerial photographs recorded in 1968 and a LANDSAT TM quick-look image recorded in November of 1989. The second goal of part I is to apply mapping techniques and methodologies currently used to discriminate and distinguish the spectral reflectance patterns of sugar-cane fields from farming crops. It was performed using a maximum likelihood classification (MLC) with the LANDSAT TM data recorded in June of 1990.

In order to properly localize the environment focused on this chapter, the *Jequia* lagoon is considered to be the upper region of the *Jequia* estuary.

4.3.2 Description of the digital methods used

The remote sensing products used within this study include: a set of aerial photographs, of quick-look image (TM) with bands 2, 3, 4 and a LANDSAT digital TM image with bands 1, 2, 3, 4, and 5.

The methods used for the remote sensing analyses were done through a visual composite analysis of the photo-interpreted elements or information classified as land-use units. This visual analysis implies that the patterns are systematically interrelated to the local elements such as texture, gray level and some mapped physiographic features and the land-use of the respective unit.

The information mapped from the aerial photographs (panchromatic images) and the quick-look multispectral image was analyzed following the standard procedures of photo interpretation. The multispectral quick look image was recorded from a 560 nm to 820 nm (TM2, TM3 and TM4) electromagnetic range, thus simulating the visible light and the near infrared photography.

The analysis of local element patterns (texture, gray level and density) was coupled to the physiographic analysis of the landscape (mainly topography and drainage). The land-use categories were then grouped according to the most frequent patterns and elements related to a given type. The composite analysis implies that the element patterns and the physiographic features show interrelated patterns.

It is relevant to state that the photo interpretation methods used in this study do not enable precise classification of land-use or land-cover units. Moreover, the interfaces between each category are fairly generalized.

The methods described in part I include results from statistical analysis and visual observation of land-use maps done through standard classification.

4.3.2.1. Mapping land-use units from the 1968 aerial photographs

4.3.2.1.1. Introduction

The main goal of part I is the overall characterization of land-use units surrounding the *Jequia* lagoon, characterization based on the qualitative composite analysis of the surface element patterns. In the composite analysis approach the elements mapped on the quick-look image and on the aerial photographs are simply divided into land-use units. It is relevant to state that the land-use units suggested hereafter do not represent a strict classification for the *Jequia* study area, since the limits between each unit are not precise nor abrupt. They represent the major land-use patterns of the area during the periods of 1968 (Figure 4.1).

Based on the interpretation of the aerial photographs from 1968, eight land-use units are proposed for the study area. They comprise: the sugar-cane fields mixed with farming (unit-SCFA), the sugar-cane fields mixed with dense forest (unit-SCFO), the dense forest (unit-FO), the farming crops (unit-FA), the coconut crops mixed with farming (unit-COFA), the tidal channel and mangrove vegetation (unit-TCMA), the *Jequia da Praia* city, the *Sinimbu* plant (or community) and the roads grouped as urban activities (unit-URB) and the *Jequia* lagoon and its tributaries (unit-LR) (Figure 4.1).

4.3.2.1.2 Description of the SCFA land-use unit

The analysis of the sugar-cane fields, as appearing on the 1968 aerial photographs, shows that they are mixed with bean, corn and manioc crops and that they are scarcely distributed along the Mesas of the *Barreiras* Formation predominating in the southern and southwestern branch of the *Jequia* lagoon.

The sugar-cane unit (SCFA) is composed mainly of sugar-cane crops presenting an irregular pattern, a very light gray level and a homogeneous texture of low roughness. The

textural pattern of the other associated farming crops is not well distinguished from the pattern of sugar-cane crops.

4.3.2.1.3. Description of the SCFO land-use unit

The sugar-cane crops mixed with forest (SCFO) mapped from the 1968 aerial photographs are scarcely distributed along the northern and western regions of the *Jequia* lagoon. They exhibit similar irregular patterns and gray levels as the crops of SCFA unit. Nevertheless, they show a coarser texture than the fields in the SCFA unit. Therefore the mixture of sugar-cane fields with some green belts of dense (remains) forest along the Mesas is considered to be a distinct category (unit) presenting a heterogeneous land-use type within the study area.

4.3.2.1.4. Description of the FO land-use unit

The interpretation of the land-use unit named dense forest (FO) on the 1968 aerial photography shows that the original forest represented more than 60% of the northern and western regions of the *Jequia* study area. Preserved forests are also mapped along the margins of the lagoon, along the Mesas, the banks and along the margins of the tributaries of the *Jequia* River. These forests show the darkest gray level in these images and a homogeneous coarse texture.

The mangroves occurring along the margins of the *Jequia* tidal channel and in the northern and eastern sides of the *Jequia* town present a very dark gray level and a homogeneous coarse texture. They are included into the FO land-use unit.

4.3.2.1.5. Description of the FA land-use unit

The farming land-use unit (FA) is composed of homogeneous fields of manioc, rice and corn. They are distributed along the southern margins of the *Jequia* lagoon, the banks

and along the margins of the tidal channel (lower part of the estuary). The farming fields show a heterogeneous texture and a soft gray level. The coconut crops show a less white and a finer and homogeneous texture compared to farming fields.

The scale prevents a differentiation among the farming crops which were very well preserved along the western margins of the *Jequia* tidal channel and different from the farming crops described within the SCFA land-use unit.

4.3.2.1.6. Description of the COFA land-use unit

This unit is composed of coconut crops mixed with manioc crops. The coconut cropping is distinctively located between the *Jequia* town and the coastal plain. The mixing of coconut and manioc is mapped mainly at mid length of the *Jequia* tidal channel.

4.3.2.1.7. Description of the TCMA land-use unit

The mangrove (TCMA) unit occurs on both margins and in the middle of the meandering tidal channel. That vegetation shows a very dark gray level and a homogeneous coarse texture. The tidal channel water shows a dark-green gray level. Therefore, mangroves and water do not show much contrast.

This absence of contrast did not permitted their differentiation on the photograph. Mangroves are then included in the same unit as the water of the tidal channel.

4.3.2.1.8. Description of the LR land-use unit

The *Jequia* lagoon, the *Poxim* lagoon and the *Jequia* River represent the natural targets classified within the LR unit. The lagoon comprises more than 50% of the study area. It is considered in this work as the upper section of the *Jequia* study area.

The targets mapped within the LR land-use unit present similar element patterns. They show dark gray levels and a homogeneous texture. Locally, the water of the *Jequia* and *Poxim* lagoons exhibits specular effects. The organization patterns of the rivers vary from coarse-textured dendritic pattern to dendritic one.

4.3.2.1.9. Description of the URB land-use unit

The urban land-use unit (URB) comprises mostly linear targets. They include roads, urban sites and the Sinimbu plant.

The town of *Jequia da Praia* is the only urban feature mapped from the aerial photographs of the study area. The scale of those panchromatic images does not enable the mapping of small worker-villages (*vilas operarias*), recognized during field surveys along the study area. *Jequia da Praia* town is located at the outlet of the lagoon (Zone I). It shows a regular polygonal coarse texture and white gray level mixed with the darker gray level of farming fields surrounding the city.

The main roads are distributed along the western margins of the *Jequia* tidal channel, crossing the northern and northeastern parts of the *Jequia da Praia* town and crossing some sugar-cane fields. Those roads are mapped as linear targets showing at most a white gray level in the aerial photographs.

4.3.2.2. Mapping the land-use units from the 1989 multispectral quick-look image

4.3.2.2.1. Introduction

Land-use change is one of the most significant factor producing expressive modifications within tropical environments. Several contributions regarding land-use

within tropical regions come from the works of Rignote *et al,* 1997, Dale *et al.*, 1993, Mantovani, 1997 and Saatchi *et al.,* 1997.

The characterization of the land-use units mapped from the quick-look multispectral image is based on the same principle as the composite analysis used for the interpretation of information recorded on panchromatic images (aerial photographs). Contrary to the interpretation of information from aerial photographs, the color levels of the different targets is the main criterion used to map the land-use units. These targets show an overall variation of their signatures recorded on the red, green, and blue coordinated systems (RGB) of the multispectral LANDSAT TM quick-look image made from the TM4 in red, TM3 in green and TM2 in blue.

It is relevant to state that the *Jequia* study area was covered by 30% of cloud shadows appearing on the quick-look multispectral image recorded in November 1989. The composite analysis of the information mapped from the 1989 multispectral LANDSAT TM2, TM3 and TM4 quick-look image consists simply of dividing and grouping the targets presenting different color level contrasts into land-use categories. Since the data is derived only from TM2, TM3 and TM4, the total spectral response comes mostly from the vegetation signature. The land-use units mapped on that multispectral image are fewer than the ones mapped from the panchromatic images (aerial photographs).

The six land-use units (Figure 4.2) mapped from the multispectral quick-look image are: the sugar-cane fields (unit-SC), the farming crops (unit-FA), the coconut crops (unit-CO), the tidal channel mixed with mangrove vegetation (unit-TCMA) and the urban sites with roads (unit-URB). The latter unit includes small roads destined to the transportation of by-products. The water body unit includes the rivers and relics of the dense forest along the margins of the *Jequia* River (unit-LRFO).

4.3.2.2.2. Description of the SC land-use unit

Analysis of the sugar-cane fields (SC) on the multispectral LANDSAT quick-look image of November 1989, shows their predominance along the study area. The sugar-cane fields represent more than 60% of the active cropping area, mostly occurring over the Mesas of the *Jequia* study area including river banks and river valleys.

The sugar-cane fields distributed along the northern and northwestern parts of the *Jequia* lagoon show a very regular and polygonal pattern and a fine texture. The fields surrounding the southern portion of the lagoon present an irregular and homogeneous pattern and a medium to fine texture. They are mixed with farming crops.

Despite the lack of syncronization between the image recording and the field surveys, it is evident from the spectral patterns within the multispectral quick-look image that sugar-cane fields show different growth stages. Four sub-levels of green enable an easy differentiation of growth stages. Therefore, these stages imply different growing crop periods.

The dark greenish crops imply an early growing period. The light greenish crops imply a mature growing period. The mixed patterns of pink and green or light green imply late growing crops. The predominant pinky gray level implies dry sugar-cane crops.

The presence of several growth stages mapped within the multispectral image finds good agreement with published information (Barbosa, 1990). Barbosa stresses the extensive use of the soil without any rest period. Therefore, the resting period required for soil regeneration is neglected within these fields.

The color level and texture patterns of the farming crops (beans, corn, manioc) on the southern part of the *Jequia* lagoon are similar to the sugar-cane patterns.

The image scale does note enable the differentiation of farming crops from sugar-cane crops. Since the image represents seasonal cropping among the sugar-cane fields, these crops were considered as belonging to the sugar-cane SC land-use unit.

4.3.2.2.3. Description of the SCFA land-use unit

The FASC land-use unit is composed of farming crops (bean, corn, and manioc) mixed with sugar-cane fields. This unit coupled with SC unit represents more than 90% of the cultivated area within the study area. This unit is geographically distributed along the southern and eastern parts of the *Jequia* lagoon surrounding its outlet and the town of *Jequia*. They exhibit a homogeneous medium to coarse texture and a color level varying from green to yellow pattern. Some sugar-cane crops are pink.

The farming crop especially beans are considered as negligible, since they are used only as a mean of preserving the soil during certain growing periods of sugar-cane. There is no information published concerning trade interests on farming crops along the *Jequia* study area.

4.3.2.2.4. Description of the URB land-use unit

The town of *Jequia* and the communities of Sinimbu (industrial plant) are the main urban agglomerations mapped using the multispectral image. They present a coarse texture, a mixed yellow, greenish and pink color level and a very regular pattern.

The town of *Jequia* is located in the southeastern side of the outlet (Zone I) of the *Jequia* lagoon and the *Sinimbu* community is located approximately 7 km from the western branch of that lake. A certain amount of clouds producing shadows over part of the *Jequia* town is shown within the quick-look image of 1989.

The discernible roads mapped on the multispectral image are distributed mainly in the area surrounding the *Sinimbu* community, the southern part of the *Jequia* lagoon and within some crossing ways along the sugar-cane fields. The roads and the roadways designed for transportation of sugar-cane by-products are mapped as linear targets presenting a white gray level.

4.3.2.2.5. Description of the TCMA land-use unit

The mangrove areas included in this unit (TCMA) are mapped mainly along the *Jequia* tidal channel. The mangrove vegetation presents a coarse texture and a color level similar to the dark greenish of the sugar-cane crops and the forest belts. The differentiation of the mangrove area from the forest area and the dark green sugar-cane crops is based on their geographic distribution. This difference is very well noticed along the *Jequia* tidal channel. Mangrove vegetation occupies the areas along the middle part of the channel banks.

4.3.2.2.6. Description of the LRFO land-use unit

The natural targets categorized as water bodies within the LRFO unit are: the *Jequia* lagoon, the *Poxim* lagoon and the tidal channel including the mangrove vegetation, the *Jequia* River and part of the Atlantic Ocean seashore.

The water bodies on the multispectral image show a similar homogeneous texture and a black color level. A dendritic drainage pattern was recognized within the *Sinimbu* area. It is generalized for the rest of the estuary, even though the information in TM2, TM3, and TM4 bands does not enable a precise description of the drainage organization along the *Jequia* estuary. The drainage is mixed with relics of forest belts and sugar-cane crops.

The remains of dense forest mapped from the image as straight green belts surrounding the northern and western margins of the lagoon represent less than 5% of this land-use unit.

4.3.2.2.7. Description of the CO land-use unit

The coconut crops are described individually due to their specific geographic distribution. They are distributed along the coast line, surrounding both margins of the *Jequia* tidal channel. They present a very irregular pattern, contrary to the pattern shown early on the aerial photographs. They also present a coarse texture and their color level varies from pink to yellowish. Any published information concerning the economy of the coconut production is unknown. The production is reserved for local consumers.

4.4. Classification and discussion of the land-use units mapped and interpreted from the aerial photographs and the quick-look image

The irradiant energy recorded in TM2, TM3 and TM4 comes mainly from the spectral response or signature of the vegetation, either from the biomass content or the vegetation cover types. The reflectance influences from the soil (roads or bare areas) are considered to have minor influence. Nevertheless, the vegetation mapped in this study, using the multispectral image, presents a generalization regarding the specific spectral response for biomass content or vegetation cover types.

The information categorized into land-use units along the study area and mapped from the 1968 aerial photographs is presented on Figure 4.1. The scale of the aerial photographs enabled a more precise differentiation of the targets compared to the quick-look image.

It is very relevant to point out that the available aerial photographs (1968) do not cover the whole study area as does the multispectral quick-look image (1989). The area of the

estuary covered by the panchromatic photographs is limited to the western branch of the *Jequia* lagoon.

The land-use units mapped from the 1989 multispectral LANDSAT quick-look image (Figure 4.2) had their geographic coordinates preliminarily integrated into Mapinfo software. A more precise differentiation of some natural targets was not performed due to the limitation of the multispectral quick-look image scale and available TM bands. The criterion used to generalize some targets within the land-use units was their geographic distribution and variation of tone and texture. Since mangroves are not distinguishable on the multispectral image scale, they are generalized and grouped with the LRFO water body unit. Roads and roadways are grouped within the urban sites land-use unit. Since the forest relics occur along the margins of rivers and lagoons, they were not excluded from URB unit.

One of the main relevant contributions of this work is the land-use classification and model proposed. This categorization is showing the effect of 20 years of deforestation along the study area. A significant clearing impact characterized by the quick replacement of dense forest (that is, its natural potentiality) by an improved and intensive industrial sugar-cane production.

Since there are only qualitative available data reporting the land-use changes during the last two decades along the study area, the above assumptions intend to be a simple qualitative analysis.

Internal and non-published reports from IMA (*Instituto do Meio Ambiente*) of *Maceio,* reports cutting of mangrove vegetation along the tidal channel and pollution resulting from vinasse dumping along the rivers. Those impacts were recognized during two field surveys in November 1989 and in March 1990 within the study area. They were considered as indicators affecting the original and natural potential land-use patterns of that environment.

From 1968 to 1989, a remarkable change in the land-use patterns is to be noticed for the areas covered once by the dense forest. Therefore, in about two decades, the dense forest was completely replaced by sugar-cane crops and farming. Social and physical environmental impacts of this deep change were never studied, except for the great improvement of sugar-cane industrial park producing sugar and alcohol in *Alagoas* state in the seventies. However, the *alagoanos* must nowadays import sugar for their internal consume.

4.5. Proposed model for the patterns of land-use within the *Jequia* study area

The interpretation of the aerial photographs recorded during the sixties demonstrates the natural potential of the soil that is, the development of forest and its biodiversity within the study area. Few areas showed farming crops. At the beginning of the eighties, the bloom of sugar-cane industries has lead the area to a major deforestation process mainly surrounding the *Jequia* lagoon. We assume that the significant slope erosion and the silting processes came along associated and/or related to that process. Nowadays, the original humid forest was completely removed, leaving only rare spots remaining along the river and the northern margins of the lagoon. The clearing of the original forest widespreading all over the study area gave place to the installation and expansion of the industry. It was completed during the early seventies (Andrade, 1973). During the application of the *Plano Nacional do Alcool* (PNA) due to the energetic crises, the impossibility of expanding the sugar-cane production was recognized. There was no more available land covered by the original ombrophylous forest.

Since a quantitative evaluation of the change on land-use patterns would require a seasonal and periodic set of comprehensive ground truth data, we propose within this study only a qualitative evaluation based on the elements mapped from the aerial photographs, the field surveys done in 1989 and 1990 and the land-use units classified using the quicklook TM data (Figure 4.3). Therefore, a preliminary diagrammatic model (Figure 4.4) summarizes the analysis of the land-use patterns and their levels of natural

vulnerability and potentiality following the concept of Rocha (2000). The model includes the land-use units mapped and the qualitative analysis of their vulnerability (V1, V2, V3) and their potentiality (P1, P2, P3) levels.

Considering the dynamic concept related to some morphogenetic and pedogenetic aspects of the study area, three levels of natural vulnerability and potentiality (level 1=high, level 2=intermediate and level 3=low) were attributed to the classified land-use units. These levels were designated as secondary data within the model (Figure 4.4). The output data are the result of crossing the land-use main characteristics with their natural potentiality and vulnerability. Five land-use classes or qualitative units were generated from the periods of 1968 and 1989. The results indicate that the URB, SCFO, SC, LR, TCMA and FO land-use units are the ones requiring the most attention due to their high natural vulnerability. However the URB, SCFO and SC units present high potentiality whereas the LR unit presents intermediate potentiality. The high potentiality of the CO, COFA and FA land-use units is facing an intermediate to a high vulnerability level due to the intensive soil use. The data suggest that no resting period between cultivation is occurring.

In spite of the tempting potential for tourism and fishery activities, we consider the study area as a very sensitive environment. The intensive land-use the area has been through requires a continuous monitoring program before any development or expansion program is established. It is pertinent to point out that intensity of use including significant area deforestation might lead to a complete loss of soil fertility and perhaps an extensive land degradation and even a decline of the biodiversity. The major natural environments (the lagoons, the tidal channel, the mangroves and the coast) of the study area are highly and spontaneously sensitivity to degradation. The main susceptibilities of these environments include: soil erosion and subsequent silting through many parts of the lagoon, the town and the channel, and the pollution potential from urban sewage and industrial activities. These sensitive environments should be managed through an

integrated seasonally preservation and/or conservation projects. Moreover, the projects should include a systematic characterization of the physical aspects coupled with education programs within the local communities.

PART II

4.6. Mapping the plumes of suspended matter along the water column of the *Jequia* lagoon using processed digital LANDSAT TM visible and near infra-red data

4.6.1. Introduction

Radiation patterns of water quality parameters distributed along water bodies can be assessed through field measurements, laboratory experiments and also through satellite (LANDSAT TM) data recording. The digital data described and analyzed in part II of this chapter comes from a LANDSAT image recorded by the TM sensor. The term irradiance used within this chapter is assumed to express the overall radiation coming from the sun, following the concept of Iqball (1985). Within the next chapter five, the overall reflectance estimated through the laboratory experiment is designated as irradiation since the energy source has an artificial origin.

Inorganic suspended matter (sediments), organic suspended matter (mostly phytoplankton) and an oil-like plume are the water quality parameters or targets qualitatively recognized within the water column of the lagoon during field surveys realized in November 1989 and March 1990. Clear water zones were also recognized.

This sub-chapter concerns the characterization of these parameters using their spectral signatures recorded by the LANDSAT TM, around 9:45 a.m., in June 1990, within the 485 nm (TM1) to 1 650 nm (TM5) wavelength range. This range hereafter covers the visible, the near infrared and the medium infrared bands. Within this study, the TM band range follows the classification proposed by Markham, *et al.* (1985).

The spectral study of the water quality targets of the lagoon comprises precisely the characterization of the overall irradiance produced by the following targets: the suspended clastic sediments, the phytoplankton species (algae), the oil-like plume and the water matter.

Considering that 99% of the spectral reflectance patterns produced by the water targets along the water column of the lagoon fall within the 485 nm to 820 nm wavelength range, only TM1, TM2, TM3 and TM4 bands were selected to support the study of the overall irradiance signatures produced by the water targets. Although some tests were performed using the medium infra-red TM5 band recording spectral signatures above 820 nm wavelength range, no new information was added to those mapped within the TM4 band. It is relevant to say that irradiance patterns recorded within the TM5 band is believed to be produced only by vegetation present within the mixed pixels surrounding the contour that masks the *Jequia* lagoon. The TM5 band is therefore neglected within this study. Within this study, we assume that the wavelength equivalence proposed by Markham *et at.*, 1985 is best suited for the *Jequia* lagoon environment. This classification uses the visible wavelengths (the blue-green corresponding to 450-520 nm, the green corresponding to 520-600 nm and the red varying from 630-690 nm) and the near-infrared wavelength ranging from 760-900 nm.

4.6.2. Definition of the mixed water quality targets along the Jequia lagoon

The suspended matter in the water column of the *Jequia* lagoon regroups three main classes: the organic, the inorganic and the anthrophogenic type. The former class includes the products of terrigenous and/or marine origin as well as the products of disintegration of other organic compounds or rests of phytoplankton shells and zooplankton exoskeleton. The clastic sediments or inorganic matter are carried into the *Jequia* lagoon mainly by the tributary rivers and by slope erosion. The anthrophogenic class includes the oil-like substance floating on the water surface witin Zone IV of the *Jequia* lagoon.

Therefore, the parameters controlling the water quality of the *Jequia* lagoon by order of magnitude are: the inorganic clastic sediments, the phytoplankton (algae) and the oil-like plume. Clear water predominates in Zones IIIa, IIIb, and IIIc.

The above parameters are hereafter grouped as a mixed target in the selected zones (Figures 1.3 and 2.1) since no zone within the *Jequia* lagoon was recognized as pertaining to only one of those parameters. However, the predominance of inorganic clastic sediments relative to the other targets is evident and might imply the effectiveness of this matter controlling the water quality of the lagoon.

Within zone IV corresponding to the industrial area, the controlling water quality targets are in order of magnitude: suspended inorganic clastic sediments, phytoplankton plume and the oil- like substance. The large variability of the targets produced by the standard satellite image classifier supports the statement that the actual numerical values recorded by the TM sensor for Zone IV are fairly low. We would expect higher numerical values for that zone compared to the others since the dominance of suspended sediments over organic matter and clear water was recognized during field surveys. During the three surveys, the water of that zone showed a very turbid aspect.

The mixed targets composed of suspended clastic sediments and mangrove vegetation (organic component) occur partly in Zone I. The mixed targets recognized within Zones IIa, IIb, IIc and Zones IIIa, IIIb, IIIc are the suspended inorganic clastic sediments and clear water. So inorganic clastic sediment is the most abundant parameter controlling the water quality of the *Jequia* lagoon.

4.6.3. Description of methods used to process data of water quality parameters of the Jequia lagoon

The methodology used in this part comprises three main steps: a pre-processing procedure which includes the selection of the TM bands containing the most suitable

spectral information regarding the targets, the correction of atmospheric scattering and the removal of bad line strips.

The second step comprises the analysis and interpretation of the overall irradiance (OvIr) for the targets within the water column of the lagoon. The procedures applied in this step involve the application of simple image arithmetic, decorrelation of data through the principal component transformation, the categorization of data using density slicing classification and a standard Gaussian (normal distribution) classifier.

The last step concerns the estimation of the overall or total irradiance (OvIr) over the *Jequia* lagoon and the irradiance produced by the suspended sediment plume, the phytoplankton (organic matter), the oil-like plume and the water matter. A simple general model of the residual radiance (ReIr) for the mixed targets is also proposed in this step.

4.6.3.1. Selection of thematic mapper bands to map water quality targets within the water column of the Jequia lagoon

The following procedures were carried out in order to isolate lagoon data from land-cover data, before each data processing step was performed. Foremost, the seven TM bands of the water body were used to mask the land surrounding that lake preventing the mixed pixels from the rest of the study area to influence the spectral reflectance produced only by the water quality parameters. Subscenes sets presenting 700 pixels per 700 lines were selected and generated from an image of 3 089 pixels per 3 600 lines.

The TM1, TM2, TM3 bands (visible light) were selected to map the spectral signature of suspended inorganic matter (turbidity), of sediment-vegetation contrast, of plant vigor and water column depth of the *Jequia* lagoon. The near-infrared TM4 was selected to map the biomass content of organic matter recognized in the water column of that lagoon. These targets produced the overall irradiance energy recorded within the visible and near infrared wavelength range (485 nm to 820 nm).

The TM5 band was discarded since it did not show any other significant spectral information regarding the water quality targets along the lagoon. The data recorded within the TM5 band is highly correlated with those recorded on the TM4 band and when used in some preliminary vegetation index processing, it has shown significant overlapping of information. Total absorption of energy was observed on the water targets from TM6 and TM7. It is also noticed that some mixed pixels of sugar-cane and farming crops along the contour of the lagoon show several spectral signatures on TM5 band.

Regarding the thermal variation along the water surface of the lagoon, a uniform emission pattern is observed on the digital image. Therefore the TM6 band was also neglected. The digital data of the land surrounding the *Jequia* lagoon was also discarded. A large variation of the vegetation spectral patterns is observed along the banks surrounding that lagoon. All the mixed pixels located on the lagoon contour, showing some data from water quality targets and some from sugar-cane and farming crops surrounding that environment, were avoided and extracted from the water mask

4.6.3.2. Removing bulk atmospheric scattering from raw data along the Jequia lagoon.

Correction of the bulk atmospheric scattering was performed by subtracting from each visible TM band a given minimum pixel value that represents the effect of scattering. The image resulting from corrected data is hereafter called the corrected image or the corrected data set. This method often called the dark pixel subtraction correction has been used by Scarpace *et al.,* 1979, Ritchie *et al.,* 1990 and Crosta 1992, 1993. It is recommended to use the empirical dark pixel subtraction method before any band ratio is performed. Therefore, in this investigation, the dark pixel method was performed before any data processing step was performed.

Based on the concept of the dark pixel subtraction method (Crosta 1992) which defines that the sun radiation might be used as an ideal or efficient normalized factor, the

minimum values of Digital Numbers (DN) within clear water (deep water) sites are used here to normalizes the rest of the digital numbers within the image . Therefore, the minimum DN values mapped on the deepest water zones (Zone IIb) of the *Jequia* lagoon and the *Poxim* lagoon were used to remove the bulk atmospheric scattering for each visible and near-infrared bands.

Considering that the dark pixel subtraction method is a linear operation which normalizes the corrected DN values out of the interval recorded by the TM sensor, the results obtained in this study were re-scaled to the interval of 0-255. The additive nature of the atmospheric scattering effects might create constrains to the effectiveness of this normalization. Nevertheless, it is assumed that for the case of the study area, the method is effective, since the region is located on a tropical humid environment with very low seasonal variations of sun irradiance. The *Jequia* study area is located in a tropical environment subjected to minor effects due to atmospheric scattering.

No significant visual differences are noticed on water quality targets between the image generated with raw data and the image generated with corrected data. However, the absolute numeric values produced by those targets show subtle differences from raw data, on the corrected image and the "destriped" image.

The only data processed without applying the dark pixel subtraction method was the Karhunen-Loeve transformation (The Principal Component Analysis). This transformation was performed using simple raw data.

4.6.3.3. Removing noise of raw data for the water surface of the Jequia lagoon

The noise signatures characterized within this study include the regular and parallel stripe zones homogeneously distributed over the study area and the irregular stripes locally distributed respectively in Zone IIIc and in Zone I of the lagoon.

The regular and parallel lines, produced by the TM sensor of the satellite, are mostly enhanced in the raw data of all visible and near infrared TM bands and on the corrected data of TM2 and TM4 bands. The striped lines are markedly recognized in TM3 and TM4 bands when applying root and equalized enhancements.

The EASY PACE (within PCI) destriping program was performed to remove the regular and parallel striped zones along the *Jequia* lagoon. The destriping program was used on a subscene image of 700 lines per 700 pixels according to a 32 cycle recommended for LANDSAT TM product.

The convoluted filters of 3 x3 were also applied on raw data and on the processed image. They produced a better performance on the spatial distribution of the data, since this type of filter is recommended as the simplest essential procedure operating on the spatial domain of any image. The unsupervised EASY PACE destriping program did not remove efficiently the striped zones. It generated randomly some regular striped zones and enhanced some others. On the contrary, filtering proved to be more efficient in removing the noise of the raw data and processed data than the destriping program.

The irregular stripes mostly enhanced on TM4 were considered in this study as random noise. The effect of random noise is believed to be the results of cloud over part of the study area and/or local currents along the water surface of the lagoon. The irregular stripes were removed by simply applying the destriping program. The dark pixel subtraction correction also proved to be efficient in removing that noise.

4.6.4. Analysis of digital raw data, derived and corrected data for the suspended matter of the Jequia water

The data analyzed in this section were obtained through: 1) linear, square and infrequency contrasts; enhancements using the Hue-Saturation Intensity index (HSI); 2) decorrelation data using the principal component transformation; 3) multispectral imaging

by band ratio and band subtraction; 4) categorization of the water quality targets using density slicing classification and 5) standard Gaussian classifier and preliminary considerations of a non parametric classifier using the EASI PACE unmixing linear spectral program.

The Digital Numbers (DN) expressed as numeric values converted to integer values, represent the digital raw data recorded by the TM sensor over the water of the *Jequia* lagoon. They also represent part of the spectral response of the water quality parameters of that lagoon. The inspection of DN values in the raw data matrix (Figures 4.5 to 4.8), of corrected or derived data and of destriped data (Table 4.1) were the first steps in the analysis of the spectral response of the water quality targets. This set of DN is the original response recorded by the TM sensor.

The inspection of the irradiance energy values converted from the above data sets illustrated respectively in tables 4.2 and 4.3 was also performed. In this study, the converted value represents a proportion of the overall irradiance energy or computed from the data recorded by the TM sensor. The radiance representing the physical absolute values of total energy recorded by the TM sensor is computed from published data. The maximum and minimum radiance was used. The computation of the radiance follows the model of Robinove (1982).

In summary, remotes sensing data discussed in part II are done by statistical analyses of the histogrammetric derived results, the corrected and converted data and the visual analysis of maps. The maps were produced by the following techniques.

4.6.4.1. Characterization of histogrammetric data

The first step used in the characterization of histogrammetric data is the plot of the absolute digital numbers (DN) in the form of a quadratic matrix (Figures 4..5 to 4.8). The simple analysis of the grouped DN in matrices suggests the subtle variability within the

spectral signatures of the targets for the selected training zones on the visible bands (TM1, TM2, TM3) and on the near-infrared band (TM4).

The absolute digital values (Figure 4.5) on the 485 nm (TM1) wavelength range vary from 50 to 55 for Zone I (lagoon outlet), from 47 to 52 for Zone IIb (mid lagoon), from 48 to 52 for Zone IIIa (secondary inlet) and 52 to 53 for Zone IV (main inlet). The absolute digital low values of 46 to 50 indicate a deepest and clearest water nature for Zone IId and IIIc. No suspended sediment was recognized within these latter zones during field work. The digital values found within the others' zones vary from 50 to 52.

The digital values (Figure 4.6) on the 560 nm (TM2) wavelength range for Zone I (lagoon outlet) vary from 21 to 22, for Zone IIb (mid lagoon) and Zone IIIa (secondary inlet) the variation is from 19 to 21 and for Zone IV (main inlet) from 22 to 24. Within the Zone IIIc that represents the clearest water site, the recorded response on TM2 varies from 18 to 20. The DN reflectances of Zones IIa, IIc, IId and IIIb vary from 19 to 23.

The absolute digital values (Figure 4.7) on the 664 nm wavelength range (TM3) vary from 14 to 16 for Zone I (lagoon outlet), from 14 to 15 for Zone IIb (mid lagoon), from 15 to 17 for Zone IIIa (secondary inlet) and from 15 to 17 for Zone IV (main inlet). The lowest absolute digital values of 11 to 15 were recorded for Zone IIIc. The other zones show values from 14 to 18.

Absolute digital values (Figure 4.8) on the wavelength range of 820 nm (TM4) vary from 4 to 6 for Zone I (lagoon outlet), from 4 to 5 for Zone IIb (mid lagoon), from 3 to 6 for Zone IIIa (secondary inlet) and from 9 to 10 for zone IV (main inlet). The lowest absolute digital values vary from 3 to 6, indicating that Zone I, IIb and IIIa are the least organically polluted water sites along the *Jequia* lagoon.

The second step in the analysis of the histogrammetric data is the plot of the mean, the standard deviation and the covariance statistics against the mean and median values. It

attempts to discriminate the best bands to map the distribution of the suspended inorganic matter and to distinguish the targets within the mixed plume. The analysis of the mean, standard deviation (Figures 4.9 and 4.10) and covariance (Figures 4.11) plotted against the mean and the median suggests the discrimination of the suitable bands which contain the most information regarding water quality targets focused in this study.

The results in figures 4.5 to 4.8 show the range of variability of the LANDSAT TM image after removing striped zones and linear atmospheric scattering. The TM4 (Figure 4.8) shows the large variation of information on the same image. Maps with destriped image and corrected images using the dark pixel subtraction method were elaborated.

The derived DN values of mean and standard deviation for TM1 and TM2 indicate (Tables 4.1) the subtle differences between the targets within these two TM bands. Nevertheless, they are not visually distinguishable in maps.

The histogrammetric data (Tables 4.1) were enhanced by infrequency contrast in order to maximize the differentiation of the water quality targets. However, the resulting graph (Figure 4.11) shows that the little variability in the digital data inhibits the discrimination of specific spectral patterns produced by each water quality target.

The results from the interpreted maps of figures 4.14 to 4.17 suggest that TM1 and TM2 are the band sets containing the most significant information regarding the suspended sediments in Zone I and Zone IV. The best TM bands for phytoplankton vigor in Zone IV are TM2 and TM3. Therefore, the TM bands 1 and 2 have recorded mostly the spectral response produced by the plumes containing dominantly suspended sediments. The TM bands 2 and 3 have recorded mostly the spectral response produced by the phytoplankton and the suspended sediments. We assume that the former target reduced the reflectance produced by the sediments within the TM1 range.

The oil-like plume considered to be mixed with the phytoplankton and sediments within Zone IV, exhibits a non-particular spectral signature. We believe that the oil-like plume might be diluted within the others targets or drained to other zones. Moreover, the oil-like plume seems to mask the specific reflectance signature of the other two targets, producing anomalous numerical values. The spectral pattern of that plume might have reduced by absorption effects the spectral signature produced by the clastic sediment plume. Consequently, the spectral response within TM2 and TM3 has been also enhanced by the signature of plant vigor.

In the case of Zone IV, we believed that the radiation is partly absorpted by the oil-like plume and algaes. Therefore that plume is the most active target controlling the residual or overall irradiance of the mixed plume within Zone IV. This argument is supported by the fact that there is a distinct spectral pattern in all results for that zone.

The above statement disregards or neglects the loss of reflectance due to random noise and scattering within the water column. The variation of grain size within the terrigenous sediments might play a significant influence on to scattered irradiance.

4.6.4.2. Producing multispectral enhanced images

Linear and infrequency band spectral contrasts were performed in attempting to maximize the oil-like plume signature and minimize the signatures from sediments and the phytoplankton within Zone IV. However, the selected methods were performed only to enable the discrimination of these targets within a mixed plume. The differentiation of those plumes along Zone IV was not obtained using simple contrast enhancements. It is assumed that the targets (oil-like substance, sediments, phytoplankton) are very well mixed in different proportion within the plumes. However, the mixed plume of Zone IV showed a specific spectral pattern on simple linear or equalization contrast, relative to the other zones. Contrast stretches were applied to classify the spectral response of the selected zones over that lagoon. Root and equalization enhancements suggest anomalous

reflectance patterns for turbidity. The turbid water is considered to be the result of high concentration of suspended inorganic matter (sediments) in the water column.

Improved results were obtained when applying Hue-Saturation-Intensity (HSI) enhancement on the transformed data by principal component analysis. The zone targets distinguished by simple contrast are very well enhanced through the HSI.

4.6.4.3. Mapping the decorrelated digital data using the principal component transformation

Principal Component Analysis (PCA) or Karhumen-Loeve (K-L) transformation has proved to be a useful tool in mapping hydrothermal alterations with TM sensors (Crosta and Rabelo, 1993). Moreover, the selective PCA transformation has also been used to minimize the problems in reducing the dimension of a large volume of data. It was performed to enable the selection of bands that contains the most data regarding the water quality parameters of the lagoon. Initially, the PCA was performed using all TM bands. The visible TM bands were used alternately with the near-infrared and the medium infrared bands. The first set comprised the TM1, TM2, TM3, TM4 and TM5 bands. The second band set included the TM1, TM2, TM3 and TM4 bands, and the third comprised only the visible TM1 and TM2 bands.

Results of tables 4.4 and 4.5 show that the TM bands set containing the most significant information regarding suspended sediments and also plant vigor are TM1 and TM2. The results also demonstrate that the principal component transformation using all bands did not add any information maximizing the separation between the water targets.

The images generated using the five principal components eigen values show that the first two principal component images with data from TM1 to TM5 account for about 98,5% of the overall irradiance recorded (93,86% for PC1 and 4,64% for PC2). The four principal component images comprising TM1 to TM4 show a similar proportion for the

first principal eigen values in the three differences images. Within the TM band set of TM1 to TM3 (Table 4.4), most of the information corresponding to 89% is covered by the first two components and 66,46% covered already by the first component.

The visible wavelength TM bands were the most highly correlated images selected. Within these subsets of bands, the amount of information lost to unused components was minimal. The best principal components images produced within this study contain decreasing proportions of scattered data within TM2, TM3 and TM4 bands.

The principal component image (Figure 4.22) was used to highlight the areas of punctual changes that were evident in all multispectral imagery TM bands. Those changes are believed to be the results of variations of the concentration of suspended sediment within the water column of that lagoon. The interpreted zones defined in figure 4.22 present generalized colors for Zones IIa, IIb, IIIa, III and IV.

To the highest correlated data within the five TM bands mapped was applied a supervised Gaussian classifier (Tables 4.6 and 4.7). The raw data were also used to produce a maximum likelihood classified regional image (Figure 4.20). The targets categorized using both data sets produced similar images.

Two spectral pattern analysis techniques were employed to determine which bands maximized the separation between the targets within the mixed plume (the inorganic clastic sediment, the oil-like plume and the phytoplankton). The Karhumen-Loeve (K-L) transformation proved to be the most appropriate technique to select the TM bands most suitable for mapping mixed water quality targets of the lagoon. Therefore, the specific reductionism of K-L transformation is appropriate to perform a series of decorrelations on correlated images of selected TM band sets.

The mixed spectral reflectance from the targets in all zones and recorded within the TM1, TM2 and TM3 bands are highly correlated. However the K-L transformation did not enable a precise separation of the specific water targets' spectral signatures.

Each distinguished zone was mapped as composed mostly of a mixed plume of several water quality targets. For Zones I and IIIa, the spectral signature for sediments predominate over the others targets. For Zone IIb, clear water spectral signature predominates. Mixed plumes in Zone IV present a specific spectral signature. They show difference from the other zones.

4.6.4.4. Producing multispectral rationed and subtracted images with estimated digital bathymetry

The estimation using the digital bathymetric data of the *Jequia* lagoon was performed using data in situ gathered by lifting down a rope attached to the dredge equipment at each sediment sample site. Four main bathymetric areas were mapped. Area 1 (Zones IIa, IIb, Iic and IIIa) represents the deepest zone with depth ranging from 9 to 12,5 meters. Area 2 (Zones I and IV) represents the shallow one with depth ranging from 3 to 4,9 meters and the two other intermediate Area 3 and 4 comprising Zones IId, IIIb and IIIc with depth ranging from 5 to 8,4 meters (Figures 1.3 and 1.4).

The estimation of the digital bathymetry of the *Jequia* lagoon using LANDSAT-TM data was performed by band rationing and band subtraction. The selection of TM bands to map the bathymetry of the lagoon was based on the assumption that light penetration within water columns is wavelength dependent. For the data processing by rationing, only the visible spectrum TM bands were used for they record the highest reflectance of suspended inorganic matter (Figure 4.13).

The TM1 (blue wavelength) band showed the highest suspended sediment signature. It also produced the highest light penetration values reaching depths of 10 m in the water

column. The TM2 (green wavelength) band is assumed to map the lagoon depth down to 5 m. The overall albedo is considered to be recorded within TM3 (red wavelength) band to a depth of 1 m. The absorption and scattering effects of the water column of the lagoon is basically deduced from the expected effect produced by the targets within the attenuated irradiance of energy. These effects are considered to be related to the variation of grain size, mineral type and concentration of sediments.

Due to the high reflectance of suspended matter, the rationed image contained only visible spectral responses. Band TM3 and band TM 4 were used to map phytoplankton plumes.

Innumerable published examples of single and multiband processed data show reflectance patterns depending on turbidity, turbulence and salinity levels. We refer to the works of Nichol (1993), Lavery *et al.* (1993), Lathrop *et al.* (1989), Khorram and Cheshire (1985), Khorram (1981) and Johnson and Harris (1980).

In this study, band ratios and band spectral differences were used to estimate and to enhance the differences between the water quality variables selected along the lagoon. The third technique used was the analysis of spectral patterns plotted from the TM2/TM1, TM1/TM2, TM2/TM3, TM3/TM2, TM3/TM4 and TM4/TM3 ratios. Enhanced and spatial filtering from TM images proved to be the best techniques to detect water circulation patterns. Regression analysis and correlations were applied to assess the physical, chemical and biological water quality parameters in polluted tropical estuaries.

4.6.4.5. Producing water types image using a multispectral subtracted method

The visible wavelength bands (TM1, TM2 and TM3) were selected to map the water quality targets of the lagoon by subtraction methods. The method enabled the enhancement of subtle spectral differences between these targets. The selected set of TM bands recorded high correlated information regarding the water quality parameters. In

addition, the spectral response of those targets showed a systematic overlapping when subtraction methods were applied to their data.

The image generated by subtracted methods (Figure 4.13) showed distinguishable signatures for Zones I, IIb, IIIa, IIIb and IV. There are subtle reflectance differences between Zones I, IIIa and IIIb. The spectral reflectance mapped from the targets of Zones IIa and IV presents specific patterns differing from the other Zones. A very large variability of information was mapped within Zone IV.

4.6.4.6. Generating a multispectral image using the density slicing classifier

Density slicing using the histogrammetric data was performed to derive target categories of classified data. The DN interval classes selected from TM1 (47 to 56), TM2 (17 to 24) and TM3 (12 to 18) using Sturges algorithm were encoded in pseudocolor values. Images generated by the density slicing classifier and the pseudocolor encoding (Figure 4.14 to 4.16) were also used to derive patterns of water quality target categories along the water body.

The results produced by pseudocolor encoding showed comparable signature patterns for Zones I, IIb, IIIa and IV for the 3 bands and some similarities with those distinguished by the PCA transformation.

4.6.4.7. Generating multispectral water types image using the standard Gaussian classifier

In order to test a maximum likelihood classification of the water types, training areas were defined for each class by analyzing pixels in several locations for each zone. The groups of pixels were arranged in quadratic matrices. Pixel matrices of 3x3, 6x6 and 9x9 for a given category of mixed targets were selected for each zone and distinguished by the techniques described in the following paragraphs.

Four TM bands were used in the selected training sites. Four to fifteen locations were defined for each zone of the lagoon. A group of 60 to 150 pixels was picked within each location. Zone IV showed very few pixels and locations.

The types of water quality classes or categories mapped with the maximum likelihood standard or Gaussian classifier showed subtle differences from the categories mapped using the density slicing classifier. We assume that these differences might be negligible and both classifiers are suitable to map the water quality classes of the *Jequia* lagoon. It was noticed that the maximum likelihood classifier performed an overall impression of noise in the signature patterns of the water quality targets mapped in the water column. This impression might result from the principle that spectral parametric classifiers assume the existence of an underlying probability distribution of the data. On the contrary, the non-parametric classifiers do not assume anything regarding the probability distribution of the data (Cortijo *et al.*, 1997). Within this study, only preliminary attempts were performed using the EASI PACE unmixing spectral program.

The image (Figure 4.17) generated by the maximum likelihood classifier showed no significant or visible differences in the reflectance patterns within the water quality targets. Those targets are not visually separable. Therefore, we assume that the water column presents mixed targets along Zone I, Zone II and Zone IV and single target within Zones IIIa and IIIb where clear water predominates.

However, the statistical results (Table 4.8) show significant differences in the targets within the water column. Standard deviation and mean values for each training location and pixels varied from zone to zone.

A preliminary categorization of the water quality targets along the lagoon was performed using the EASI PACE spectral linear unmixing program. Although the results are preliminary they suggest more details than the results generated by standard classifiers, disregarding the mixed nature of some water targets. Therefore, we refer to the unmixing

spectral program as a more performing and adequate technique to enable the separation of mixed homogeneous water quality targets of the *Jequia* lagoon. Published data (Mertes *et al.*, 1996) using the spectral unmixing method for mapping suspended inorganic matter (sediments) have proven to be more efficient than standard Gaussian classifiers for mixed or homogeneous targets.

Due to the limited tests performed in this study, the spectral unmixing classified data are preliminary and require more systematic testing and analysis.

4.6.4.9. Statistical analysis and interpretation of the decorrelated data from the principal component and maximum likelihood classification

The covariance matrix (Table 4.5) and confusion or error matrix (Table 4.6) shows significant differences between data recorded in each individual TM bands within the four zones classified. Both statistical techniques were used respectively to analyze the distribution of classified data in the principal component and maximum likelihood classification.

The error matrix is the technique used in this study to express the accuracy of the supervised classification (Table 4.7). It contains along the first column the training zones assumed to be corrected and interpreted from the aerial photographs. The first rows are assigned to the classified classes performed by the supervised maximum likelihood classifier. The Kappa (KHAT empirical statistic measure) test statistic as suggested by Fitzgerald *et al.*, 1994, was computed to measure the classification accuracy. The KHAT measures of accuracy (0,59) and the automated average accuracy (61,23%) show close agreement. The KHAT measures have not improved the overall accuracy of the classification.

Even though the overall accuracy of this classification lies around 60,96%, the individual land-use classes accuracy varies significantly. The land-use units or categories

(Table 4.7) designated as Jeq-water, Pox-lagoon, Atla-water and Jeq-channel indicate a very good accuracy ranging from 78,4% to 92,3%. The land-use classes designated as Farming, Sugarcane mixed and Bare soil present accuracy ranging from 42,1% to 53,6%. The Urb-sites (built up area) and Routes land-use classes show the least accuracy classification with 29,7% and 33,6% respectively.

The covariance matrix generated with the principal components 1, 2, 3, 4 an 5 is used to express the classified water quality targets with the five TM bands selected. The albedo pattern was mapped considering the absence of any contrast in the first principal component (PC1). The PC2 and PC3 show a contrast within TM4 and TM5 bands that we consider to be the spectral pattern of phytoplankton. The principal components 4 and 5 show contrast within TM1 and TM2 that corresponds to the spectral signatures of suspended sediments.

4.7. Interpretation of digital raw and corrected data for suspended matter in the water column of the *Jequia* lagoon

The inorganic particles are a common element in natural (fresh) waters, differing widely in size, shapes, distributions and optical properties. Those characteristics determine and alter the spectral properties of light upwelling in any water body. Therefore, we consider that the spectral differentiation of these particles is fundamental due to their influence on attenuating the light penetration by scattering and absorption.

The best fit linear regression analysis computed with data of selected TM bands (Figures 4.18 and 4.19) shows high correlation between two simultaneous and non-simultaneous TM bands. TM1 and TM2 show high correlation and TM1 and TM3 even higher correlation information. These results imply strong similarities between the targets in the water column of the lagoon.

Concerning the visible TM1 band and medium infrared TM5 band (Figure 4.19), there was a poor correlation whereas for TM1 and TM4, there was a strong correlation.

High correlation recognized in the above TM band sets implies that the spectral signatures of water quality targets in the visible wavelength show straight similarities. Poor correlation between TM1 and TM5 supports the statement of vegetation signatures perceived only in the mixed pixels surrounding the lagoon and some sugar-cane crops.

It is therefore assumed that the water column of the *Jequia* lagoon presents a composite distinctive nature. It is mainly composed of mixed homogeneous targets. The strong correlation in figure 4.19 supports the selection of only two pairs of TM bands to process data through band rationing and through principal component transformation. The selected pairs of bands enable a full characterization of water quality targets. Otherwise overlapped information would have masked most of the significant data.

4.8. Modeling the overall residual irradiance for the water column of the *Jequia* lagoon

4.8.1. Introduction

It is assumed that the most controlling targets playing a significant role on the optical characteristics of the water column of the lagoon are: the sediment properties (grain size, mineral type and their concentration), the content of phytoplankton and nekton, and the content of dissolved organic and inorganic matter including the content of vinasse within Zone IV. Therefore, a preliminary simple residual irradiance model is proposed within this study. It consists of describing the relationship between the spectral reflectance produced by each of the above water targets and the residual irradiance recorded by the TM sensor in 1990 within a 485 to 820 nm range (from blue to near-infrared).

The term irradiance is widely applied within the next chapter. Irradiance refers to the wavelength energy recorded by the TM sensor and also includes the concept of Iqball, 1985. It represents the rate of solar energy arriving at a surface per unit of time and per unit of area. The term irradiation indicates simply the radiation arriving at a surface and coming from any source or origin. It is discussed within chapter five of this study.

The spectral reflectance as well as the residual irradiance are wavelength dependent functions. Nevertheless, the scattered irradiance produced by the particles is assumed to be wavelength independent. Considering the general principles of Kirchoffs' law (Maul, 1985) and omitting the emitted energy along the visible light (constant temperature), the spectral reflectance-Sa (l) within the model can be written as:

$$Sa(l) = a(l) / r(l) \qquad \text{equation 4.1}$$

in which;

Sa (l): Spectral reflectance[(% (Table 4.3) or MW /cm^{-2} sr.mm (Table 4.2)]

a (l): Energy reflected from the water surface

r (l): Energy incident on the water surface

The model includes also considerations regarding the relationship between the residual spectral reflectance, the particle sizes and the lagoon depth. The scattering coming from the atmosphere is neglected within this model.

Considering that no previously spectral reflectance data existed from the study area, the main objective of the proposed model is to estimate a residual overall reflectance that could represent the first preliminary reference data recorded by satellites. It is very pertinent to point out that, within the model, some parameters that might control the residual reflectance are neglected. The solar elevation angle (40°) as a function of the satellite nadir for the *Jequia* region was taken from Hartmann *et al.* (1989). However, the

possible variations in solar zenith angle, atmospheric scattering and random noise were neglected.

Within this study, the proposed residual irradiance model expresses the radiation balance for the water quality of the *Jequia* lagoon. The overall residual irradiance includes the irradiance produced by suspended sediment, by phytoplankton matter, by dissolved matter and by the oil-like substance specially recognized on the western portion (Zone IV) of that lagoon. Clear water response, mixed plume signature, noise effects and albedo are also accounted for in the model discussion. The concepts of overall irradiance (OIr(l), overall absorptance -OAb(l) and overall scattering -OSc(l) from the water quality targets (equation 4.1, 4.2) considered in this study are based on the fundamental theory presented by Maul, (1985), Iqball (1985), Zbindem (1981) and Novo (1989).

The spectral residual irradiance is considered as the sum of the irradiance reaching the water surface and the irradiance transmitted within the water column. The latter irradiance includes the fractions of absorpted and scattered irradiance produced respectively by the suspended organic and inorganic matter, by the water itself and by the sediments.

The total irradiance from the water targets within the visible wavelength range for Zones I, IIb, IIIa and IV along the lagoon was estimated by converting all the digital numbers (DN) into spectral irradiance. The mean DN values were selected from figures 4.5 to 4.8 and converted into radiance (Table 4.8). The differentiated effects of light with depth was also considered, as proposed by the work of Smith *et al.* (1978), Moore (1980), Smith *et al.* (1981), Bukata *et al.* (1984), Maul (1985), Nanu *et al.* (1990), Bierwirth *et al.* (1992), Ji, *et al.* (1992), Dantas (1994) and Lyon *et al* . (1995).

The conversion of DN into radiance was empirically computed using equation 4.1. Lillesand *et al.* (1994) present a linear fit function showing the relationship between radiance and DN values for any given TM. They define the maximum radiance (Rmax) as the irradiance at which the channel saturates and the minimum radiance (Rmin) as the

spectral reflectance corresponding to a DN equals to zero. Markham (1985) using a band-by-band relative spectral response method demonstrates some spectral characteristics of the TM sensor that enable the conversion empirically.

$$CRa = \{(Rmax-Rmin)/255\}DN+Rmin \qquad \text{equation 4.2}$$

in which;

CRa: Converted radiance

Rmax: Maximum radiance

Rmin: Minimum radiance

To estimate the total irradiance within the sensor bands, the CRa were multiplied by each TM band width (Lillesand *et al.*, 1995). The band width (Bw), the maximum radiance (Rmax) and the minimum radiance (Rmin) from the TM1, TM2, TM3 and TM4 bands were extracted from Markham (1985). The converted spectral irradiances are presented in table 4.8. The overall incident solar irradiance is extrapolated from Souza, 1994. He has determined an overall solar irradiance of 5,3 kWhm 2 (June) and 7,7 kWhm 2 (December) for the coast of *Alagoas* and in *Maceio* for the period of 1997-1999. Those values are reduced of 28% during cloudy sky and also for the months of February and November (Nicacio *et al.*, 2001).

We assume that the overall irradiance flux (r) is directly related to the overall albedo recorded within the TM band 3 along the *Jequia* lagoon. It corresponds also to the irradiance that is produced by attenuation effects coming from the specific characteristic of the targets within the water column. They include the grain size, the mineral type and the nature of the inorganic (oil-like substance) and organic dissolved matter. The effects due to absorption and scattering are hereafter considered as the attenuated irradiance flux (k). The attenuation pattern is controlled mainly by the suspended matter (Sathyendranath, 1981).

Within this study we also assume that the spectral reflectance of suspended sediments, organic and dissolved matter controls the irradiance balance for the lagoon. The incident flux-r(l) is also a target-dependent function and represents the irradiance produced by the sun and the atmospheric scattering. Therefore, the overall irradiance (OIr) based on converted DN can be written as follow:

$$OvIr = Ca(l) / Cr(l), \qquad \text{equation 4.3}$$

in which;

OvIr: Overall solar irradiance

Ca(l):Converted reflected irradiance

Cr(l): Converted incident irradiance

The residual irradiance can be expressed using the principle (equation 4.1 to 4.6) of electromagnetic conservation of energy or radiation. Therefore a general irradiance balance can be written as:

$$IrB = a(l) + k(l) \qquad \text{equation 4.4}$$

in which;

IrB: Irradiance balance

a(l): Reflected irradiance flux

k(l): Attenuated irradiance flux

The attenuated irradiance flux represents the sum of the absorpted-a(l) and scattered-sc(l) fraction of energy produced by the suspended matters within the water column of the lagoon. The coefficient of attenuation is designated as the k(l) and their relationship can be written as:

$k(l) = (a)l + sc(l)$ equation 4.5

in which;

k(l): Attenuated irradiance

(a)l : Absorpted irradiance

sc(l): Scattered irradiance

The scattering and absorption coefficients are also split into partial coefficients (equations 4.5 and 4.6) relating the main properties of the targets to wavelength and to water depth. It is also considered that attenuation is dominated mainly by absorption, by two orders of magnitude (Maul, 1985). Since we assume an overall pure water nature for the *Jequia* lagoon, the absorpted irradiance along the four zones is simplified to a factor of 0,025 computed empirically from equation 4.5. The attenuation and scattered values used within the water factor computation come from published data (Maul, 1985). Therefore, the major contribution to the residual irradiance is controlled mainly by the suspended inorganic and organic matter. Moreover, the inorganic particles (sediments) are assumed to be large enough so that their scattering coefficient is independent of wavelength (l) and that the absorpted water irradiance = 0 for all zones. Similar assumption has been reported by Sathyendranath (1981).

It is also considered that the incident irradiance flux Ir(l) is constant therefore corresponding to 1 or 100% of the attenuated irradiance Irk(l) produced within the water column. The incident flux (r) is also a target-dependent function and represents the radiant energy produced by the sun and atmospheric scattering. Therefore, the overall irradiance (OIr) can also be written as follow:

$Ira(l)/Ir(l) + Irk(l)/Ir(l) = Ir(l)/Ir(l)$ equation 4.6

in which;

Ira(l) : Reflected irradiance

Irk(l) : Attenuated irradiance

Irr(l): Incident irradiance

So, a differential residual irradiance model (equation 4.8 to 4.11) is proposed for the water column of the *Jequia* lagoon for each of the selected zones (I, IIb, IIIa and IV). The empirical spectral irradiance model for each zone (I, IIb, IIIa and IV) and the residual irradiance model for the lagoon are respectively expressed within equations 4.7 to 4.11. They express the digital irradiances as a function of wavelength. The spectral reflectance component Sa (l) is taken from equation 4.1 and is assumed to be the ratio between the overall albedo recorded within TM3 (%) and the overall irradiance (OveIR) of about 15 MJ m^{-2}, proposed by Souza (1994) for the *Alagoas* coast.

$Ir(l)_{zone\ I} = Sa(l) + 0{,}025[k(TM2-TM4)]$ equation 4.7

in which;

$Ir(l)_{zone\ I}$: Residual irradiance for Zone I

Sa(l): Ratio of albedo (TM3) and the OveIR

k(l): Attenuated irradiance

TM2: Spectral reflectance (%) within band 2

TM4: Spectral reflectance (%) within band 4

$Ir(l)_{zone\ IIb} = Sa(l) + 0{,}025[k(TM1-TM2)]$ equation 4.8

in which;

$Ir(l)_{zone\ IIb}$: Residual irradiance for Zone IIb

Sa(l): Ratio of albedo (TM3) and the OveIR

k(l): Attenuated irradiance

TM1: Spectral reflectance (%) within band 1

TM2: Spectral reflectance (%) within band 2

$Ir(l)_{zone\ IIIa} = Sa(l) + 0{,}025[k(TM2-TM4)]$ equation 4.9

in which;

$Ir(l)_{zone\ IIIa}$: Residual irradiance for Zone IIIa

Sa(l): Ratio of albedo (TM3) and the OveIR

k(l): Attenuated irradiance

TM2: Spectral reflectance within band 2

TM4: Spectral reflectance within band 4

$Ir(l)_{zone\ IV} = Sa(l) + 0{,}025[k(TM2+TM4)]$ equation 4.10

in which;

$Ir(l)_{zone\ IV}$: Residual irradiance for Zone IV

Sa(l): Ratio of albedo (TM3) and the OveIR

k(l): Attenuated irradiance

TM2: Spectral reflectance (%) within band 2

TM4: Spectral reflectance (%) within band 4

$OReIr = \sum(Ir(l)_{zone\ I} + Ir(l)_{zone\ IIb} + Ir(l)_{zone\ IIIa} + Ir(l)_{zone\ IV}$

equation 4.11

in which:

OReIr: Overall residual irradiance [(% (Table 4.3) or MW/cm^{-2} sr.mm (Table 4.2)]

$Ir(l)_{zone\ I}$: Irradiance of Zone I

$Ir(l)_{zone\ IIb}$: Irradiance of Zone IIb

$Ir(l)_{zone\ IIIa}$: Irradiance of Zone IIIa

$Ir(l)_{zone\ IV}$: Irradiance of Zone IV

Within the above empirical model, the first component (Sa(l)) of equations 4.7 to 4.10 is considered to be constant therefore the attenuated irradiance coefficient controlling the overall residual irradiance (OReIr) along the *Jequia* lagoon

4.8.2. Application and discussion of the irradiance model for the Jequia lagoon

The preliminary residual irradiance model proposed above expresses only part of the overall spectral irradiance recorded by the TM sensor along the *Jequia* lagoon, since not all zones were computed. The model includes the partial irradiance produced by the suspended matter within the water column of the lagoon.

It is assumed within this model that the irradiance is controlled mainly by attenuation effects within the water column. Absorption from the water and from the organic matter is considered only within Zone IV. Phytoplankton and the oil-like substance were abundant along that zone during the field survey, therefore, we assume that they play a major role in increasing the attenuated irradiance. There is also a high turbidity along Zone IV, that is, a significant amount of suspended sediments.

The spectral irradiance estimated for the shallow zones (I and IV) was mainly due to the varying energy scattered and absorpted by the inorganic and organic matter. These matters are distributed along the layers of the water column and the bottom of the lagoon. The spectral irradiance estimated for the clearest and deepest zones (IIIa, IIb) was mainly due to scattering by the suspended sediments. Moreover, part of the signal recorded by the sensor has included the water surface reflection that is, the overall albedo of TM3. The DN results (Figures 4.5 to 4.8) indicate that the proportion of reflected energy, that is the albedo, is higher in Zones IIIa and IV than Zones I and IIb. Zone IIb shows the lowest albedo, which is coherent with the highest values of depth.

The inorganic suspended matter, which are the sediments (quartz+kaolinite), is treated in this study as non-absorpting spherical matter. According to Mie theory's, it is possible to estimate the light scattering from these particles when the index of refraction is known. These minerals (quartz+kaolinite) present index of refraction larger (about 1,554) than the water one (1,333). Then, we assume that light scattering from the water column of the lagoon is largely dominated by the effects of several layers of suspended sediments. Therefore, these sediments contribute mainly to the fraction of scattered energy within the residual irradiance balance. Their spectral response was neglected specially for Zones I and IV since the organic and inorganic matters are the targets controlling the overall irradiance. The fraction of the absorpted effect dominates.

The residual irradiance detected for the shallow zones (I and IV) was mainly produced by the absorption effects of inorganic and organic matter. It is believed that part of the signal recorded by the sensor has included the water surface reflection, that is the overall albedo of the lagoon. The surface of the lagoon is assumed to have a dominating diffuse nature since the characterization of the residual reflectance within this study accounts also for the information recorded on the color of that targets.

The depth variation from the shallow Zones I and IV (3 to 5 m) to the deepest Zones III and IIb (6 to 12 m) plays also a significant role within the residual irradiance recorded

by the LANDSAT TM sensor. This parameter might create constraints on any comparison between the residual irradiance detected by the TM sensor and the residual spectral reflectance (irradiation) recorded by the spectro-radiometer in laboratory for a constant depth. The results indicate a high attenuation due to the significant absorption and scattering effects from the targets within Zones I and IV and a low attenuation effect produced by the targets within the water column of the deepest Zones II and III of the lagoon. Therefore, the higher overall residual irradiance is controlled mainly by the partial irradiance estimated for the shallow Zones IIIa and IV. The interpretation of the model suggests at least two uniform layers of water for Zones I, IIb and IIIa and a very mixed one for Zone IV. It is assumed that two deepest layers exist along Zones I and IIb and a shallow one within zone III. These results show good agreement with the bathymetric data.

FIGURES AND TABLES FOR CHAPTER 4

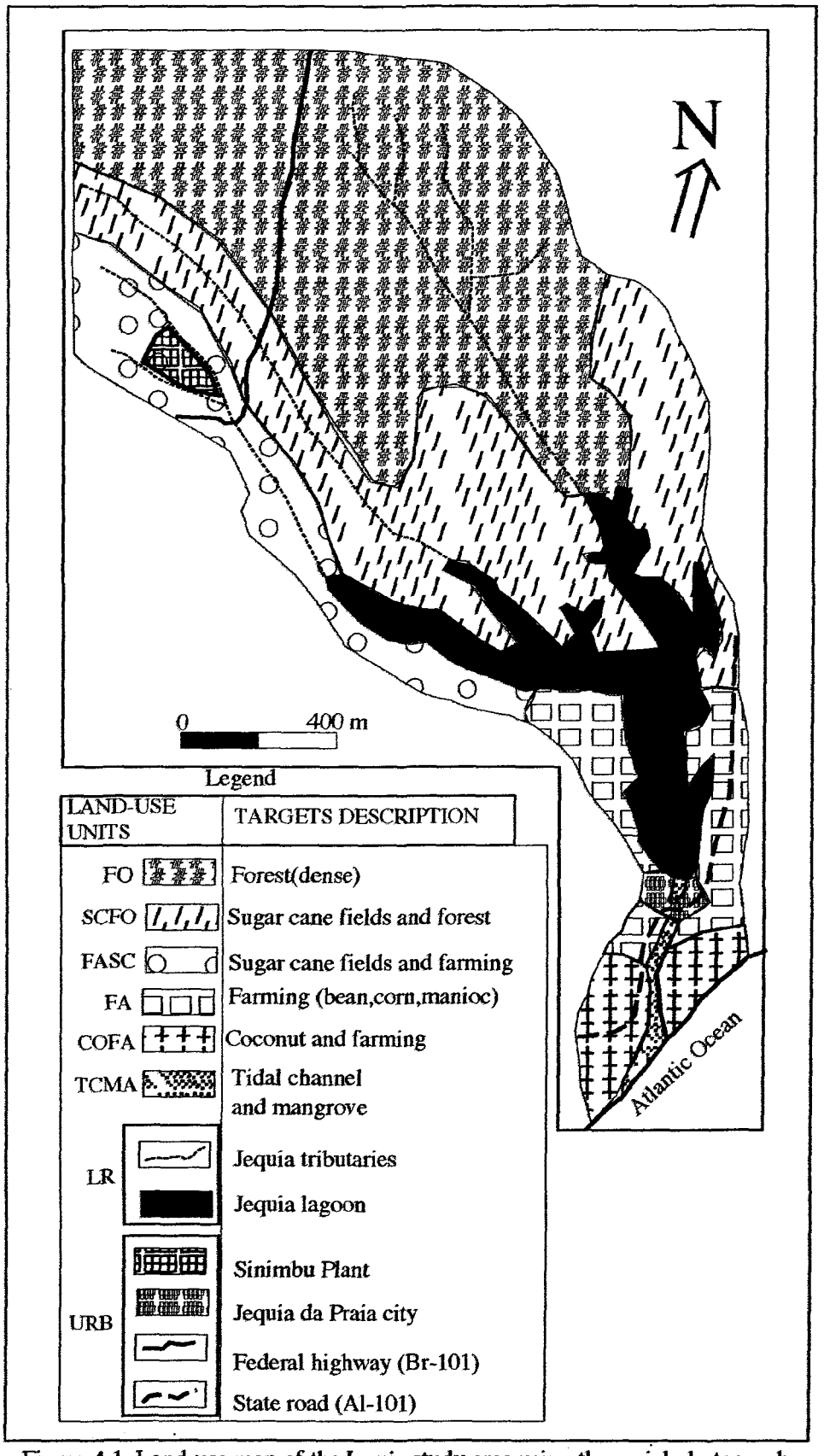

Figure 4.1. Land-use map of the*Jequia* study area using the aerial photographs recorded in 1968

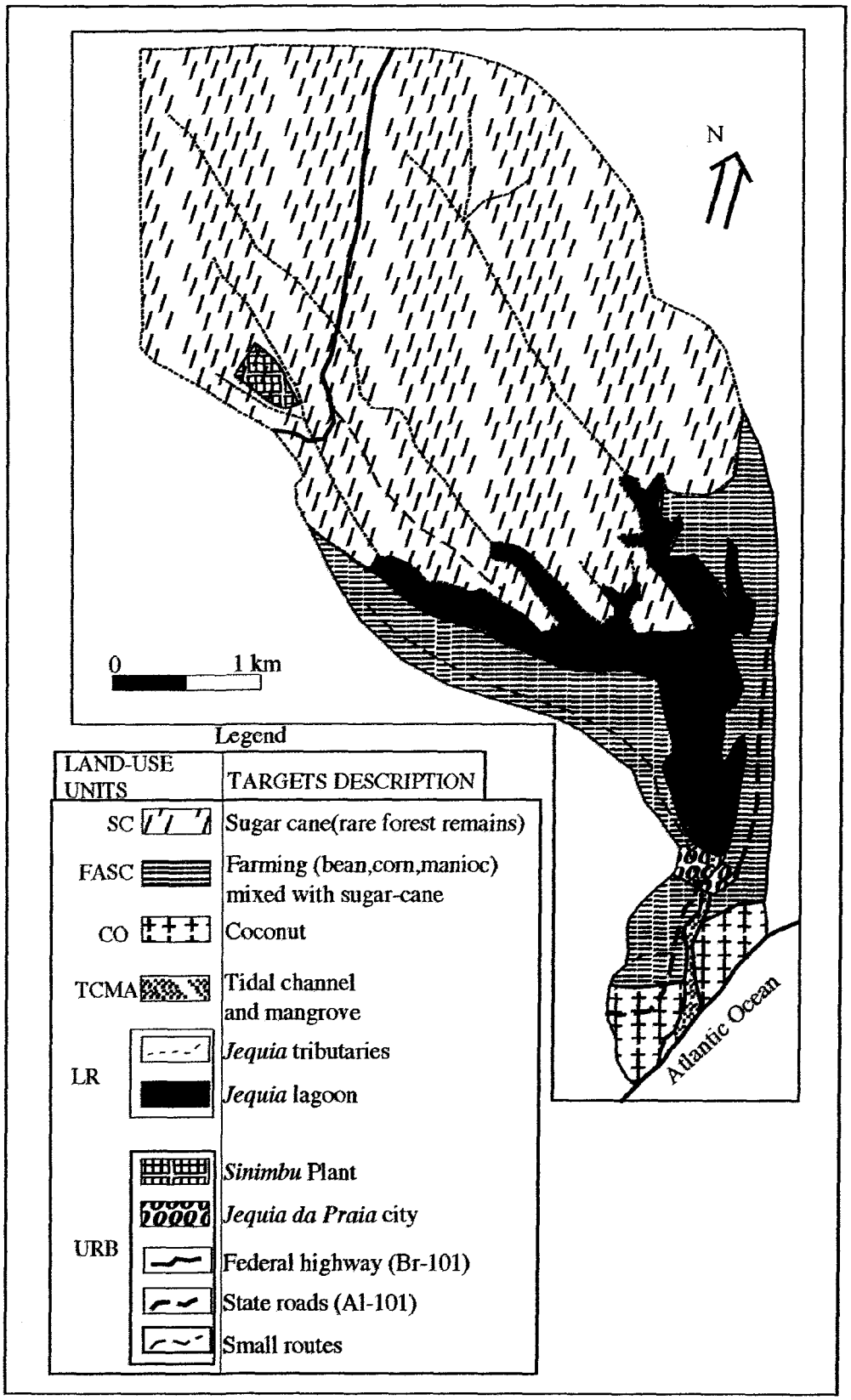

Figure 4.2. Land-use map of the *Jequia* study area based on the LANDSAT quick-look recorded in November 1989.

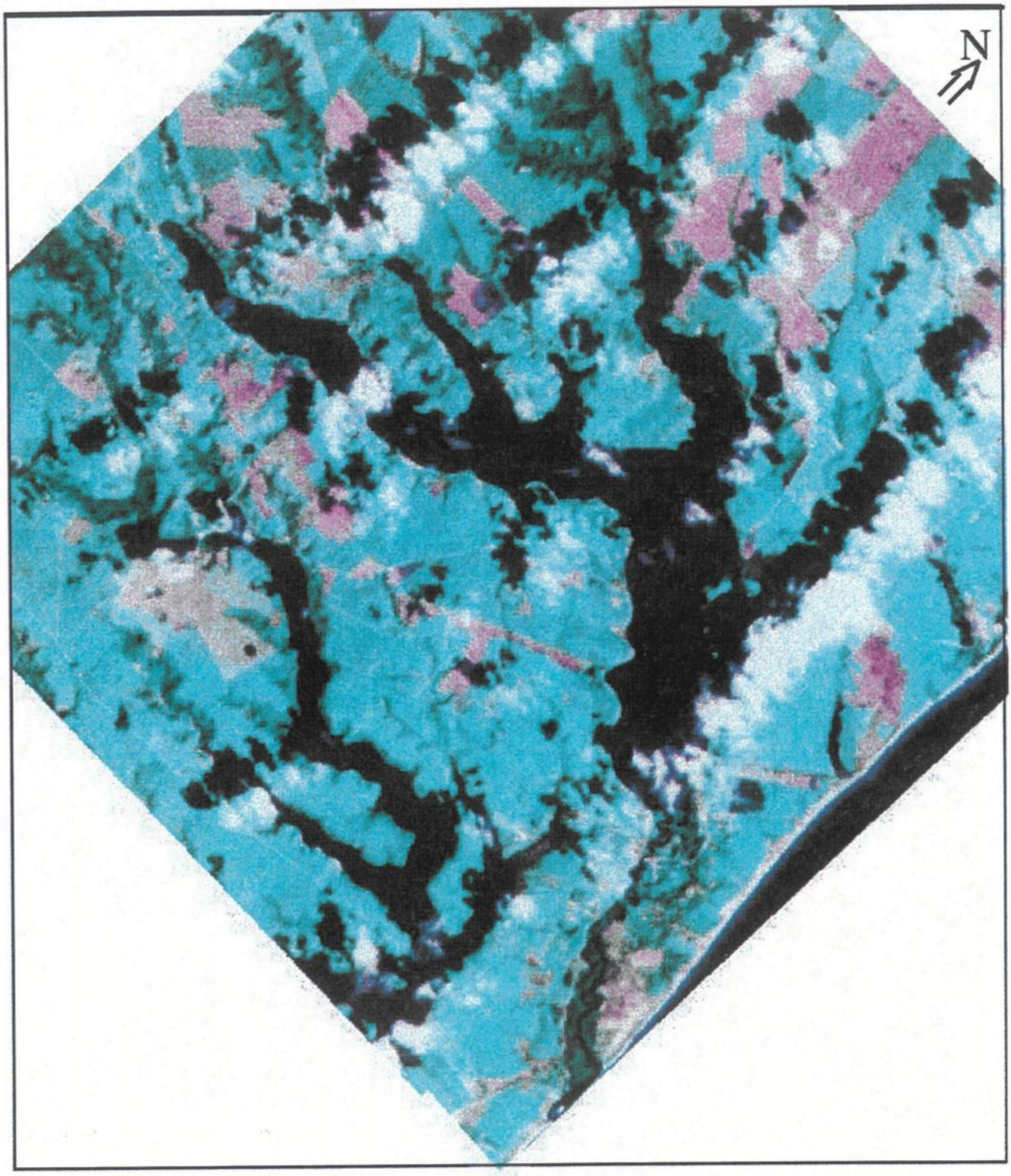

Figure 4.3: Landuse patterns of the Jequia estuarine-lagoon system from a quick-look LANDSAT-TM image recorded in November of 1989.

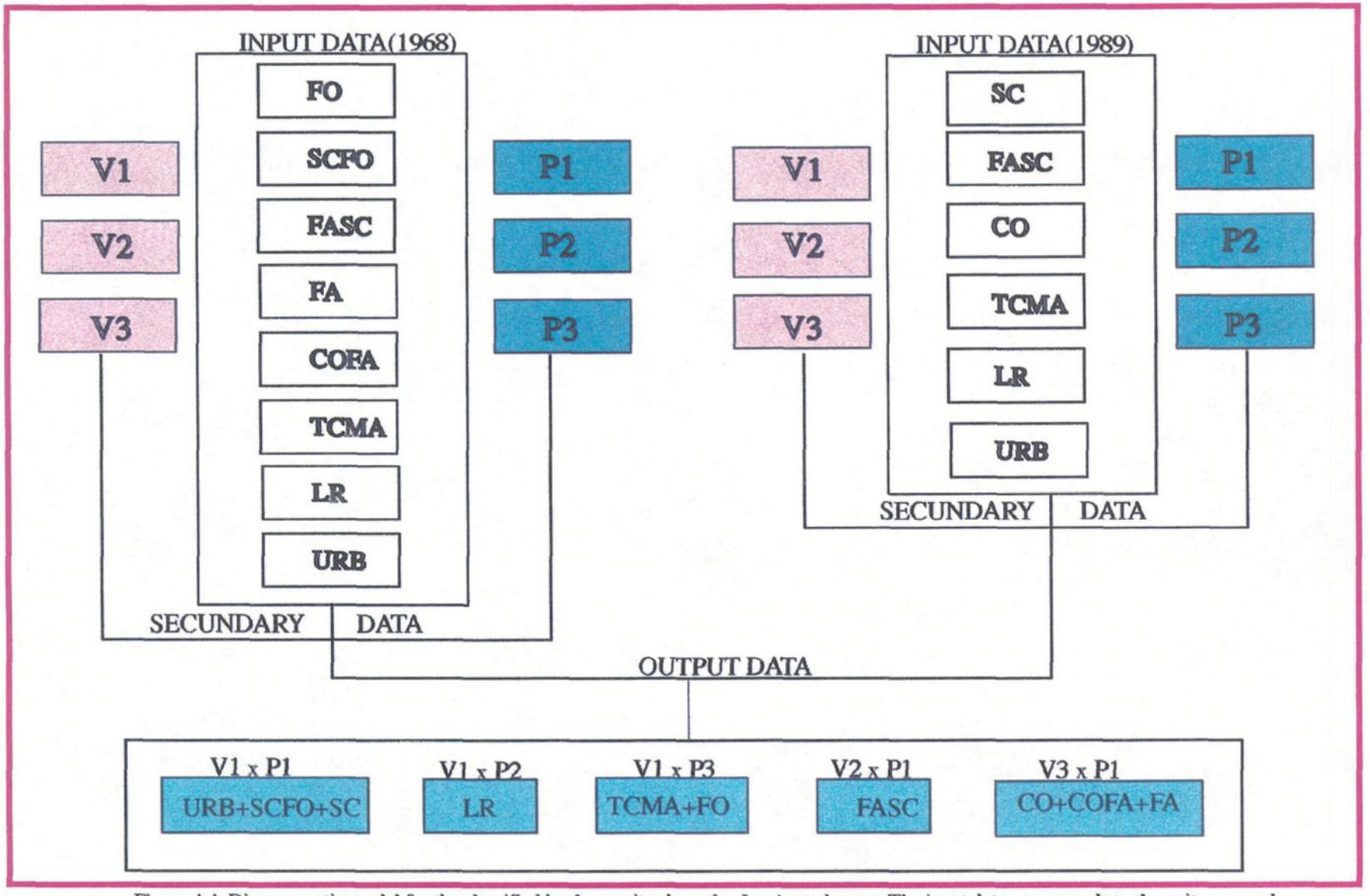

Figure 4.4: Diagrammatic model for the classified landuse units along the *Jequia* study area. The input data corresponds to the units grouped in figures 4.1 and 4.2. The designated analytic V1, V2, V3, P1, P2 and P3 correspond respectively to qualitative levels(1=high, 2=intermediate, 3=low) of natural vulnerability and potentiality of the landuse units.

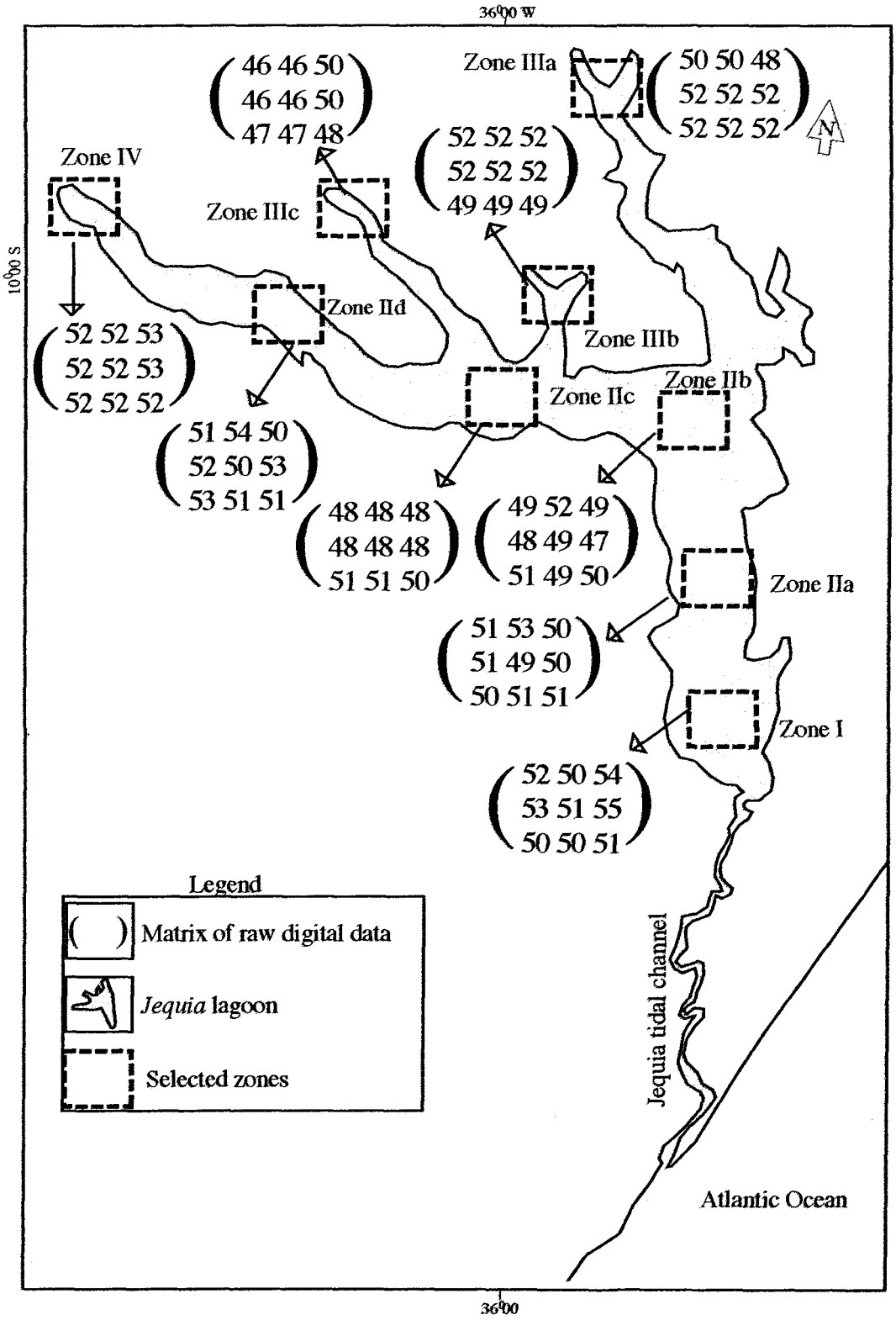

Figure 4.5. Landsat TM1 raw digital data expressed as digital numbers (DN), of the selected zones along the water surface of the *Jequia* lagoon, *Alagoas* Brazil

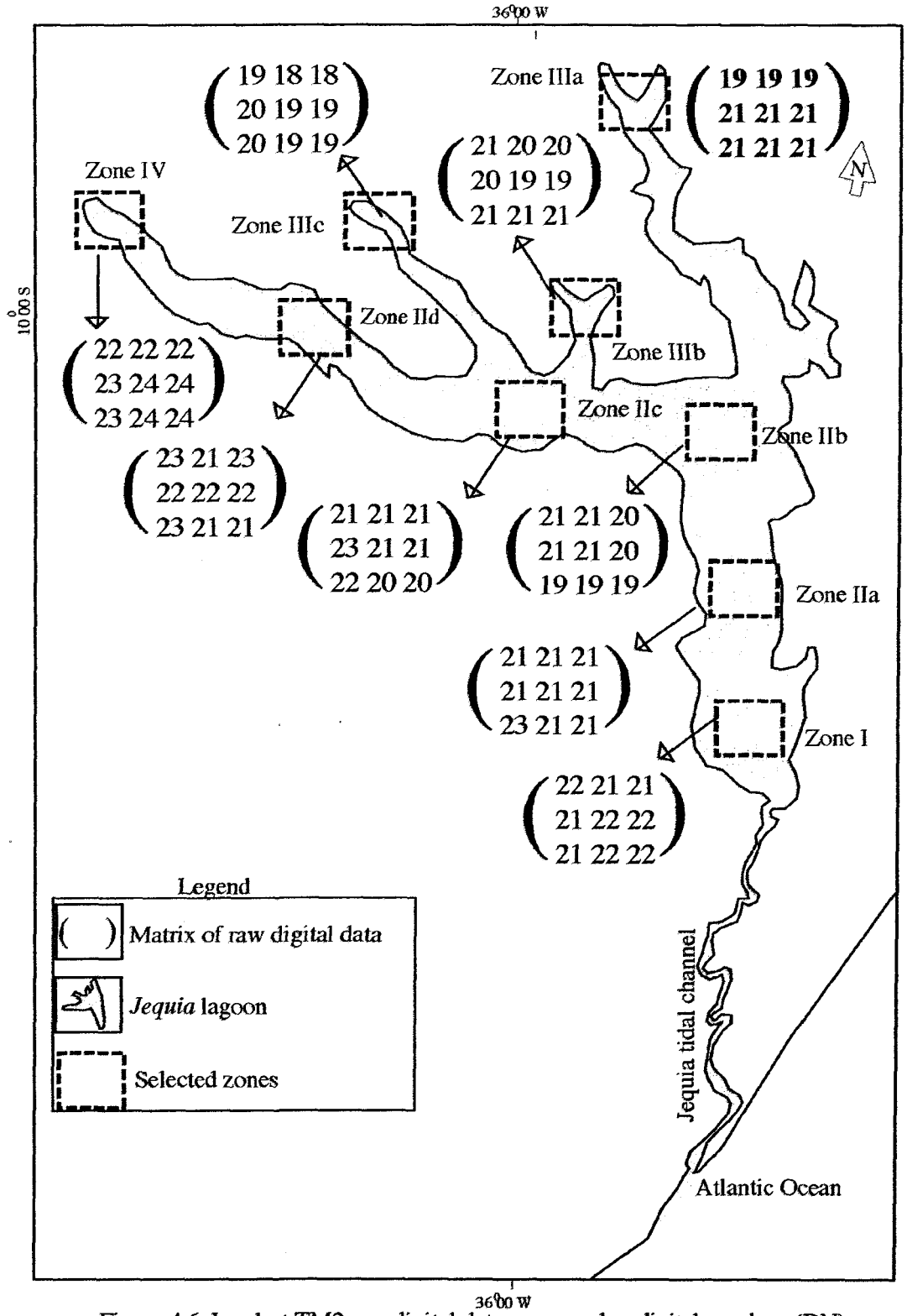

Figure 4.6. Landsat TM2 raw digital data expressed as digital numbers (DN), of the selected zones along the water surface of the *Jequia* lagoon, *Alagoas* Brazil

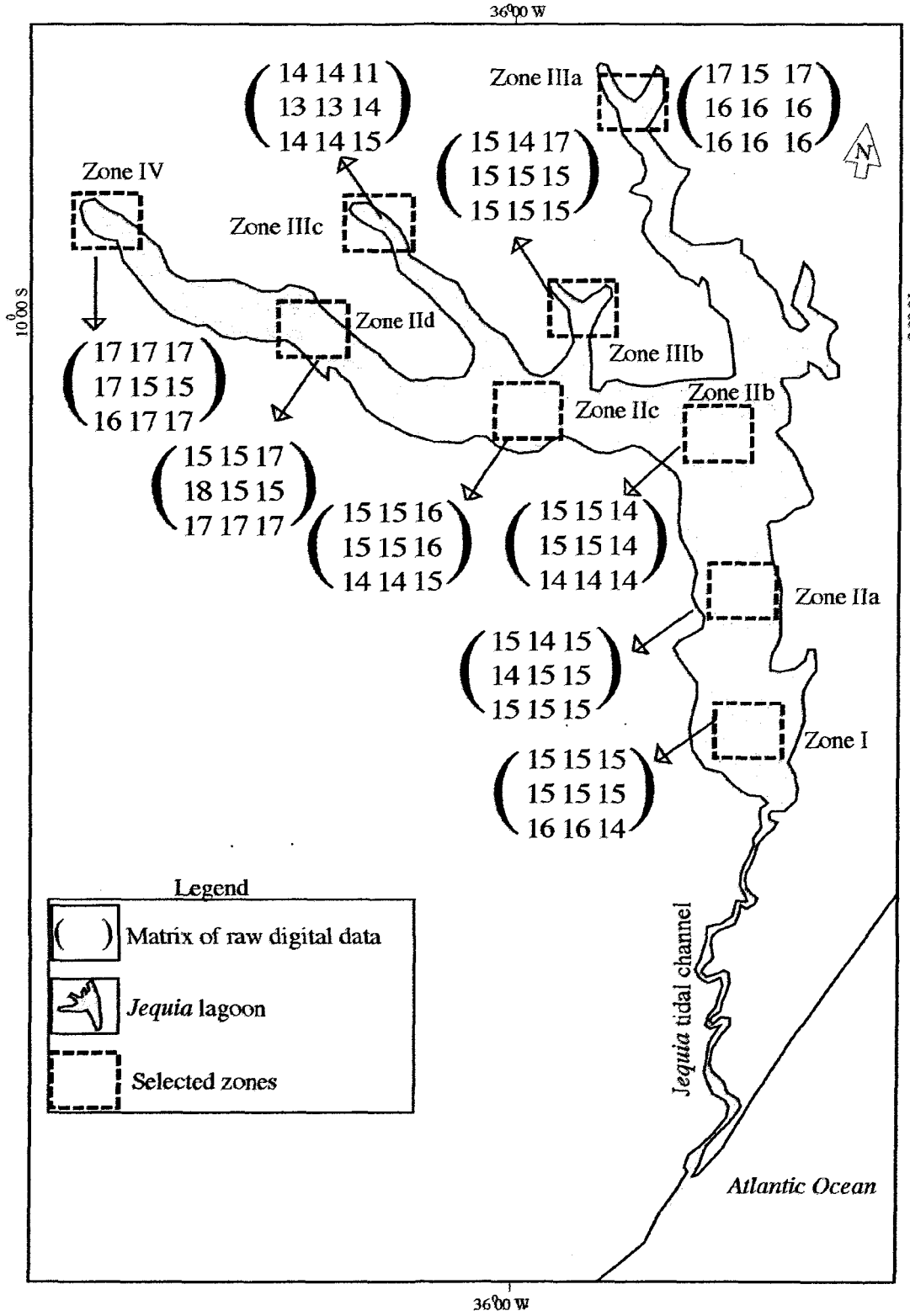

Figure 4.7. Landsat TM3 raw digital data expressed as digital numbers (DN), of the selected zones along the water surface of the *Jequia* lagoon, *Alagoas* Brazil

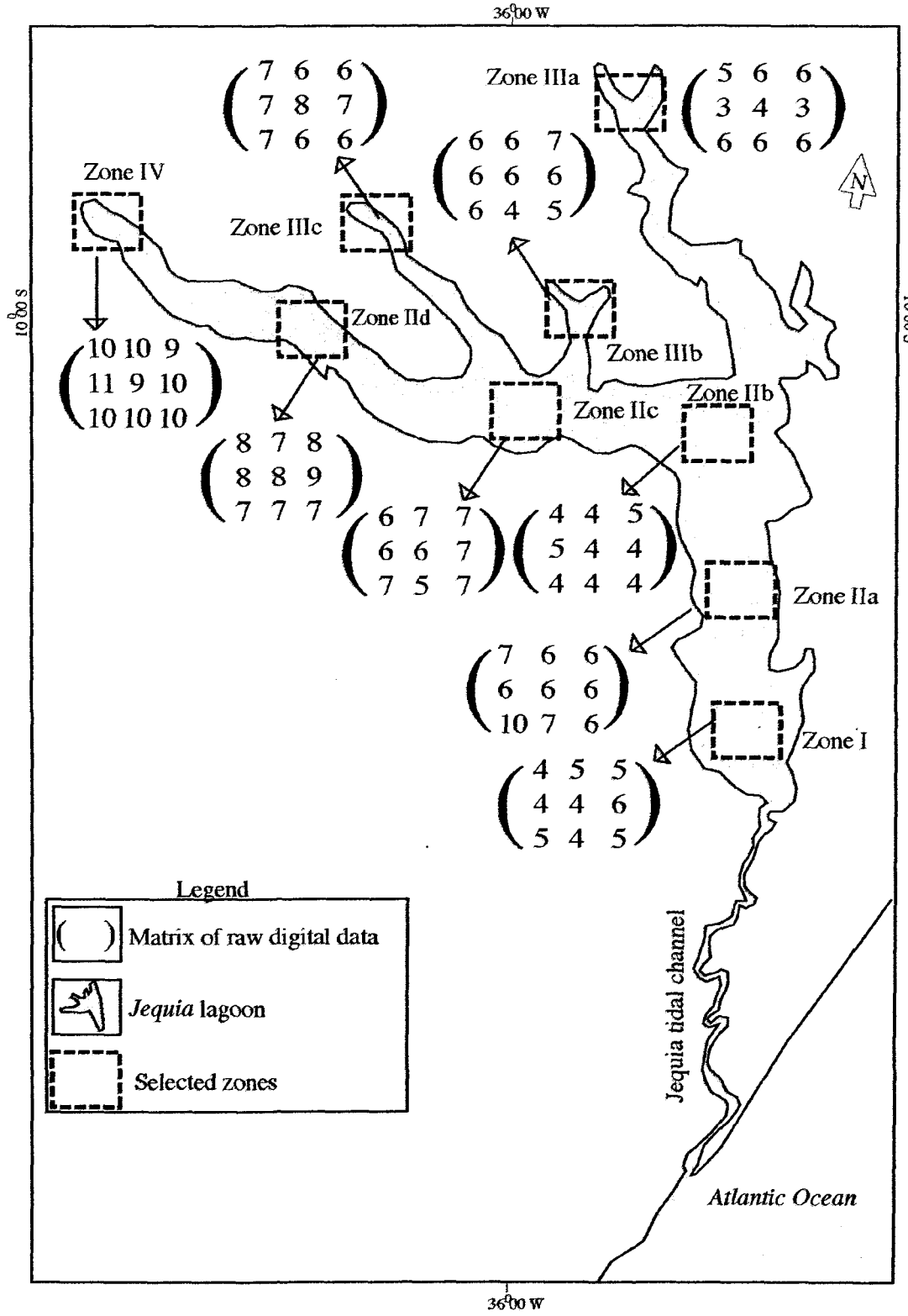

Figure 4.8. Landsat TM4 raw digital data expressed as digital numbers (DN), of the selected zones along the water surface of the *Jequia* lagoon, *Alagoas* Brazil

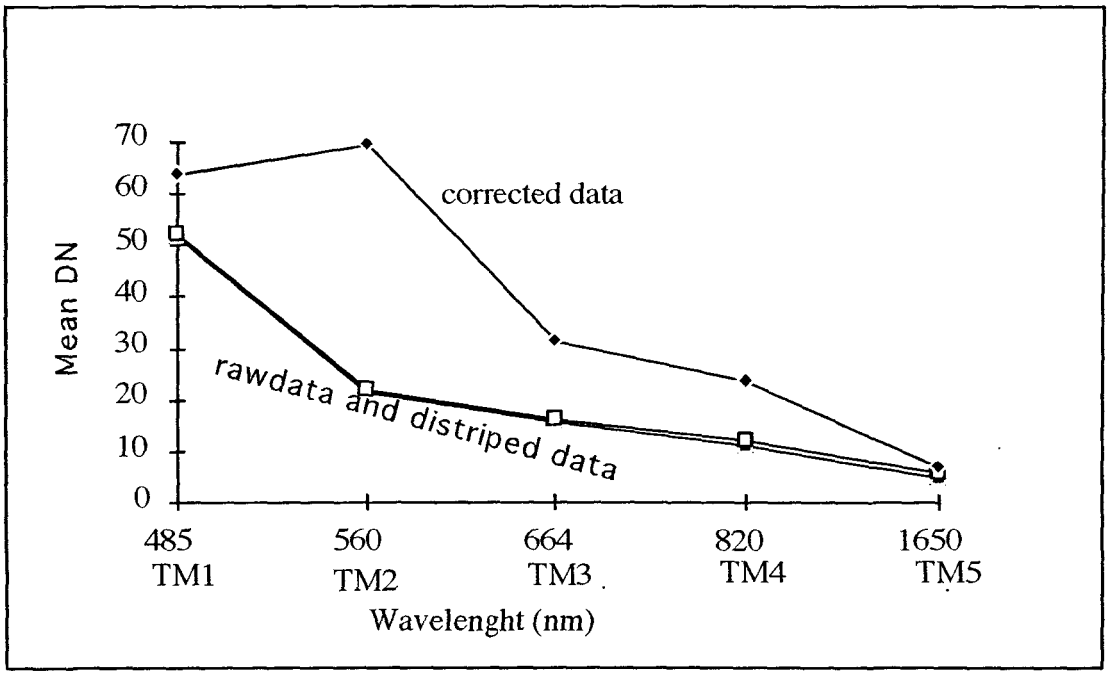

Figure 4.9. Correlation analysis of mean digital data for a Landsat TM image of the *Jequia* lagoon, *Alagoas*, Brazil. Corrected for atmospheric scattering and random noise from rawdata.

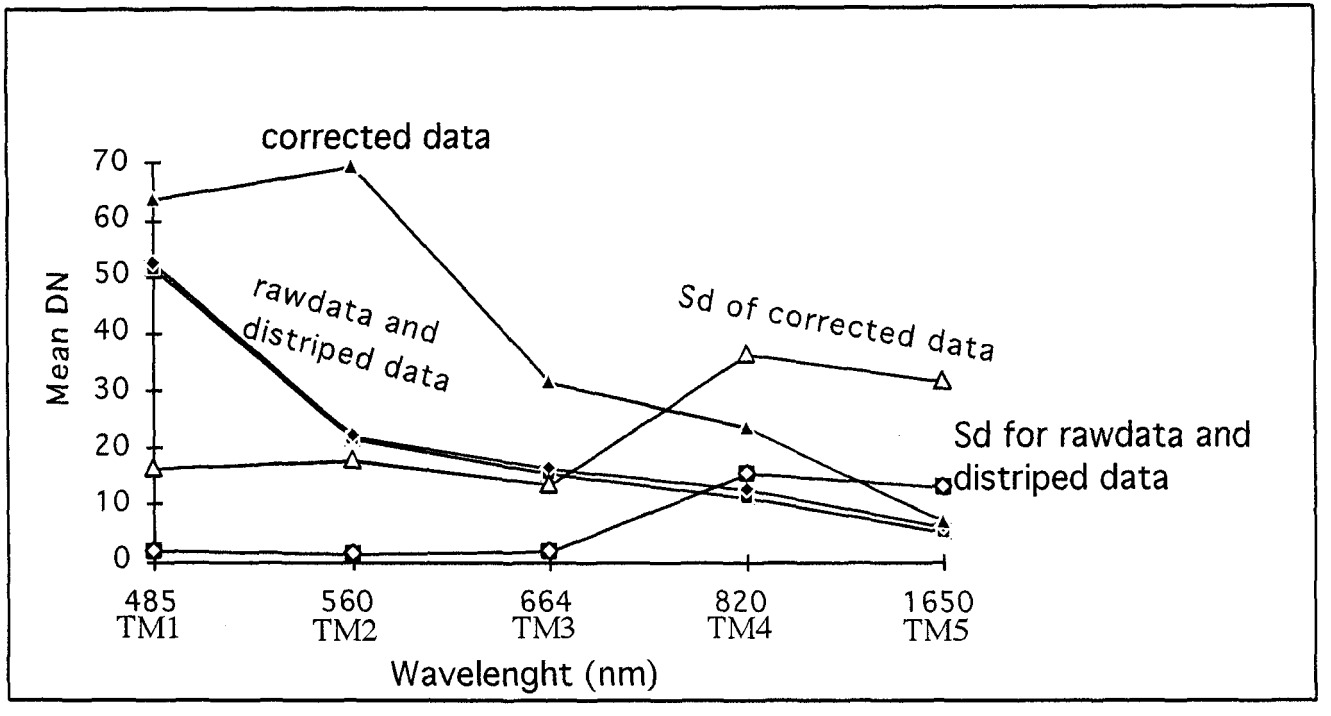

Figure 4.10. Spectral pattern analysis of mean and standard deviation(Sd) of digital data for a Landsat TM image of the *Jequia* lagoon, *Alagoas*, Brazil. Corrected for atmospheric scattering and noise from rawdata.

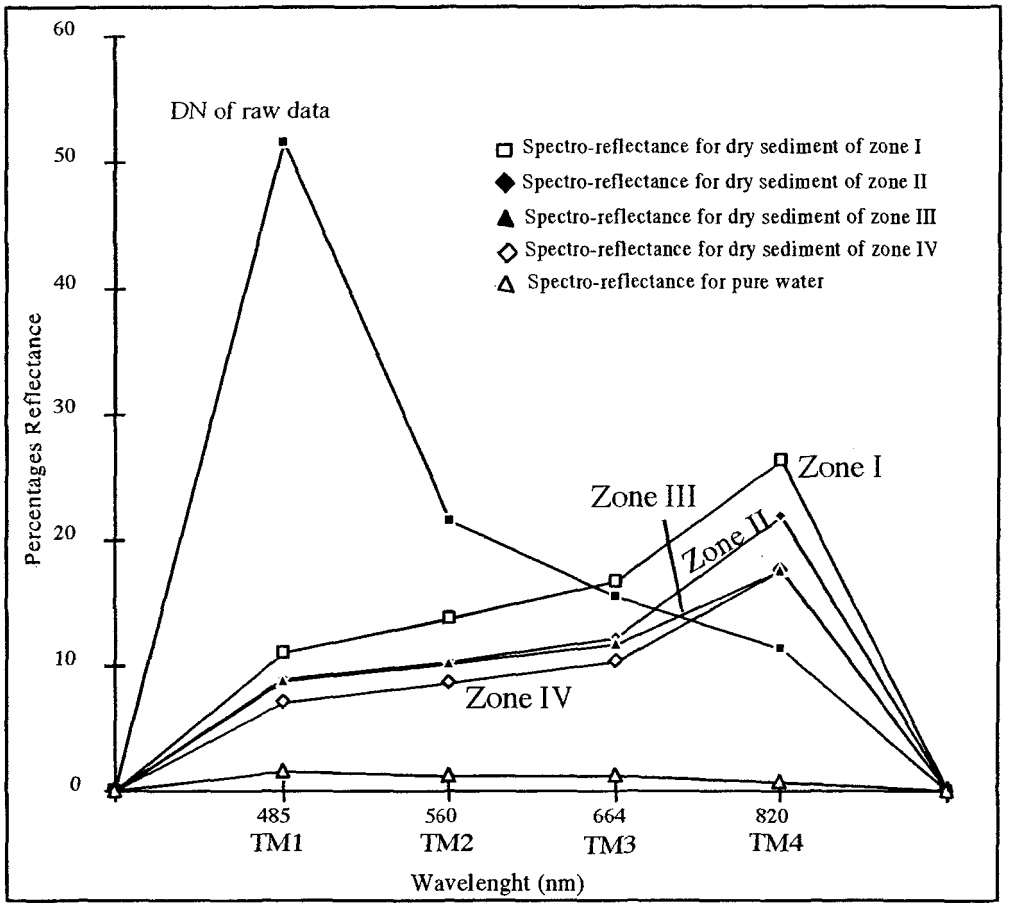

Figure 4.11. Spectral patterns of radiometric data and Landsat TM digital data of the water quality parameters of the Jequia lagoon, Alagoas, Brazil

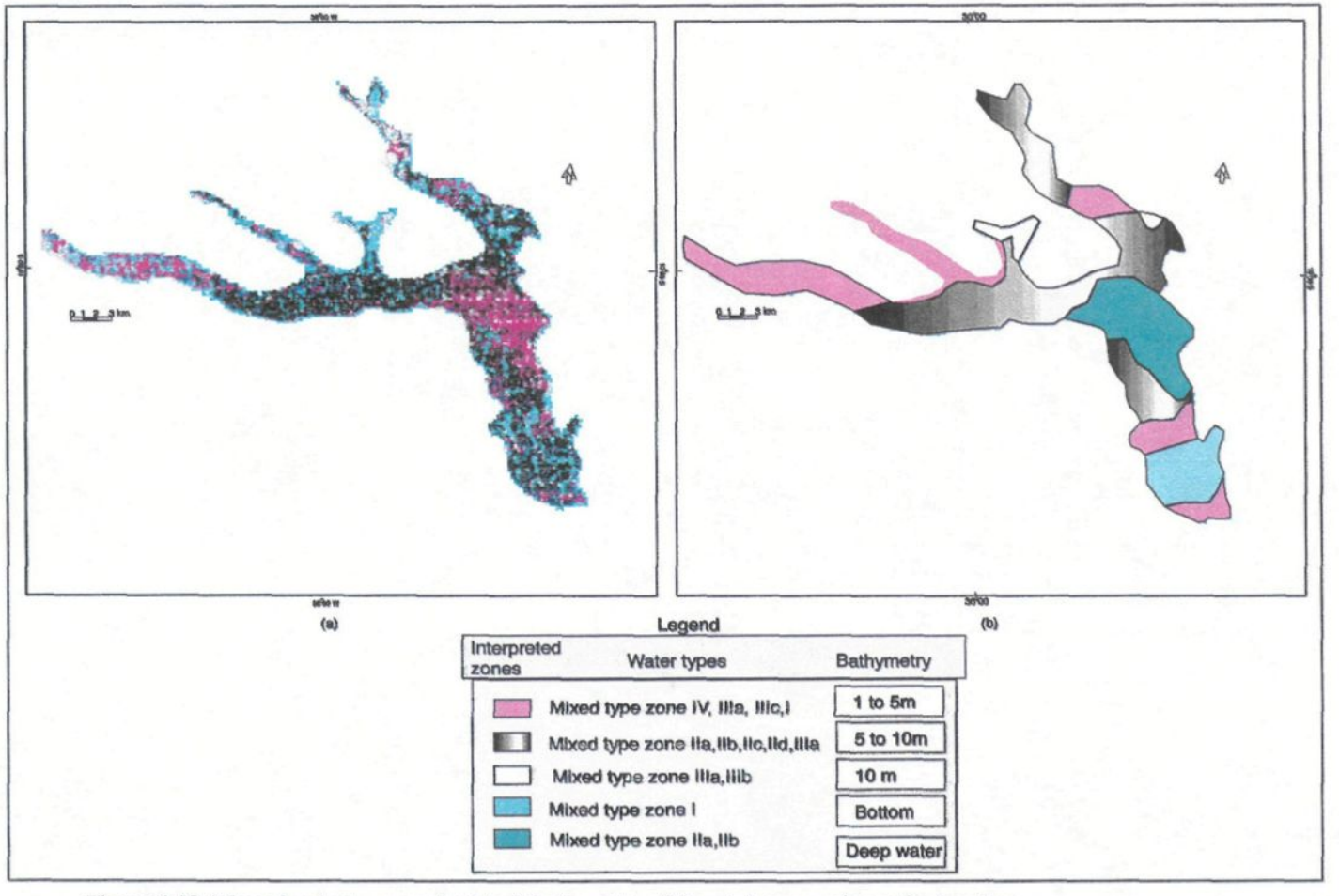

Figure 4.12. Map of water types and related bathymetry of *Jequia* lagoon using rationing data.
(a) rationing image displayed on [R,G,B] 3,2,1 system, (b) interpreted image from (a) image.
TM2/TM1 displayed in the red channel 3; TM2/TM3 displayed in the green channel 2; and TM3/TM1 in the blue channel 1.

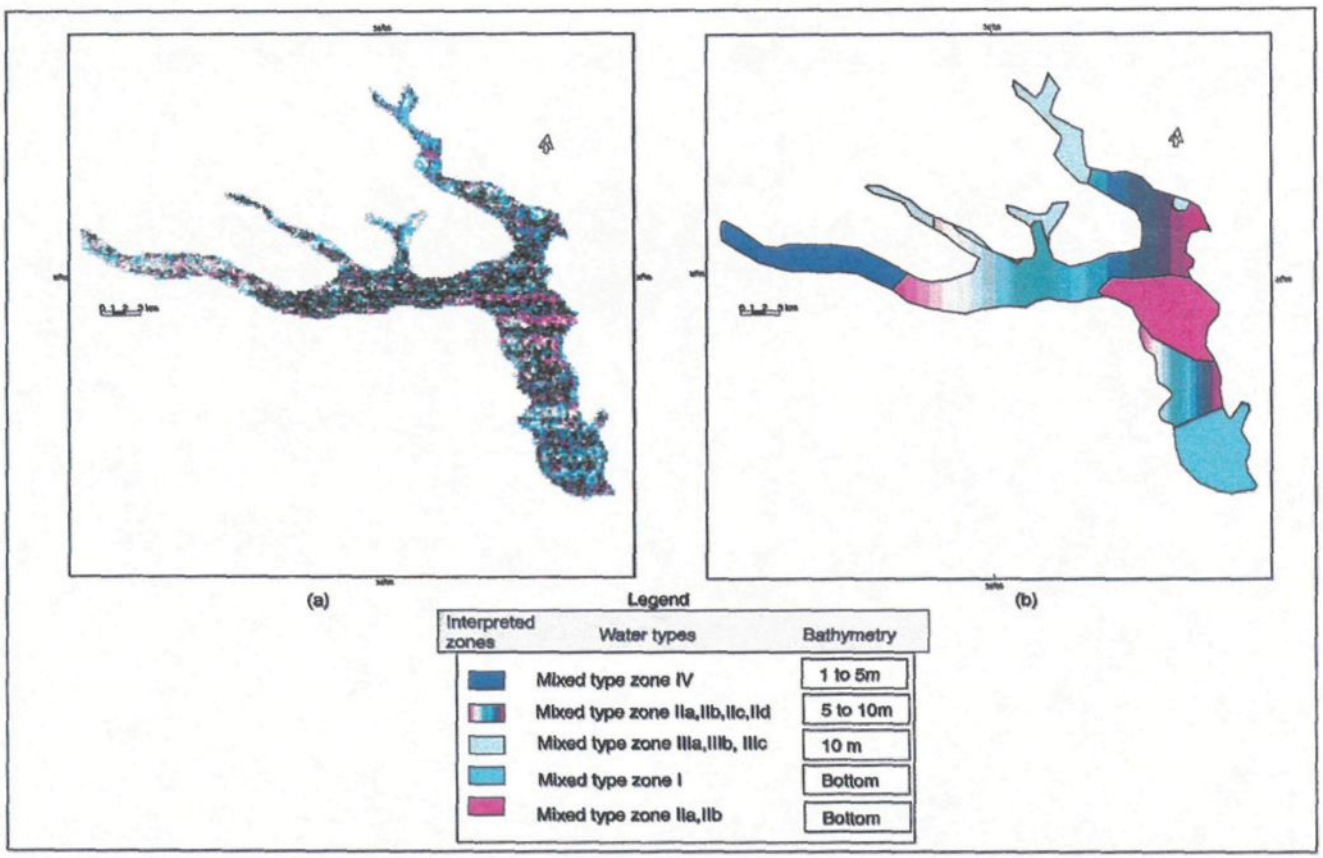

Figure 4.13. Map of water types and related bathymetry of *Jequia* lagoon using subtracted data.
(a) subtracted image displayed on [R,G,B] 3,2,1 system.
(b) interpreted image from (a) image. TM1-TM3 displayed in the red channel, 3, TM2-TM3 displayed in the green channel 2, and TM1-TM3 displayed in the blue channel, 1.

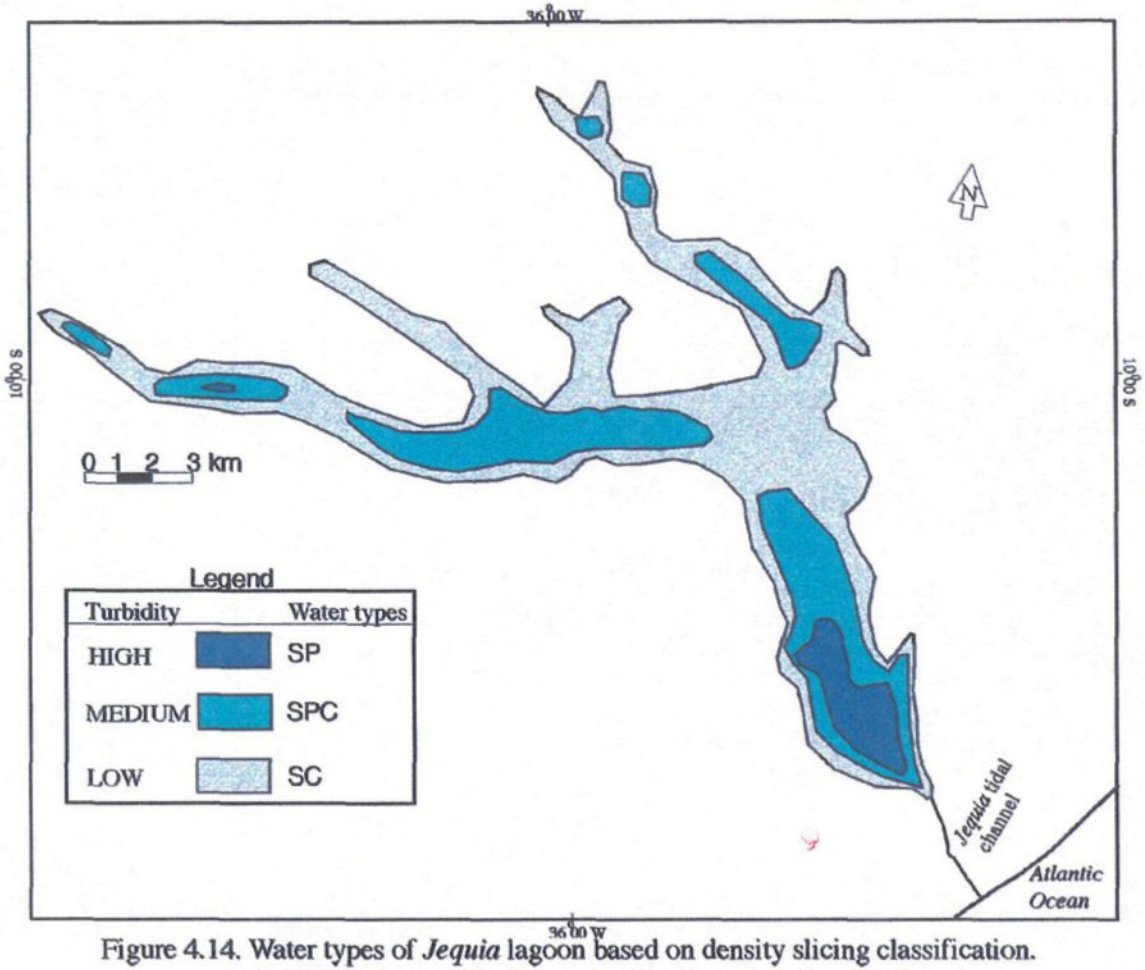

Figure 4.14. Water types of *Jequia* lagoon based on density slicing classification. Pseudocolor encoding using the Landsat TM1 data.
SP-Sediment+Phytoplankton, SPC-Sediment+Phytoplankton+Clear water
SC-Sediment+Clear water

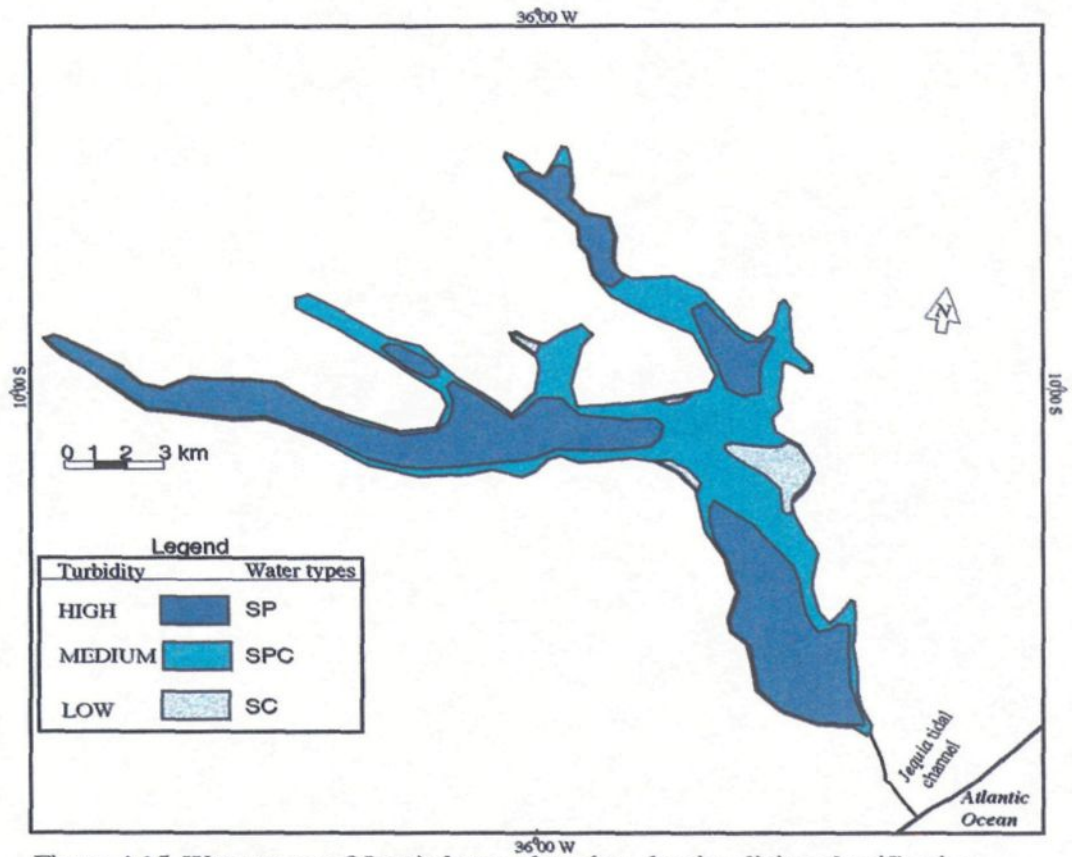

Figure 4.15. Water types of Jequia lagoon based on density slicing classification.
Pseudocolor encoding using the Landsat TM2 data.
SP-Sediment+Phytoplankton, SPC-Sediment+Phytoplankton+Clear water
SC-Sediment+Clear water

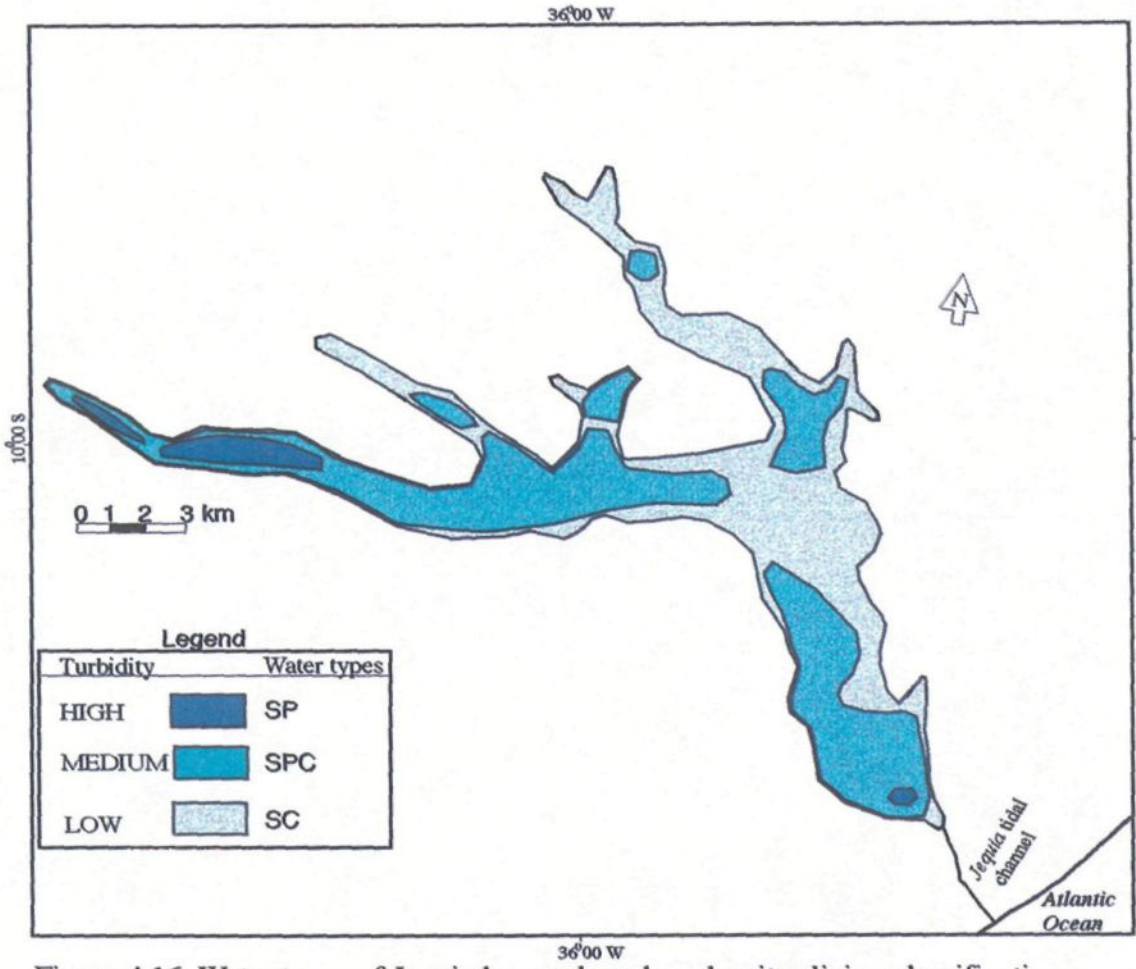

Figure 4.16. Water types of Jequia lagoon based on density slicing classification.
Pseudocolor encoding using the Landsat TM3 data.
SP-Sediment+Phytoplankton, SPC-Sediment+Phytoplankton+Clear water
SC-Sediment+Clear water

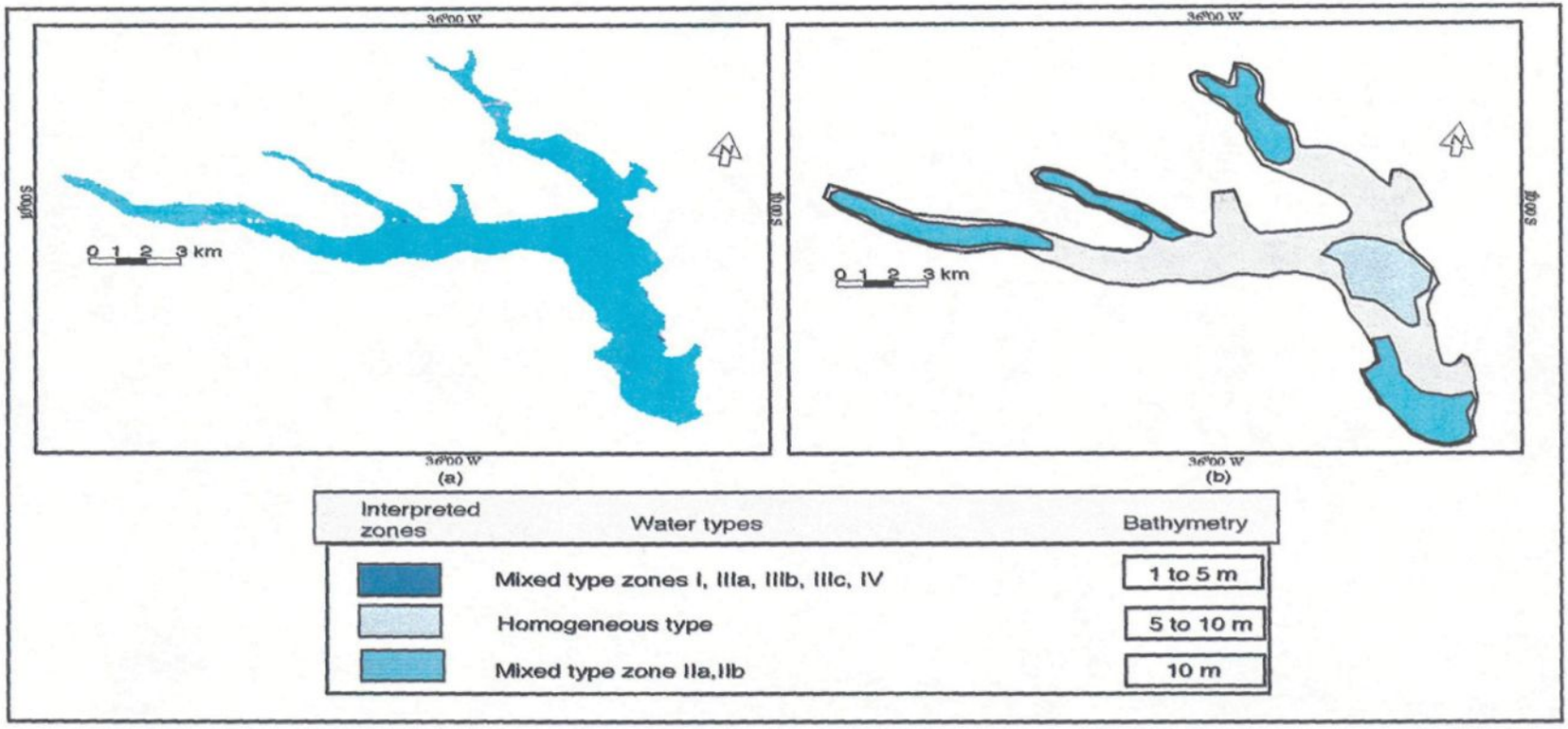

Figure 4.17. Map of water types and related bathymetry of *Jequia* lagoon using a maximum likelihood (MLC) classified data. Maximum likelihood classified image (a) displayed on [R,G,B] 3,2,1 system and (b) interpreted image from image (a).

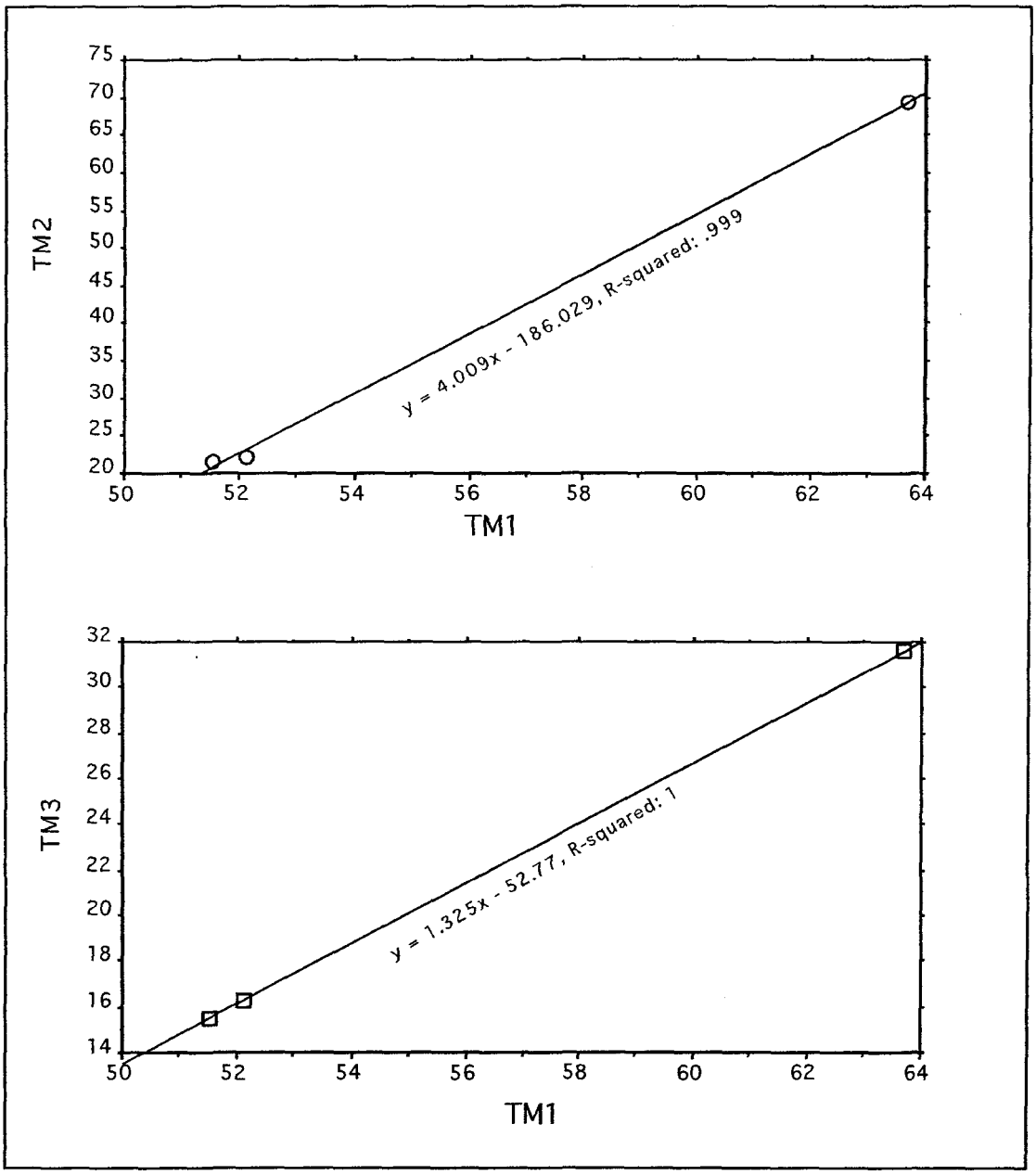

Figure 4.18. Best fit regression analysis for the Landsat TM123 raw digital data of the water quality parameters of the *Jequia* lagoon, *Alagoas*, Brazil

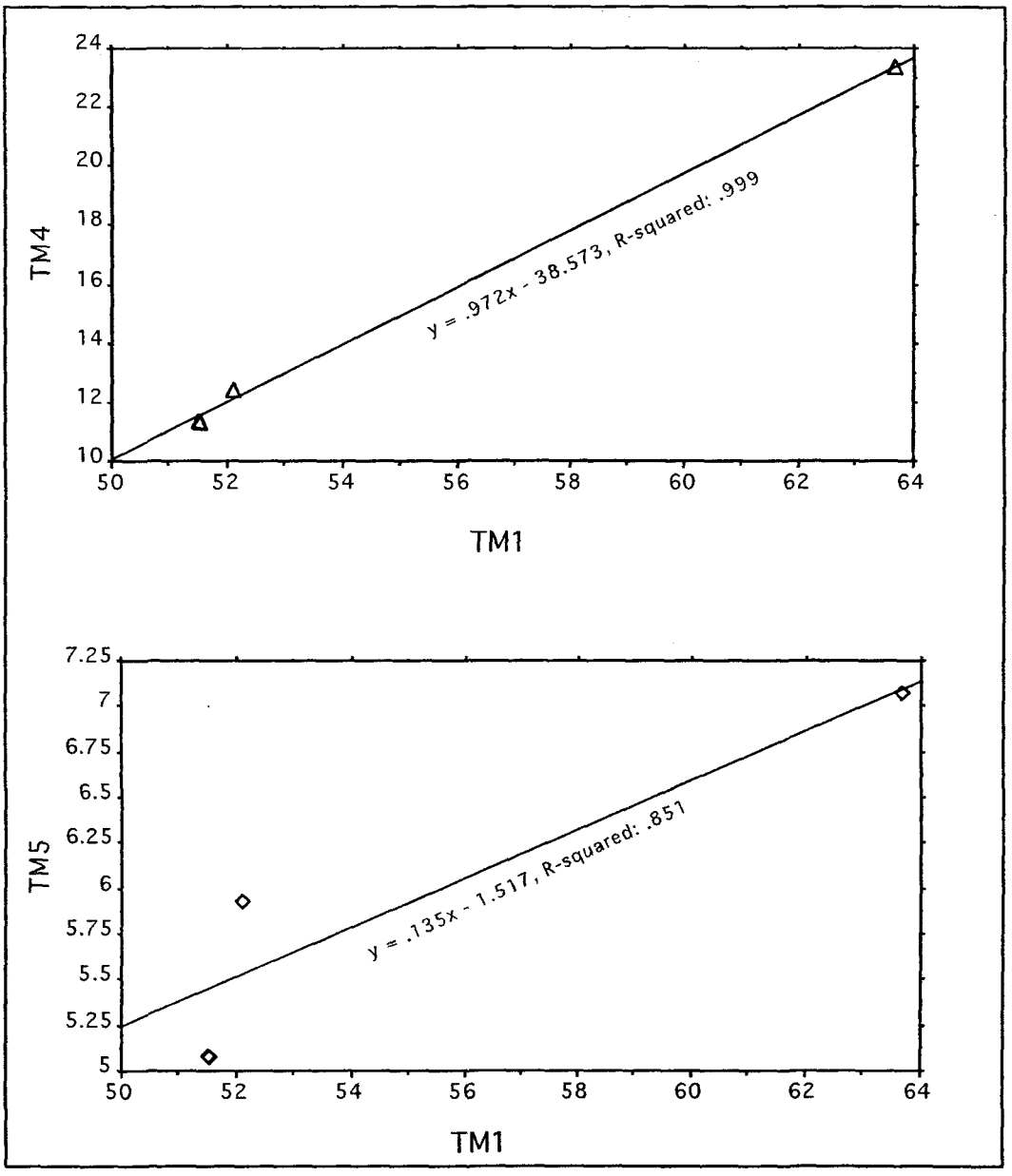

Figure 4.19.Best fit regression analysis for the Landsat TM145 using the mean of the raw digital numerical values of the water quality parameters of the *Jequia* lagoon, *Alagoas*, Brazil

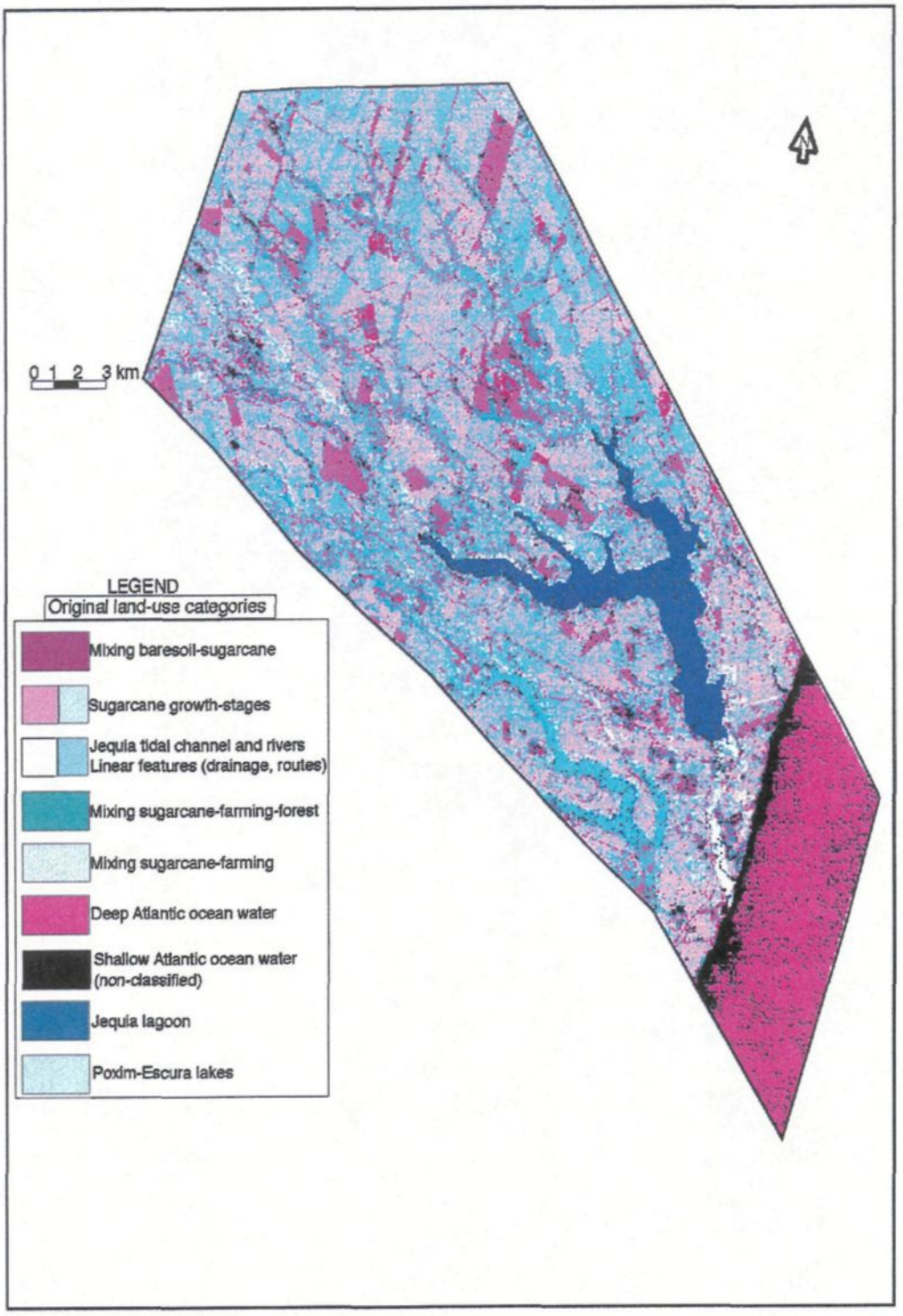

Figure 4.20: Maximum likelihood classified (MLC) image of land use categories sourounding *Jequia* lagoon using Landsat TM data.

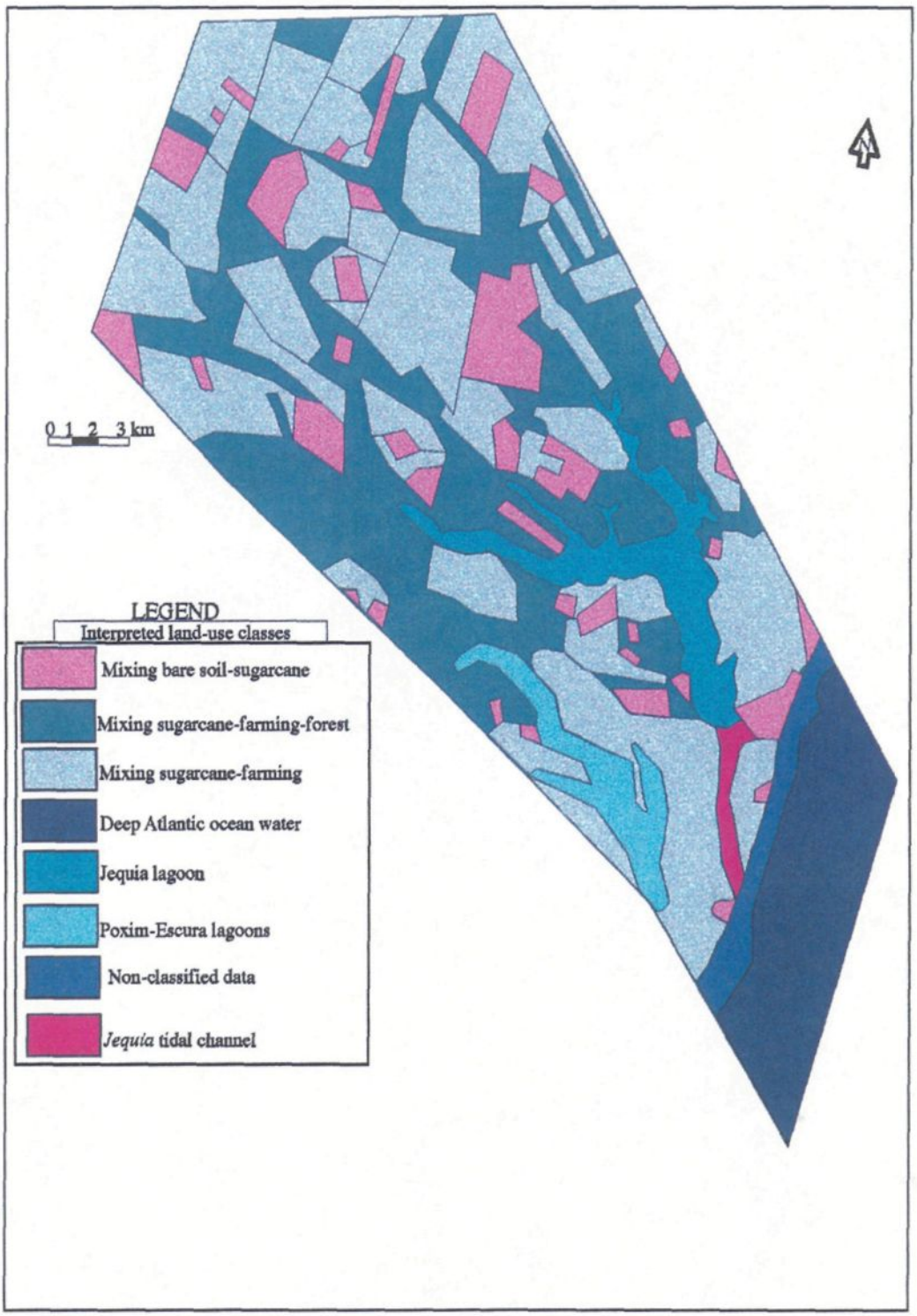

Figure 4.21: Map of land use interpreted categories and related crop types sourounding Jequia lagoon using MLC classified data (Figure 4.20).

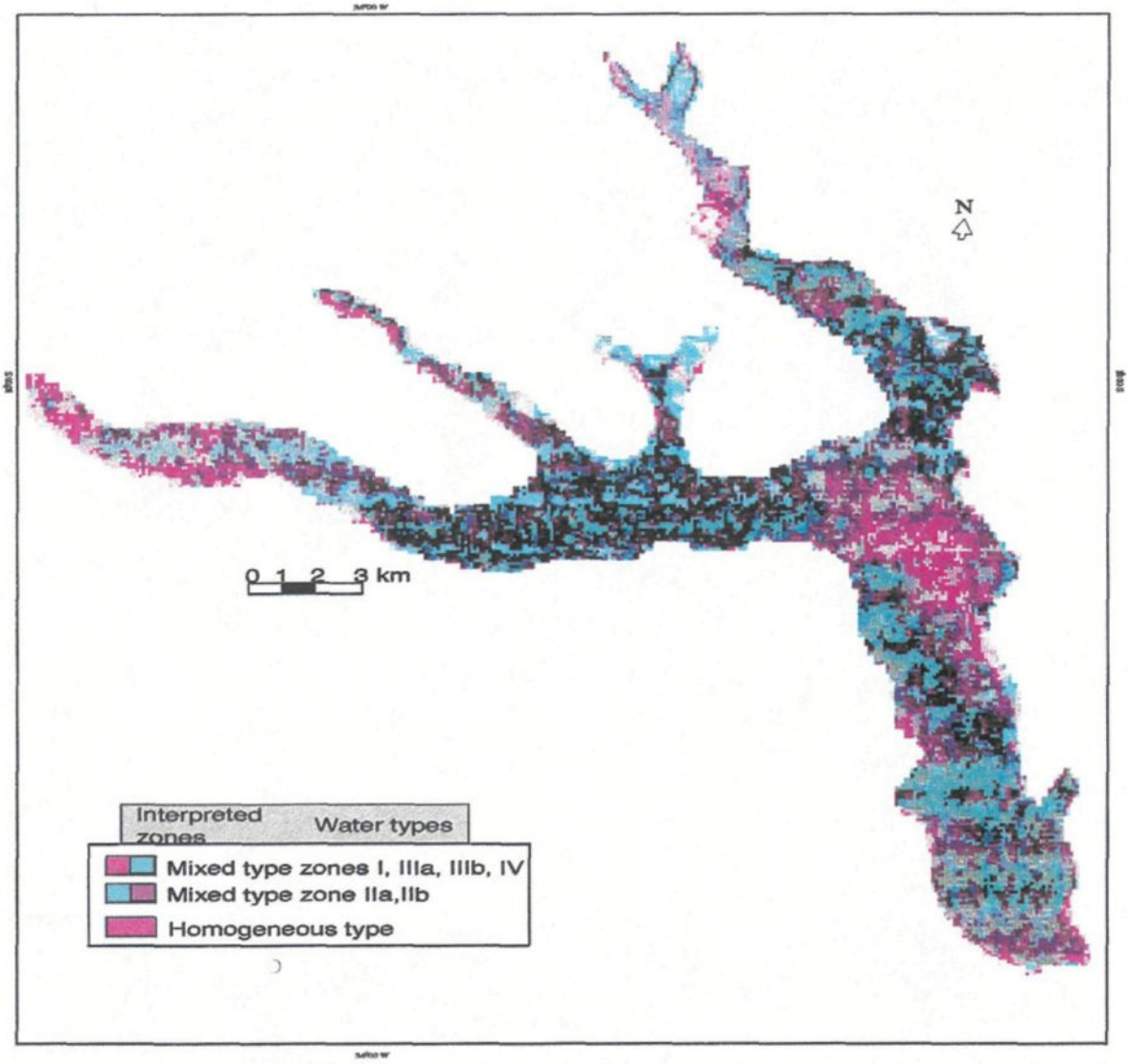

Figure 4.22. Map of water types and related bathymetry of Jequia lagoon using a Principal Component Analysis(PCA). The image is displayed on [R,G,B] 3,2,1 system

Landsat visible and near-infrared TM bands	Digital Numbers(DN) for rawdata		Digital Numbers(DN) for corrected data		Digital Numbers(DN) for destriped data	
	Mean values(XDN)	Standard deviation(StDN)	Mean values(XDN)	Standard deviation(StDN)	Mean values(XDN)	Standard deviation(StDN)
1	51.548	1.691	63.673	16.585	52.117	1.646
2	21.468	1.401	69.295	17.860	22.056	1.445
3	15.510	1.916	31.579	13.482	16.278	1.445
4	11.319	15.508	23.332	35.989	12.353	15.461

Table 4.1. Summary of the digital raw, destriped and corrected data for the water quality parameters of the *Jequia* lagoon.The values represent the recorded digital response or signatures expressed as digital numbers(DN).

Landsat visible and near-infrared TM bands	Rawdata	Corrected data	Destriped data
	Irradiance values(Ir) (mW/cm.sr.mm)	Irradiance values(Ir) (mW/cm.sr.mm)	Irradiance values(Ir) (mW/cm.sr.mm)
1	2.819	3.482	2.850
2	2.348	7.579	2.412
3	1.393	2.837	1.462
4	0.972	2.005	1.061

Table 4.2. Summary of the converted digital data(digital numbers-DN) to irradiance(reflectance) data for the water quality parameters of the *Jequia* lagoon.

Landsat visible and near-infrared TM bands		Rawdata	Corrected data	Destriped data
	DN white reference values (*)	Reflectance (%)	Reflectance (%)	Reflectance (%)
1	**245**	21.04	25.98	21.27
2	**126**	17.03	54.99	17.50
3	**177**	8.76	17.84	9.19
4	**138**	8.20	16.90	8.95

Table 4.3. Summary of the converted mean digital data (DN=digital numbers) to reflectance percentage for the water quality parameters of the *Jequia* lagoon. The mean digital values were normalized to the white reference values (*) from a corbonate(calcite) mine in Quebec.

Principal Components	TM1	TM2	TM3	Variance (%)	Water quality parameters
PC1	- 0.5170	- 0.4663	- 0.7177	66.46	Albedo
PC2	- 0.8255	0.0499	0.5621	22.52	Suspended Sediment
PC3	0.2262	- 0.8831	0.4108	11.01	Suspended Sediment

Table 4.4: Covariance matrix of a principal component classified image of water quality parameters along *Jequia* lagoon, *Alagoas*, Brazil. Landsat TM1, TM2, and TM3 bands were used as input data.

Principal Components	TM1	TM2	TM3	TM4	TM5	Variance (%)	Water quality parameters
PC1	0.0094	0.0200	0.0513	0.7675	0.6385	93.86	Albedo
PC2	0.1433	0.1058	0.1700	-0.6291	0.7372	4.64	Phytoplankton
PC3	0.6298	0.4793	0.5585	0.1220	- 0.215	0.89	Phytoplankton
PC4	-0.7403	0.2169	0.6349	- 0.0064	- 0.0391	0.39	Suspended Sediment
PC5	0.1857	- 0.8435	0.5032	0.0070	- 0.0251	0.22	Suspended Sediment

Table 4.5. Covariance matrix of a principal component classified image of water quality parameters along *Jequia* lagoon, *Alagoas*, Brazil. Landsat TM1, TM2, TM3, TM4 and TM5 bands were used as input data.

CLASSIFIED DATA		Zone I	Zone II	Zone III	Zone IV	Un-classified pixels	Number of pixels	Total row of pixels
TRAINING ZONES	Zone I	92,9	0	2,4	0	0	42	95,3
	Zone II	0	68,4	26,3	0	0	19	94,7
	Zone III	1,2	1,2	87,5	8,8	1,2	80	99,9
	Zone IV	0	4,2	12,5	75	8,3	24	100
Un-classified pixels		21,3	4,3	41,5	8	21,4	961	96,5
Column		115,4	78,1	170,2	91,8	30,9	-	486,4
Producer's Accuracy (%)		80,50	87,58	51,41	81,69	69,25	Automated average accuracy = 69,04 % Automated overall accuracy = 30,73 %	
User's Accuracy (%)		97,48	72,22	87,58	75	22,17	Descriptive overall accuracy = 70,97 % Kappa statistic accuracy = 63 %	

Table 4.6. Error matrix of a maximum likelihood classification using supervised training zones of the water types along the *Jequia* lagoon, *Alagoas*, Brazil

	CLASSIFIED DATA	Un-classified pixels	Jeq-water	Pox-lagoon	Atla-water	Jeq-channel	Urb-sites	Routes	Farming	Sugarcane mixed	Baresoil	Total row of pixels	Number of pixels
TRAINING ZONES	Jeq-water	2.4	**92.3**	1.6	0.0	2.4	0.0	0.1	0.3	0.4	0.5	97.6	11456
	Pox-lagoon	2.4	1.9	**80.7**	0.0	5.1	0.3	0.1	2.0	1.5	5.9	97.5	6340
	Atla-water	10.2	0.0	0.0	**89.8**	0.0	0.0	0.0	0.0	0.0	0.0	89.9	32096
	Jeq-channel	2.7	4.5	4.0	0.0	**78.4**	0.7	0.6	5.4	2.3	1.4	97.3	1149
	Urb-sites	8.7	0.0	0.7	0.0	1.0	**29.7**	21.9	19.7	10.8	7.4	91.2	2502
	Routes	4.0	0.0	0.3	0.0	0.6	14.6	**33.6**	25.5	16.7	4.7	96	5444
	Farming	0.8	0.0	1.4	0.0	7.7	2.9	4.7	**53.6**	26.2	2.7	99.2	4415
	Sugar-cane mixed	0.4	0.0	0.7	0.0	0.8	1.8	3.7	41.1	**50.8**	0.6	99.5	79049
	Baresoil	4.2	0.0	1.5	4.6	1.2	3.5	4.2	20.7	18.2	**42.1**	96	19312
Total column of pixels		-	98.7	90.9	94.4	97.2	53.5	68.9	168.3	126.9	65.3	864.1	-
Producer's Accuracy (%)		-	94	89	95	80	55	48	32	40	64	-	-
User's Accuracy (%)		-	95	83	100	80	33	35	54	51	44	AAA=61.23% AOA=60.96% EOA=64% KHATa=0.59	

Table 4.7: Error matrix of a maximum likelihood classification using supervised training zones of land-use categories along the *Jequia* estuary. *Alagoas*. Brazil. AAA: Automated average accuracy, AOA:Automated overall accuracy, EOA: Empirical overall accuracy and KHATa: Kappa statistic accuracy

Lagoon Zones		I		IIb		III		IV	
Thematic Mapper Bands	Rmax Rmin	DN	CIr	DN	CIr	DN	CIr	DN	CIr
TM1 Bw= 65.4	10.0 8.0	51.77	91.975	49.33	88.220	51.11	90.962	52.22	92.670
TM2 Bw= 81.3	7.0 5.0	21.55	194.689	20.11	184.130	20.33	185.743	23.11	206.128
TM3 Bw= 66.8	7.5 4.0	15.11	94.882	14.44	91.371	16.11	100.120	16.44	101.849
TM4 Bw= 128.1	20.0 11.0	4.66	86.535	4.22	84.104	4.55	83.914	9.88	115.379

Table 4.8. Spectral irradiances($MW/cm^{-2}\mu m$) converted from digital numbers from the visible TM bands, within the zones of *Jequia* lagoon. The Bw corresponds to the band width.

CHAPTER 5

CHARACTERIZATION OF THE OPTICAL REFLECTANCE PATTERNS OF SUSPENDED SEDIMENTS FROM THE *JEQUIA* LAGOON

5.1. Introduction

The spectral reflectance or irradiation patterns of a given target can be acquired by in situ measurements, laboratory experimentations or remote sensing sensors. The objective of this chapter is to study the correlations between the laboratory reflectance and the physical characteristic of the bottom sediments (particle size and concentration) sampled in the tropical lagoon of *Jequia*.

The reflectance or irradiation data produced in this chapter were recorded by a Personal Spectro-Radiometer (PSR) in simulated laboratory conditions. The terms reflectance and irradiation are used interchangeably within this chapter. They refer to the proportion of overall energy or radiation coming from an artificial source of energy and recorded by the spectroradiometer. Moreover, this irradiation is concerned with the proportion of reflected and incident energy flux (simply reflectance), transmitted (simply transmittance) and quantified for several concentrations of suspended sediments simulated in a tank of water. The latter includes the absorpted (simply absorptance) and backscattered energy upwelling the water column since it was assumed that the water is clear and that attenuation is the major energy controlling the overall irradiation detected. Within the overall irradiation, the effect of particle size and the experiment viewing geometry are also discussed.

Numerous remote sensing researches have contributed to the characterization of laboratory reflectance or irradiation related to particle size, soil type, depth and sediment concentration through a water column. We refer to the contributions of Ritchie *et al.* (1988), Novo *et al.* (1989a), (1989b), (1991), Bhargava *et al.* (1990), (1991), (1992), Chen *et. al* (1992), Mantovani *et al.* (1992), Ji *et al.* (1992), Braga *et. al.* (1993) and Ferrier (1995). Bhargava *et al.* (1991) have recognized the relationship between reflectance and the properties of sediments (type, size, shape and concentration). Curran *et al.* (1988) have discussed the influences of the environment and the viewing geometry within the detected laboratory reflectance. Mantovany *et al.* (1992) pointed out that the optimum tank

dimension should have a horizontal measurement greater than the depth. Moreover, they argued that inadequate tank dimension will produce significant effects from bottom and wall on the overall detected reflectance.

The optical characterization of the inorganic suspended and dry sediments were estimated using a water tank set up in a close environment. The sediments used for this experimentation were sampled (Figure 1.2) on the bottom of the *Jequia* lagoon and were randomly grouped in Zones to enable overall analyses. This chapter also attempts to establish the correlation between the suspended matter spectral laboratory reflectance and the irradiance estimated using the satellite digital data (DN and converted DNs). Analogies regarding the optical characterization of water quality parameters of the lagoon were assumed.

The analyses were based on the spectral irradiation measured for low (150 mg/L and 300 mg/l), intermediate (600 mg/L) and high (900 mg/L and 1 200 mg/L) sediment concentrations.

Since the *Jequia* lagoon presents a maximum average daily sediment discharge of about 1,4 m^3/sec (Cavalcante *et al.*, 1993) during the dry season, which corresponds to the range of low sediment concentration simulated in laboratory, we assume that the spectral results discussed in this chapter might be extrapolated to natural conditions expected within the water column of that lagoon.

The empirical model (equation 5.1) proposed by Rowe *et al.* (1995) was used to estimate the sediment discharge into the *Jequia* lagoon. The discharge data previously published and the conductivity determined in situ in 1990 for this study were computed in the above model. The sediment discharges might vary from 1,7 mg/l to 3,3 mg/L during winter (low exchange in total suspended matter) to 1,45 m^3/sec during the summer period (high exchange).

$$Tds = [(EC)\ (ds)] * K \qquad \text{(equation 5.1)}$$

in which;

Tds:Total dissolved solids (mg/L),

EC:Electrical conductivity (mhoms/cm),

ds:Mean outflow from the *Jequia* River (m/s),

K:Empirical factor (0,59) for pure water

5.2. Description of the spectroradiometric experimentation

The spectral irradiance data presented in this chapter were recorded using a CCD personnel spectro-radiometer II (Analytical spectral devices corporation (ASD)), in a laboratory setup at the University of Quebec at Chicoutimi. The experimental set-up was arranged in a closed laboratory condition (Figure 5.1). Several concentrations of sediments were simulated and their reflectance determined. It consisted of a 400 liter cylindrical tank presenting a diameter of 121,1 cm and a depth of 34,5 cm. The tank was previously coated with optically flat black paint to minimize backscattering from the bottom and wall.

The spectro-radiometer illumination field was provided by a combination of two incandescent artificial light sources. A 150 W spotlight was used providing the near infrared and most red energy and also a near infra-red 300 W tungsten halogen slide projector bulb. The slide projector, with its infrared blocking filter in place, compensated for the lack of blue light in the first source. A 30 degrees incidence angle was set between the light beam and the normal. The sensor field of view (FOV) was of 1^{o}.

The head of the sensor was set vertically to measure the irradiation at a height of 117 cm from a target area of 21 mm over the water surface. The spectro-radiometer was equipped of 512 channels covering a 316 to 1 040 nm wavelength interval. The spectral values obtained in the experiment ranged from 400 to 900 nm. Within that wavelength interval we used a software-selected channel group simulating the visible and near infrared TM bands (Figure 5.1)

The irradiation for the corresponding dry sediment samples as well as the pure distilled water spectrum was measured in the experimentation. A plate or panel (5 mm thick) with barium sulfate $BaSO_4$ was used to calibrate the spectra-radiometer. The dark current level was automatically subtracted from the equipment before each measurement.

The required channels (400 to 900 nm) were automatically grouped by the ASD software to simulate the Thematic Mapper (TM) bands. The equivalent overall irradiance (chapter 4) bands recorded in this study were corresponding to theTM1, TM2, TM3 and TM4 wavelengths of the LANDSAT satellite.

The spectral reflectance for the different suspended sediment concentration was measured by adding known amounts of composite sediments (quartz+kaolinite) for each zone into the tank filled with pure distilled water.

Four mixtures of sediment samples, collected on the bottom of the *Jequia* lagoon in March 1990 were randomly grouped (Figure 1.2) in Zones I, II, III, IV. The spectral irradiation of the mixtures was determined for two groups of samples in each Zone. The first group presented two lower (150 mg/L and 300 mg/l) concentrations and an intermediate sediment concentration of 600 mg/L. The second group contained the higher (900 mg/L and 1 200 mg/L) sediment concentrations simulated.

It is pertinent to note that the referred bed sediment samples presented a significant amount of organic matter in Zones II, III and IV. The organic matter was not removed or

chemically attacked on the original samples before the experimentation. Therefore, the spectral reflectance recorded for the mineralogical assemblage of quartz+kaolinite and minor illite might account also for the presence of organic matter or more precisely the suspended phytoplankton matter. There were no floating biological or organic species along Zones I, IIb and IIIa of the lagoon during the sampling surveys. Algae, phytoplankton and an oil-like plume dominated within Zone IV.

5.3. Interpretation of the spectral reflectance patterns from the suspended inorganic matter

5.3.1. Introduction

The optical characteristics interpreted in the analyses of the spectral irradiation simulated in laboratory include the water color and several turbidity levels controlled by the sediments sampled along the bottom of the *Jequia* lagoon. The color and turbidity of the water mass are considered within this study as a similar water quality parameter. Considering that the sediments used within the simulation come from the *Jequia* lagoon, we extended several considerations from the laboratory results to that environment. We assume that the quantified laboratory reflectance for low sediment concentration might approach the real environment.

The empirical suspended sediment concentration reflectance data measured for the sediments grouped in zones is illustrated in figure 5.2 . Reflectance spectrum for pure water, for barium sulfate white reference, for the dry sediments and for the black bottom are shown also in figure 5.2.

5.3.2. Interpretation of laboratory reflectance data from sediment concentrations

The raw spectrum radiometer results for the five different suspended sediment concentrations and expressed in terms of percentage of reflectance recorded along the visible and near-infrared wavelength range, are illustrated in tables 5.3 to 5.8.

The spectral irradiation patterns for dry sediments were considered to be the spectral signatures of the mineralogical assembly of Kaoline + Quartz and minor Illite. These minerals represent the major inorganic phases within the bottom sediments of the *Jequia* lagoon. Considering this fact, we have assumed that the irradiation detected by LANDSAT TM and by the spectroradiometer corresponded to the spectral signal produced mostly by the inorganic matter (sediments). However, as said before, the organic matter was not removed from some samples. Two groups of sediment concentration sample (a lower and a higher) were selected in order to avoid overlapping of some spectral curve plots and to enable a readily analysis of the results.

The higher sediment concentration samples for Zones I, II, III and IV are shown respectively in figure 5.3 and 5.4. The lower sediment concentration samples for all zones are illustrated in figures 5.5 and 5.6. They are also drawn individually due to overlap within the results.

The analysis of the spectral patterns produced by the various sediment concentrations indicates an overall percentage increase of energy related to the wavelength recorded by the radiometer. The spectral patterns were more discernible for the longest wavelength ranges. The results for Zones II and IV showed distinguishable reflectance patterns for all concentrations of sediment particularly in the wavelength longer than 664 nm.

An overall analysis of Zone I (Figures 5.3 and 5.7) indicates a higher proportion of reflectance (6 to 12%) than the other zones (4 to 9%). This fact might be related to the dominance of quartz relative to the other minerals present within the sediments of Zone I.

The observed overlapping of data from the sediment concentrations higher than 600 mg/L suggests a saturation of one mineral over the other phases. The spectral irradiation recorded for concentrations over 600 mg/L might be the one produced mostly by the presence of kaolinite.

The presence of the quartz as the major mineral is offering a faster settling velocity therefore resting in suspension less than clayey minerals. This fact corroborates the assumption of a predominance of the kaolinite spectral pattern. Since clay minerals stay in suspension for longer period than quartz must have added the high reflectance values for suspended sediment concentration of 1 200 mg/L for Zone II (Figures 5.3 and 5.4). We consider that the backscattering effect comes mainly from the bottom, which is mostly filled with particles in the range of silt fraction.

The reflectance patterns for the suspended sediment concentrations higher than 600 mg/L (Figures 5.3 and 5.4) present overall overlapping. Subtle differences are noted for the concentrations of 900 mg/L and 1 200 mg/L within Zone IV. There are also slight differences for concentrations of 600 mg/L, 900 mg/L and 1 200 mg/L with wavelength range longer than 664 nm for the sediments from Zone IIb.

For the intermediate concentration of sediments of 600 mg/L, there is an overall similar trend spectral irradiation for all zones. However, there is remarkable inversion on the reflectance value for the 600 mg/l sediment concentration relative to the 300 mg/l concentration for the sediments from Zones II (Figures 5.5 and 5.6). Another inversion of the irradiation is noticed for the 300 mg/L sediment concentration relative to the 150 mg/L concentration for Zone III (Figure 5.5). The former inversion (600 mg/L) might be the result of quick deposition of quartz particles over the other minerals. This behavior is notice for wavelengths shorter than 485 nm. The suspended matter for the 300 mg/L concentration was still in suspension, which led to a higher reflectance value.

The similar inversion spectral irradiation was noticed for Zone III (Figures 5.5 and 5.6) and must have been due to the same argument as above. The difference of reflectance between these two sediment concentrations is less than 1% for both zones. Therefore, for wavelengths shorter than 485 nm, the lowest sediment concentrations of 150 to 600 mg/L were not a controlling factor of the spectrum of water quality parameters.

The high proportion of organic matter in the sediments of Zone II (5 to 11%) and III (7 to 8%) must also control the inversion pattern. Since organic matter presents a low reflectance pattern in shorter wavelength ranges, it tends to mask spectral signatures produced only by inorganic matter that in turn should show distinguishable reflectance patterns. The irradiation detected for the sediments from Zone I show good agreement with this assumption. Their reflectance patterns for low and intermediate sediment concentrations are very similar (5,9% for 150 mg/L, 6,1% for 300 mg/L and 6,2% for 600 mg/L concentration).

It is remarkable that the increase of reflectance or spectral irradiation values with increasing concentration of inorganic suspended matter was not a linear function. The most important effect observed was the shift of spectral pattern for the longer wavelength range (TM3 and TM4) for higher concentrations.

The spectral irradiation recorded for Zone IV sediments showed different patterns for shorter wavelength range. The reflectance for the lowest concentration (150 mg/L) was of 3.5%. It was lower than the reflectance for 300 mg/L and 600 mg/L sediment concentrations. There is an overlapping reflectance for the latter concentration (4.5%).

The above difference might be related to the high amount of organic matter fixed to the sediments of Zone IV (6 to 7%). Organic matter increases attenuated irradiation within the water column and as a result, influences a decrease in the overall reflectance. This target has shown a low reflectance and high absorptance within any wavelength range. Moreover, the predominant mineral in Zone IV sediments was kaolinite. The spectral

irradiations for wavelength lower than 450 nm and 485 nm are not defined. It showed a dominant overlapping of data for all sediment concentrations that might suggest a non-dependence of suspended sediment concentration spectral reflectance to wavelength increase along short ranges.

Thus, the inorganic matter was not a significant factor within the TM1 band range. On the contrary, the spectral pattern for wavelength ranges between 664 to 820 nm demonstrates that the suspended sediment concentrations were the major controlling water quality parameter.

In this study, the various sediment concentrations were controlling water quality parameters only for wavelength range longer than 664 nm. High optical spectral irradiation for shorter wavelength range and high absorption in longer wavelength range support this assumption. This is a remarkable contrast between similar published data. Therefore, we assume that sediments are not the controlling water quality parameter for different given water bodies with similar total solid with low concentrations.

For wavelength ranges shorter than 400 nm to 500 nm and for suspended sediment concentrations lower than 150 to 300 mg/L, there was a uniform increase of spectral irradiation for inorganic suspended matter. For wavelength ranges higher than 400 nm, the spectral irradiation of suspended sediments decreased anomalously with respect to standard published trends. For the spectral reflectance of suspended sediment concentrations higher than 600 mg/L and over wavelength range of 600 nm, there is a sharp increase of reflectance with increasing wavelength range.

The lighting and viewing geometry, as well as the degree of field of view (FOV) used for the experimentation were very small. A remarkable quick deposition of the sediments towards the tank wall away from the sensor field of view was observed. The FOV of 1 degree was considered very small. Although the viewing geometry of the experiment was not monitored, we believe it might have produced some effects on the detected reflectance.

Therefore, we assume that attenuation of backscattering from wall and bottom is the major component controlling the overall irradiation of the sediments in the laboratory experimentation.

Even though the sediments were kept in suspension by continuous agitation and stirring, the deposition was remarkably effective and quick. This fact might have inhibit accurate determination of the spectral reflectance corresponding to low concentrations of suspended matter.

After stirring, we observed a quick deposition and concentration of sediments towards the extreme border of the tank. Few sediments were kept in suspension along the field of view surface area. These phenomena might also have contributed to the overlap of spectral patterns recorded for wavelength shorter than 485 nm, depicted in Figures 5.4 and 5.5. We believed that multiple scattering from the sediments quickly deposited and attached respectively along the bottom and wall of the tank, therefore, far from the FOV surface area, influenced the overall detected reflectance. So, scattering played a significant role in the total spectral reflectance recorded by the spectro-radiometer.

The strong effect of light backscattering within the spectral patterns for dry sediments was supported by spectral results for black bottom reflectance. It is very close to the reflectance patterns of Zones I (1,2%), II (0,85%), III (0,85%) and IV (0,88%) (Figures 5.7 and 5.8). The black bottom showed a lower reflectance pattern than the dry sediments of Zone IV. This fact is anomalous since this target should show high optical irradiance or absorptance (the rate of absorptance and incidence flux).

The spectral reflectance for Zone IV was very high relative to the others zones. The sediments from that zone behaved as a target having an optically higher irradiance. This result shows a good agreement with the field observation regarding the abundant floating organic matter within Zone IV. This abundance lowers the reflectance in the blue range and increases it in the green. We also believe that backscattering from the bottom had a

great influence on the reflectance. The dry inorganic matter spectral results for other zones showed higher reflectance values.

Backscattering effect from the wall and bottom is therefore the controlling factor within the overall laboratory irradiation. This effect might explain the higher spectral reflectance values for the black bottom (Figures 5.1 and 5.2) relative to the irradiation recorded for all suspended sediment concentration and for dry sediments for Zone IV (Figure 5.2). These results were noticed for the blue wavelength (485 nm) range.

Although the content of organic matter determined for the sediments within Zone IV was not the highest, we believe that the predominating phytoplankton matter (60% referred by Lira *et al*, 1991) "in situ" and within the sediments of Zone IV explains the decrease in reflectance values for that zone relative to the others zones. The spectral reflectance curves recorded for the dry sediments of Zone IV and all sediment concentrations for Zones I, II and III for short wavelengths, had a strong influence on the black bottom optical characteristic. We assume that the sediments had already deposited towards the extreme border of the tank, away from the field of view surface. The low reflectance for Zone IV might have also been the response of a high rate of absorptance within the water column.

The analysis of the spectral reflectance patterns recorded for the dry sediment samples illustrated in figures 5.7 and 5.8 indicated a similar overall increase in reflectance values with increasing wavelength ranges. For wavelengths in the TM1 range, the sediments of Zone IV presented a spectral reflectance (0,7%) similar to the black bottom one in the 485 nm wavelength range. The spectral pattern for higher wavelength range varied from 0,7% to 16%. The spectral patterns for Zones II (0,85% to 21%) and III (0,85% to 16%) sediments were similar.

The only dry sediment spectral irradiation that can be differentiated from the other sediment reflectance patterns was that of Zone I (1,1 % to 25%). The result is markedly higher than the results for others in all wavelength range. The sediments within Zone I

presented a larger grain size and a lower content in organic matter, supporting the higher reflectance values recorded. The spectral irradiation recorded for the various suspended sediment concentrations for all wavelength ranges for Zone IV shows a distinctive spectral reflectance pattern (Figures 5.4, 5.6 and 5.8). It is distinct from the black bottom response that is contrary to the sediment spectral reflectance in the other zones.

Considering that the reflectance of any water body should increase with increasing suspended sediment concentration, we believe that the viewing geometry defined in the experimentation (1 degree for the FOV, the 30 degree azimuth angle for the lamp position, and the bottom and diameter depth for the tank), might have influence the spectral reflectance patterns detected for dry sediments and wet sediments (suspended sediments) mostly for blue, TM1 wavelength range.

Furthermore, the anisotropy nature of the sediment distribution for each composite sample of each zone coupled with the selected 1 degree FOV biased the spectral reflectance values expected. It is pertinent to state that the random noise was not assessed.

The presence of many bubbles during the emersion of the sediments along the water surface also influences a non linearity within the spectral irradiation detected for all concentration of sediments. It might also have caused possible spectral interference produced by the laboratory environment. These are considered random noise during experimentation for radiance acquisition.

In addition, a corresponding increase in forward scattering was also observed for each suspended sediment concentration increase. Changes in the viewing FOV and solar zenith angles during data acquisition controlled the patterns of reflectance of the water body for high concentration of inorganic matter. In a way, the spectral reflectance detected can be related to the water properties of the studied lagoon.

Laboratory studies (Novo *et al*, 1989a, 1989b; Mantovani and Cabral, 1992) have reported the significant role of viewing geometry in the determination of the relative proportion of sub-surface and water reflectance recorded by a given sensor. Mantovani and Cabral (1992) suggested an optimum tank depth greater than 41 m for determining spectral reflectance for concentration of 140 mg/L for red silt and depth values of 41 to 63 m for bentonite.

The low concentration of 140 mg/L is a close value to the low concentration (150 mg/L) of this study. Even though the sediments sampled in situ are silt and clay, the depth tank value selected for this experimentation was very low, strongly favoring bottom scattering. Several studies concerning the detection of spectral irradiation patterns of suspended sediments, have demonstrated that for very low concentrations of suspended sediment (less than 10 mg/L), the backscattering effect from bottom reflectance is the controlling factor. Therefore, a similar backscattering effect is assumed within this experimentation. Comparative analyses between the spectral reflectance (Figures 5.5 and 5.6) for the 150 mg/L concentration and the corresponding wavelength range from all targets indicated that the spectral reflectance for the lower concentrations might approximate ground truth values. There was an increase in reflectance values and wavelength with the lagoon depth (Figures 5.9 and 5.10). Furthermore, the increase in reflectance varied from Zones I to III and from Zones IV to II.

The shift from lower reflectance values in the blue range to higher reflectance values in higher wavelength range for zone IV might be due to the predominance of one mineral (quartz +kaolinite) relative to the other within the sediments of Zone II. Sediments containing mostly kaolinite have been reported to present higher spectral reflectance than the results in this study.

The relationships between the depth of the lagoon and the corresponding spectral irradiation patterns for the mineralogical assemblage were determined only for dry sediments from the lagoon bottom. They are illustrated in figure 5.10. The average depth

determined for the mapped zones within the lagoon proved to play a significant role within the corresponding spectral reflectance recorded by the spectro-radiometer for the dry sediment samples.

The analysis of the spectral irradiation trends of the curves in Figure 5.10 suggested a direct asymptotic relationship between the depth, the reflectance and the wavelength range. The sediments deposited along Zone IV present higher spectral irradiation values relative to the other zones and kaolinite is the dominant mineral.

It is observed that Zone I presents the lowest values of spectral reflectance. This fact might be related to the predominance of quartz relative to the clay minerals within the sediments of that zone. Zones II and III present spectral reflectance values between those of Zones I and IV. The granulometric analyses presented in chapter two indicate that the silt fraction predominates within Zone I. The X-ray results indicate that quartz is the predominant phase in that fraction and kaolinite dominates within the clay fraction.

Within the analysis through centrifugation it is not possible to establish precisely for Zone III which mineralogical phase predominated, although a tendency showing silt as the predominant grain particle was observed.

The determined bi-directional reflectance factor (BDF) according to the concept of Mantovani et Cabral (1992) indicates that, for the selected tank depth of 34,5 cm, the bi-directional reflectance was controlled by the wavelength range. There was an increase of BDF (Figures 5.11 and 5.12) and wavelength range at low concentrations of 150 and 300 mg/L for Zone I and at low concentrations of 150 mg/L for Zone III. There was a shift in concentrations decreasing from sediment concentrations higher than 600 mg/L for Zone II to sediment concentrations between 300 and 600 mg/L for Zone III. For concentrations higher than 600 mg/L for Zone III, there was an increase of the bi-directional reflectance factor with increasing concentrations and wavelength ranges. The bi-directional reflectance factor (BDF) for Zone IV has showed a linear increase with wavelength range

with the 150 mg/L to 600 mg/L concentration and a decrease with the 900 mg/L. The highest concentration of 1 200 mg/L increases with all wavelength range.

The depth values (Figures 5.9 and 5.10) mapped for the Zones along the *Jequia* lagoon can be compared to the bi-directional factor that normalizes all spectral reflectance to the reflectance of the white barium reference panel.

Scatterplots (Figures 5.9 and 5.10) of the bi-directional reflectance factor and the spectral reflectance for dry sediments for all zones did not indicate distinguishable trends as it did for the reflectance of suspended sediment and normalized factor.

The dry BDF increased from Zone I to Zones II and IV with increasing wavelength range. For the sediment concentrations of Zone III, the BDF values were the lowest and increased with wavelength range.

Assuming that the total estimated suspended solids discharged empirically for the *Jequia* lagoon varied from 17 to 33 mg/L and that they corresponded to the sediments sampled, we might deduce that the reflectance of the lowest simulated sediment concentration (150 mg/L) recorded by the spectro-radiometer is at least 3 times higher than the irradiance (converted DN) detected by the TM sensor. Thus, if the laboratory spectral reflectance for a low concentration of suspended sediments varies from 0,38% to 0,76% within the zones, then the real overall irradiance expected should be of 3 orders of magnitude higher, including the attenuated effect produced by the organic matter. Within these considerations, the contribution from atmospheric transmittance (scattering) is neglected and also solar elevation and zenith angles.

The spectral irradiation model for the water quality parameters proposed in this study is computed using the conductivity measures, the temperature, the sechi depth and the bathymetric data. Also used are the empirical measures of sediment discharges, the

sediment properties and the laboratory suspended sediment concentrations. Published annual water discharge (1,4 m^3/sec) data were also taken into account.

The average sediment discharge is empirically determined using the concept of Moursy (1987) which defines that constant flow velocity of sediments occurs along the upper layers of a given water body. The suspended sediment discharge values used in the model are derived from the relationship between conductivity determined in situ and total solids estimated in laboratory conditions.

5.4. Modeling the laboratory irradiation balance (IRaB) produced by the water targets

5.4.1. Fundamental theory solving the irradiation balance model

The balance of energy conservation is related to the interactions between the flux of energy reflected (reflected/incident) and the one transmitted (scattered+absorpted) (Sathyendranath, 1981; Wetzel, 1975; Iqbal, 1983; Maul, 1985 and Dantas, 1994) within a given target. Wetzel (1975) states that as light reaches a water surface it is first refracted, then absorpted, reflected, scattered or transmitted. Only the absorpted light is transformed in energy. The light coefficients of incidence, reflectance, absorptance and transmission are optically dependent of the water optical characteristics (Dantas, 1994) that is, the sediments (grain size and mineral type) and the water dissolved matter. We also assume the effect of any organic or inorganic matter fixed within the spherical particles. Within this study, the coefficients of absorption and transmission are denominated as the coefficients of attenuation.

The basic equations solving the problems regarding the downwelling and upwelling irradiation recorded by the spectro-radiometer are based on the general radioactive energy transfer model for any given environment. They can be written in the form of equations 5.1 to 5.5 as:

$R_\lambda = I_\lambda - [A(\lambda) + T(\lambda)]$, equation (5.1)

in which;

R_λ:Reflected energy from the water surface,

I_λ: Incident energy on the water surface,

A_λ: Absorpted energy by the water column matter

T_λ:Transmitted or backscattered energy by the water column matter

The fraction of reflected, absorpted and transmitted irradiation can also be expressed as:

$a + r + t = 1$ equation (5.2)

in which;

a: Coefficient of reflection

r: Coefficient of absorption

t: Coefficient of transmission or backscattered

Within this model the fraction of absorpted and transmitted irradiation is assumed to be the attenuated irradiation (K). It can be expressed, based on the numerical model of Dantas (1994) as:

$K = k_w + k_{ss} + k_{dm}$ equation (5.3)

in which;

k_w: Attenuation coefficient due to water molecules

k_{dm}: Attenuation coefficient due to dissolved matters

k_{ss}: Attenuation coefficient due to suspended sediments

It is assumed that the sediment particle sizes are not wavelength dependent and that the absorpted (r) irradiation produced by the water molecules and dissolved matter is omitted (r =0). The water used within the simulation was distilled (pure). Therefore, the relationship of equation 5.2 is simplified to:

$$a = 1 - t \qquad \text{equation (5.4)}$$

in which;

a: Coefficient of reflection

t: Coefficient of transmission (backscattered)

The absorptance and transmitance are assumed within this work as the backscattered energy or simply attenuated irradiation. Since pure water equals the aborptance and transmitance (r = t= 0) due to the suspended sediments and dissolved matter (Dantas, 1994) we assume that the residual irradiation corresponds to a simple linear energy balance model.

The significant amount of bubbles generated by the stirring of the sediments in the water column is accounted for within the model. It is also considered as a controlling factor of the backscattering from the wall and bottom of the tank.

Therefore the attenuated irradiation (K) of equation 5.4 is simply reduced to:

$$K = k_{ss} + k_{bu} \quad k_{wb} \qquad \text{equation (5.5)}$$

in which;

K : Overall attenuated irradiation

k_{bu}: Attenuation coefficient due to bubbles

k_{ss}: Attenuation coefficient due to suspended sediments and fixed matter

k_{wb} : Attenuation coefficient due to wall and bottom backscattering

5.4.2. Discussion on the irradiation balance models

Two simple linear models are proposed. The first model is related to the correlations between the dry sediments (grain size and mineral type) reflectance with the wavelength range and their distribution on the bottom of the lagoon. The second model discusses the relationship between the sediment concentrations with wavelength and their distributions along the zones from where they were sampled.

Dantas (1994) estimated that, in a pure water tank, the reflected coefficient must be constant and around 5% for the solar radiation with incident angles less than 45°. Within the experiment, we assumed an incident angle of 30°. Therefore, we extended his estimation of 5% to the maximum laboratory reflectance recorded by the spectro-radiometer.

Within the IraB, we assume that the suspended sediments (size and mineral type) are the major significant target controlling the spectral reflectance that is, the attenuated irradiation detected by the spectro-radiometer.

The assumptions of Dantas (1994), for the application of Fresnel model estimating the proportions of water reflectance, are extented to this study. Therefore, the physical parameters assumed are: an environment temperature of about 20^0 C, a water refractive index of 1,33, minerals refraction index of 1,555 and a normal or vertical incidence of the light. So, the Fresnel (Maul, 1985) general model can be simply reduced to:

$Ab(\%)= 100(n-1/n+1)^2$ equation 5.11

in which;

Ab: Overall irradiance (albedo) produced by water molecules

n: Index of refraction for water.

The relationship expressed in equation 5.11 can also be applied to the mineral properties. Therefore, one might achieve the influences of the mineral in the overall irradiance (albedo).

The overall irradiation produced by pure water was empirically estimated using equation 5.11. The estimated empirical value of 2,4% (0,024) presents a good agreement with an average value of 0,02 within the blue (TM1) range detected in laboratory. This value might be accounted for within the two linear models (equations 5.12 and 5.13) as a constant factor of 0,024 for all the following considerations.

Therefore, it is assumed that the inorganic and organic matters respectively for Zones I and IV were the parameters affecting the water quality (color) of the lagoon.

The first spectral reflectance (irradiation) model describes a simple linear relationship between the irradiation for the dry sediments from TM1 to TM4 and their characteristics along the sampled four zones. The simple linear model is expressed as:

$OvIrds_l = 0.024(Bsc_l + Aog_l + Adw_l)$ equation (5.12)

where;

$OvIds_l$: Overall reflectance from dry sediments

Bsc_l: Backscattering from wall and bottom

within Zone IV present the higher irradiation from 485 nm to 820 nm, compared to the sediments from Zones I, IIb and III. Their reflectance shows an increased peak at the blue-green range (485-560 nm) three times higher for Zone IV than the same range for the sediments collected within Zone III. The reflectance of the dry sediments for all zones presents an increase within the blue-green range and a subsequent decrease from 560 nm to 820 nm. The results also indicate a decreasing in the laboratory reflectance with the water depth estimated in the field. The explanation for the unexpected reflectance result for the sediments from Zone IV might be related to the particle size of the sediments and the presence of organic and inorganic (oil-like substance) matter fixed within the sediments.

The second linear model relates the five selected sediment concentrations to their reflected and attenuated irradiation recorded within the visible (TM1, TM2),(TM3) and near infrared (TM4) wavelength range. Therefore, the relationship between the variation from lower concentrations (150 mg/L and 300 mg/L) through intermediate concentrations (600 mg/L) and to high concentration (900 mg/L 1 200 mg/L) of sediments sampled within the four Zones (I, IIb, IIIa and IV) can be discussed through the general form of equation 5.12.

$$OvIRssc_1 = 0.024[OvIds_1 - [(Irlssc + Irhssc)_{Zone\ III+IV} + (Irissc)_{Zone\ I+IIb}] \quad \text{equation (5.12)}$$

in which:

$OvIRssc_1$: Overall irradiation from suspended sediment concentrations (ssc)

$OvIds_1$: Overall reflectance from the dry sediments

$(Irlssc + Irhssc)_{Zone\ III+IV}$: Reflectance from low and high concentration of sediments

$(Irissc)_{Zone\ III+IV}$: Reflectance from intermediate concentration of sediments.

The reflectance of low and high concentrations of sediments was computed in one single term within the model due to their similar trend for all wavelength ranges.

The results (Figures 5.2 to 5.9) indicate a general trend of increasing irradiation with increasing wavelength. The highest reflectance is shown within the red range. In the case of low concentration of sediments, all zones see their reflectance decreasing after the red (TM3) range. On the contrary, the high concentrations (900 and 1 200 mg/L) maintain the increasing tendency within the TM3 range and longer range. For their part, the intermediate concentration (600 mg/L) of sediments presents increasing trends within wavelength longer than TM3 only for Zones IIIa and IV. It shows a decrease of reflectance for the sediments from Zones I and IIb. The explanation can be related to the depth of zone IIb and the presence of organic matter in the latter. These results show strong disagreement with the effects of deep water, that is, low attenuation due to water mass absorption and/or backscattering within successive layers. The two proposed linear irradiation models enable only general assumptions concerning the influence of variation on the size and type of the mineral within the sediments and their overall reflectance. The analysis of the grain size distribution indicates a mixture of the type and size within the samples used in the laboratory reflectance. The sediments collected within Zones IV and IIIa present larger dimensions than the other zones. Therefore, from published data (Bhargava *et al.*, 1991), it is expected a lower reflectance for those zones. However, for this study, the irradiation from the dry sediments and from the concentration of sediments shows a strong tendency of increased reflectance for the zones within the blue-green range and a smooth decreasing reflectance for the longer wavelength range.

FIGURES FOR CHAPTER 5

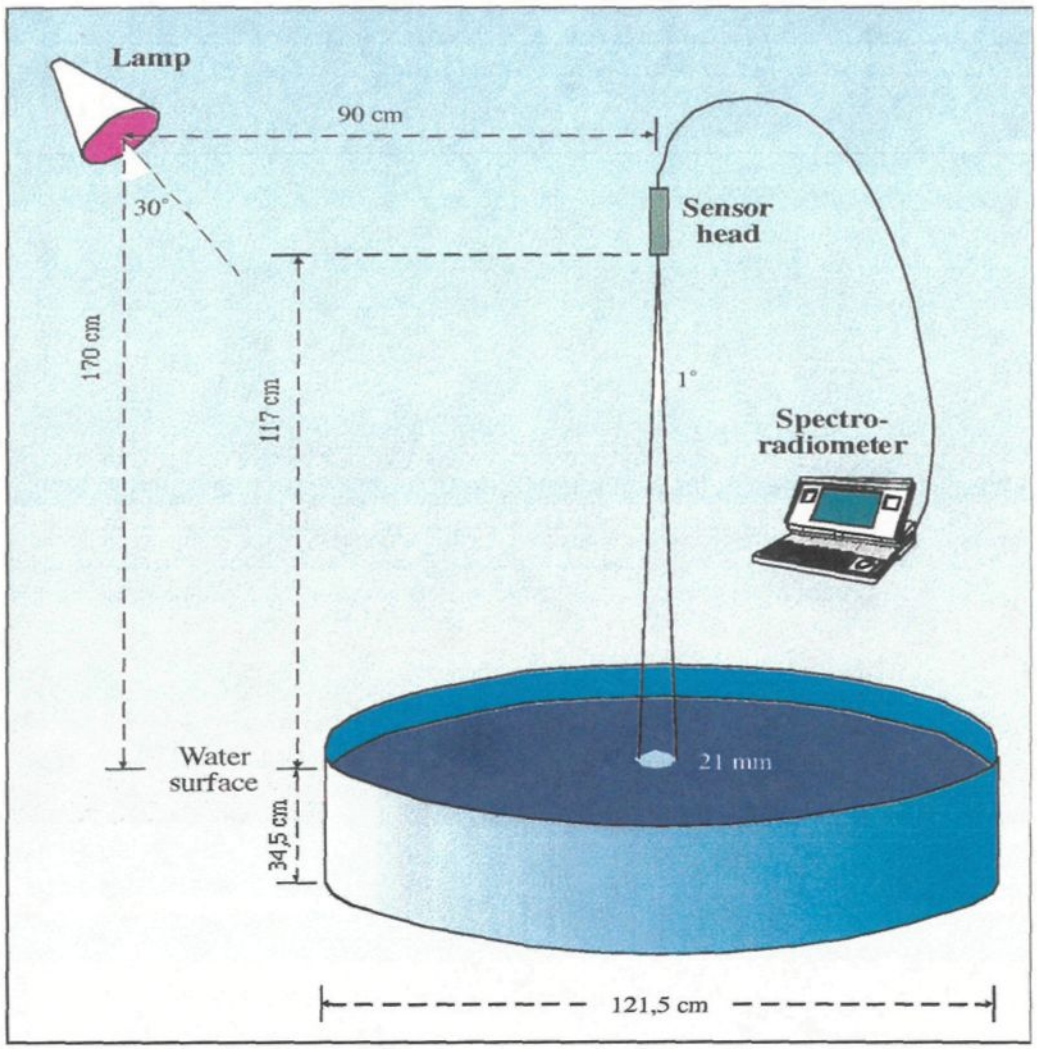

Figure 5.1. Scheme of the laboratory set-up used for determining spectral reflectances for several concentrations of sediments.

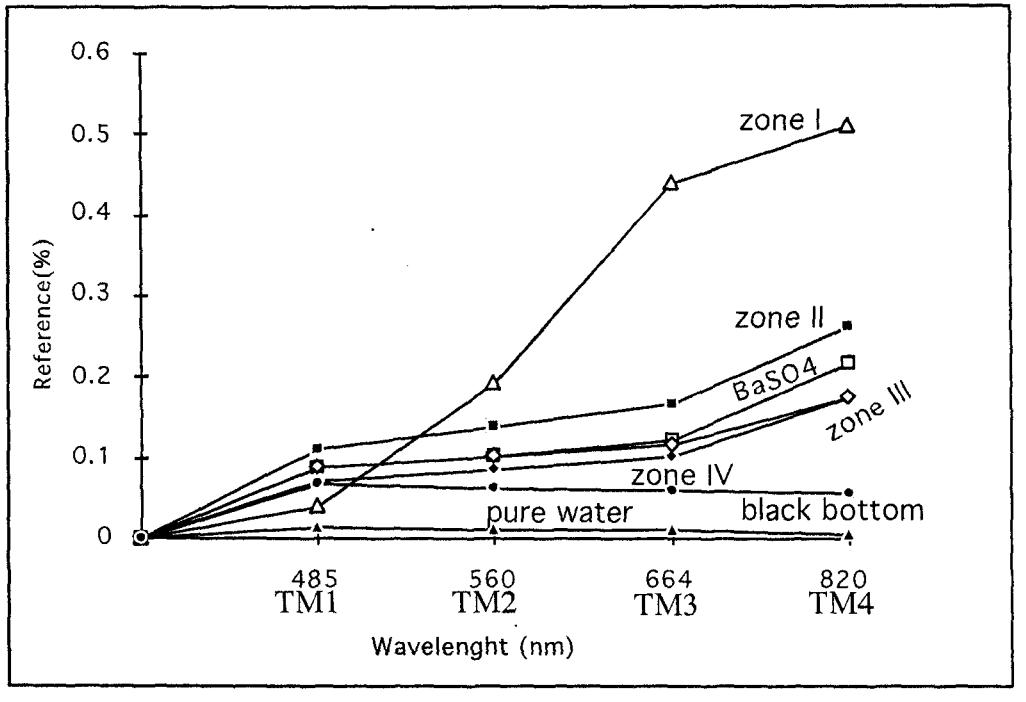

Figure 5.2:Spectroradiometer reflectance of dry sediments, pure water, black bottom and $BaSO_4$ reference panel for the simulated concentration of suspended sediments collected along the *Jequia* lagoon,*Alagoas*, Brazil.

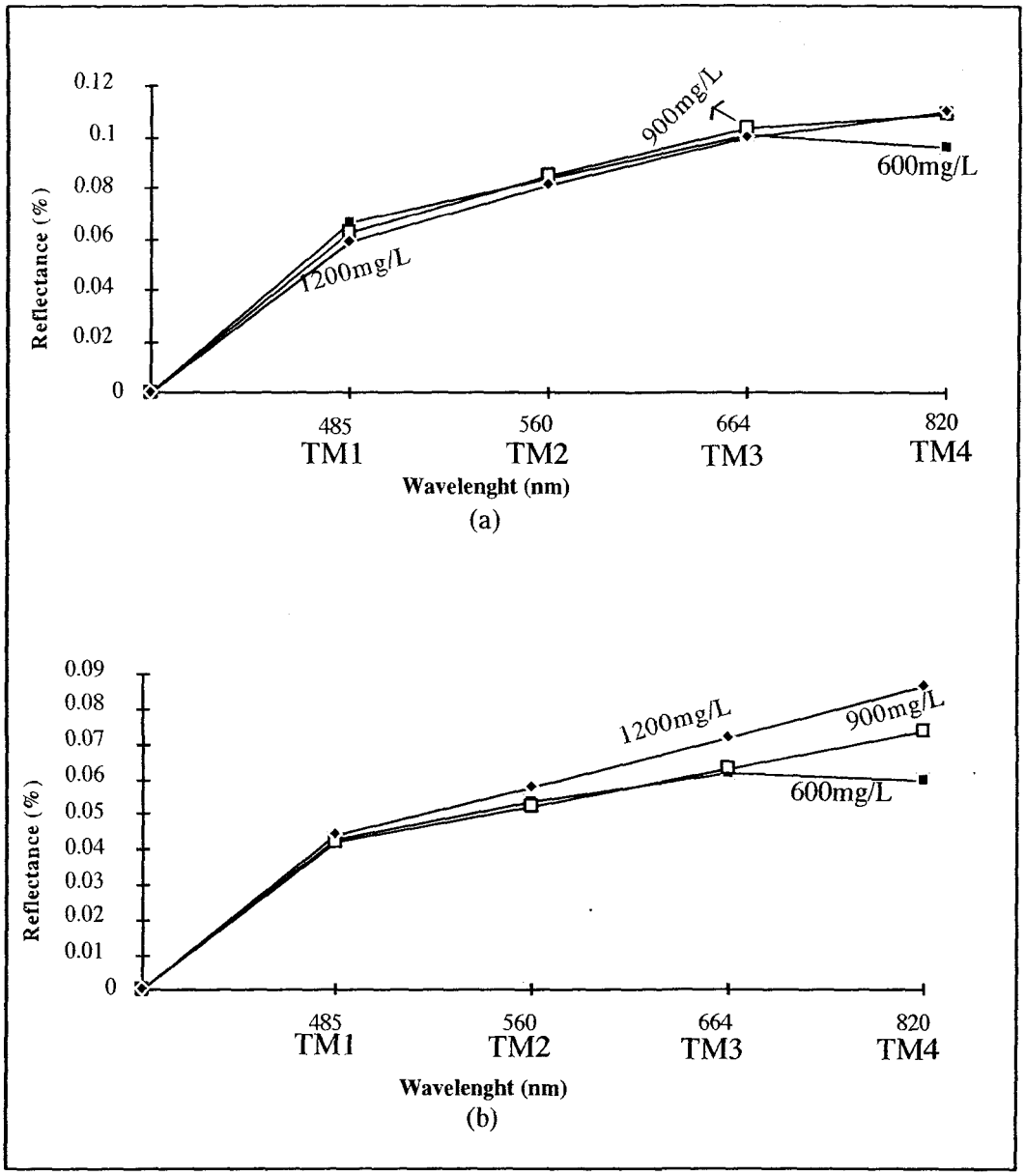

Figure 5.3: Spectroradiometer reflectances of the suspended sediment concentrations of 600mg/L, 900mg/L and 1200mg/L for zoneI (a) and II(b) of the *Jequia* lagoon. *Alagoas*, Brazil

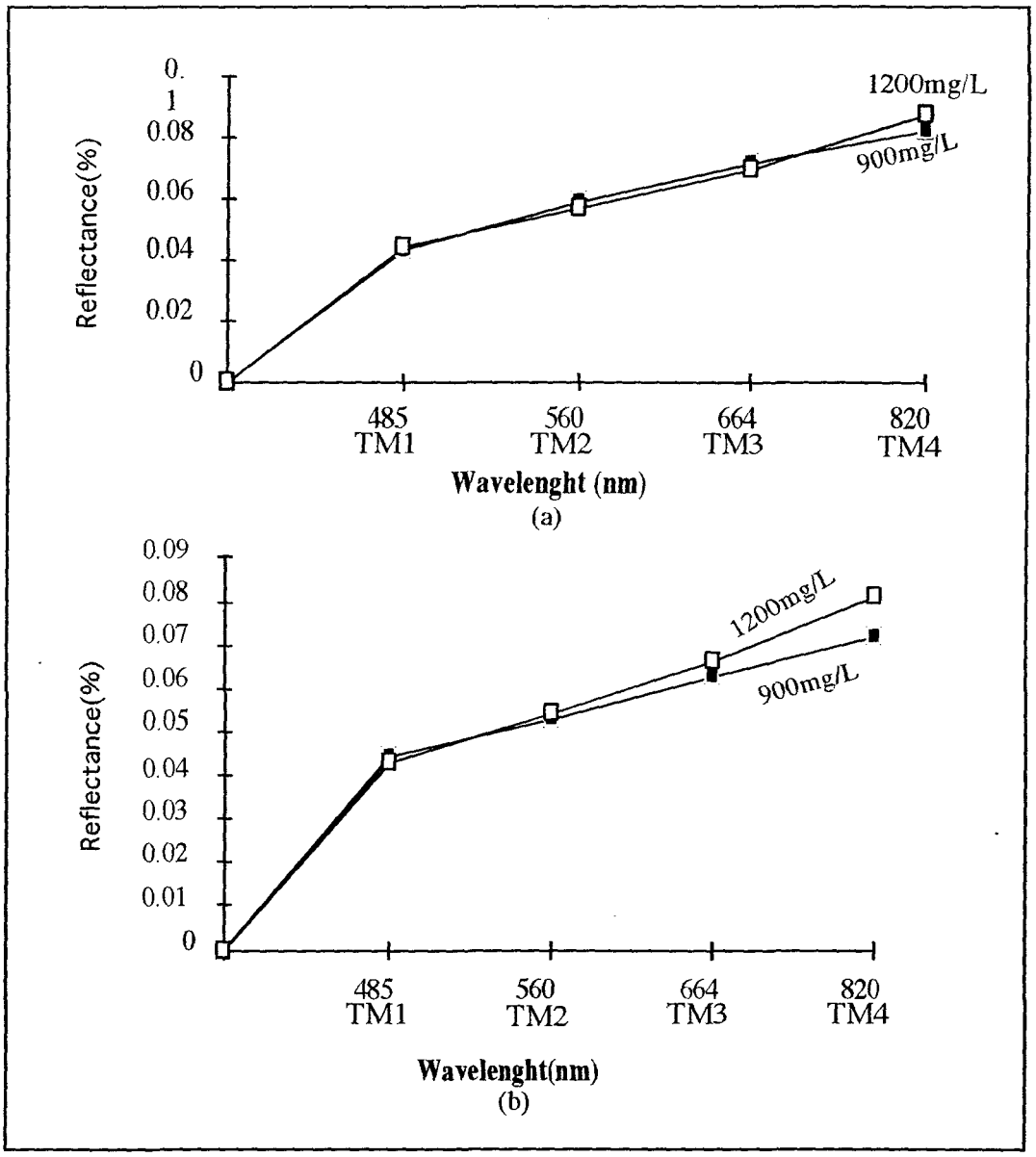

Figure 5.4: Spectroradiometer reflectances for the high concentration of suspended sediment of 900mg/L and 1200mg/L for zones IIIa (a) and IV (b) of the *Jequia* lagoon *Alagoas*, Brazil

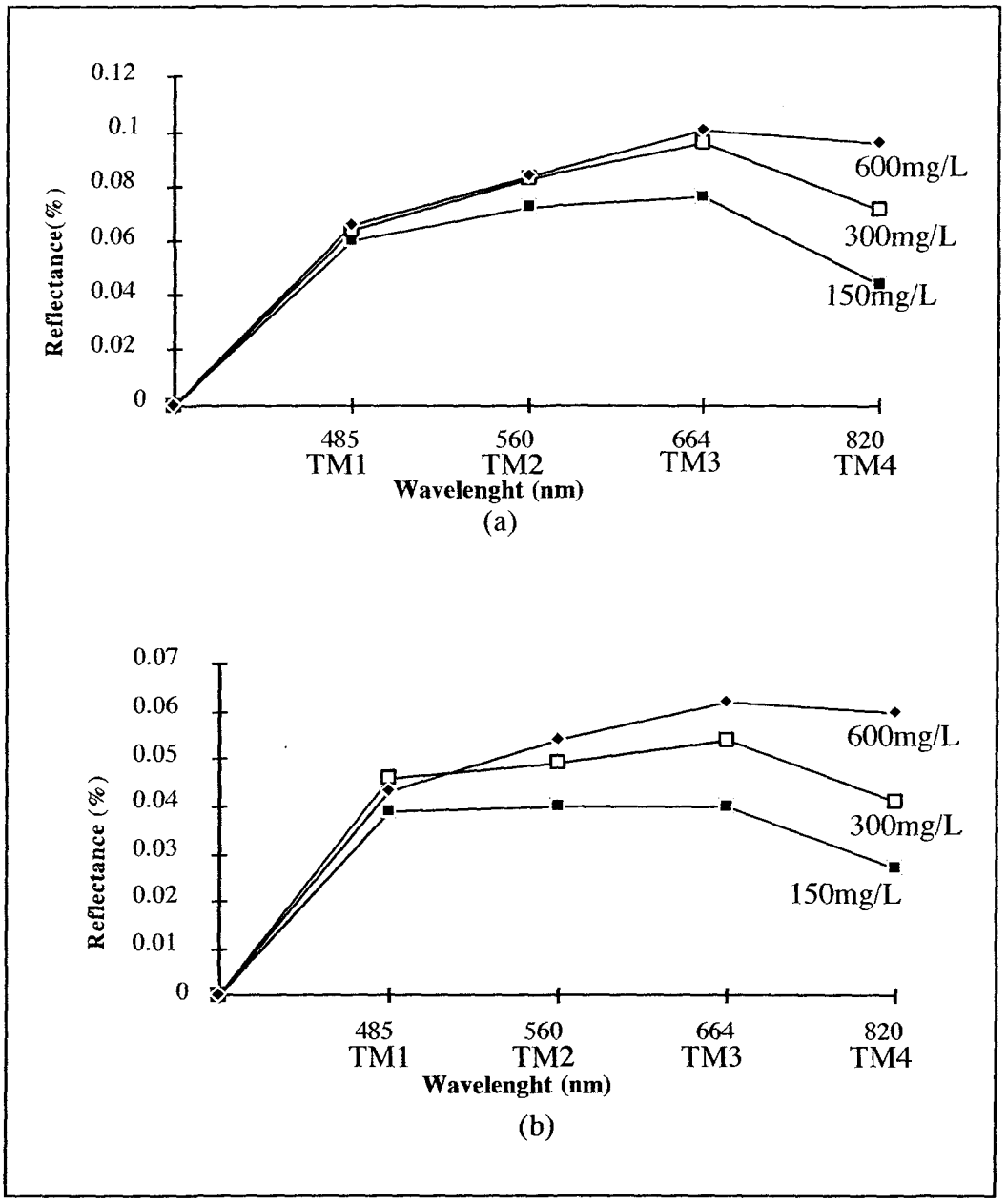

Figure 5.5:Spectroradiometer reflectances of the suspended sediment concentration of 150mg/L, 300mg/L and 600mg/L of zones I(a) and IIb(b) of the *Jequia* lagoon *Alagoas*, Brazil

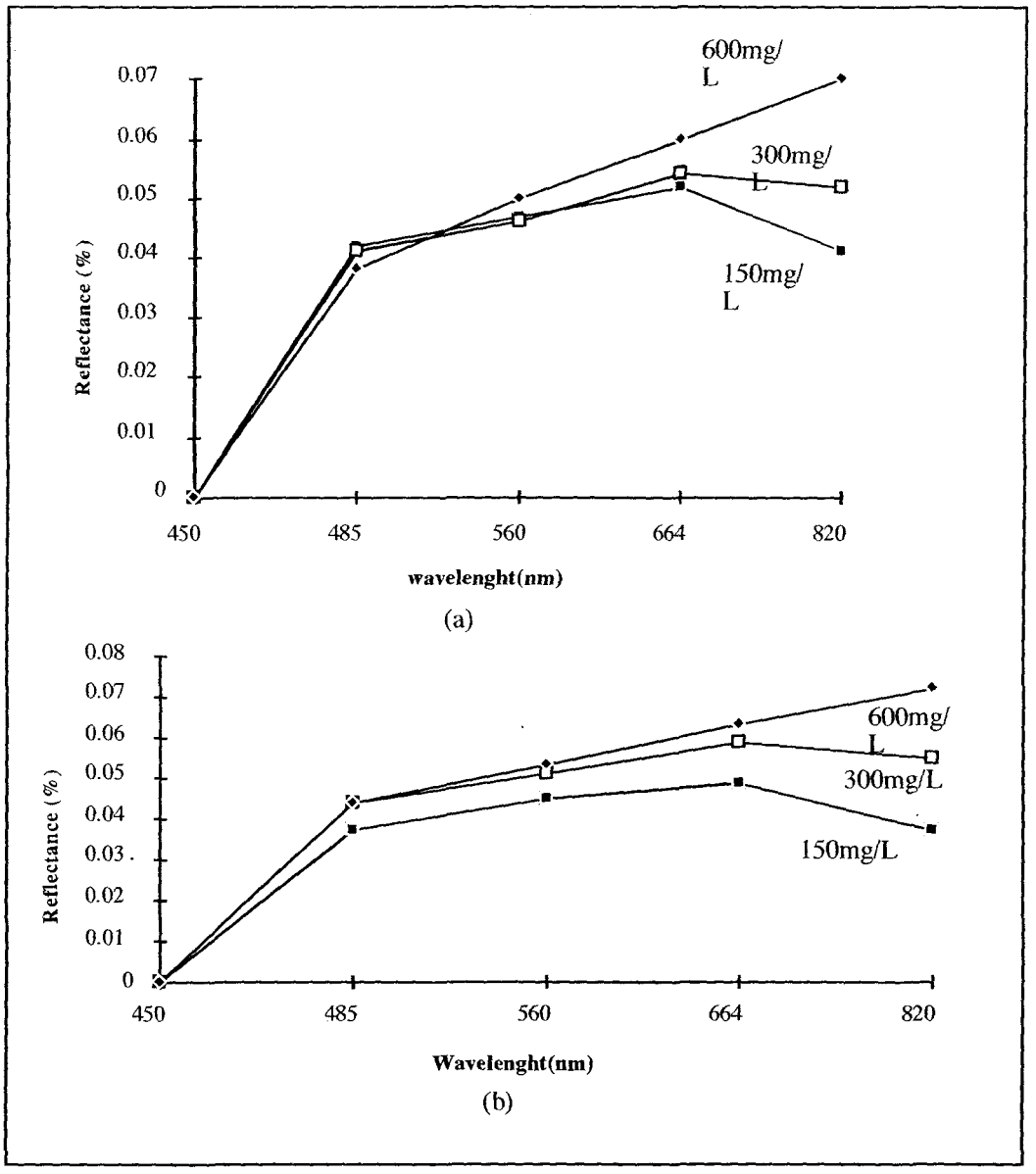

Figure 5.6: Spectroradiometer reflectance of the suspended sediment concentration of 150mg/L, 300mg/L and 600mg/L of zone IIIa(a) and IV (b) of the *Jequia* lagoon *Alagoas*, Brazil

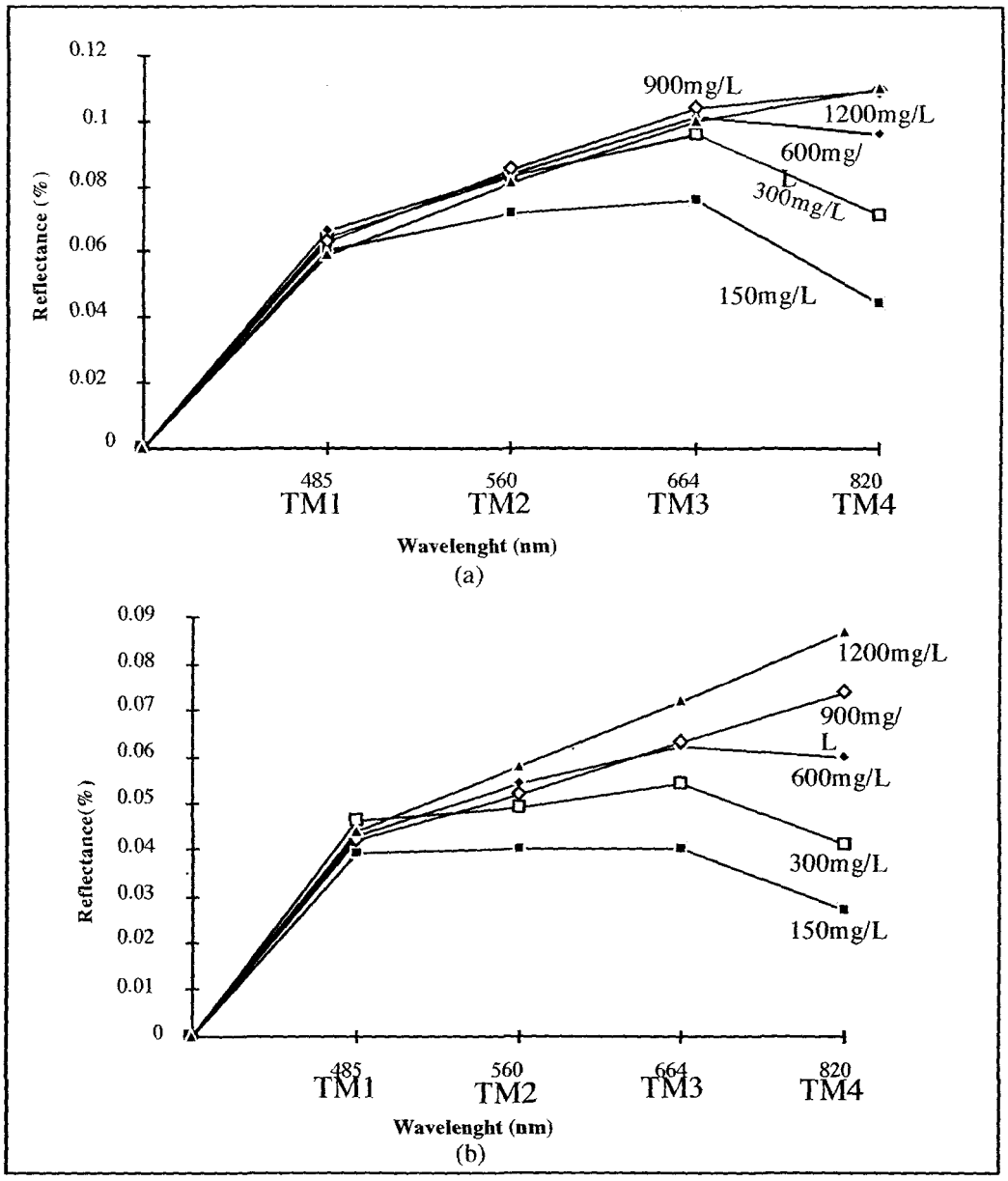

Figure 5.7: Spectroradiometer reflectances of suspended sediment concentrations for zone I (a) and IIb(b) of the *Jequia* lagoon, *Alagoas*, Brazil

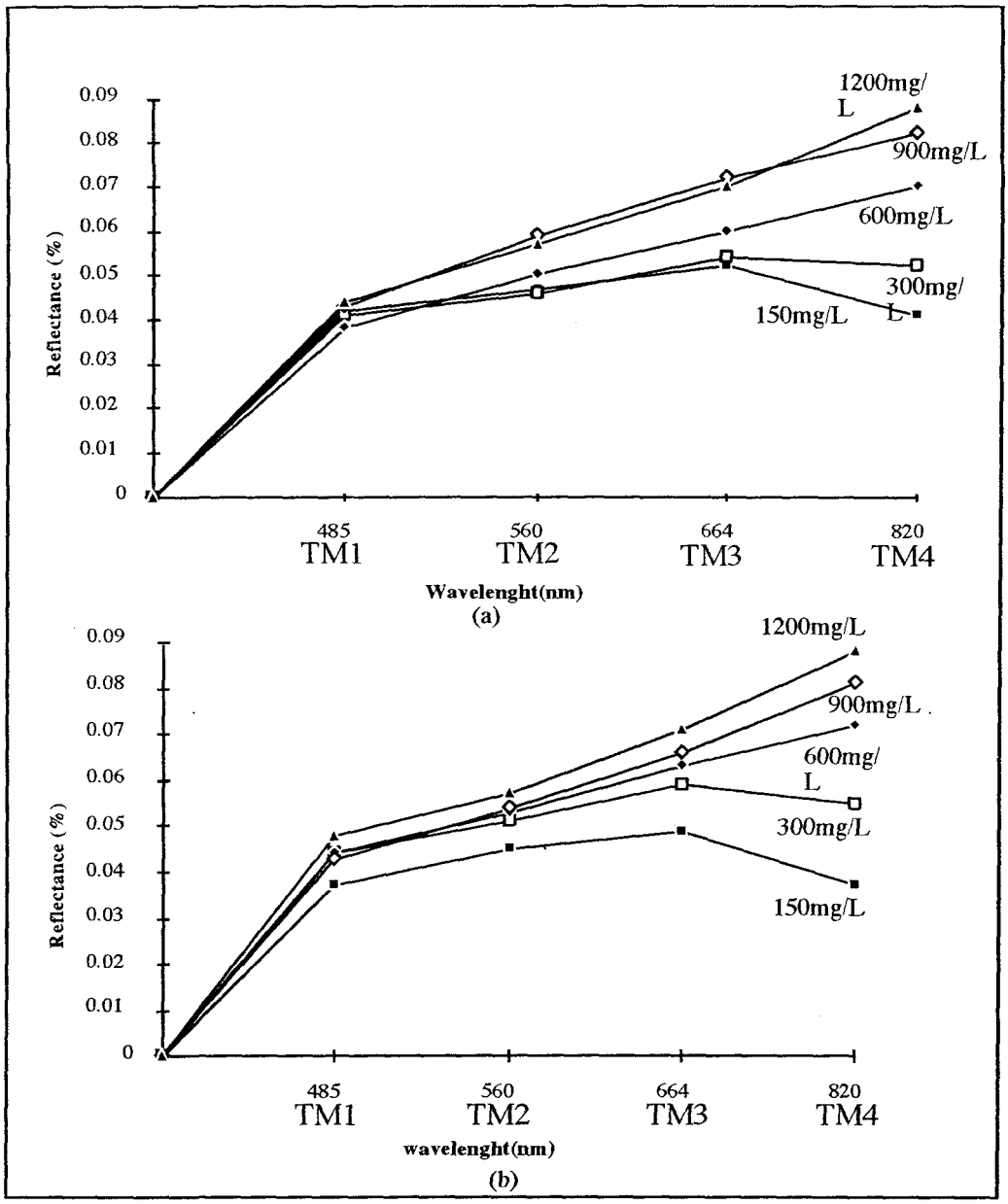

Figure 5.8: Spectroradiometer reflectances of several suspended sediment concentration for zone IIIa (a) and IV(b) of the *Jequia* lagoon, *Alagoas*, Brazil

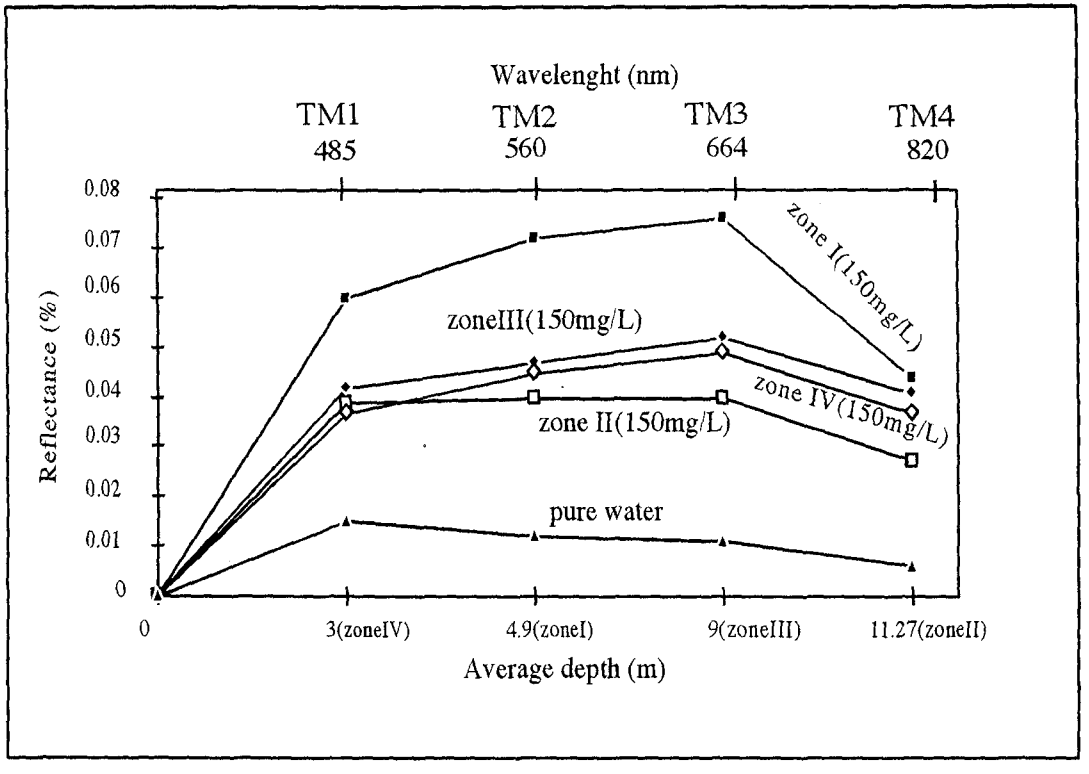

Figure 5.9. Scatterplot of bathymetric data (sites in situ) and the corresponding laboratory reflectance

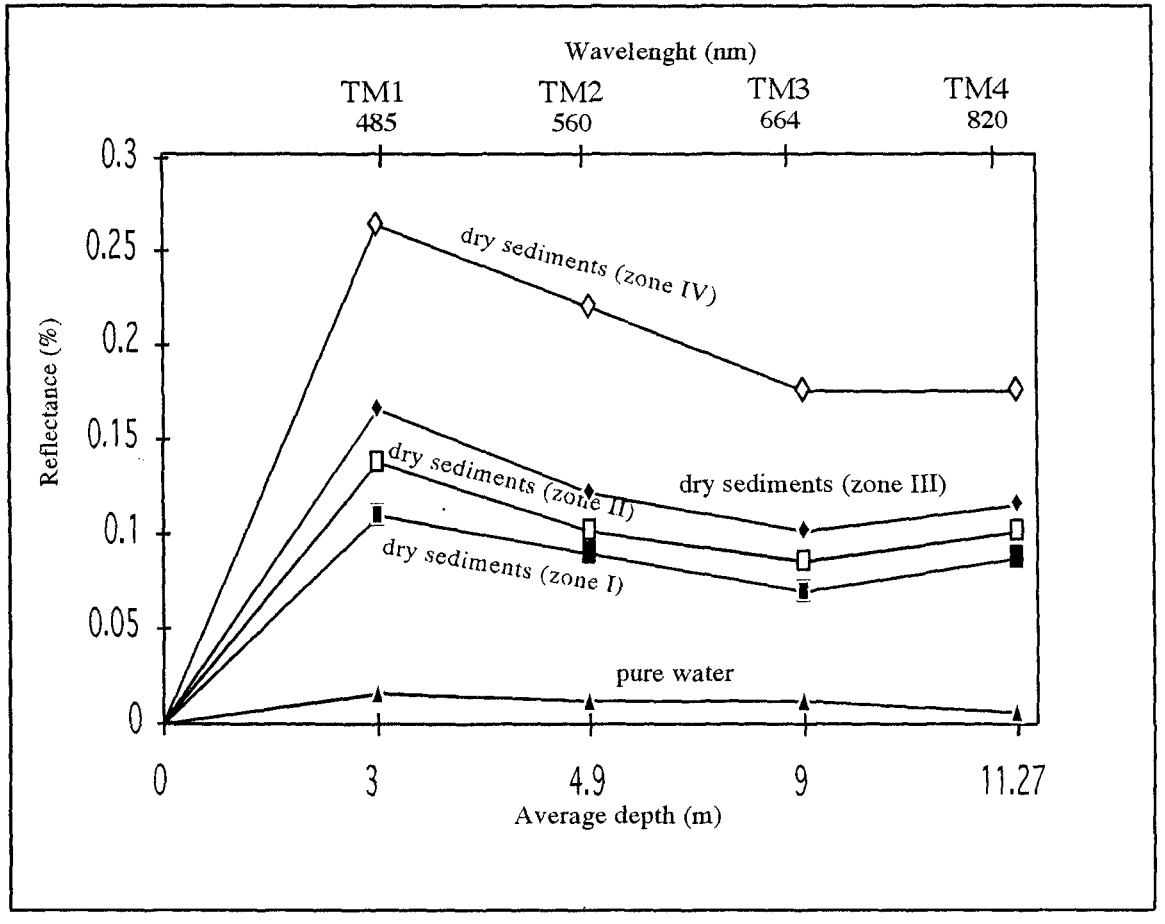

Figure 5.10: Scatterplot of the relationship between the batymetryc data determined in situ along the *Jequia* lagoon and the corresponding spectra-reflectance and wavelenght of the sediments sampled along the same zones and sites.

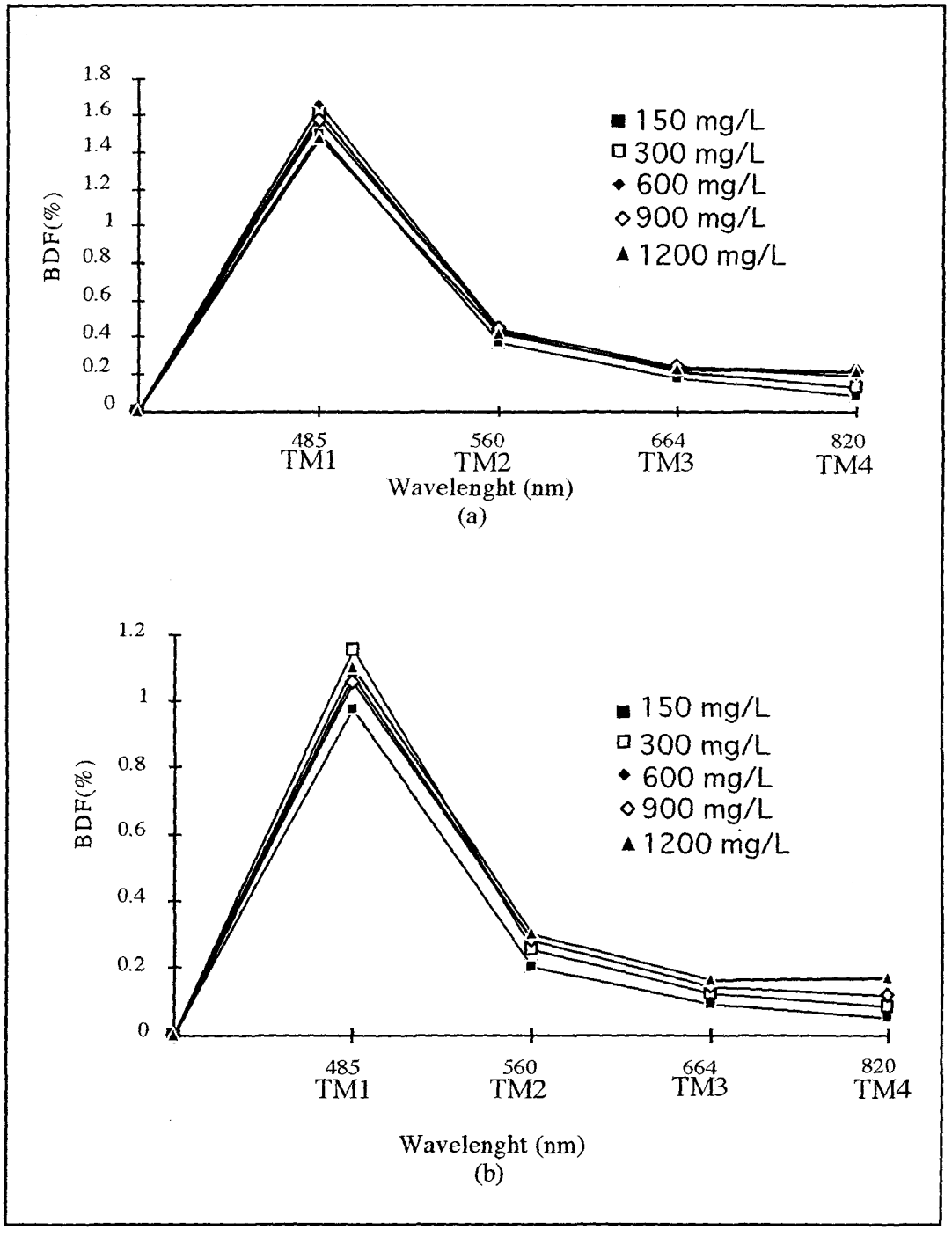

Figure 5.11: Bidirectional normalized spectro-reflectance (BDF) curves for the suspended sediment concentration using the bed clastic sediments of the *Jequia* lagoon, *Alagoas*, Brazil. Zone I (a) and zone IIb(b)

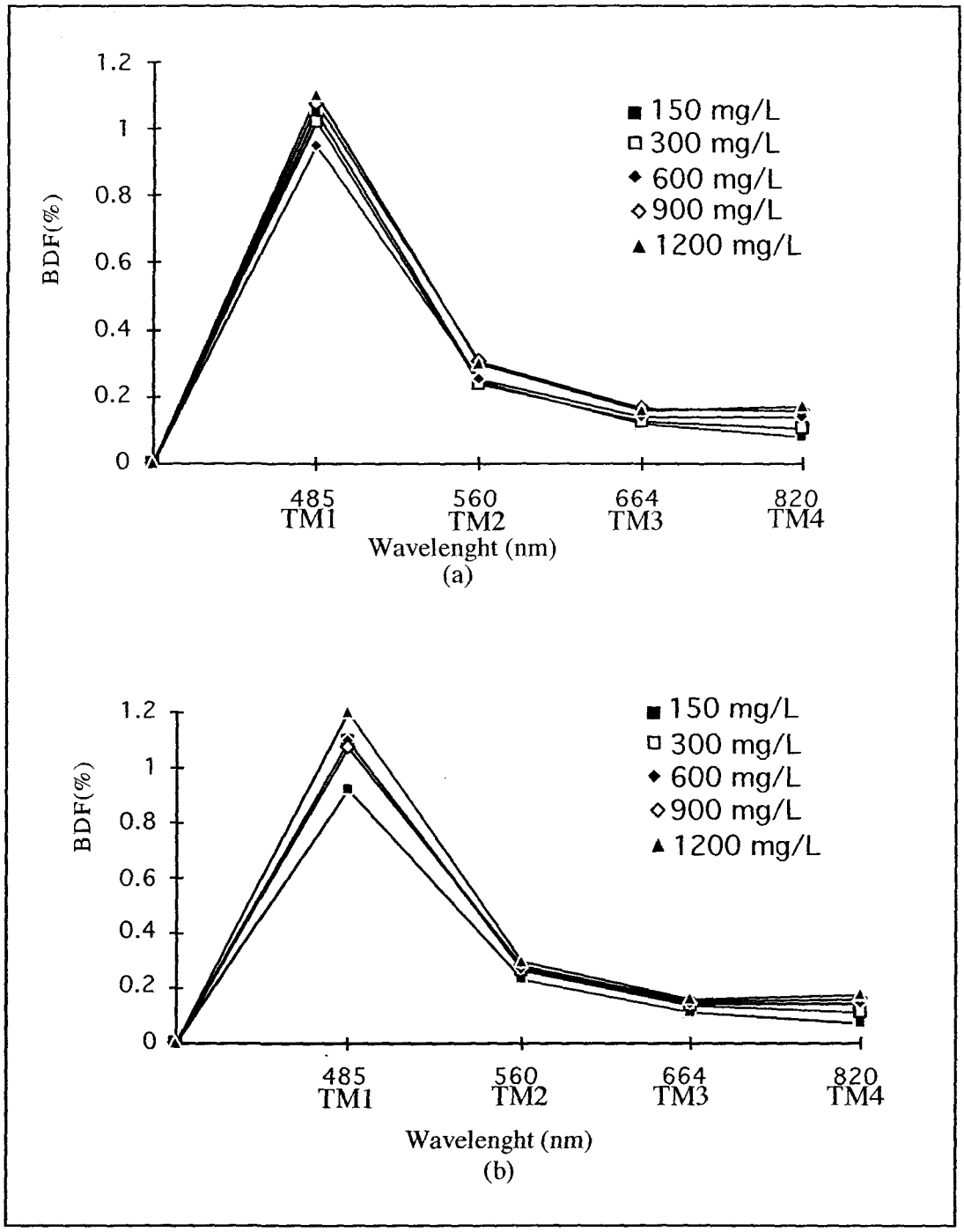

Figure 5.12: Bidirectional normalized spectro-reflectance (BDF) curves for the suspended sediment concentration using the bottom clastic sediments of the *Jequia* lagoon, *Alagoas*, Brazil. Zone III (a) and zone IV(b)

CHAPTER 6

DISCUSSION AND CONCLUSIONS

6.1. Introduction

This chapter aims to integrate and discuss the information acquired mainly by remote sensing technique and by few ground truth data. It also attempts to point out the correlations between the various types of information characterized and described in the preceding chapters.

The main objective of this work was to study the correlation between two factors: land use and sedimentation processes. The idea was to evaluate and point out changes in the land use patterns during the last three decades. As for the sedimentary processes, the thrust was to characterize sediment properties (grain size, mineral type and concentration) and their impact on transport mechanisms and the reflectance produced by the suspended matter. It was assumed that the sediments are the predominant element within suspended matter and they control the turbidity (water types) of the lagoon.

During fieldwork on the lagoon, an oil-like plume and some floating phytoplankton were recognized within Zone IV. Sediment plumes were abundant within Zones I and IV. The other zones presented a relatively pure water state during the surveys.

6.2. Correlation of results

The study area represents a complex-sensitive tropical ecosystem. The *Jequia* lagoon contains a homogeneous distribution of terrigenous clastic sediments carried mainly by near bottom (bed load) traction and suspension. Quartz and kaolinite are the dominant phases within the bottom sediments. These minerals are the result of tropical climate weathering. Slope and bank erosion of the Barreiras Formation was recognized during sampling survey near the lagoon outlet. During the course of this work, a significant amount of organic matter was identified in these sediments.

The turbidity of the lagoon assumed to be the distribution of the inorganic suspended sediments, can be easily mapped by using any of the remote sensing techniques described in this study. At least three water types are differentiated by enhancement, principal component, rationing or standard classification. However, the distinct reflectance from each of the plume components was not precisely detected.

Land-use units are mapped and considered to be representative of three decades of intensive development. The major impact recognized within this study is the removal of almost 100% of the original humid forest. The results from the quick-look and digital images indicate several growing stages for the sugar-cane fields.

The Gaussian standard classifier was not efficient to discriminate water types, nor suspended matter within the plumes. Moreover, we consider that at least two seasonably images coupled with simultaneous ground truth data are required to enable better discrimination of those targets. The classifiers show good accuracy for the discrimination of land-use categories although, within mixed crops, there is still some data generalization.

It is clear that a pixel by pixel variation is the norm within some crops and the water type of Zone IV. It is relevant to point out the necessity of considering the variation, even subtle, of zenith solar angle in the estimation of digital spectral patterns. It is impossible to detect precise temporal variation of sugar-cane or farming growing crops using only one satellite image. However, a spatial variability map of sugar-cane fields can be performed.

Furthermore, during the data acquisition time, the fields were filled with water since it is the high hydric period (Figure 2.7). The water flows into sugar-cane fields and may reduce the actual sugar-cane reflectance. The crop vigor controls the reflectance pattern as well as the biomass influences the spectral response of a given crop. The estimation of the vegetative index surely enables the distinction of growth stages and cropping vigor. It is known that the maximum difference of reflectance between two different targets should

not exceed 10%. Therefore, it is impossible to detect subtle differences within the same crop with limited temporal data.

Correlations between spectral responses for a given target in a given environment (tropical) are often difficult to transfer as a reference to other environments (temperate). Even similar tropical environments may present seasonal differences. However, the overall irradiance and irradiation estimated might be used as reference for further studies in similar tropical lagoons.

It is highly probable that the majority of the parameters (suspended phytoplankton and suspended sediments) within the water column of the lagoon are not optical Lambertian targets, therefore presenting difficulties in being distinguished. The intrinsic properties of the sediments and the other suspended matter might imply a non-uniform surface, therefore of non-homogeneous nature. These targets neither behave as free surfaces in which light propagates nor are located in horizontal surface uniformly illuminated.

Due to the little indication of zones containing only pure water, the total reflectance response mapped along the *Jequia* lagoon is mostly produced by the presence of sediment in suspension in Zones I, IIb and III and the existence of floating algae in Zone IV.

It is believed that the oil-like inorganic substance (oil-like plume) mixed with very strong turbid (high concentration of sediment) water, recognized qualitatively along Zone IV, is distinguishable using standard classifiers. Polluted sites can be better detected if long term data (with water chemical monitoring program) is available to enable the isolation of ground control points and the establishment of their reflectance. The most important constraint to discriminate the oil-like plume was the absence of sufficient pixel clusters to determine representative training sites. A few dozens (30 to 60) of pixels were insufficient to assess precisely the oil-like plume, the algae and the sediments within the water column of the lagoon, with any standard band to band processing methods.

Some terrigenous inorganic sediment, a punctual oil-like plume called the polluted plume and a phytoplankton plume were identified within Zone IV (Figure 1.2). These parameters showed interactions very difficult to be differentiated using standard remote sensing methods with limited temporal satellite data.

Spectro-radiometric data and digital data obtained in this study led to a simple model of overall irradiation (reflectance) of the sediments sampled within the lagoon. However, the spectral characterization of those targets is validated only punctually and in laboratory conditions.

We suggest, for further investigation, that a systematic and periodic semi-diurnal sampling of chemical data from the water column of Zone IV, may reveal the spectral signature of the pollutant plume. Moreover, investigation and analyses of the suspended and bottom sediments using this systematic sampling program would permit a better characterization of the environmental parameters of the lagoon.

Water starts to fill the sugar-cane crops during June for most years due to the high hydric excess (Figure 2.7) found during that month. Viewed from space, that fact justifies the reduction of the expected reflectance of sugar-cane fields since water shows strong absorptance in visible wavelength ranges. Sugar-cane crop vigor might influence the reflectance as the biomass affects the spectral response of a given crop.

It is considered that the irregular patterns of sugar-cane crops within the study area contributed to the enhancement of the differences in green colors due to several growth stages. These stages imply that the total or residual reflectance recorded by the LANDSAT TM might be mixed with spectral responses derived from bare soil areas distributed within the sugar-cane fields, adding then to their specific reflectance. This fact leads to the assumption that only a non-standard classifier (non-parametric) is adequate to differentiate the multiple patterns of reflectance within the sugar-cane crops and also within the homogeneous targets (water parameters).

From the above considerations, we assume that the results and correlations of this work present enormous spatial and temporal limitations. The correlations between spectral signatures, sedimentation and land-use patterns require an intensive synchronicity of data. Taking into account that the discharge of sediments within the study area varies in a dynamic way (intrinsic properties) and that the reflectances of a homogeneous water body (lagoon) are hardly assessed with standard classifiers, the correlations between these aspects become a hard task. Nevertheless, we consider that correlations between grain size, mineral type, concentration of sediment and their respective reflectance can be precisely assessed if data is collected simultaneously with satellite recording.

One original contribution of this study is presented in chapter five on remote sensing. Foremost, the data is considered original since there are no previous investigations with a focus on the estimation of the reflectance of suspended and dry sediments of the *Jequia* lagoon. Another originality of this study is based on the fact that the sediments used within the simulation are natural, differing then from most of the published works that simulate soil types. Therefore, natural sampled sediments might approach the real environment. Moreover, the reflectances estimated in laboratory conditions are very useful, because we can isolate the parameters controlling the overall irradiation from any targets (plumes).

The mineral assemblage of quartz and kaolinite produces the residual radiance estimated in the laboratory. It is assumed that the spectral values estimated correspond to interchangeable overall irradiance (Chapter 4, Part II) and irradiation (Chapter 5) produced mainly by the suspended sediment (low concentration) in laboratory and in real environment (*Jequia* lagoon).

The two linear irradiation models are applied only to bottom sedimentation occurring under physical (flux, spatial distribution and seasonality) conditions prevailing during the sampling period (March 1990) in the *Jequia* lagoon. On the contrary, the land-use models

present several original contributions on the conditions that prevail nowadays along the study area.

6.3. Conclusions

The results of this study can be summed up as follows:

1) The textural characterization of the sediments based on combined sieve and hydrometer methods present significant laboratory error. We consider that simply using sieve data produces more pertinent and significant data. Sieve data coupled with few X-ray analyses easily enable precise comparison between the sediment properties and their reflectance. We assume that the errors produced during hydrometric reading prevent better results.

2) The Barreiras Formation and the Quaternary deposits produce the major sediment input into the lagoon, therefore, their detailed mapping is required.

3) It is clearly noticed that a pixel by pixel variation is the norm within the digital data of the water type of Zone IV. The distinction of these pixels requires non-parametric techniques. It is relevant to point out the necessity of considering the variation, even subtle, of zenith solar angle in the estimation of digital spectral patterns. The detection of precise temporal variation of sugar-cane or farm grown crops requires seasonable satellite imagery. Therefore, targets presenting mixed pixels within the study area are more the rule than the exception. Within these assumptions, the need to estimate the subtle variations of the zenith solar angle (FOV), very present in tropical environments, should also be taken into account. The maximum differences in reflectance between two different targets have exceeded 10%, though subtle differences along the same crop field of sugar-cane were impossible to differentiate due to limitation of temporal data. However, a spatial variability map of sugar-cane fields was performed.

4) The simulation of a larger variation of concentration of sediments can be considered relevant in laboratory experiments. Several low (lower than 150 mg/L), intermediate and high concentrations of sediment should be simulated. Previous knowledge of the amount of organic matter within the sediments and their removal from the sample is necessary before reflectance estimation is performed. Within this study, the removal of organic matter was performed after the experiment.

5) It is recommended in this investigation that the discrimination of polluted plumes using spectral signatures be done, for these plumes can be detected with periodic data obtained simultaneously with the satellites overpass.

6) We assume that the three decades of inflow of effluents from the distilleries into the *Jequia* lagoon and the lack of monitoring programs have contributed to aggravate the impacts on its ecosystems. The impacts are now being recognized and they have to be taken into account in the establishment of long term monitoring and managing programs of the coastal lagoon of *Jequia*.

REFERENCES

AB'SABER, A. N. (1992). Painel das Interferencias Antropicad na fachada Atlantica do Brasil: litoral e retroterra imediata. S.P: USP, 23 p.

ALLEN, P. G (1971). Relationship between grain size parameter distribution and current patterns in the Gironde estuary (France). Journal of Sedimentary Petrology, 41: 74-88.

ANDERSON, L. G., HANSOM, D. J., and HAAS, H. R. (1993). Evaluating LANDSAT thematic mapper derived vegetation indices for estimating above ground biomass on semiarid-rangelands. Remote Sensing of Environment, 45:165-175.

ANDRADE, M.C. (1973). A Terra e o Homem do Nordeste.Ed. Brasiliense. 3th. Ed. SP. 251 p.

ASSIS, S. de A. (1998). Fitogeografia, uso do espaco e protecao ambiental: o caso de uma reliquia paleoambiental ameaçada de extinção. Recife: DCG/CFCH-UFPE. Dissertação. 70 p.

ASSIS, S. de A. (1999). A Vegetacao dos Tabuleiros Costeiros Alagoanos: Caracterizacao e Zoneamento Geoambiental. Relatorio Tecnico para EMBRAPA.

ASSIS, S. de A. (2000). Biogeografia e Conservacao da Biodiversidade. Ed. Catavento

BAGNOLD, A. R. and NIELSEN, B. O. (1980). The pattern of natural size distribution. Sedimentology, 27: 199-207.

BARBOSA, F. R. A. (1990). Impacto ambiental causado nos recursos hidricos pelas industrias sucro-alcooleiras no estado de Alagoas. Relatorio interno do Instituto do Meio Ambiente de Alagoas. pp. 1-33.

BARBOSA, M. L. (1986). Quaternário costeiro no estado de Alagoas: influencias das variacoes do nivel do mar. Master thesis, Federal University of Bahia, Salvador, Bahia, Brazil.

BARROS, P. B. J., MAGALHAES, M. M. E., SILVA, S. C., SILVA, J J., LIRA, A. C. M., CORREIA, D. M., SOVIERZOSKI, H. H., JUNIOR, O. M. P., and MACEDO, J. S. (1992). Levantamento preliminar de dados bioecologicos da lagoa de Jequia: relatorio interno. Laboratorios Integrados de Ciencias do mar e naturais (LABMAR)-Universidade Federal de Alagoas (UFAL). 45 p.

BHARGAVA, S. D. (1983). Very Low Altitude Remote Sensing of the Water Quality of Rivers. Photogrammetric Engeneering and Remote Sensing. No.6, 49: 805-809.

BHARGAVA, S. D., and MARIAM, W. D. (1990). Spectral Reflectance Relationship to turbidity generated by different Clay Materials. Photogrammetric Engineering and Remote Sensing. No.2, 56: 519-529.

BHARGAVA, S. D., and MARIAM, W. D. (1991). Effects of Suspended Particle Size and Concentration on Reflectance Measurements. Photogrammetric Engineering and Remote Sensing. No.5, 57: 519-529.

BHARGAVA, S. D., and MARIAM, W. D. (1992). Cumulative effects of salinity and sediment concentration on reflectance measurements. International Journal of Remote Sensing. No.11,13: 2151-2159.

BIERWIRTH, P.N and LEE, T. J and BURNE, R. V.(1993). Shallow sea-floor reflectance and water depth derived by unmixing multispectral imagery. Photogrammetric Engineering & Remote Sensing. No. 3, 59: 331-338.

BIGARELLA, J.J. (1975). The Barreiras Group in Northeastern Brasil. Separata dos Anais da Academia Brasileira de Ciencias, Curitiba-Porto Alegre, 47: 365-394.

BITTENCOURT, P. Da S. C. A., DOMINGUEZ, L. M. J., MARTIN, L., and FERREIRA, De A. Y. (1982). Dados preliminares sobre a evolucao do delta do rio Sao Francisco (SE/Al) durante o Quaternario, influencia das variacoes do nivel do mar. Atas do IV Simposio do quaternario no Brasil, pp. 49-68.

BITTENCOURT, P. Da S. C. A., MARTIN, L.,DOMINGUEZ, L. M. J., and FERREIRA, De A. Y.(1983). Evoluçao Paleogeografica Quaternaria da Costa do estado de Sergipe e da Costa Sul do Estado de Alagoas. Revista Brasileira de Geociencias. No.13, 2: 93-97.

BOWKER, D. E and DAVIS, R. E and MYRICK. D. L and STACY, K. and JONES, W. T. (1985). Spectral Reflectances of Natural Targets for Use in Remote Sensing Studies. National Aeronautics and Space Administration. NASA Scientific and Technical Information Branch. 184 p.

BRAGA, F. Z. C., SETZER,W. A and DE LACERDA, D. L. (1993). Water quality assessment with simultaneous LANDSAT 5-TM Data at Guanabara Bay, Rio de Janeiro, Brazil. Remote Sensing of Environment, 45: 95-106.

BRAKEL, H. W. (1984). Seasonal dynamics of suspended-sediment plumes from the Tana and Sabaki Rivers, Kenya: analysis of LANDSAT imagery. Remote Sensing of Environment, 16:165-173.

BRYANT, R. C., and LEDREW, F. E. (1989). The Scope of Land-use change research, in Remote Sensing and Methodologies of Land-use Change Analysis. Edited by Bryant,

LeDrew, Marois and Cavanyas. Department of geography Publications Series, No. 6, pp. 1-5.

BUKATA, P. R. and BRUTON, E. J. and JEROME, H. J and JAIN, C. S. and ZWICK, H. H. (1981). Optical water quality model of Lake Ontario: determination of chlorophyll a and suspended mineral concentrations of natural waters from submersible and low altitude optical sensors. Applied Optics, 20: 1704-1714.

BULL, B. W. (1962). Relation of textural (CM) patterns to depositional environments of alluvial-fan deposits. Journal of Sedimentary Petrology, 32: 211-216.

BUSH, J. (1951). Derivation of a size-frequency curve from the cumulative curve. Journal of Sedimentary Petrology, 21: 178-182.

CASTRO, A. C. (1989). Structural evolution of the Sergipe-Alagoas Basin, Brazil. Ph.D. thesis, Rice University, Houston, Texas.

CAVALCANTE, T. A and ROCHA, C. de A. L.R, and ROCHA, P. M, and LIMA, M de P. V and BRITO, L. C. (1993). Contribuição de água doce na lagoa de Jequia-Alagoas-Brasil. Revista de Geociencias do Departamento de Geologia e Topografia.No.05, pp.1-68.

CHAVEZ, S. P. Jr., and KWARTENG, Y. A. (1989). Extracting spectral contrast in LANDSAT thematic mapper image data using selective principal component analysis. Photogrammetric Engineering and Remote Sensing. No. 3,55:339-348.

CHAVEZ, S. P. Jr., GUPTILL, C.S., and BOWELL, J. (1984). Image processing techniques for Thematic Mapper data, Proceedings, 50th Annual ASP-ACSM Symposium, American Society of Photogrammetry, pp. 728-743.

CHEN, Z., CURRAN, J. P., and HANSOM, D. J. (1992). Derivative reflectance spectroscopy to estimate suspended sediment concentration. Remote Sensing of Environment, 40: 67-77.

CONGALTON, G. R. and ODERWALD, G. R. and MEAD, A. R. (1983). Assessing LANDSAT Classification Accuracy Using Discrete Multivariate Analysis Statistical Techniques. Photogrammetric Engineering & Remote Sensing, 49: 1671-1678.

CORTIJO, F.J and De La BLANCA, N. P. (1997). A comparative study of some non-parametric spectral classifiers.Aplications to problems with high overlapping training sets. International Journal of remote Sensing. No.6, 18: 1259-1275.

CRACKNELL, P. A. and IBRAHIM, M. (1987). Use of Satellite and Aircraft Data for Bathymetry Studies. 13th Annual Conference of the Remote Sensing Society. September 7-11.

CROSTA, P. A. (1992). Processamento Digital de Imagens de Sensoriamento Remoto. Universidade de Campinas (UNICAMP). Instituto de Geociencias.Departamento de Metalogenese e Geoquimica.

CROSTA, P. A., and RABELO, A. (1992). Deteçao de alteraçao hidrotermal em regioes subtropicais atraves do processamento digital de imagens LANDSAT/TM: possibilidades e limitaçoes. 37th Brazilian Geologicalal Congress: Sociedade Brasileira de Geologia. Sao Paulo. pp. 145-146.

CROSTA, P. A., and RABELO, A. (1993). Assessing LANDSAT/TM for Hydrothermal Alteration Mapping in Central- Western, Brazil. Ninth Thematic Conference on Geologie and Remote Sensing, Pasadena, California., vol. II. , pp. 1053-1061.

CURRAN, J. P., HANSOM, D. J., PLUMMER, E. S., and PEDLEY, I. M. (1987). Multispectral remote sensing of nearshore suspended sediments: a pilot study. International Journal of Remote Sensing. No.1, 8:103-112.

DALE, V.H and O'NEILL, V. R. and PEDLOWSKI, M and SOUTHWORTH, F. (1993). Causes and effects of land-use in Central Rondonia, Brazil. Photogrammetric Engineering & Remote Sensing. No 6, 59:997-1005.

DANTAS, A. R. J., CALHEIROS, V. E. M., TORRES, G. A., De BRITO, N. B. B., BARBOSA, M. L., BITTENCOURT, P. S. C. AA., DOMINGUEZ, and L. M., MARTIN, L. (1986). Mapa geologicalo do estado de Alagoas. DNPM. 77 p.

DOMINGUEZ, L. M. J., BITTENCOURT, P. Da S. C. A.,and MARTIN, L. (1981). Esquema evolutivo da sedimentaçao Quaternaria nas feiçoes deltaicas dos rios sao Francisco (SE/AL), Jequitinhonha (BA), Doce (ES) e Paraiba do Sul (RJ). Revista Brasileira de Geociencias. No. 11, 4: 227-237.

FERREIRA, E.R. and BRAY, S.C. (1984). As Influencias do Pro-Alcool e do Pro-Oeste nas transformacoes das area canavieiras do estado de Sao Paulo. Geografia, 9: 101-104.

FOLK, L. R. (1966). A review of grain size parameters. Sedimentology, 6: 73-93.

FOLK, L. R. and WARD, C. W. (1957). Brazos River bar: a study in the significance of grain size parameters. Journal of Sedimentary Petrology, 27: 3-26.

FOLK, L. R. (1980). Petrology of sedimentary rocks. Hemphill P. Company.

FITZGERALD, W. R. and LEES, G. B. (1994). Assessing the Classification Accuracy of Multisource Remote Sensing Data. Remote Sensing and Environment, 47: 362-368

FRIEDMAN, M. G. (1962). Comparison of moment measures for sieving and thin-section data in sedimentary petrological studies. Journal of Sedimentary Petrology, 32: 15-25.

FRITZ, J. W and MOORE, N. J. (1988). Basics of Physical Stratigraphy and Sedimentology. John Wiley &Sons, New York.

GIBBS, J. R. and CHAKRAPANI, J. G (1994). Sediment particle size in the Hudson River estuary. Sedimentology, 41: 1063-1068.

GIBBONS, E. D., WUKELIC, E. G., LEIGHTON, P. J., and DOYLE, J. M. (1989). Application of LANDSAT Thematic Mapper Data for Coastal Thermal Plume Analysis at Diablo Canyon. Photogrammetric Engineering and Remote Sensing. No. 6, 55:903-909.

GLORIA, A. N and ORLANDO, F. J. (1983). Aplicaçao da vinhaça como fertilizante. Boletin Tecnico do PLANALSUCAR. No.5, 1: 5-38.

GOMES, A. (1980). Projeto RANDAMBRAZIL: cap. Geologia e Geomorfologia, 30: 27-444.

GOWARD, N. S. (1989). LANDSAT 1989: Remote Sensing at the Crossroads. Remote Sensing of Environment, 28:3-4.

GRIFFITHS, C. J. (1953). Estimation of error in grain size analysis. Journal of Sedimentary Petrology, 23:75-84.

GRIFFIN, M.G and INGRAM, L. R. (1955). Clay Minerals of the Neuse River estuary. Journal of Sedimentary Petrology.No.3, 25:194-200.

GUIMARAES, P. de T. (1988). Basin analysis and structural development of the Sergipe-Alagoas Basin, Brazil. Ph.D. thesis, University of Texas at Austin.

HARRINGTON, A. J., SCHIEBE, R. F., and NIX, F. J. (1991). Remote Sensing of Lake Chicot, Arkansas: Monitoring Suspended Sediments, Turbidity, and Secchi Depth with LANDSAT MSS data. Remote Sensing of Environment, 39: 15-27.

HARTMANN, C. and ADORNES, A and HARKOT, P. F.G. (1989). O Sistema LANDSAT com enfase no sensor Thematic Mapper(TM). Sociedade & Natureza. 1(2):107-121.

HUANG, G.H., CRACKNELL, P.A., and VAUGHAN, A.R. (1993). Satellite thermal observations of the Shannon River plume. Estuarine, Coastal and Shelf Science, 36: 207-219.

IQBAL, M. (1983). An Introduction to Solar Radiation. Academic Press, p.389.

JI, W. and CIVCO, L. D and KENNARD, C. W. (1992). Satellite Remote Bathymetry: a New Mechanism for Modeling. Photogrammetric Engineering & Remote Sensing, 58: 545-549.

JOHNS, D.W and GRIM, E. R and BRADLEY, F. W. (1954). Quantitative estimations of clay minerals by diffraction methods.Journal of Sedimentary Petrology, 24: 242-251

JOHNSON, R., and HARRIS, R. (1980). Remote Sensing for Water Quality and Biological Measurements in Coastal Waters. Photogrammetric Engineering and Remote Sensing. No. 1,46: 77-85.

JONES, F. B and WEIR, H.A. (1983). Clay minerals of lake abert, an alkaline, saline lake.Clays and Clay Minerals, 31:161-172.

KADDAH, M. T. (1974). The hydrometer method for detailed particle-size analysis: 1. Graphical interpretation of hydrometer readings and test of method. Soil Sciences, 118: 102-108.

KAWASHIMA, S. (1994). Relation between vegetation, surface temperature, and surface composition in the Tokyo region during winter. Remote Sensing of Environment, 50: 52-60.

KENNEDY, K. S. and MELOT, P. T. and DURNEY, E. T. (1984). Sieve data-size and shape information. Journal of Sedimentary Petrology, 55: 356-360.

KHORRAM, S. (1981). Water quality mapping from LANDSAT digital data. International Journal of Remote Sensing. No. 2, 2:145-153.

KHORRAM, S., and CHESHIRE, M. H. (1985). Remote sensing of water quality in the Neuse River estuary, North Carolina. Photogrammetric Engineering and Remote Sensing. No.3, 51: 329-341.

KLEMAS, V., and PHILPOT, D. W. (1981). Drift and Dispersion Studies of Ocean-Dumped Waste using LANDSAT Imagery and Curret Drogues. Photogrammetric Engineering and Remote Sensing. No.4, 47: 533-542.

KLOVAN, E.J, (1986). The use of factor analysis in determining depositional environments from grain-size distributions. Journal of Sedimentary Petrology, 36:115-125.

KOFFLER, F. N and DONZELI, L. P (1985). Avaliacao dos Solos Brasileiros para a Cultura da Cana-de-Açucar. Boletim Tecnico do IAA/PLANALSUCAR.

KOZLOV, D. V. and SAMSON, M. N. (1974). Measurement of the Light Attenuation Factor in Water from the Backscattered Light. Atmospheric and Oceanic Physics No.10, 10: 1093-1096.

LAMBE, W. T. (1967). Series in soil testing for engineers. John Wiley & Sons, 163p.

LANA, Da C. M. (1990). Bacia de Sergipe-Alagoas: uma hipotese de evolucao tectono-sedimentar. Edited by Raja Gabaglia, Guilherme Pederneiras and Milani, Edison Jose: PETROBRAS. pp. 311-332.

LATHROP, G. R. Jr., and LILLESAND, M. T. (1989). Monitoring water quality and river plume transport in Green Bay, Lake Michigan with SPOT-1 imagery. Photogrammetric Engineering and Remote Sensing. No.3, 55:349-354.

LAVERY, P., PATTIARATCHI, C., WYLLIE, A., and HICK, P. (1993). Water quality monitoring in estuarine waters using the LANDSAT thematic mapper. Remote Sensing of Environment, 46: 268-280.

LE DREW, F. E. (1989). Remote Sensing as a Diagnostic Science, in Remote Sensing and Methodologies of Land-use Changes Analysis. Edited by Bryant, LeDrew, Marois and Cavanyas. Department of geography Publications Series, No. 6 pp. 1-5.

LEMIEUX, G.-H.., BRISSON, C., PERRON, S., VACHON, G., and BÉGIN, R. (1993). Étude exploratoire d'une image satellitaire LANDSAT TM du Parc Marin du Saguenay. 16th.Canadian Symposium on Remote Sensing. pp. 533-539.

LEWIS, W. D and McCONCHIE, D. (1994). Analytical sedimentology. Chapman & Hall, 196 p.

LILLELAND, M. T. and KIEFER, W. R. (1994). Remote Sensing and Image Interpretation. Third Edition. John Wiley & Sons, Inc.

LINDELL, T. L., STEINVALL, O., and CLAESSON, TH. (1985). Mapping of coastal-water turbidity using LANDSAT imagery. International Journal of Remote Sensing. No.5, 6: 629-642.

LINST, W. G. (1966). Relationship of sediment-size distribution to ecologic factors in Buttonwood sound, Florida bay. Journal of Sedimentary Petrology, 36: 66-74.

LIRA, de A. C. M. and MAGALHAES, de M. M. E. and CORREIA D. M and SOVIERZOSKI, H. H. (1992). Relatorio Interno do Laboratorio de Ciencias do Mar da Universidade Federal de Alagoas.

LYNTS, W.G. (1966). Relationship of sediment-size distribution to ecologic factors in Buttonwood Sound, Florida Bay. Journal of Sedimentary Petrology.No.1,36:66-74.

LYON, G. J. and HUTCHINSON, S. W. (1995). Application of a Radiometric Model for Evaluation of Water Depths and Verification of Results with Airborne Scanner Data. Photogrammetric Engineering & Remote Sensing, 61: 161-166.

MANIKIAM, B., GOWDA, H. H., MANAVALAN, P., and JAYARAMAN, V. (1993). Study of sediment dynamics using satellite remote sensing. Advances in space research: the official journal of the Committee on Space Research. No.5, 13:75-78.

MANTOVANI, A.C.DI.M. (1997). Deforestation in the Amazon with an AVHRR-based system. International Journal of Remote Sensing. No 2, 18:273-286.

MARINHO, S., T., V. (1994). Coletania de legislacao ambiental: Federal-Estadual. Projeto IMA/GTZ. Governo do estado de Alagoas. pp.255.

MARTIN, L., SUGUIO, K., FLEXOR, J. M., BITTENCOURT, A. C. S. P., and VILAS BOAS, G. S. (1980a). Le Quaternaire marin bresilien (Littoral Paulista, Sud Fluminennse et Bahianais). Cah. Serie Geologie, X1: 95-124.

MARKHAM, L. B. and BARKER, L. J. (1985). Spectral characterization of the LANDSAT Thematic Mapper sensors. International Journal of Remote Sensing, no.5, 6:697-716.

MARKHAM, L. B. (1985). The LANDSAT sensor spatial responses. IEEE Transactions on Geoscience and Remote Sensing, no.6. GE-23:864-875.

MAUL, G. A. (1985). Introduction to satellite oceaonography. Martinus N.P. 599 p.

MAZUMDER, S. B. (1994). Grain size distribution in suspension from bed materials. Sedimentology, 41: 271-277.

McLAREN, P. (1981). An interpretation of trends in grain size measures. Journal of Sedimentary Petrology, 51: 611-624.

McLAREN, P and BOWLES, D. (1985). The effects of sediment transport on grain-size distributions. Journal of Sedimentary Petrology, 55: 457-470.

MEDEIROS, C., and KJERFVE, B. (1993). Hydrology of a tropical estuarine system:Itamaraca, Brasil. Estuarine, Coastal and Shelf Science, 36:495-515.

MERTES, K.A. L., SMITH, O. M., and ADAMS, B. J. (1993). Estimating suspended, Sediment Concentrations in Surface Waters of the Amazon River Wetlands from LANDSAT Images. Remote Sensing of Environment, 43: 281-301.

MOIOLA, J.R and WEISER, D. (1968). Textural parameters: An evaluation. Journal of Sedimentary Petrology, 38:45-53.

MOORE, M. D. and REYNOLDS, C. Jr. R. (1989). X-Ray Diffraction and the Identification and Analysis of Clay Minerals Oxford University Press, p 327.

MOORE, K. G. (1980). Satellite remote sensing of water turbidity. Hydrological Sciences-Bulletin-des- Sciences Hydrologiques. No.25, 4: 407-421.

MOUSSA, M. O. (1987). Satellite data based sediment-yield models for the Blue Nile and the Atbara River watersheds. Dissertation, 360 p. The Ohio State University.

MOUSSA, T. M. (1977). Phi mean and Phi standard deviation of grain-size distribution in sediments method of moments. Journal of Sedimentary Petrology, 47:1295-1298.

NANU, L. and ROBERTSON, C. (1978). Estimating suspended sediment concentration from spectral reflectance data. International Journal of Remote Sensing.No.5, 11: 913-920.

NICACIO, M. R. and De SOUZA, J. L. and BERNARDO, S. De O. (2001). Estimativa da irradiancia solar global para Maceio utilizando o modelo linear de Angstrom-Prescott. XII Congresso Brasileiro de Agrometeorologia-III Reuniao Latino-Americana de Agrometeorologia. V-I:279-280.

NICHOL E. J,. (1993). Remote Sensing of Water Quality in the Singapore-Johor-Rian Growth Triangle. Remote Sensing of Environment, 43: 139-148.

NITROUER, A. C. and SHARARA, T. M and DeMASTER. J. D. (1983). Variations of sediment texture on the Amazon continental shelf. Journal of Sedimentary Petrology, 53: 179-191.

NOVO, M. M. E. (1986). Aplicacoes de sensoriamento remoto em hidrologia e recursos hidricos. Revista Brasileira Engenharia, No.2, 3: 5-16.

NOVO, M. M. E., HANSOM, D. J., and CURRAN, J. P. (1989a). The effect of viewing geometry and wavelenght on the relationship between reflectance and suspended sediment concentration. No.8,10:1357-1372.

NOVO, M. M. E., HANSOM, D. J., and CURRAN, J. P. (1989b). The effect of sediment type on the relationship between reflectance and suspended sediment concentration. No.7, 10:1283-1289.

NOVO, M. M. E., and CURRAN, J. P. (1989c). Fatores ambientais que afetam a estimativa de concentracoes de sedimentos em suspensao a superficie a partir de dados de sensores remotos. RBE. No.1, 7: 49-63.

PASSEGA, R. (1964). Grain size representation by CM patterns as a geologicalal tool. Journal of Sedimentary Petrology.No.4, 34: 830-847.

PASSEGA, R. and BYRAMJEE, R. (1969). Grain size image of clastic deposits. Sedimentology, 13: 233-252.

REYNOLDS, C. Jr. R. (1989). Modern Power Diffraction Reviews in Mineralogy, 20:3-17. Editors Bish, L. D and Post, E.J. Mineralogical Society of America.

RICHARDSON, J. A and WIEGAND, L. C. (1977). Distinguishing Vegetation from Soil Background Information. Photogrammetric Engineering & Remote Sensing, 43: 1541-1552.

RIGNOT, E. and SALAS, A.W. and SKOLE, D. L. (1997). Mapping deforestation and secondary growth in Rondonia, Brazil, using imaging RADAR and Thematic Mapper data Remote Sensing and Environment, 59: 167-179.

RITCHIE, C. J., SCHIEBE, R. F., and McHENRY, R. (1976). Remote sensing of suspended sediments in surface waters. Photogrammetric Engineering and Remote Sensing. No.12, 42: 533-542.

RITCHIE, C. J., COLLINS, B. M., and PATTIARATCHI, B. C. (1987). Mapping of water quality in coastal waters using Airborne Thematic Mapper data. International Journal of Remote Sensing. No.1, 8:85-102.

RITCHIE, C. J., and COOPER, M. C. (1988). Comparison of measured Suspended sediment concentration with Suspended sediment concentrations estimated from LANDSAT MSS data. International Journal of Remote Sensing. No.3, 9:379-387.

RITCHIE, C. J., and COOPER, M. C., and SCHIEBE, R. F. (1990). The relationship of MSS and TM digital data with suspended sediments, chlorophyll, and temperature in Moon Lake, Mississippi. Remote Sensing of Environment, 33: 137-148.

RIZZO, L.T. B. and ORLANDO, F. J. (1987). Estimativa de distribuicao da cultura de cana-de-acucar nos solos do Estado de Sao Paulo, Brasil Acucareiro, RJ, No.96, 5: 37-44.

ROCHA, B. H. C. (2000). Geoprocessamento:Tecnologia Interdisciplinar. Editora do Autor.

ROSSETTO, J. A. (1980). Utilizacao Agronomica dos Subprodutos e Residuos da Industria Açucareira e Alcooleira. Boletim Tecnico do PLANALSUCAR.

ROWE, R. D. and ABDEL-MAGID, M. I. (1995). Handbook of waste water reclamation and reuse. CRC Press, Inc. Lewis Publishers.

SAATCHI, S. S. and SOARES, J.V and ALVES, D.S. (1997). Mapping Deforestation and Land-use in Amazon Rainforest by using SIR-C Imagery. Remote Sensing and environment, 59: 191-202.

SABINS, F. F. Jr. (1986). Remote Sensing: principles and interpretation. 2nd. Edition, W. H. Freeman and Company, New York, 449 p.

SAHU, K. B. (1964). Depositional mechanism from the size analysis of clastic sediments. Journal of Sedimentary Petrology, 34: 73-83.

SALDANHA, R. A.L. and CAVALCANTE, T. A. and WANDERLEY, M. R. P and ROCHA, C. R. (1975). Grupo Barreiras: contribuição ao seu conhecimento no estado de Alagoas. ANAIS do VII Simposio de Geologia, p 113-119.

SALOMONSON, V. V., and STUART, L. (1989). Thematic Mapper Research in the earth Sciences. Remote Sens. Environ. 28: 5-7.

SATHYENDRANATH, S. (1981). Influence des substance en solution et en suspension dans les eaux de mer sur l'absorption et la réflectance. Modélisation et application à la télédétection. Thèse. Université Pierre et Marie Curie.Paris IV

SCHALLER, H. (1989). Revisao estratigrafica da Bacia Sergipe-Alagoas, Boletim Tecnico da Petrobras, 12:21-86.

SENGUPTA, S. (1979). Grain-size distribution of suspended load in relation to bed materials and flow velocity. Sedimentology, 26: 63-82.

SENGUPTA, S. and GHOSH, K.J and MAZUMDER, S. B. (1991). Experimental theoretical approach to interpretation of grain size frequency distributions, in Principles, methods and application of particle size analysis. J.P.M. Syvitski (Editor). Cambridge University Press, p. 382.

SMITH, C. R. and BAKER, S. K. (1978). Optical classification of natural waters. Limnology and Oceanography, 23: 260-267.

SMITH, C. R. and BAKER, S. K. (1981). Optical properties of the clearest natural waters Applied Optics, No. 2, 20: 177-184.

SMITH, M. O., and ADAMS, J. B. (1985). Interpretation of AIS images of Cuprite, Nevada using constraints of mixtures in Proc. airborne Imaging Spectrometer Data Analysis. Workshop, Jet Propulsion Lab Publication, 85-41, Pasadena, CA, pp. 62-68.

SOLOHUB,T. J and KLOVAN, E.T (1970). Evaluation of grain-size parameters in lacustrine environments. Journal of Sedimentary Petrology.No.1, 40:81-101.

SOUZA, De. J. L. (1994). Caracteristicas da Irradiancia Solar na Costa Alagoana. 450 Congresso Brasileiro de Agrometeorologia.

SOUZA, J. L. (2000). Area de Protecao Ambiental de Piacabucu:Diagnostico Avaliacao e Zoneamento. Cap.5: 107-203. Editora EDUFAL.

SPENCER, W. D. (1963). The interpretation of grain size distribution curves of clastic sediments. Journal of Sedimentary Petrology, 33: 180-190.

STERNBERG, W. R and CREAGER, S. J. (1961). Comparative efficiencies of size analysis by hydrometer and pipette methods. Journal of Sedimentary Petrology, 31: 96-100.

STONE, A. T. and SCHLESINGER, P. and HOUGHTON, A. R. and WOODWELL, M. G. (1994). A Map of the Vegetation of South America Based on Satellite Imagery. Photogrammetric Engineering & Remote Sensing, 60: 541-551.

SUGUIO, K. (1999). Geologia do Quaternario e mudanças ambientais. São Paulo's Comunicação e Artes Graficas, p. 275.

SWIFT, P. J. D.and SCHUBEL, R. J and SHELDON, W. R. (1972). Size analysis of fine-grained suspended sediments: a review. Journal of Sedimentary Petrology, 42: 122-134.

TASSAN, S. (1981). A method for the retrieval of phytoplankton and Suspended Sediment concentration from remote measurements of water color, in Proceedings 15th Int. Symp. on Remote Sensing of Environment. 15. Ann Arbor, MI, 2.

THENKABAIL, S. P and WARD, D. A. and LYON, G. J. and MERRY, J. C. (1994). Thematic Mapper Vegetation Indices for Determining Soybean and Corn Growth Parameters. Photogrammetric Engineering & Remote Sensing, 60: 437-442.

THORNNTHWAITE, C. W and MATHER, R.J. (1995). The Water Balance. Pbl. Climatology, 8. No 1. p. 104

TASSAN, S. (1988). The effect of dissolved 'yellow substance' on the quantitative retrieval of chlorophyll and total suspended sediment concentrations from remote measurements of water colour. International Journal of Remote Sensing. No.4, 9: 787-797.

TASSAN, S., and D'ALCALA, R. M. (1993). Water quality Monitoring by Thematic Mapper in Coastal Environments. A performance Analysis of Local Bio-optical Algorithms and atmospheric Correction Procedures. Remote Sensing of Environment, 45: 177-191.

VANONI, A. V. (1975). Sedimentation Engineering. Edited by ASCE. No.54, pp.87.

VASCONCELOS, N. J., and OLIVEIRA, G. C. (1985). Composiçao quimica dos diferentes tipos de vinhaça das destilarias de alcool de Alagoas. Boletin Tecnico da Planalsucar. No 14, pp.32-35.

VERDIN, P. J. (1985). Monitoring water quality conditions in a large western reservoir with LANDSAT imagery. Photogrammetric Engineering and Remote Sensing. No.3, 51:343-353.

VILAS BOAS, Da S. G., BITTENCOURT, P. Da S. C. A.., and MARTIN, L. (1985). Leques aluviais Pleistocenicos da regiao costeira da Bahia: Implicacoes paleoclimaticas. Revista Brasileira de Geociencias. No. 15, 3: 255-258.

VISHER, S. G. (1969). Grain size distribution and depositional processes. Journal of Sedimentary Petrology, 39:1074-1106.

WAKE, M and VIANA, C. D. B. and SOUZA, C. G (1983). Pedologia: levantamento exploratorio de solos. In: BRASIL/MME/PROJETO RADAMBRASIL. Folhas SC. 24/25 Aracaju/Recife, 30: 445-572.

WEISER, D. and MOIOLA, J.R. (1968). Textural parameters: an evaluation. Journal of Sedimentary Petrology. No.1, 38:45-53.

WEISMILLER, A. R. and KRISTOF, J. S. and SCHOLZ, K. D and ANUTA, E. P. and MONIN, A. S. (1977). Change Detection in Coastal Zone Environments. Photogrammetric Engeneering & Remote Sensing, 43: 1533-1539.

WETZEL, R. G. (1975). Limnology.Philadelphia:W. B. Sanders, p.743

YATES, G. M., JONES, R. A., McGRORTY, S. and GOSS-CUSTARD, D. J. (1993). The use of satellite imagery to determine the distribution of intertidal surface sediments of the Wash, England. Estuarine, Coastal and Shelf Science, 36:333-344.

ZBINDEN, R. (1981). Les suspension de la Baie du Mont Saint-Michel: étude microgranulométrique et radiométrique. Thèse de Troisième Cycle, 288 p. Université de Paris I.

APPENDICES

APPENDIX I: Sieve procedure

1. The samples were dryed in natural conditions for two weeks,

2. Aproximately 100g of dry sample was subjected to10 minutes of shaking. Screening was done mechanicaly using a series of screens; 16 (1,2 mm), 30 (0,6 mm), 40 (0,42 mm), 50 (0,3 mm), 100 (0,15 mm), and 200 (0,074 mm) mesh sieves,

3.The sediment retained in each sieve was weightened,

4. Determination of the percentage of the total dry sample (Pr) retained in each sieve, which can be written as,

Pr= (Sr wt / Ts wt) x 100% where, (equation 3.1)

Pr- Percentage retained in each sieve (%),

Sr wt- Weight of soil retained in each sieve,

Ts wt- Weight of total dry soil (some samples was 50 g, others vary from 10 to 28 g)

5. Determination of the cumulative weight percentage (Cwt) of sediments retained in each sieve, computed as the sum of all coarser sieves. Some samples were computed using Folk's (1980) formula, written as;

Cwt = (Cc wt / Cl wt) x 100% where, (equation 3.2)

Cc wt- Each coarser cumulative weight,

Cl wt- Last cumulative weight

6.Determination of the percentage of finer (Pf) than any sieve size, which can be writen as,

Pf= 100%- Cwt% (equation 3.3)

7. Plots of cumulative percentage and and cumulative frequency curves, using the percentage of finer (Pf) values were done in arithmetic and probability graphs.

APPENDIX II: Hydrometer procedure

1. 70g of claily sediments, of a diameter smaller than 2 mm, were taken for weighting with a resolution of 0,01g. 100g of the same material was weightened to posterior determination of hygroscopic humidity of those sediments,

2. A 1000 cm^3 solution of 125 cm^3 of Sodium Hexametafostate with a concentration of 45,7g was added to the sample and left to rest for 24 hours. The Sodium Hexametafostate is normally used as a deflocculating agent among the particles.

3. The resulted suspension was emptied into the cup of an electrical mixer for 15 minutes,

4. A jar with distilled water was prepared aside, to store the hydrometer in between readings,

5. The mixed suspension was washed in a 1000 cm^3 graduated cylinder in which distilled water was added up to 5 cm from the top,

6. Mixing of the solution was again done using the palm of our hands over the open end of the cylinder and turning it upside down and back. This procedure was done during 1 minute in order to avoid any soil from sticking to the base of the cyllinder,

7. The graduated cyllinder was then placed on a cimented balcony, and the designated ASTM 152H Bouyoucos hydrometer was inserted to start the readings. The hydrometer is graduated to read directly grams of sediment or soil per liter at 68 ^oC and is assumed to determine the density of the sediments in suspension at about its center of volume after correcting the displacement of the suspended sediment.

8. Hydrometer readings for 1, 2, 4, 8, 15 and 30 minutes were done and followed by readings at total elapsed time intervals of 1, 2, 4, 8, and 24 hours. The temperature was taken for every hydrometer reading within the suspension. Paralel hydrometer readings

were taken in the jar of distilled water at each elapsed time interval for a few samples. Some other tests were repeated at the Soil Mechanics laboratory at the University of Quebec in Chicoutimi. Due to the unchange state for the last three readings observed, the test was limited to 10 samples distributed among the four selected zones.

9. The suspension was poured into evaporating jars and placed in an oven for 24 hours. The dry sediments were weightened again and the hygroscopic humidity was calculated.